Multifunctional PBLG nanoparticles for bone targeting and anticancer drug delivery into bone tissues

Laura De de Miguel Miguel Martínez de Aragón

UNIVERSITE PARIS-SUD

ÉCOLE DOCTORALE : INNOVATION THÉRAPEUTIQUE:

DU FONDAMENTAL A L'APPLIQUÉ

Laboratoire *UMR CNRS 8612 Institut Galien Paris-Sud*

DISCIPLINE: PHARMACOTECHNIE ET PHYSICO-CHIMIE

PHARMACEUTIQUE

THÈSE DE DOCTORAT SUR TRAVAUX

soutenue le 01/10/2013

par

Laura DE MIGUEL MARTÍNEZ DE ARAGÓN

Nanoparticules multifonctionnelles de poly(L-glutamate de gamma-benzyle) destinées au ciblage et à la délivrance d'anticancéreux aux tissus osseux

Directeur de thèse :	M. **Gilles PONCHEL**	Professeur, Université Paris-Sud
Composition du jury :		
Président du jury :	M. Elias FATTAL	Professeur, Université Paris-Sud
Rapporteurs :	Mme Sandrine CAMMAS	CR CNRS, UMR CNRS 6226
	M. Philippe LEGRAND	Professeur, Université Montpellier 1
Examinateurs :	M. Pierre MARIE	DR CNRS, UMR INSERM 606

ACKNOWLEDGEMENTS

I would like to thank everybody that has collaborated in this project and has helped me during my PhD. First, I would like to thank Pr. Gilles Ponchel for accepting my demand to do a PhD under his supervision. I am very grateful for your kindness and for the interesting discussions that we have shared. I would also like to show my greatest appreciation to Pr. Elias Fattal for having accepted me in the research lab, for his advices, the time he dedicated to me and his natural approach towards me.

I would like to express my gratitude to the thesis referees Dr. Sandrine Cammas- Marion and Dr. Philippe Legrand and all the members of the jury for their evaluations and critics of my work, for their work and their availability.

I would also like to thank all the members of the laboratory, who have helped me during this PhD period. I would like to express my deepest appreciation to Bénédicte, for all those years sharing the office, for her friendship, her support and advice. To Dr. Christine Charrueau; since I have known her, she has always been available to help me and to give me her always useful advices. For her attention, kindness and responsibility towards me and her help with the manuscript corrections. Also for her help with the animal experiments. To Dr. Christine Vauthier, for her kind help and useful advices. To Dr. Iuliana Popa, for her friendly approach, her useful advices and for all her experimented help working with cells. To Christelle for her help and moments shared together and also to Dr. Kawthar, Silvia, Junior, Claudio Freimar, Olivier, Anne Laure, Mounira, Donato and all others students of the UMR 8612 for their kindness and attention.

I would particularly like to thank Magali, for her kindness and comprehension, her help, useful advice and work accomplished with the ITC experiments!

To Nicolas, Benjamin and Julien for their advice in chemistry. To Davide for his always useful help in the lab and for the discussions. I have greatly benefited from Pr. Didier Desmâele's altruistic help with my chemistry synthesis and NMR decoding!

I would like to thank Dr.Bogdan Iorga and Dr. Georgiana Surpatenau from the UPR 2301, Institut de Chimie des Substances Naturelles for collaborating with us in the alendronate -hydroxyapatite interaction and for the interesting discussions we shared together.

I am deeply grateful to Cynthia Gillet for her help and expertise with the TEM images and the Platform for Transmission Electronic Microscopy of IMAGIF and also to Vincent Guérineau for the MALDI-TOF analyses.

I would like to express my gratitude to the Pharmacy Service of Georges-Pompidou European Hospital and especially Dr. Eric Caudron and Sophie He for their availability and help with the AAS experiments.

I want to thank the laboratory of Analytical Chemistry of University of Valencia, Dr. Antonio Doménech-Carbó and especially my friend Gerardo, for accepting to carry out electroanalytical experiments.

I am particularly grateful for the assistance given by Alice, Simona, and Pauline and Julie from the Animal Platform, for their teaching and patience with the animal experiments and for being there whenever I needed.

I would like to thank the laboratory Inserm U606 and all their members for their kindness and help with the histological experiments. To Dr. Pierre Marie for accepting to collaborate with us in this project. To Caroline Marty for showing me very patiently the mysteries of histology. To Julia for her kind help in my initial contact with mice experiments. To Aurore and Eric for their help with the Apotome.

I would also like to thank the Unité de Pharmacologie Chimique et Génétique et d'Imagerie UMR 8151 CNRS U1022 INSERM and especially Michel Bureau for his availability and help with the imaging experiments.

I owe my deepest gratitude to Giovanna, Patricia, Gopan and Ludivine for their generosity towards me and their help with the manuscript. To Nicolas, Bettina, Nadège, Chantal, Odile, Hervé, Nadège, Valentina, Nadia, Violeta and all other members of the UMR 8612 who have always been very kind to me.

I would like to offer my special thanks to the two students, Ludovica and Guillaume, who have collaborated with me on this work. I sincerely hope you enjoyed the work accomplished with this project and that it contributed positively for you and your future. Thanks a lot for all your efforts and help.

I would like to thank also my family who have supported and encouraged me all the long way through these four years. Thanks a lot to Alexandre for his endless patience and support. To Gerardo, who was already at Châtenay when I arrived to start my PhD. For all those dinners around science! To my friends from Spain and from the Houses of both Canada and Spain, for those moments shared together that have given me the strength to accomplish this task.

INDEX

List of abbreviations

AAS	atomic absorption spectroscopy
ABC	accelerated blood clearance
Asp	aspartic acid
ATCC	American type culture collection
ATR	attenuated total reflection system
BLG-NCA	γ-benzyl-L-glutamate-N-carboxylic anhydride
BMUs	basic multicellular units
bnz	benzyl
$CaCl_2$	calcium chloride
$CDCl_3$	deuterated chloroform
CDDP	cisplatin
CF_3COOK	potassium trifluoroacetate
CuBr	copper(I) bromide
DCC	N,N'-dicyclohexylcarbodiimide
DCM	dichloromethane()
DCTB	*trans*-2-[3-(4-*tert*-butylphenyl)-2-methyl-2-propenylidene]malonitrile
DMSO	dimethyl sulfoxide
DMSO (d_6)	dimethyl sulfoxide
DEE	diethyl ether
DLS	dynamic light scattering
ds-DNA	double stranded deoxyribonucleic acid sodium salt from salmon testes
DP_n	degree of polymerization
EtOH	ethanol
FDA	Food and Drug Administration

FITC	fluorescein isothiocyanate
FTIR	fourier transform infrared spectroscopy
GCE	glassy carbon working electrode
Glu	glutamic acid
H^+	protons
HAP	hydroxyapatite
^{1}H NMR	proton nuclear magnetic resonance
HSC	hematopoietic stem cells
ITC	isothermal titration calorimetry
K_{Ca}^{+2}	calcium binding affinity
K_{HAP}	hydroxyapatite binding affinity
MALDI-TOF	matrix-assisted laser desorption/ionization time-of-flight
MMPs	matrix metalloproteinasas
MeOH	methanol
MeO-PEG-NH2	α-Methoxy-ω-amino poly(ethylene glycol)
MSC	mesenchymal stem cells
MTS	([3-(4,5-dimethylthiazol-2-yl)-5-(3-carboxymethoxyphenyl)-2-(4 sulfophenyl)-2H-tetrazolium, inner salt)
N_A	number of Avogadro
NaOH	sodium hydroxyde
NCA	N-carboxylic anhydride
NHS	N-hydroxysuccinimide
α,ω-Bis-NHS-PEG$_{6k}$	α -N-hydroxysuccinimide- poly(ethylene glycol)$_{6000}$- ω- N-hydroxysuccinimide
α-NHS-PEG- ω alkyne	α-N-Hydroxysuccinimide-poly(ethylene glycol)- ω-alkyne

NMR	nuclear magnetic resonance
N_3-PEG-NH_2	azide- poly(ethylene glycol)-amine
OPG	osteoprotegerin
PBCA	polybutylcyanoacrylate
PBLG	poly(γ-benzyl-L-glutamate)
PBLG-*b*-PGlu	poly(γ-benzyl-glutamate)-*block*-poly (glutamic acid)
PBS	phosphate buffer saline
PEG	poly(ethylene glycol)
ph/sr/s/cm^2	photon per steradian per second per square centimeter
Pd/C	palladium on carbon
PI	polydispersity index
PGlu	poly (glutamic acid)
PGlu-CDDP	poly(glutamic acid)-cisplatin
PLA	polylactic acid
PLGA	poly(lactic-co-glycolic acid)
PMDETA	pentamethyldiethylenetriamine
^{31}P NMR	phosphorus nuclear magnetic resonance
PSMA	prostate-specific membrane antigen
PVP	polyvinylpyrrolidone
PEO-PAGE	poly(ethylene oxide)-*b*-poly (allyl glycidyl ether)
RANK	receptor activator of nuclear factor κ-B
RANKL	receptor activator nuclear factor κ-B ligand
RES	reticuloendothelial system
RGD	arginylglycylaspartic acid
ROP	ring opening polymerization

SEC	size exclusion chromatography
SD	supplementary data
SI	supplementary information
siRNA	small interfering RNA
SWVs	square wave voltammetry
TEA	triethylamine
TEM	transmission electron microscopy
THF	tetrahydrofuran
UV	ultraviolet
VEGF	vascular endothelial growth factor
VPA	vinyl phosphonic acid

INTRODUCTION GÉNÉRALE

INTRODUCTION

Après son administration dans l'organisme tout principe actif est soumis à une multitude de processus complexes qui vont déterminer sa biodistribution et par conséquent non seulement son efficacité mais aussi les éventuels effets indésirables et sa toxicité. L'amélioration de l'efficacité des molécules actives peut être recherchée tant par la voie de la pharmaco-modulation que par celle de la vectorisation, en les associant à des vecteurs capables de modifier leur distribution et d'améliorer leur efficacité tout en diminuant leurs effets secondaires. C' est une idée déjà ancienne, proposée il y a plus de 100 ans par le prix Nobel Paul Ehrlich qui proposa de « cibler » de manière spécifique les cellules tumorales ou les organismes provocant des maladies. Cette stratégie a donc pour ambition de restreindre l'effet thérapeutique à un organe ou des cellules pathologiques, c'est-à-dire une modification de la biodistribution naturelle de la molécule, ce qui permettrait en théorie une diminution des doses administrées ainsi qu'une réduction des effets secondaires.

Le présent travail s'inscrit pleinement dans le champ de la nanomédecine, un domaine dans lequel on désire mettre en jeu, à l'échelle nanométrique, des phénomènes variés entre un objet artificiel et l'organisme d'un patient. Plus précisément, ce travail a consisté à concevoir, préparer et caractériser des nanoparticules polymères possédant un tropisme pour les tissus osseux, en vue d'améliorer la distribution des molécules actives vers ces tissus.

Cet objectif nécessite d'être capable de conférer simultanément aux nanoparticules de nombreuses fonctionnalités différentes, capables d'aider les particules dans leur progression vers leur cible, depuis leur point d'administration. Dans ce cadre, lors de thèses entreprises au sein de notre équipe [1-3] il a été montré qu'il était possible de préparer des nanoparticules multifonctionnelles en mélangeant en proportions variables des polymères dérivés du poly (glutamate de benzyle) et portant différentes fonctionnalités. De façon intéressante, il a été montré que les propriétés de surface de ces nanoparticules pouvaient être aisément modulées. En effet, la maîtrise des propriétés de surfaces de

ces particules est indispensable puisque c'est elle qui va induire ou non les phénomènes d'interactions avec les composants du milieu biologique et qui sont souhaités ou non selon leur nature.

Dans ce contexte, l'objectif de ce travail de recherche a été le développement de nanoparticules multifonctionnelles polymères préparées à partir de dérivés du poly (glutamate de benzyle) (PBLG) possédant des propriétés de ciblage des tissus osseux de manière à pouvoir les immobiliser de manière suffisamment longue et d'assurer la délivrance d'un principe actif qui leur est associé dans les tissus osseux, de façon contrôlée dans le temps. De cette manière, ces nanoparticules pourraient constituer des réservoirs de principe actif intéressants en vue d'améliorer le traitement de diverses maladies du squelette.

Dans ce but, une mini-librairie de copolymères dérivés du PBLG et portant différentes fonctionnalités a été synthétisée. Ces copolymères, mélangés dans des proportions différentes ont montré des propriétés d'auto-assemblage pour former des nanoparticules de petite taille, typiquement inférieures à 80 nm et présentant une morphologie souvent ellipsoïdale. Leurs propriétés d'attachement aux tissus osseux, conférées par la présentation en surface de différents ligands ostéotropes (biphosphonates, acide poly(glutamique), ont été évaluées *in vitro* en utilisant l'hydroxyapatite comme modèle, puis *ex vivo* et *in vivo*.

Le traitement des métastases osseuses a été identifié comme une possible application de ces nanoparticules ciblées aux tissus osseux. De nombreux cancers ont une forte tendance à métastaser dans l'os ce qui induit des problèmes majeurs de santé publique, notamment dans le cancer du sein et de la prostate, en raison de leur incidence élevée. Différentes stratégies ont donc été étudiées visant à associer à ces nanoparticules des molécules anticancéreuses et à leur conférer ainsi des propriétés anticancéreuses. Parmi celles étudiées, la complexation du cisplatine aux groupements carboxylates de nanoparticules formées à partir du copolymère PBLG-PGlu a été retenue puisque de cette manière la libération du cisplatine peut être contrôlée très efficacement dans le temps, avec une cinétique de

libération compatible avec la stratégie envisagée, où les nanoparticules ciblées aux tissus osseux constituent réellement des réservoirs de principe actif une fois arrivées à leur cible.

Le travail de thèse présenté se décompose en plusieurs chapitres. Un premier chapitre bibliographique a tout d'abord été consacré à une revue des différentes stratégies imaginées pour concevoir et préparer des systèmes d'administration doués d'un tropisme pour l'os. Ce chapitre, qui comprend une présentation de l'anatomie et de la physiologie osseuse, a pour ambition de déterminer les barrières actuellement identifiées et que les nanoparticules envisagées devront donc franchir pour rejoindre les tissus osseux. Une revue des différents systèmes d'administration proposés, particulièrement axée sur les vecteurs nanoparticules termine cette partie.

Le deuxième chapitre est ainsi consacré à la préparation de nanoparticules décorées avec des molécules d'alendronate, qui sont des molécules possédant des propriétés osteotropiques et qui sont utilisées largement dans la thérapeutique de maladies osseuses. L'interaction de ces nanoparticules avec l'hydroxyapatite et les ions calcium divalents, qui sont en grande partie les responsables de l'interaction alendronate-hydroxyapatite, a été comparée.

Le troisième chapitre, décrit la préparation de nanoparticules décorées avec le poly(acide glutamique). Ce ligand confère aux nanoparticules de façon simultanée des propriétés d'attachement à l'os et d'encapsulation et de contrôle de la libération du cisplatine grâce à la capacité des groupements carboxylate de former de complexes réversibles avec le cisplatine. Les propriétés d'interaction, d'association et de libération du cisplatine ainsi que le maintien d'un effet cytotoxique ont été explorés.

Le quatrième chapitre est axé sur la mise au point de nanoparticules multifonctionnelles décorées simultanément avec des chaînes de poly(acide glutamique) et de poly(éthylène glycol). De manière originale, une technique d'électrochimie a été utilisée comme un outil novateur et complémentaire à

d'autres techniques pour le suivi des différents processus impliquant les nanoparticules chargées en cisplatine.

Le cinquième chapitre de la thèse présente différents types de nanoparticules multifonctionnelles et fluorescentes, possédant des propriétés d'attachement aux tissus osseux grâce à leur décoration à l'aide de l'alendronate ou bien du poly(acide glutamique), ou encore d'une combinaison de deux. La modulation des propriétés de surface des nanoparticules préparées par une méthode de nanoprécipitation et plus particulièrement leur capacité d'attachement à l'hydroxyapatite, a été démontrée uniquement lorsque les particules portent un ligand osteotrope. De plus, leur capacité à atteindre les tissus minéralisés a été étudiée *in vivo* par des techniques d'histologie.

Enfin, une discussion générale reprend ces résultats expérimentaux afin de les présenter de manière synthétique et aussi de façon à les mettre en perspective avec des travaux décrits dans la littérature.

Références

[1] M.E.M. Barbosa, Synthèse de dérivés du poly(L-glutamate de γ-benzyle) : préparation et caractérisation de nanoparticules multifonctionnelles, in, Physico-chimie, Pharmacotechnie, Biopharmacie, UMR 8612, Université Paris-Sud, Paris, 2006.

[2] F.S. Sanchez, Nanoparticules multifonctionnelles de poly (L-glutamate de γ-benzyle) conçues pour être aisément décorées par des ligands de reconnaissance par la mise en oeuvre du système biotine-avidine, in, Physico-chimie, Pharmacotechnie, Biopharmacie, UMR 8612, Université Paris-Sud,Paris 2009.

[3] O. Cauchois, Conception, Préparation & Caractérisation de Nanoparticules de Formes Complexes. Etude de leur Devenir In Vivo, in, Physico-chimie, Pharmacotechnie, Biopharmacie, UMR 8612, Université Paris-Sud, Paris 2011.

TRAVAUX ANTERIEURS

CHAPITRE I

BONE TARGETED

NANOPARTICLE THERAPEUTICS

BONE TARGETED NANOPARTICLE THERAPEUTICS

Laura de Miguel[1] and Gilles Ponchel[1]*

[1] Univ. Paris Sud, UMR CNRS 8612, Institut Galien, 92296 Châtenay-Malabry Cedex, France.

*Corresponding author: Gilles Ponchel, Univ. Paris Sud, UMR CNRS 8612, Institut Galien Paris Sud, 92296 Châtenay-Malabry Cedex, France. E-mail: gilles.ponchel@u-psud.fr

Résumé

Les maladies squelettiques sont devenus de plus en plus répandues principalement en raison du vieillissement de la population. Elles sont caractérisées par une morbidité très élevée, impliquant des complications métaboliques invalidantes et dont la prise en charge est coûteuse. La vectorisation de principes actifs aux tissus osseux constitue une stratégie prometteuse dans l'objectif d'obtenir des traitements tout à la fois plus efficaces et dont les effets secondaires seraient moindres. L'hydroxyapatite, composant très spécifique de l'os, constitue une cible très spécifique pour la conception de vecteurs nanoparticulaires doués d'un tropisme osseux. Cette revue bibliographique présente une approche rationnelle de la conception de vecteurs nanoparticulaires en considérant les barrières biologiques à franchir pour atteindre leur cible et la manière dont les propriétés physico-chimiques des nanoparticules peuvent être ajustées de manière à favoriser leur franchissement. Enfin, l'état de la littérature dans le domaine de cette stratégie émergeante est présentée.

Abstract

Skeletal diseases are becoming increasingly important in nowadays society, due mainly to the aging of the population and are characterised by a high morbidity involving metabolic complications, which may be quite invalidating for patients and would require costly treatments. The need for safer and more effective bone therapeutics is thus of major importance. In this way, targeting drugs to bone would increase therapeutic efficacy while decreasing side effects. In view of bone targeting, hydroxyapatite, a very specific component to bone, offers a highly specific target to be exploited by

nanomedicine. This review deals with a rational approach for bone targeted nanoparticles and discuss their physicochemical requirements and their relationships with *in vivo* biological barriers that they have to overcome from the site of delivery to bone tissues. Finally a review of the scarce literature of this emerging approach is presented.

Keywords: nanoparticles, bone-targeting, drug-delivery, multivalency, hydroxyapatite, skeletal diseases.

1- Introduction

Bone diseases such as osteoporosis, Paget's disease, osteopenia, osteogenesis imperfecta or bone cancer constitute a major public health problem in our society. They are characterised by a high morbidity involving metabolic complications, pain or fractures. Besides and due primarily to the aging of the population, age-related bone diseases are to increase: in 2020: more than half of Americans over 50 years old are expected to risk or to actually develop osteoporosis in any part of the skeleton [1]. Moreover, the skeleton is the most common organ for cancers to metastasize, breast and prostate cancers having the highest incidence of bone metastasis, with 73% and 68% of bone metastases found respectively at post-mortem studies followed by thyroid and lung cancers [2].

Nanotechnology offers a unique strategy for the development of more effective and safer treatments. Nanomedicine has revealed a promising approach, more than thirty nanotechnology based products have been approved by the Food and Drug Administration (FDA) [3]. Nanoparticles offer many advantages such as improved drug solubility, longer half-life pharmacokinetics, more specific drug biodistribution or controlled release of the drug. Active targeted nanoparticles involves the specific drug delivery into a diseased tissue or cell. This will result in safer treatments, with lower therapeutic dose and less sides effects, derived from the pharmacological action of the drug at other sites. Bone diseases could benefit from the nanotechnological approach for improved therapeutics.

Several drug carriers have been designed to target bone tissue as shown in figure 1: drug-conjugates, polymeric conjugates and nanoparticles. This review will focus on the targeting of bone tissue via the approach of bone targeted nanoparticles, discussing important characteristics that will determine optimal targeting and *in vivo* fate. Drug conjugates and polymeric conjugates are beyond the scope of this review.

2- Bone targeting systems: approach via bone targeted nanoparticles

Different strategies have been conceived for improving drug delivery to bones as shown in figure 1. Bone targeting moiety-drug conjugates consist of the chemical coupling between a bone seeking agent and a therapeutic drug. and they have been extensively reviewed elsewhere [5-7]. As pointed out in Hirabayashi's review, some of them are under preclinical research. A particular issue is the delivery of proteins to bone, by chemical conjugation via a spacer to a bone targeting which has been extensively developed by the group of Uludag [8, 9]. Bone targeted polymer-drug conjugates consist on the conjugation of drugs and diagnostic tools to a water soluble polymeric backbone. This strategy has been extensively developed by Kopecek et al. [7, 10]. As pointed out , all this strategies has been extensively previously reviewed and they are therefore out of the scope of this review.

The bone targeted nanoparticle approach constitutes the scope of this review and it consists of the building up of nano objects such as micelles or nanoparticles. They can be formed by different materials depending on the type of nanoparticles. As shown in figure 1, they should bear different functionalities including a shielding protective layer which is usually formed by the flexible and hydrophilic poly(ethylene glycol) (PEG) chains. This functionality is mandatory for preventing premature removal of the nanoparticles by the immune system and favouring long circulating systems that would allow nanoparticles to attain their target in larger amounts. The bone targeting moiety should be situated at the surface of nanoparticles, so as to be able to display its targeting efficiency. The therapeutic drug is usually protected inside nanoparticles and an imaging agent can be associated

to the nanoparticles. Methods to fabricate multifunctional targeted nanoparticles are beyond the interest of this review and have been reviewed elsewhere [4].

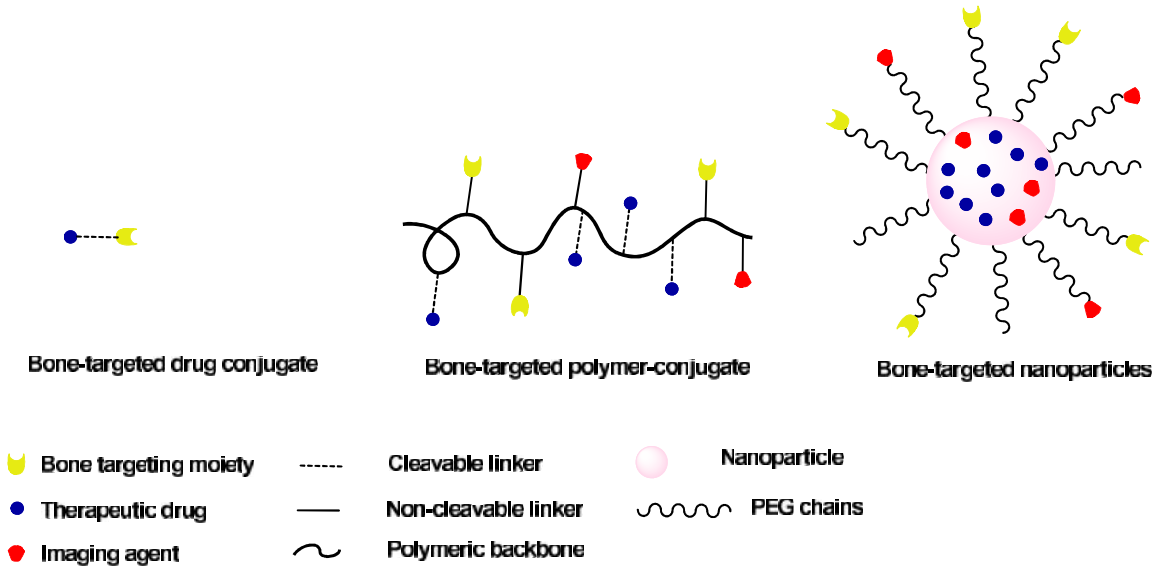

Figure 1: Bone targeted drug delivery systems

3- The targeted organ: introduction to bone anatomy and physiology

3.1- Bone

Bone is a highly specialized connective tissue that provides all higher vertebrates with an internal mechanical support thanks to its mineralized extracellular matrix. It is also involved in the homeostasis of calcium and other ions. Bone is composed of 50-70% mineralized matrix, 20-40% organic matrix, 5-10% water and 5% of lipids. The organic matrix, is mainly constituted of (~85-90%) type I collagen and also other collagenous proteins and non collagenous proteins (~10 %), such as albumin or α2-HS-glycoprotein. The mineralized matrix is mainly constituted by hydroxyapatite (HAP), $Ca_{10}(PO_4)_6(OH)_2$, which provides the skeleton with rigidity and strength, maintaining at the same time a certain degree of elasticity. Morphologically, bone can be cortical and trabecular or cancellous, whose ratios changes depending on the type of bones. Cortical bone is dense, has an outer periosteal surface and an inner endosteal surface that surrounds the marrow space. It is formed by

osteons called Harvesians systems. Trabecular bone consists of a high porous spongy-like network of trabeculae interspersed in the bone marrow and is formed by osteons called packets. Trabecular bone is more vascularised and typically more metabolically active.

The cellular elements of bone are osteoblasts, osteoclasts, osteocytes and bone lining cells. Osteoblasts, osteoclasts and bone lining cells are situated on bone surfaces whereas osteocytes are embedded in the matrix. Bone lining cells cover inactive trabeculae bone surfaces that are not undergoing remodellation, whereas osteoblasts and osteoclasts are on active surfaces which are undergoing modelling and remodelling. Bone remodelling is the process by which bone is renewed in order to maintain bone strength and homeostasis and it takes place continuously throughout life. Bone resorption and formation are coupled. Osteoclasts, which are responsible for bone resorption, and bone forming cells, osteoblasts, constitute basic multicellular units (BMUs), where osteoblasts always trail behinds osteoclasts, ensuring that the removed bone is replaced by newly formed bone. The triad receptor activator of nuclear factor κ-B ligand / osteoprotegerin / receptor activator of nuclear factor κ-B (RANKL/OPG/RANK) is the key regulator in bone metabolism [11].

3.2- Bone marrow

Bone marrow is located in the medullar cavity of the bone, situated next to the endocortical surfaces of trabecular bone. Bone and bone marrow are highly connected and thus have been suggested to function as a single unit. Bone marrow and bone blood supply are highly interconnected and age-related marrow composition changes are known to influence bone remodelling [12]. Bone marrow contains haematopoietic and non-haematopoietic cells, from which osteoclasts and osteoblasts are derived, respectively. Mesenchymal stem cells (MSC) are non hematopoietic multipotent cells capable of multilineage to the majority of marrow stromal cell lineage including osteoblasts, chondroblasts, bone marrow stromal cells, adipocytes, fibroblasts and dermal and other cells of the connective tissue. Hematopoietic stem cells (HSC) are pluripotent cells regulated by humoral factors which can

differentiate into multiple cellular lineages such as erythrocytes, platelets, segmented neutrophils, monocytes, eosinophils basophils or T and B limphocytes [13]. The HSC have been shown to localize to specific microenviroments called niches. The HSC osteoblastic niche, situated next to the endosteal bone surface and regulated partly by osteoblasts, is known to favour quiescence whereas the vascular one allows differentiation and further mobilization of mature cells, which enter the peripheral circulation through the endothelial cells. Once in the vascular systems, HSC cells remain in constant contact with the endothelial cells. Homing of stem cells implies the returning of circulating stem cells to the bone marrow [14].

3.3- Bone vascularisation

Bone blood supply and flow plays a major role in the delivery of bone targeted nanoparticles to bone.

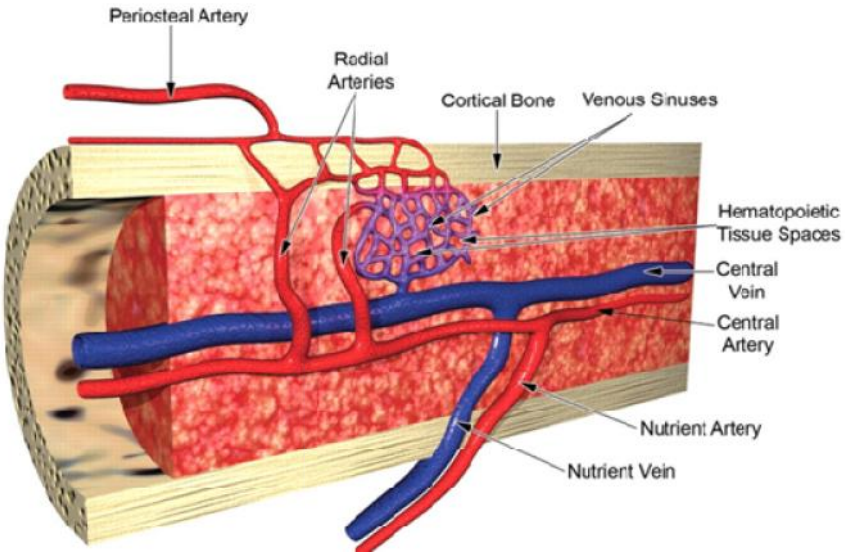

Figure 2: Vasculature in bone adapted from Williams Hematology, 6th edition [15]

As shown in figure 2, blood is supplied to long bones by six groups of arteries that are interconnected by a rich network of anastomoses: superior epiphyseal and metaphyseal artery, periosteal arterioles, dyaphyseal or nutrient arteries, and inferior metaphyseal and epiphyseal artery. The nutrient artery constitutes the major blood supply and it passes the cortex of long bones and enters the bone marrow

as shown in figure 2. Once entered into the marrow cavity, it divides into ascending and descending branches that will split into smaller vessels in the medullar cavity: mostly capillaries, some of them arteries and veins that will extend outwards to the cortical bone to form the Harversian and Volkmann's canals. Plexus venous are formed which then go into the medullar cavity to drain into the central vein that is parallel to the ascending and descending branches derived from the nutrient artery in the medullar cavity [16, 17]. The trabecular bone lacks blood vessels unlike the cortical bone, but is vascularised through the adjacent bone marrow.

Differences in the vasculature will play a major role in the delivery of bone targeted therapeutics. Intraosseous blood flow varies depending in the type of bone, type of bone marrow and in between species. It has been determined in all animals and human bones studies that intraosseous blood flow ranges from 1 mL/min/100 g in the cortical marrow to 20 mL /min/100 g in the cancellous bone while this value is of 5 mL/min/100 g for cortical bone [18].

Vasculature plays an important role in bone metabolism and remodelling [19]. Red bone marrow, that is retained mainly in the spine, pelvis, ribs and sternum in the human adult, is highly vascularised and is the site of large scale transport between the extracellular compartment and blood stream. On the other hand, fat bone marrow is less vascularised than red bone marrow [20] and its content has been shown to rise in reduced vascularised states [21].

4- Bone targeting moiety

Attachment of ligands to nanoparticles as a way to improve selective biodistribution into the targeted organ or cell has attracted much interest in the last few years. The ideal target should be expressed in the target tissue or cells but not expressed at all in non targets. For example, most of cancer targeting approaches are based on the overexpressed receptors of tumour vasculature associated to angiogenesis (vascular endothelial growth factor (VEGF), α_v β_3-integrin receptors) or up-regulated receptors in cancer cells associated to cell proliferation markers (transferrin, folate receptors) compared to healthy

cells [22]. However, receptors do in fact exist in healthy cells and vasculature. α_v β_3 integrins are overexpressed in breast cancer bone metastases; however the specificity of this receptor is low since it is also highly expressed in osteoclasts and it is ubiquitously expressed in diverse cell types, interacting with the extracellular matrix proteins or with other cells and being involved in different biological processes. [23]. Due to this limitation, few approaches are based on the targeting of more specific cell receptors, such as prostate-specific membrane antigen (PSMA) to target prostate cancer cells or CD33 in acute myeloma leucemia. [24]

Bones, thanks to their unique anatomic characteristic, the presence of HAP, $(Ca_{10}(PO_4)_6(OH)_2)$, that is only present also in teeth and pathological calcifications, offers a unique and highly specific target. Because of this, it is not surprising that most of the bone targeting approaches are based on HAP targeting, which is also facilitated by the fact that many aminoacids, proteins and other compounds have been shown to bind to HAP [25, 26].

Biological HAP in vertebrates is a poorly crystallized, non -stoichiometric HAP that has multiple deficiencies at all ionic sites and that undergoes multiple substitutions. It is known to contain less hydroxyl groups than the synthetic HAP and more carbonates groups which substitutes phosphate ions [27].

There are several moieties that were shown to have HAP affinity such as biphosphonates, acidic oligopeptides, tetracyclines [28] and tetracycline analogs [29]. For the latter, the tricarbonylmethane of ring A and the keto-enol function of B and C rings have been suggested to be involved in HAP binding [30]. Small heterocycles related to the thiadiazole structure were found to bind HAP with a similar affinity as tetracycline [31] and poly(malonic acids) [32]. In general, these molecules present groups in their structure that are able to chelate calcium atoms present in the HAP crystallite. Besides, some metals such as strontium, which is incorporated into the HAP by surface exchange or ionic

substitution [33], lanthanides or fluorides [34, 35] have shown affinity for bone. To impart osteotropicity to drugs the most used moieties are biphosphonates and acidic oligopeptides.

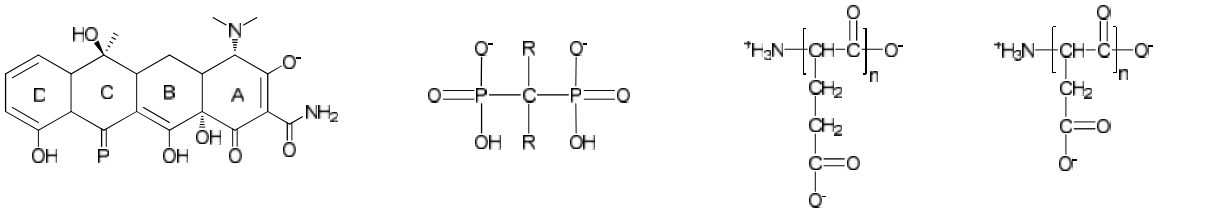

Figure 3: Most commonly used bone targeting moieties at physiological pH

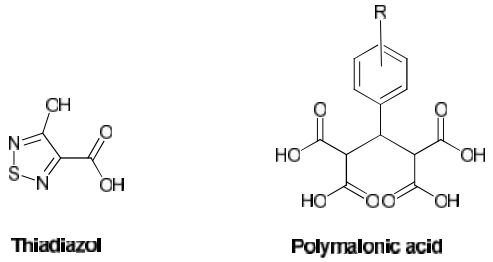

Figure 4: Other bone binding moieties

4.1- Biphosphonates

Biphosphonate are commonly used drugs in the treatment of skeletal pathologies. They are analogous of the endogenous pyrophosphate, where the labile P-O-P linkage has been substituted by the hydrolysis resistant P-C-P structure. The O-P-C-P-O backbone is responsible for the strong affinity for calcium ions, the presence of hydroxyl groups in side chains usually enhances the affinity for calcium ions via a tridentate rather than a bidentade binding. The substituents in the R_2 side chains might also have an effect on the mineral affinity [36]. Biphosphonates show poor oral bioavailability and have a very short plasma half life due to high renal excretion and high bone uptake [37].

The HAP binding affinity of biphosphonates is of great importance in terms of skeletal distribution and retention. It was found to be in the range of 10^6 M^{-1} whereas with bone powder, affinities were found to be much lower, in the range of 10^4 M^{-1} [38]. Significant differences between biphosphonates

could be inferred, being the decreasing affinity order as follows: zoledronate > alendronate > ibandronate > risedronate > etidronate > clodronate [36]. The adsorption isotherm, which is an equilibrium between HAP adsorbed biphosphonate and free biphosphonates in the bone extracellular fluid, was found to follow a Langmuir model.

Once administered intravenously, biphosphonates that are not excreted via kidneys are rapidly distributed to bone. It was found that biphosphonates accumulate in a non homogeneous way, preferentially at active sites where remodelling process is taking place. This might be due to the fact that HAP is highly exposed at these areas and is available for biphosphonate adsorption. Indeed, active surfaces are minoritary, since they are found in less than 10% of the trabecular bone surfaces of the iliac crest in adult humans [39], although it could vary depending on the type of bone and age. Besides, biphosphonates distribute preferentially to trabecular bone [40], possibly due to its increased blood flow and metabolic activity. Studies in rats with radioactive labelled biphosphonates, alendronate and etidronate showed a dose dependence for skeletal biodistribution, with preferential binding to bone resorption sites. At much higher doses, however, etidronate was almost equally distributed although still slightly preferentially accumulated in bone resorption [38, 41].

Once biphosphonates are bound to HAP, they can either be released or become embedded within the bone matrix as osteoblasts produce osteoid. There are theoretically two release mechanisms for biphosphonates from bone mineralized surfaces: chemical resorption and osteoclast resorption. The first one is thought to be relatively more important in the short term after dosing and it is dependent on the concentration in the extracellular fluid, being desorbed when its concentration in the extracellular fluid is low. In the long term and being the most relevant *in vivo* mechanism globally, it is the osteoclast resorption which will mainly release biphosphonates by the secretion of protons (H^+) into the resorption lacunae. The acidic pH of the resorption lacunae causes the protonation of the

phosphonate groups, decreasing HAP affinity and provoking its release. Sato et al. have shown *in vitro* that at a pH of 3.5 50% of alendronate molecules could be released from bone mineralized tissue [38].

Some of the released biphosphonates could reattach to the bone surface, be eliminated from the bone organ or be available for internalisation by osteoclasts and other cells and this would depend on the bone affinity of biphosphonates. Higher rather than lower affinity biphosphonates will be expected to be soon reattached to the mineralized surfaces. Bone affinity can also provoke different skeletal distribution of biphosphonates. Higher affinity biphosphonates will expect to diffuse lower through the osteocyte canalicular network as it was recently shown: lower affinity compounds penetrate deeper into the bone matrix and thus more osteocytes were in contact with these low affinity compounds [42, 43].

Skeletal retention of biphosphonates is long, although the exact retention time remains controversial. Some studies have estimated the skeletal retention of alendronate to 10 years in humans, establishing an intermediate half-life of 6 months, perhaps due to the chemical desorption [44]; pamidronate was detected in urine in young patients with juvenile osteoporosis up to seven years later [45]. Biphosphonate retention may be also dependent on bone turnover although there is little data on this issue.

4.2- Acidic oligopeptides

Acidic non collagenous proteins, such as osteonectine and bone sialoproteine, were shown to bind to HAP with high affinity (binding constants in the range of 10^6-10^7 M), preferentially on the (100) face of HAP crystals [46]. The identification of glutamic-acid rich sequences as possible HAP binding sites opened the way to the use of acidic oligopeptides as bone targeting moieties [47]. The acidic oligopeptides containing at least six L-aspartic acid (Asp) and L- glutamic acid (Glu) aminoacids were shown to be selectively distributed to bone .There were no *in vitro* bone binding differences between the two isomeric forms, D and L. However, *in vivo* L-Asp was eliminated considerably in 7 days,

attributing this to a possible degradation by peptidases or to the acidic pH present in the bone microenvironment. The HAP binding affinity constant for both $(L\text{-}Asp)_6$ or $(L\text{-}Glu)_6$ were in the same range and were approximately $1.6\ 10^5\ M^{-1}$ [48]. It was suggested that $(Asp)_6$ had a non homogeneous distribution in bone and that it would accumulate preferentially to the active bone surfaces [49]. It could be hypothesised from their affinity constant, which is ~100 times lower than that of biphosphonates, that acidic oligopeptides would chemically desorp more from the mineralized tissue, would reattach less to the bone, would penetrate deeper into the osteocyte network and would have shorter skeletal retention.

4.3- Targeting specific sites of bone surfaces

Newly deposited HAP differs substantially from the matured one. Newly deposited HAP has a non-apatitic domain at the surface of the nanocrystals, that consists of a well developed hydrated layer, responsible for the high ion exchange reactivity of HAP, where labile phosphates and carbonates groups are easily and reversibly exchangeable. During maturation, the non-apatitic domain progressively decreases and the apatitic one increases, evolving towards a highly crystalline phase involving the relocation of labile phosphate and carbonates and an increase of the phosphate apatite [50]. In physiological conditions, in normal bone mineral, maturity evolves generally in parallel with the crystallinity index. However, both have different parameters and their crystallinity index can be modified by the presence of ionic substitutions in the apatite lattice. Moreover, some pathologies, such as skeletal fluorosis and osteoporosis, as well as the use of several drugs are known to modify the degree of crystallinity of HAP [51].

Some bone binding moieties have shown to have specific affinity for either resorption or formation sites. HPMA targeted to bone by $D\text{-}(Asp)_8$ peptide was found to bind preferentially to bone resorption sites, which are characterised by a higher crystallinity compared to bone formation sites whereas alendronate bound to both resorption and formation sites. This could be attributed to the lower affinity

of $(Asp)_8$ for HAP and to a more dependent binding on HAP crystallinity [52] than for the biphosphonate moiety. Moreover, specific sequences, $(Asp\text{-}Ser\text{-}Ser)_n$ based on dentin phophoroprotein, one of the major non collagenous protein of dentin extracellular matrix and involved in nucleation of HAP, have been shown to have a specific binding to calcium phosphates (HA and amorphous calcium phosphate) and have shown specificity for emerging sites of mineralization such as dentin. The optimal length has been established to be six, with the maximum affinities values being for eight repeating sequences [53]. Another specific peptidic binding sequence has been identified with specific affinity for dental or enamel. Interestingly, such peptidic sequence that binds specifically with enamel does not contain the known bone binding motifs and is uncharged, which would open new insights into the mechanisms of interaction with bone surface [54]. Differences in binding between dentin and enamel might be also due to differences in HAP crystals, as dentin is poorly mineralized and has smaller and randomly oriented HAP whereas enamel is highly mineralized and composed of elongated well-oriented HAP crystals.

These findings are of major importance since they open a higher level of bone targeting: the targeting of specific sites in bone -resorption or formation- according to pathologies and drugs used. In this way, Zhang et al. showed the sequence $(Asp\text{-}Ser\text{-}Ser)_6$ binds specifically to bone formation surfaces and used it as a bone targeting ligand to specifically deliver through liposomes small interfering siRNAs that silenced bone formation inhibitory genes in osteoblasts [55].

Targeting the bone offers the possibility to concentrate the therapeutic drug in this tissue and thus minimizing side effects derived from the distribution of the drug in other organs. However, once in the bone, drug can interact with the different bone cells and thus intra bone side effects cannot be excluded. Therefore, in a new emerging approach attempts are made to target more precisely intraskeletal localizations depending on the type of pathological disease to address, which can result in more specific drug delivering and thus reduced intra-bone side effects.

5- Biological barriers for nanoparticles to overcome to attain bone mineralised tissue

Biodistribution and clearance of nanoparticles will depend both on the physiological characteristics of the organism and on their physicochemical characteristics. In order to attain bone mineralised surfaces, nanoparticles have to overcome numerous barriers, which are discussed below.

5.1- Reticuloendothelial system (RES)

A main parameter that would determine nanoparticle distribution is avoidance by the RES. Long circulating times are required so that bone-targeted nanoparticles can attain the target bone tissue. The process of recognition by the RES is the major obstacle to long circulation time and to efficient targeting. It starts typically by an opsonization process in which opsonins (plasma proteins) bind to nanoparticles. This leads to the attachment of the phagocytes, principally located in the liver (Kuppfer cells), spleen and also bone marrow and thus, favouring their accumulation in this tissue and further ingestion and digestion or accumulation of the phagocytosed material. However, the involved processes are much more complex since it has been shown that opsonizated sterically stabilized liposomes may not necessarily induce engulfment by the macrophages [56] and that protein binding cannot correlate with plasma circulation lifetimes [57]. Opsonin independent mechanisms may be involved in the recognition by macrophages via scavenger receptors and via direct interactions with macrophages, where surface characteristics of nanoparticles have shown to play a major role [58, 59].

There are many physicochemical factors that play a role in the clearance and biodistribution of nanoparticles, such as particle size, shape, composition, surface charge, pegylation and functionality. Although some generalisations are widely accepted, each nanoparticle system has unique overall characteristics. It is generally accepted that nanoparticles should be under 100 nm in diameter to be able to display reduced protein adsorption and enhanced blood circulation [60]. Slightly negative and neutral nanoparticles are known to have reduced plasma protein adsorption, macrophage uptake and enhanced target tissue accumulation compared to positive ones [61]. Shape has also proven to have a

major role in the engulfment of micro and nanoparticles by the macrophages [62, 63], worm-shaped microparticles exhibiting a very long half life of up to one week [64].

To reduce opsonization and thus to enhance long circulating time in the bloodstream the preferred method is the PEGylation of nanoparticles, although other materials such as other PEG containing polymers[65], polysaccharides [66], poly(acrilamide), poly(vinyl alcohol), poly-(N-vinyl pirrolidone) [67] or poly(aminoacids) have also been used [68]. Recently, a combination of PEG and water soluble chitosan have shown to synergistically enhance blood half lives [68, 69].The PEGylation provides nanoparticles with a hydrophilic neutral and flexible shield that reduces hydrophobic interaction with the RES. However, the exact mechanism of PEG shielding remains largely unknown. PEG can be linked to nanoparticles through different ways, among which covalent link has shown to be the most effective. There are many factors affecting the efficacy of the PEG shield in conferring stealth properties such as the PEG length, conformation and density. The fact that pegylation enhanced blood circulation time was firstly reported with PLGA-PEG nanoparticles [70]. PEG optimal length varies depending on other physicochemical parameters of nanoparticles. Some authors found an optimal PEG length of 5 kDa [71, 72] or longer [60]. A PEG grafting density ranging from approximately 1.4 to 2.2 nm between the PEG chains has shown to reduce protein adsorption [71, 73]. PEG chains can adopt different conformations depending on the surface coverage. At low surface PEG density, PEG adopts a mushroom conformation and nanoparticles are prone to opsonization and RES capture. The brush conformation, where PEG chains are extended at higher surface densities, or the brush-mushroom intermediate, are more resistant to phagocytosis and activated poorly the human complement system [74]. The effect of pegylation length and size in poly (ethylene glycol) cyanoacrylate-co-*n*-hexadecyl cyanoacrylate nanoparticle on protein adsorption was studied, revealing slower blood clearance for smaller nanoparticles. This may be due also to a higher surface PEG density exhibited on smaller nanoparticles [60].

However, some drawbacks concerning the use of PEG have been reported. In some PEGylated liposomes and nanoparticles at repeated dose regimens, the accelerated blood clearance (ABC) phenomena has been described, where a first dose of PEGylated liposomes administered intravenously would alter the pharmacokinetic properties of a second dose administered within an interval of several days after the first dose. The second dose presents an accelerated clearance from the blood due to an enhanced liver and spleen capture [75-77]. There are several factors that can have an influence on the ABC phenomenon, such as the dose, size and charge of liposomes administered, the PEG density, the drug encapsulated or the interval between injections [78-81]. In order to reduce this phenomena, changes in the time interval between consecutive doses [77] as well as the use of other shielding polymers such as polyvinylpyrrolidone (PVP) as coating for polylactic acid (PLA) nanoparticles have been proposed [82]. However, this issue still remains a big challenge to overcome in order to have reproducible pharmacokinetics for multiple dose treatments. Another inconvenient of PEGylation has been described for gene delivery applications, such as small interfering RNA (siRNA) or plasmid DNA. In order to be active, they have to attain their intracellular target (cytosol and nucleus, respectively). However, PEGylation reduces transfection efficiency due to a lower interaction and uptake by cells [83] and to an inhibition of the endosomal escape of the nucleic acids, being degraded by the DNAases in the endosome [84]. Therefore, the PEG dilemma refers to the advantageous effect of PEGylation in terms of prolonged blood residence and improved pharmacokinetics in opposition to the reduced transfection efficiency inconvenient. To overcome the PEG dilemma, targeting by specific ligands [85], cleavable PEG from the carrier system in response to intracellular or extracellular environment [86-88] and the acceleration of membrane fusion or disruption [89] have been proposed.

5.2- Blood-organ barrier

Unlike small molecules, nanoparticulate systems due to their size are dependent on the structure of the capillary microvasculature to attain the desired tissue. In order to attain longer circulating times, nanoparticles should avoid renal clearance through excretion as well as hepatic and spleen uptake also

related to the RES, as previously discussed in section 5.1. Organs with leaky vasculature, such as liver or spleen will favour an accumulation of nanoparticles in these tissues, whose accumulation is also related to the RES system capture, and therefore preventing nanoparticles from getting into the targeted bone organ. Liver capillary microvasculature consists of reticuloendothelial sinusoids with open fenestrae vessels that allow transvascular flow of nanoparticles up to 180 nm in humans and rabbits and up to 280 nm in mice and rats. Spleen consists of sinusoidal non reticuloendothelial microvasculature in the terminal splenic red pulp arterial blood capillary that allows a transvascular flow of particles up to 5 μm. So as to avoid renal excretion, nanoparticles should be larger than 6 nm [90, 91]. Pathological conditions such as tumours, which can undergo angiogenesis results in abnormal leaky vasculature with gap sizes ranging from 100-2μm and present limited lymphatic drainage, which results in the enhanced permeability effect [22]. Therefore, biodistribution of nanoparticles will be modified in this disease state and will also tend to accumulate in the organs affected by cancer.

5.3- Blood -bone barrier

Bone targeted nanoparticles will have to extravasate from the bone marrow sinusoids to attain bone marrow and then bone surfaces. Information regarding extravasation through bone marrow sinusoids remains controversial in spite of the inter-species differences [92]. Some authors proposed the existence of pores of around 80 nm, as observed in 7 weeks old chicken [93]. Two ways of extravasation have been reported: intracellular via endocytosis by the endothelial cells through the caveolae and bristle coated pits or transcelullar via the diaphragmed fenestrated capillaries of around 80-150 nm [94]. However, a recent review by Sarin establishes that red bone marrow sinusoids are sinusoidal reticuloendothelial capillaries which are transiently fenestrated for blood cell transmigration, and these fenestrations are regulated by diverse adhesion molecules and receptors in the endothelial cells [95] and close rapidly after cells. Under this theory, the transvascular physiologic upper limit of the pore size is limited to 5 nm. Localization of non endogenous nanoparticles of around 60 nm in the bone marrow is attributed to the phago-endocytic capacity of the endothelial cells

through the bristle coated pits, which is restricted to a narrow size range of nanoparticles [96]. In any case, this topic requires deeper research and further understanding in order to explain how nanoparticles could attain this tissue and if any receptor mediated uptake could be involved. For all theories of bone microvasculature, the rational approach would be the development of small nanoparticles (around 60-80 nm) with high stealth properties.

Bone marrow diseases, such as myelofibrosis, have been associated to thickened or continuous basement membranes. Therefore, delivery to fat bone marrow containing bones or to myelofibrosis diseased bone marrow might be hampered by nanoparticles and would constitute an additional challenge. Disease states such as osteoporosis, osteopenia, osteonecrosis or bone infarction, that are associated with reduced vascularization [97-99] makes the delivery of bone targeted nanocarriers into the bone more difficult. On the other hand, in other diseases such as bone metastases lesions, specifically from Walker 256/B cells, an increased vascularization with irregular and increased in diameter new formed blood vessels have been observed [100], in accordance with the general feature of tumour related angiogenesis. Besides, a production of enzymes that digest extracellular matrix [101] could enhance the delivery of the bone targeted nanoparticles and their better diffusion throughout the bone [102].

5.4- Intra-bone barriers

Once in the bone marrow, bone mineralised surfaces are not readily next to the vessels and there are still important barriers to overcome as shown in figure 5. To attain the mineralised tissue nanoparticles will have to overcome a major obstacle: the endocytosis of nanoparticles by the macrophages present in the bone marrow. Again, as for the biodistribution of nanoparticles into the bone organ, avoidance of the RES is a major obstacle for nanoparticle to attain bone surfaces. However, macrophages are not the only obstacle as nanoparticles will be surrounded by a large number of cells, hematopoietic or not,

that are being differentiated from the HSC and the MSC. As a result, a lesser number of nanoparticles may attain the mineralized surfaces.

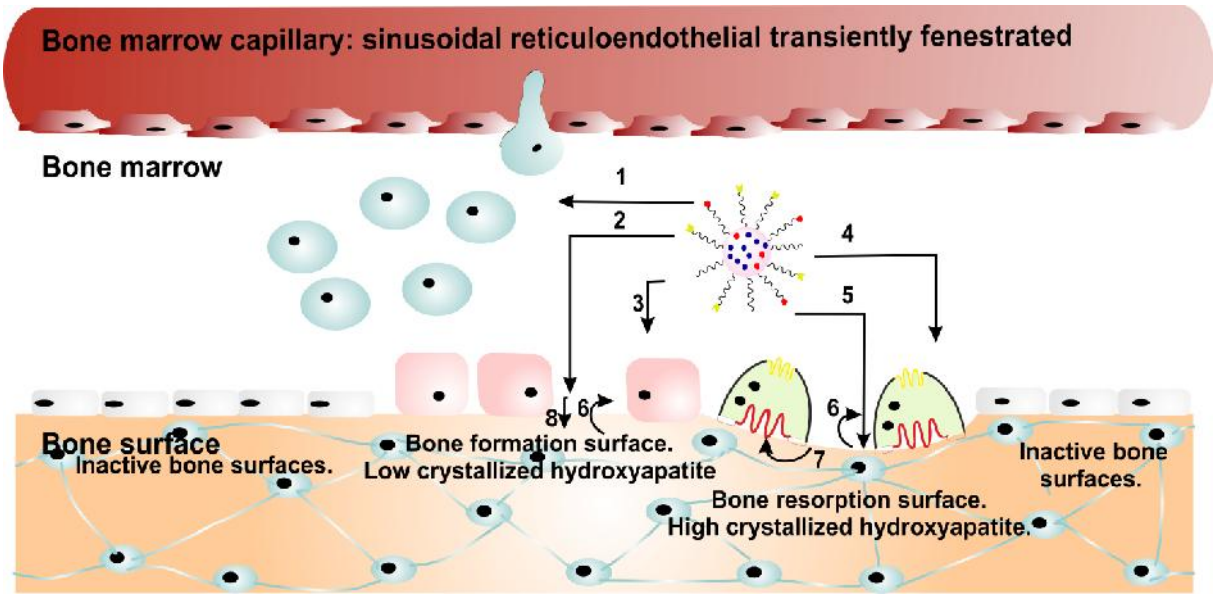

Figure 5: Nanoparticle interaction in the bone microenvironment once attained the bone tissue. Nanoparticles can interact with different cell types and extracelullar matrix domains present in the bone microenvironment: 1- bone marrow cells including phagocyting cells; 2- low crystallized HAP corresponding to bone formation sites; 3- osteoblasts; 4- osteoclasts; 5- highly crystallized HAP corresponding to bone resorption sites. Once attached to the bone surface nanoparticles could: 6-detach from it, being available to interact with bone cells, eliminated from bone or reattach to the bone surface; 7- being resorbed by osteoclasts; 8- being embedded within the osteoid.

If interacting with cells, different general routes for nanoparticles to be endocytosed have been established: clathrin dependent, caveolae mediated, clathrin and caveolae independent or macropinocytosis. These distinct pathways determine the post-endocytic trafficking, involving different type of vesicles with different pH that nanoparticles will encounter. Most nanoparticles have been shown to use more than one of the pathway to enter cells. Several factors, such as the cell type and physicochemical characteristics of nanoparticles, including targeting ligands for any of the cell

surface receptors, will determine the entrance route. The detailed routes have been carefully reviewed [103-105].

Once the bone marrow space passed, bone surface is heterogeneous as shown by figure 5. Non active surfaces are covered by a layer of bone lining cells. It is a nearly continuous layer where bone lining cells are interconnected among them and with osteocytes via gap junctions. Bone binding ligands have been shown to bind preferentially to active surface, where HAP is more exposed. Thus, in order to attain bone mineralised tissue, nanoparticles will be more likely to pass around or through osteoclasts and osteoblasts rather than around or through the nearly continuous layer of quiescent bone lining cells. If interacting with osteoclasts and osteoblasts, as shown for vinyl phosphonic acid (VPA) nanoparticles of approximately 200 nm [110] a lesser number will be available for binding to HAP

Then, they will pass a connective tissue layer formed mainly by collagen and the lamina limitans [39] [106]. To attain mineralized tissue far from vasculature, as bone is a dense tissue and moreover, due to nanoparticles' size, transport may be hampered in some vascular and extravascular spaces, [107] Harvesians canals and the lacunocanalicular system could be involved.

Specifically to osteoclasts, they have in addition the ability to phagocytose. Since they are multinucleated cells of the phagocyte system, which are specialized in internalization and processing of the degraded bone matrix, they share this ability with the RES cells. Vesicular trafficking is of major importance in osteoclasts as shown in figure 6. When osteoclasts are active, they are highly polarised with four different plasma membrane domains. Among the intense vesicular trafficking in osteoclasts, a transcytotic pathway has been described for the degradation products, which are endocytosed from the ruffled border and secreted to the functional secretory domain. There are also endocytic pathways described from the basal plasma membrane to the ruffled border [109].

Polymeric and metallic particles ranging from the submicron up to 10 μm particles have been shown to be phagocytosed by osteoclasts *in vitro* [108]. However, no evidence of the mechanism and route

involved has been described. More insight into these routes would be necessary to fully understand the endocytic trafficking of actively osteoclast and the entry for nanocarriers.

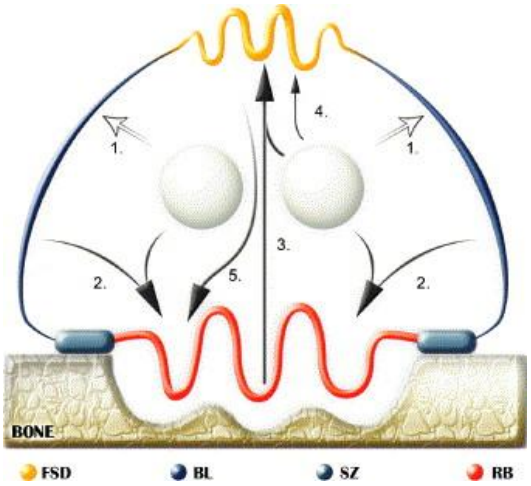

Figure 6: Actively resorbing osteoclast showing different endocytic pathways, adapted from [111]. (1) RB: ruffled border; SZ: sealing zones; BL: basolateral membrane; FSD: functional secretory domain. Biosynthetic pathway from Golgi to basolateral membrane (2) Biosynthetic pathway from Golgi to endosomal pathway join to form fusion zone of ruffled border. (3) Transcytotic pathway from ruffled border to functional secretory domain carrying bone degradation products and. (4) Biosynthetic pathway from Golgi to transcytotic pathway and or to functional secretory domain. (5) Retrieval pathway from functional secretory domain to ruffled border

6. Bone targeted nanoparticles reported in the literature

The design of the appropriate drug carrier depends on many aspects, one of them being the affinity of drug carriers for their target. Nanoparticles can display multivalency by conjugation of multiple targeting units to their surface or the multiassembly of targeted polymers. Multivalent interactions occur in several processes in nature and are known to be much stronger than their monovalents interactions [112]. This might be less important for high affinity ligands, such as alendronate [113]. The effective *in vivo* bone targeting of nanoparticles will be the result of various complex factors, an essential one being the avoidance of the RES. Indeed, the number of ligands exposed on nanoparticles

can have an influence on the recognition by the RES and thus an optimal number of ligands with an optimal bone targeting properties and avoidance of the RES should be established.

Concerning drug release and contrary to the proposed drug controlled release systems discussed in section 7, up to date no responsive bone targeted nanoparticle systems have been achieved (see table 1); therapeutic drug is physically entrapped and there is no controlled release. More concern regarding this issue should be devoted, as for drug conjugates and polymer drug conjugates, in order to increase drug therapeutic efficiency and reduce side effects.

Bone targeted drug delivery by nanoparticles is an emerging field and thus there are still relatively few papers on this field that are shown in table 1 and discussed below.

6.1- Polymeric nanoparticles

Poly(lactic-co-glycolic acid) (PLGA) nanoparticles

Bone targeted (PLGA) nanoparticles have been employed by several authors. PLGA-alendronate decorated nanoparticles that showed *in vitro* HAP affinity were the first bone-targeted nanomedicine to be reported [114]. Then, PLGA-alendronate nanoparticles loaded with doxorubicin were studied in terms of biocompatibility and were employed to treat skeletal metastases derived from breast cancers and for the prevention of osteolytic lesions. The therapeutic effect of alendronate nanoparticle was not found to be higher than the free doxorrubicin [115, 116].

In another study, PLGA -alendronate nanoparticles containing bortezomir and curcumine showed to have increased therapeutic efficacy in reducing bone tumor metastasis derived from breast cancer compared to non targeted nanoparticles and both of them to control vehicle group. Surprisingly and despite the absence of surface PEGylation of the nanoparticles, biodistribution of bone targeted nanoparticles was much higher initially (after 0.5 hours), than for control nanoparticles but diminishes to a very low concentration (the same as for control nanoparticles), after 13 hours. Nanoparticles were thus rapidly eliminated from bone and hardly accumulated in the bone tissue. This is difficult to

conciliate with the long term skeletal retention shown by biphosphonates and the involvement of the bone marrow as a RES organ could account partly for it. [117].

However, PEGylation of nanoparticles is expected (i) to prolong the half life in the bloodstream, and thus is expected to allow bone delivery of a larger amount of nanoparticles. and (ii) once in the bone, to avoid the phagocytosis by the macrophages present in the bone marrow. Accumulation of PLGA-PEG- zoledronate nanoparticles containing docetaxel was enhanced *in vivo* bone compared to non targeted PEGylated nanoparticles. Interestingly, these authors evidenced an EPR effect of metastatic tumour in bone for that model since the delivery of bone targeted PLGA-PEG-zoledronate nanoparticles to tumour bone was 5 times higher and 3 times higher compared to non-diseased bone after 1 and 24 hours, respectively [102].

Poly(γ-benzyl-L-glutamate)(PBLG) nanoparticles

Our group reported PBLG-PEG-alendronate nanoparticles that showed an enhanced accumulation in bone tissue [118].

Poly(butylcyanoacrylate) (PBCA) nanoparticles

PBCA-PEG-zoledronate nanoparticles were shown to enhance biodistribution towards bone metastasis. Interestingly, they showed that not only the anticancer encapsulated drug but also the covalently linked zoledronate showed an *in vitro* pharmacological action. Interestingly, the initially covalently-linked zoledronate exerted an enhanced pharmacological action (ApppI production) compared to that of free zoledronate [119].

6.2- Lipid-based nanoparticles

The binding characteristics of nanoparticles to HAP was specifically studied with alendronate-PEGylated liposomes [120]. In another research, PEGylated liposomes composed of PEG-DPG encapsulating adriamycin showed significantly increased therapeutic effect in reducing osteosarcome

growth as well as pulmonary metastases, increasing the survival time compared to the corresponding control groups [121].

A very interesting approach that selectively delivers siRNAs to bone formation sites was achieved by means of liposomes decorated with a novel bone targeting moiety (AspSerSer), with enhanced bone distribution and knockdown efficiency. This enhanced biodistribution might be also the sum up of different factors, bone affinity and reduced RES capture accounting for this. Some specific unkown uptake mechanism could also be involved as it has been suggested for modified liposomes [122].

Type of nanoparticle	**Bone targeting ligand**	**Therapeutic drug**	**Mechanism of release**	**Application**	**Ref.**
Polymeric- PLGA	Alendronate	-			[114]
Polymeric- PLGA	Alendronate	Doxorubicin	Physically entrapped	Bone metastases	[123]
Polymeric- PLGA	Alendronate	Bortezomir Curcumin	Physically entrapped	Bone metastases	[117]
Polymeric- PLGA-PEG	Zoledronate	Docetaxel	Physically entrapped		[102]
Polymeric PBLG-PEG	Alendronate	-			[118]
Polymeric PBCA-PEG	Zoledronate	Docetaxel Zoledronate	Physically entrapped	Bone metatases	[119]
PEGylated Liposomes	Alendronate	-			[120]
Liposomes	Methylene diphosphonate	Adriamycin	Physically entrapped	Osteosarcome	[121]
Liposomes	$(Asp\text{-}Ser\text{-}Ser)_6$	siRNA	Physically entrapped	Impaired bone formation	[55]
Composite scaffold Collagen/HA	Biphosphonate	Model drugs (Doxorubicin,	Physically entrapped		[124]

		carboxyfluores-cein, lysozime)			
Phospholipid vesicles	Poly-phosphoester	-			[125]
Inorganic- Au	Alendronate Phosphonate Glutamate	-		Potential: imaging. X-ray contrast	[126]
C_{60} fullerene	Biphosphonate	-		-	[127]

Table 1: Bone targeted nanoparticles reported in the literature

Other types of lipid-based systems have been proposed, such as biphosphonate liposomes [128], subcutaneous implants formed of scaffolfds of collagen and HAP, containing biphosphonates liposomes [124, 129], or polyphosphoester ionomer-phospholipid vesicles [125], although there is no data concerning their biodistribution or bioefficacy.

6.3- Inorganic nanoparticles

The binding characteristics of nanoparticles to HAP has been studied with gold (Au) nanoparticles presenting three different bone targeting ligands on their surface: alendronate, phosphonate and glutamate [130]. Gold nanoparticles functionalized with glutamate were suggested as potential targeted-x-ray contrast agent for damaged tissue after effective results *ex vivo* [126]. Biphosphonate decorated fullerenes C_{60} have also been reported [127].

Conclusive remarks

Some of the researches commented above have reported interesting data concerning nanoparticle uptake and interactions with cancer cells metastasized to the bone tissue, specifically an enhanced cellular uptake of nanoparticles decorated with biphosphonate ligands [102, 119]. Enhanced biodistribution for these bone targeted nanoparticles might partly be due to this enhanced uptake. Therefore, it would be interesting to know the *in vivo* fate of nanoparticles in bone diseased state models. Further, as shown above, most attempts are directed to the targeting of the mineral surfaces.

However, the actual contribution of HAP binding by the means of targeting ligands should also be evaluated in terms of enhanced delivery and efficiency. As an alternative to irreversible HAP targeting, following bone tissue distribution, nanoparticles can also be designed so as to be transiently adherent to HAP surfaces and to become available for interaction with different cells types, including bone cancer cells and others including osteoclasts. It is noteworthy that bone cancer cells and these specialized phagocytic cells might be active in endocytosing nanoparticles. In summary, once bound to bone and depending on their affinity for HAP, nanoparticles could either remain bound to the bone mineralized surface, and in this case the release of the drug might take place in the bone extracellular microenvironment, by osteoclast-mediated resorption or not, or they could be desorbed and progressively detached, making them available for further uptake by cells. More insight into the bone healthy and diseased microenvironment would be necessary so as to predict and to control nanoparticles *in vivo* fate in the bone microenvironment.

7- Drug loading and controlled release , a major issue for bone targeted nanoparticles

As discussed above, it is necessary to impart simultaneously various functionalities to bone targeted nanomedicines and more specifically into nanoparticles. It is not the purpose of this chapter to discuss these functionalities and the best ways to implement them into bone targeted sytems. Rather, it has been decided to end this review by considering drug loading and the control of drug release from nanoparticles designed for bone targeting, as it is a major concern for their efficiency.

As an evidence, nanoparticles should carry a therapeutic drug in a sufficient dose to treat skeletal diseases. Because the potency of drugs is highly variable, ranging from the need of sufficiently high concentrations in the vicinity of their pharmacological receptor for many small molecules, to the need for only few copies in the case of siRNA for example, nanoparticles should be carefully engineered from this point of view. A broad overview of the literature shows that small drug molecules (typically under 1,000 Da in molecular weight) can be either physically entrapped in the core of nanoparticles or chemically linked to one of its components.

The classical method of encapsulating is based on physical interactions between the drug and the carrier. However, conventional physically entrapment of drugs into nanoparticles has two major drawbacks: the generally low (or very low) payloads and the usual lack of controlled release or at least difficulties to control release kinetics. Indeed, it should be considered that there are strong exigencies in this area, as release kinetics profiles should ideally ensure drug delivery once at the targeted site and possibly according to a time prolonged kinetics. Drug release before the target is attained will result in subsequent side effects, and a redhibitory loss of the payload before attaining the target. On the other hand, the chemical approach consisting in covalently linking the drug, either directly to nanoparticles or to the carrier which is further formulated into nanoparticles, with a cleavable bond in physiological conditions represent an attractive approach so as to maximize the pharmacological activity. In this approach, not only the drug release should be triggered by the local environment, but also time-controlled from this moment.

Smart nanoparticles responsive to physio-pathological conditions of the targeting microenvironment is another promising approach. Here we discuss the advantages and drawbacks of several approaches for controlling drug loading and release kinetics in bone targeted nanoparticles using triggers in specific physiological conditions present in the bone microenvironment.

7.1- Acid triggered release

There are several bone conditions where acid triggered drug release could be useful.

First, osteoclasts create an acidic microenvironment for bone resorption. Initially, osteoclasts attach to the bone surface through integrins and secrete protons and chloride ions through the ruffled border via direct pumping or by fusions of acidic vesicles extracellularly into the resorption lacunae that will dissolve the mineral content of the matrix, the HAP. The pH of the resorption lacunae has been estimated to be about 4.0-4.5 [131]. Although active surfaces are a minority, (found in less than 10% of the trabecular bone surfaces of the iliac crest in adult humans [39]) bone targeted nanoparticles are

likely to bind to the active bone sites, where HAP is more exposed and available. Osteoclast resorption takes only 2-4 weeks in humans to be completed [132] and thus osteoclast mediated drug release from nanoparticles could be foreseen. However, such a triggering of drug release by acidity could reveal slow in the case of nanoparticles once they have attained bone formation sites rather than resorption ones and toxic effects to osteoclast cannot be excluded.

In addition to the osteoclast mediated acidic pH in the resorption lacunae, if nanoparticles are endocytosed by cells in bone, they will encounter acidic pH in early endosomes where pH ranges from 6.8-6.0, while lysosomes are more acidic (pH 5.2-4.5) [104]. Moreover, if bones are affected by cancers, tumoral areas could present a mild acidic extracellular pH in the tumour microenvironment. Cancerous cells, as a result of the increased metabolic activity exports H^+ to the extracellular space via a Na^+/H^+ exchanger, creating a mild acidic space (pH 6.60-6.98 in various tumours) [133].

Two main approaches in nanoparticulate systems have been used to trigger drug release in response to acidic conditions, including (i) nanoparticles whose components undergo structural changes or destabilization resulting in drug release or (ii) the use of an acid cleavable linker between the drug and the polymer in the case of polymer-drug conjugates that can be further conjugated into nanoparticles or not.

7.1.1.- Acid induced structural changes or destabilization of micelles

Nanoparticulate systems formed by pH-sensitive polymers, based on their pK properties, such as carboxylic acid containing polymers or polyhistidine, have been proposed to trigger drug release in acidic environments. Ionic core-cross linked micelles with enhanced stability against dilution derived from poly(ethylene oxide)-b-polymethacrylate were achieved in the presence of divalent ions such as calcium and further crosslinking of carboxylates with 1,2-ethylenediamine. Cores of micelles presented swelling properties in response to pH. Then, cisplatin was incorporated to the carboxylic groups of polymethacrylate that could be released in a pH dependent manner, being faster at pH 5.5

than 7.4 [115]. Release from micelles derived from polyhistidine show a pH dependency due to the physical destabilization of micelles at mildly acidic pH caused by the protonation of the histidine groups, resulting in an enhanced release of their cargos [116].

7.1.2--Acid cleavable linker between the drug and the polymer

Micelles formed by self-assemblying of folate-PEG-poly(aspartic acid) polymer linked to the adriamicine through hydrazone acid cleavable linkers were shown to selectively release their cargo in the acidic intracellular compartments [134]. Ulbrich et al also designed pH sensitive micelles formed by poly(ethylene oxide)-b-poly (allyl glycidyl ether) (PEO-PAGE) which showed faster release of doxorubicin at pH 5 compared to the physiological pH 7.4, both showing incomplete release due to an equilibrium between physically entrapped and free doxorubicin [135]. Polymeric micelles formed by PLA-mPEG were chemically linked to doxorubicin by two acid cleavable linkers: hydrazone and cis-acotinyl, which present an enhanced release at acidic pH compared to the neutral ones, the hydrazone linked doxorubicin showing a slower release profile [136]. Prodrugs linked by cis-aconityl have shown an incomplete release probably due to the formation of a trans isomer that cannot be cleaved [137]. Other acid clevable linkers such as acetals were used. Hydrophobic groups were attached via acetal groups to the core forming dendrimer copolymer of the micelles, that were charged in doxorubicin. Upon pH decrease hydrophobic groups were cleaved, rendering copolymers more hydrophilic and destabilizing micelles and enhancing drug release [138].

7.2 Chloride triggered release

During osteoclast resorption, secretion of protons is accompanied by secretion of chloride anions via specific chloride channels. In the resorption lacunae, there is a high microconcentration of chloride due to the secretion of chloride anions via specific chloride channels. Polycarboxylates are known to form complexes with cisplatin derivates whose release depends mainly in the chloride [139] and to a lower extent on other nucleophile concentration. Kataoka's group in parallel to Kabanov's group,

designed cisplatin core cross-linked micelles where cisplatin acted as a crosslinking agent . This nanomedicines presented a very high loading of cisplatin (almost 40 % w/w) and its release was dependent mainly on the concentration of chloride anions [140, 141]. Cisplatin carriers involving a coordinate bond with carboxylate groups could take advantage of the high concentration of chloride ion present in the resorption lacunae that would enhance the release of cisplatin. The disadvantage of this approach is that chloride ions are abundant in the bloodstream. Depending on the release kinetics, drug release could take place in the bloodstream, and thus reducing the percentage of still encapsulated drug attaining the target tissue, while side effects could occur due to the biodistribution of the free drug to other organs rather than the bone.

7.3 Enzyme triggered release

During osteoclast resorption, secretion of proteolytic enzymes such as lysosomal cystein proteinases and matrix metalloproteinases (MMPs) into the resorption lacunae occurs. Among them, cathepsin K has been shown to play a major role in the degradation of the organic matrix, although other cystein proteases, such as cathepsin B and L might also be involved [111, 142]. Therefore, peptide sequences sensitive to these proteolytic enzymes have been proposed as cleavable linkers in bone targeted drug delivery systems.

7.3.1 - Cathepsin K sensitive spacers

Cathepsin K belongs to the cysteine protease family and is mainly expressed by osteoclasts although also in other organs to lesser extents, such as ovary, heart and skeletal muscle, lung, testis or small intestine and colon. It requires an acidic microenvironment for its activity and thus is active in lysosomes and acidic resorption lacunae. It is secreted into the resorption lacunae where it is responsible for the degradation of the organic matrix collagen and other non collagenic proteins including matrix embedded growth factors once they have been released from the matrix by proton secretion. It is known to cleave collagen at multiple sites within the triple helix of collagen type I and

II. Deficiency of its activity causes severe bone sclerosing disorder. Cathepsin K inhibitors suppress degradation of organic matrix while allowing demineralization. Unlike other antiresorptive agents, bone formation is not suppressed [143, 144].

Specific cleavage sites of cathepsin K are different from those of cathepsin L, in spite of sharing 40 % of homology, and have been revealed using a peptide containing six sequences Gly-Pro-Z-Gly. The study revealed three major cleavable sites where Z was Met, Arg and Ser and a minor one where Z is Gln [145]. An additional specific cleavage sequence Gly-Pro-Z-Gly where Z was Trp was found using hydrogels, which underwent specific osteoclast degradation [146]. Moreover, Gly-Gly-Pro-Nle sequence was used to design a HPMA-prostaglandin E_1conjugate, whose cleavage was majorly performed by cathepsin K [147].

7.2.2-Matrix metalloproteinases (MMPs) sensitive spacers

MMPs are a type of endopeptidases. They structurally possess a zinc (Zn) binding catalytic domain. They are ubiquitously expressed throughout the organism, although substrate specificity differs depending on the type of MMP. Collagenases are a subfamily of MMPs which have the ability to degrade fibrilar collagen in its triple helical structure. In type I collagen, the most abundant in bone, cleavage occurs between Gly_{775}/Ile_{776} and Gly_{775}/Leu_{776} of the α 1 (I) and α 2 (I) chain, respectively. Octapeptides sequences containing similar sequences to the cleavage sites in native type I collagen have been identified. [148]. However, the degradation of the organic matrix in bone is mainly carried out by the cathepsin K and the role of MMPs is limited. MMP 13 has been suggested to contribute to matrix solubilisation in specific areas of the skeleton and in some pathological and developmental conditions and to play a role in the removal of collagen leftovers at the end of the resorption cycle [149]. Some types of MMPs have been involved in the skeletal development and in the modulation of extracellular signals since MMPs can cleave cytokines, growth factors, cell surface molecules or

matrix molecules [150]. No MMPs specific sequences have been used to trigger drug release; MMPs are ubiquitously expressed and have a limited role in bone matrix degradation.

8. Conclusions

The development of bone targeted nanomedicines could be an interesting approach considering the bone disease state and the associated pathological characteristics. It is also a very complex issue, because of the complexity of the barriers to overcome before reaching bone mineralized tissue, including bone marrow, which is an hematopoietic organ with numerous cell types and also a RES organ. Although being an emerging field, bone targeted nanoparticles have already shown considerable therapeutic improvements in the treatment of cancers and delivery of nucleic acids. More insight into the mechanisms by which nanoparticles can overcome barriers, such as blood capillaries extravasation in physiological and specific disease state or microdistribution pattern in the bone marrow environment, would be really useful to optimise the nanomedicine approach. Further, more detailed studies are necessary to understand the actual contribution and efficacy of active targeting approaches using specific ligands in order to challenge this strategy and conclude about its pertinence. Finally, toxicological concerns equally have to be considered. The seek for specific cell targeting and not only HAP surfaces, should be considered and may constitute a valuable approach for efficient intra bone targeting.

References

[1] Bone health and osteoporosis: a report of the surgeon general, in, Office of the surgeon general (US), 2004.
[2] R.E. Coleman, Clinical features of metastatic bone disease and risk of skeletal morbidity, Clin. Cancer Res., 12 (2006) 6243s-6249s.
[3] Y. Zhang, H.F. Chan, K.W. Leong, Advanced materials and processing for drug delivery: The past and the future, Adv. Drug Delivery Rev., 65 (2013) 104-120.
[4] C. Vauthier, K. Bouchemal, Methods for the Preparation and Manufacture of Polymeric Nanoparticles, Pharmaceutical Research, 26 (2009) 1025-1058.
[5] H. Hirabayashi, J. Fujisaki, Bone-specific drug delivery systems: approaches via chemical modification of bone-seeking agents, Clin. Pharmacokinet., 42 (2003) 1319-1330.
[6] J. Ishizaki, Y. Waki, T. Takahashi-Nishioka, K. Yokogawa, K.-i. Miyamoto, Selective drug delivery to bone using acidic oligopeptides, J. Bone Miner. Metab., 27 (2009) 1-8.

[7] D. Wang, S.C. Miller, P. Kopecková, J. Kopecek, Bone-targeting macromolecular therapeutics, Adv. Drug Delivery Rev., 57 (2005) 1049-1076.
[8] S. Zhang, G. Gangal, H. Uludag, 'Magic bullets' for bone diseases: progress in rational design of bone-seeking medicinal agents, Chem. Soc. Rev., 36 (2007) 507-531.
[9] S.A. Gittens, G. Bansal, R.F. Zernicke, H. Uludag, Designing proteins for bone targeting, Adv. Drug Delivery Rev., 57 (2005) 1011-1036.
[10] S.A. Low, J. Kopeček, Targeting polymer therapeutics to bone, Adv. Drug Delivery Rev., 64 (2012) 1189-1204.
[11] S.C. Marks Jr, P.R. Odgren, P.B. John, L.G.R. Lawrence G. Raisz and Gideon A. Rodan A2 - John P. Bilezikian, A.R. Gideon, Chapter 1 - Structure and development of the skeleton, in: Principles of bone biology (second edition), Academic press, San Diego, 2002, pp. 3-15.
[12] J.E. Compston, Bone marrow and bone: a functional unit, J Endocrinol, 173 (2002) 387-394.
[13] G.S. Travlos, Normal structure, function, and histology of the bone marrow, Toxicol Pathol, 34 (2006) 548-565.
[14] T. Yin, L. Li, The stem cell niches in bone, The Journal of Clinical Investigation, 116 (2006) 1195-1201.
[15] E. Beutler, W.J. Williams, Williams hematology 6. Ed, McGraw-Hill, Medical Publishing Division, 2001.
[16] M. Laroche, Intraosseous circulation from physiology to disease, Joint Bone Spine, 69 (2002) 262-269.
[17] G.E. Nelson, Jr., P.J. Kelly, L.F. Peterson, J.M. Janes, Blood supply of the human tibia, J Bone Joint Surg Am, 42-A (1960) 625-636.
[18] I. McCarthy, The physiology of bone blood flow: a review, J Bone Joint Surg Am, 88 Suppl 3 (2006) 4-9.
[19] M.-H. Lafage-Proust, R. Prisby, B. Roche, L. Vico, Bone vascularization and remodeling, Joint Bone Spine, 77 (2010) 521-524.
[20] S.C. Miller, W.S.S. Jee, The microvascular bed of fatty bone marrow in the adult beagle, Metabolic Bone Disease and Related Research, 2 (1980) 239-246.
[21] J.F. Griffith, D.K.W. Yeung, P.H. Tsang, K.C. Choi, T.C.Y. Kwok, A.T. Ahuja, K.S. Leung, P.C. Leung, Compromised Bone Marrow Perfusion in Osteoporosis, J. Bone Miner. Res., 23 (2008) 1068-1075.
[22] J.D. Byrne, T. Betancourt, L. Brannon-Peppas, Active targeting schemes for nanoparticle systems in cancer therapeutics, Adv. Drug Delivery Rev., 60 (2008) 1615-1626.
[23] Y. Zhao, R. Bachelier, I. Treilleux, P. Pujuguet, O. Peyruchaud, R. Baron, P. Clément-Lacroix, P. Clézardin, Tumor αvβ3 Integrin Is a Therapeutic Target for Breast Cancer Bone Metastases, Cancer Res., 67 (2007) 5821-5830.
[24] X.-Q. Zhang, X. Xu, N. Bertrand, E. Pridgen, A. Swami, O.C. Farokhzad, Interactions of nanomaterials and biological systems: Implications to personalized nanomedicine, Adv. Drug Delivery Rev., 64 (2012) 1363-1384.
[25] A. El Rhilassi, M. Mourabet, M. Bennani-Ziatni, R. El Hamri, A. Taitai, Interaction of some essential amino acids with synthesized poorly crystalline hydroxyapatite, Journal of Saudi Chemical Society, (2013).
[26] T. Yamamoto, H. Tamaki, C. Katsuda, K. Nakatani, S. Terauchi, H. Terada, Y. Shinohara, Molecular basis of interactions between mitochondrial proteins and hydroxyapatite in the presence of Triton X-100, as revealed by proteomic and recombinant techniques, J. Chromatogr. A, 1301 (2013) 169-178.
[27] T. Leventouri, Synthetic and biological hydroxyapatites: Crystal structure questions, Biomaterials, 27 (2006) 3339-3342.
[28] D.D. Perrin, Binding of Tetracyclines to Bone, Nature, 208 (1965) 787-788.

[29] J.R. Neale, N.B. Richter, K.E. Merten, K.G. Taylor, S. Singh, L.C. Waite, N.K. Emery, N.B. Smith, J. Cai, W.M. Pierce, Jr., Bone selective effect of an estradiol conjugate with a novel tetracycline-derived bone-targeting agent, Bioorg. Med. Chem. Lett., 19 (2009) 680-683.
[30] H.M. Myers, H.J. Tochon-Danguy, C.A. Baud, IR absorption spectrophotometric analysis of the complex formed by tetracycline and synthetic hydroxyapatite, Calcif. Tissue Int., 35 (1983) 745-749.
[31] T.M. Willson, P.S. Charifson, A.D. Baxter, N.G. Geddie, Bone targeted drugs 1. Identification of heterocycles with hydroxyapatite affinity, Bioorg. Med. Chem. Lett., 6 (1996) 1043-1046.
[32] W.J. Thompson, D.D. Thompson, P.S. Anderson, G.A. Rodan, Polymalonic acids as bone affinity agents, in: I. Merck & Co. (Ed.), 1989.
[33] S.G. Dahl, P. Allain, P.J. Marie, Y. Mauras, G. Boivin, P. Ammann, Y. Tsouderos, P.D. Delmas, C. Christiansen, Incorporation and distribution of strontium in bone, Bone, 28 (2001) 446-453.
[34] N.D. Priest, G. European Late Effects Project, C. Commission of the European, Metals in bone: proceedings of a EULEP symposium on the deposition, retention, and effects of radioactive and stable metals in bone and bone marrow tissues, October 11th-13th, 1984, Angers, France, MTP Press, 1985.
[35] T. Das, S. Chakraborty, H.D. Sarma, M. Venkatesh, S. Banerjee, 166Ho-labeled hydroxyapatite particles: a possible agent for liver cancer therapy, Cancer Biother. Radiopharm., 24 (2009) 7-14.
[36] G.H. Nancollas, R. Tang, R.J. Phipps, Z. Henneman, S. Gulde, W. Wu, A. Mangood, R.G.G. Russell, F.H. Ebetino, Novel insights into actions of bisphosphonates on bone: Differences in interactions with hydroxyapatite, Bone, 38 (2006) 617-627.
[37] J.H. Lin, Bisphosphonates: A review of their pharmacokinetic properties, Bone, 18 (1996) 75-85.
[38] M. Sato, W. Grasser, N. Endo, R. Akins, H. Simmons, D.D. Thompson, E. Golub, G.A. Rodan, Bisphosphonate action. Alendronate localization in rat bone and effects on osteoclast ultrastructure, J. Clin. Invest., 88 (1991) 2095-2105.
[39] S.C. Miller, B.M. Bowman, J.M. Smith, W.S.S. Jee, Characterization of endosteal bone-lining cells from fatty marrow bone sites in adult beagles, The Anatomical Record, 198 (1980) 163-173.
[40] J.H. Lin, I.W. Chen, D.E. Duggan, Effects of dose, sex, and age on the disposition of alendronate, a potent antiosteolytic bisphosphonate, in rats, Drug Metab Dispos, 20 (1992) 473-478.
[41] P. Masarachia, M. Weinreb, R. Balena, G.A. Rodan, Comparison of the distribution of 3H-alendronate and 3H-etidronate in rat and mouse bones, Bone, 19 (1996) 281-290.
[42] R. Russell, N. Watts, F. Ebetino, M. Rogers, Mechanisms of action of bisphosphonates: similarities and differences and their potential influence on clinical efficacy, Osteoporosis International, 19 (2008) 733-759.
[43] F. Coxon, A. Roelofs, A. Boyde, M. Lundy, C. McKenna, K. Blazewska, S. Sun, B. Kashemirov, X. Duan, G. Russell, A. Khalid, M. Rogers, F. Ebetino, The ability of bisphosphonates and their analogues to penetrate the osteocyte network is dependent on affinity for bone, Bone, 46 (2010) S22.
[44] S.A. Khan, J.A. Kanis, S. Vasikaran, W.F. Kline, B.K. Matuszewski, E.V. McCloskey, M.N.C. Beneton, B.J. Gertz, D.G. Sciberras, S.D. Holland, J. Orgee, G.M. Coombes, S.R. Rogers, A.G. Porras, Elimination and biochemical responses to intravenous alendronate in postmenopausal osteoporosis, J. Bone Miner. Res., 12 (1997) 1700-1707.
[45] S.E. Papapoulos, S.C.L.M. Cremers, Prolonged bisphosphonate release after treatment in children, New England Journal of Medicine, 356 (2007) 1075-1076.
[46] R. Fujisawa, Y. Kuboki, Preferential adsorption of dentin and bone acidic proteins on the (100) face of hydroxyapatite crystals, Biochim. Biophys. Acta, 1075 (1991) 56-60.
[47] R. Fujisawa, Y. Wada, Y. Nodasaka, Y. Kuboki, Acidic amino acid-rich sequences as binding sites of osteonectin to hydroxyapatite crystals, Biochim. Biophys. Acta, 1292 (1996) 53-60.

[48] T. Sekido, N. Sakura, Y. Higashi, K. Miya, Y. Nitta, M. Nomura, H. Sawanishi, K. Morito, Y. Masamune, S. Kasugai, K. Yokogawa, K.-I. Miyamoto, Novel drug delivery system to bone using acidic oligopeptide: pharmacokinetic characteristics and pharmacological potential, J. Drug Targeting, 9 (2001) 111-121.
[49] S. Kasugai, R. Fujisawa, Y. Waki, K. Miyamoto, K. Ohya, Selective drug delivery system to bone: small peptide (Asp)6 conjugation, J Bone Miner Res, 15 (2000) 936-943.
[50] S. Cazalbou, C.l. Combes, D. Eichert, C. Rey, M.J. Glimcher, Poorly crystalline apatites: evolution and maturation in vitro and in vivo, J. Bone Miner. Metab., 22 (2004) 310-317.
[51] D. Farlay, G.r. Panczer, C. Rey, P. Delmas, G. Boivin, Mineral maturity and crystallinity index are distinct characteristics of bone mineral, J. Bone Miner. Metab., 28 (2010) 433-445.
[52] D. Wang, S.C. Miller, L.S. Shlyakhtenko, A.M. Portillo, X.M. Liu, K. Papangkorn, P. Kopeckova, Y. Lyubchenko, W.I. Higuchi, J. Kopecek, Osteotropic peptide that differentiates functional domains of the skeleton, Bioconjug. Chem., 18 (2007) 1375-1378.
[53] D.K. Yarbrough, E. Hagerman, R. Eckert, J. He, H. Choi, N. Cao, K. Le, J. Hedger, F. Qi, M. Anderson, B. Rutherford, B. Wu, S. Tetradis, W. Shi, Specific binding and mineralization of calcified surfaces by small peptides, Calcif. Tissue Int., 86 (2010) 58-66.
[54] D.K. Yarbrough, R. Eckert, J. He, E. Hagerman, F. Qi, R. Lux, B. Wu, M.H. Anderson, W. Shi, Rapid probing of biological surfaces with a sparse-matrix peptide library, PLoS ONE, 6 (2011) e23551.
[55] G. Zhang, B. Guo, H. Wu, T. Tang, B.T. Zhang, L. Zheng, Y. He, Z. Yang, X. Pan, H. Chow, K. To, Y. Li, D. Li, X. Wang, Y. Wang, K. Lee, Z. Hou, N. Dong, G. Li, K. Leung, L. Hung, F. He, L. Zhang, L. Qin, A delivery system targeting bone formation surfaces to facilitate RNAi-based anabolic therapy, Nat Med, 18 (2012) 307-314.
[56] S.M. Moghimi, A.J. Andersen, D. Ahmadvand, P.P. Wibroe, T.L. Andresen, A.C. Hunter, Material properties in complement activation, Adv. Drug Delivery Rev., 63 (2011) 1000-1007.
[57] N. Dos Santos, C. Allen, A.-M. Doppen, M. Anantha, K.A.K. Cox, R.C. Gallagher, G. Karlsson, K. Edwards, G. Kenner, L. Samuels, M.S. Webb, M.B. Bally, Influence of poly(ethylene glycol) grafting density and polymer length on liposomes: Relating plasma circulation lifetimes to protein binding, Biochimica et Biophysica Acta (BBA) - Biomembranes, 1768 (2007) 1367-1377.
[58] S.M. Moghimi, J. Szebeni, Stealth liposomes and long circulating nanoparticles: critical issues in pharmacokinetics, opsonization and protein-binding properties, Prog Lipid Res, 42 (2003) 463-478.
[59] A. Vonarbourg, C. Passirani, P. Saulnier, J.-P. Benoit, Parameters influencing the stealthiness of colloidal drug delivery systems, Biomaterials, 27 (2006) 4356-4373.
[60] C. Fang, B. Shi, Y.-Y. Pei, M.-H. Hong, J. Wu, H.-Z. Chen, In vivo tumor targeting of tumor necrosis factor-α-loaded stealth nanoparticles: Effect of MePEG molecular weight and particle size, European Journal of Pharmaceutical Sciences, 27 (2006) 27-36.
[61] C. He, Y. Hu, L. Yin, C. Tang, C. Yin, Effects of particle size and surface charge on cellular uptake and biodistribution of polymeric nanoparticles, Biomaterials, 31 (2010) 3657-3666.
[62] J.A. Champion, S. Mitragotri, Role of target geometry in phagocytosis, Proceedings of the National Academy of Sciences of the United States of America, 103 (2006) 4930-4934.
[63] S.-Y. Lin, W.-H. Hsu, J.-M. Lo, H.-C. Tsai, G.-H. Hsiue, Novel geometry type of nanocarriers mitigated the phagocytosis for drug delivery, J. Control. Release, 154 (2011) 84-92.
[64] Y. Geng, P. Dalhaimer, S. Cai, R. Tsai, M. Tewari, T. Minko, D.E. Discher, Shape effects of filaments versus spherical particles in flow and drug delivery, Nat. Nanotechnol., 2 (2007) 249-255.
[65] I. Hamad, O. Al-Hanbali, A.C. Hunter, K.J. Rutt, T.L. Andresen, S.M. Moghimi, Distinct polymer architecture mediates switching of complement activation pathways at the nanosphere-serum Interface: implications for stealth nanoparticle engineering, ACS Nano, 4 (2010) 6629-6638.

[66] I. Bertholon, C. Vauthier, D. Labarre, Complement activation by core-shell poly(isobutylcyanoacrylate)-polysaccharide nanoparticles: influences of surface morphology, length, and type of polysaccharide, Pharm Res, 23 (2006) 1313-1323.
[67] G.v. Gaucher, K. Asahina, J. Wang, J.-C. Leroux, Effect of Poly(N-vinyl-pyrrolidone)-block-poly(d,l-lactide) as Coating Agent on the Opsonization, Phagocytosis, and Pharmacokinetics of Biodegradable Nanoparticles, Biomacromolecules, 10 (2009) 408-416.
[68] J.M. Metselaar, P. Bruin, L.W.T. de Boer, T. de Vringer, C. Snel, C. Oussoren, M.H.M. Wauben, D.J.A. Crommelin, G. Storm, W.E. Hennink, A Novel Family of l-Amino Acid-Based Biodegradable Polymerâˆ'Lipid Conjugates for the Development of Long-Circulating Liposomes with Effective Drug-Targeting Capacity, Bioconjugate Chem., 14 (2003) 1156-1164.
[69] Y. Sheng, C. Liu, Y. Yuan, X. Tao, F. Yang, X. Shan, H. Zhou, F. Xu, Long-circulating polymeric nanoparticles bearing a combinatorial coating of PEG and water-soluble chitosan, Biomaterials, 30 (2009) 2340-2348.
[70] R. Gref, Y. Minamitake, M.T. Peracchia, V. Trubetskoy, V. Torchilin, R. Langer, Biodegradable long-circulating polymeric nanospheres, Science (New York, N.Y.), 263 (1994) 1600-1603.
[71] R. Gref, M. Lück, P. Quellec, M. Marchand, E. Dellacherie, S. Harnisch, T. Blunk, R.H. Müller, "Stealth" corona-core nanoparticles surface modified by polyethylene glycol (PEG): influences of the corona (PEG chain length and surface density) and of the core composition on phagocytic uptake and plasma protein adsorption, Colloids Surf., B, 18 (2000) 301-313.
[72] A.S. Zahr, C.A. Davis, M.V. Pishko, Macrophage uptake of core-shell nanoparticles surface modified with poly(ethylene glycol), Langmuir, 22 (2006) 8178-8185.
[73] M.l. Vittaz, D. Bazile, G. Spenlehauer, T. Verrecchia, M. Veillard, F. Puisieux, D. Labarre, Effect of PEO surface density on long-circulating PLA-PEO nanoparticles which are very low complement activators, Biomaterials, 17 (1996) 1575-1581.
[74] J.K. Gbadamosi, A.C. Hunter, S.M. Moghimi, PEGylation of microspheres generates a heterogeneous population of particles with differential surface characteristics and biological performance, FEBS Letters, 532 (2002) 338-344.
[75] P. Laverman, A.H. Brouwers, E. Th. M. Dams, W.J.G. Oyen, G. Storm, N. van Rooijen, F.H.M. Corstens, O.C. Boerman, Preclinical and clinical evidence for disappearance of long-circulating characteristics of polyethylene glycol liposomes at low lipid dose, Journal of Pharmacology and Experimental Therapeutics, 293 (2000) 996-1001.
[76] T. Ishida, R. Maeda, M. Ichihara, Y. Mukai, Y. Motoki, Y. Manabe, K. Irimura, H. Kiwada, The accelerated clearance on repeated injection of pegylated liposomes in rats: laboratory and histopathological study, Cell. Mol. Biol. Lett., 7 (2002) 286.
[77] T. Ishihara, M. Takeda, H. Sakamoto, A. Kimoto, C. Kobayashi, N. Takasaki, K. Yuki, K.-i. Tanaka, M. Takenaga, R. Igarashi, T. Maeda, N. Yamakawa, Y. Okamoto, M. Otsuka, T. Ishida, H. Kiwada, Y. Mizushima, T. Mizushima, Accelerated blood clearance phenomenon upon repeated injection of PEG-modified PLA-nanoparticles, Pharmaceutical Research, 26 (2009) 2270-2279.
[78] E.T. Dams, P. Laverman, W.J. Oyen, G. Storm, G.L. Scherphof, J.W. van Der Meer, F.H. Corstens, O.C. Boerman, Accelerated blood clearance and altered biodistribution of repeated injections of sterically stabilized liposomes, J Pharmacol Exp Ther, 292 (2000) 1071-1079.
[79] T. Ishida, M. Harada, X.Y. Wang, M. Ichihara, K. Irimura, H. Kiwada, Accelerated blood clearance of PEGylated liposomes following preceding liposome injection: Effects of lipid dose and PEG surface-density and chain length of the first-dose liposomes, J. Control. Release, 105 (2005) 305-317.
[80] T. Ishida, K. Atobe, X. Wang, H. Kiwada, Accelerated blood clearance of PEGylated liposomes upon repeated injections: Effect of doxorubicin-encapsulation and high-dose first injection, J. Control. Release, 115 (2006) 251-258.

[81] X.Y. Wang, T. Ishida, M. Ichihara, H. Kiwada, Influence of the physicochemical properties of liposomes on the accelerated blood clearance phenomenon in rats, J. Control. Release, 104 (2005) 91-102.
[82] T. Ishihara, T. Maeda, H. Sakamoto, N. Takasaki, M. Shigyo, T. Ishida, H. Kiwada, Y. Mizushima, T. Mizushima, Evasion of the accelerated blood clearance phenomenon by coating of nanoparticles with various hydrophilic polymers, Biomacromolecules, 11 (2010) 2700-2706.
[83] S. Mishra, P. Webster, M.E. Davis, PEGylation significantly affects cellular uptake and intracellular trafficking of non-viral gene delivery particles, European Journal of Cell Biology, 83 (2004) 97-111.
[84] K. Remaut, B. Lucas, K. Braeckmans, J. Demeester, S.C. De Smedt, Pegylation of liposomes favours the endosomal degradation of the delivered phosphodiester oligonucleotides, J. Control. Release, 117 (2007) 256-266.
[85] M. Ogris, G. Walker, T. Blessing, R. Kircheis, M. Wolschek, E. Wagner, Tumor-targeted gene therapy: strategies for the preparation of ligand–polyethylene glycol–polyethylenimine/DNA complexes, J. Control. Release, 91 (2003) 173-181.
[86] J.X. Zhang, S. Zalipsky, N. Mullah, M. Pechar, T.M. Allen, Pharmaco attributes of dioleoylphosphatidylethanolamine/cholesterylhemisuccinate liposomes containing different types of cleavable lipopolymers, Pharmacol Res, 49 (2004) 185-198.
[87] H. Hatakeyama, H. Akita, K. Kogure, M. Oishi, Y. Nagasaki, Y. Kihira, M. Ueno, H. Kobayashi, H. Kikuchi, H. Harashima, Development of a novel systemic gene delivery system for cancer therapy with a tumor-specific cleavable PEG-lipid, Gene Ther, 14 (2007) 68-77.
[88] H. Hatakeyama, H. Akita, H. Harashima, A multifunctional envelope type nano device (MEND) for gene delivery to tumours based on the EPR effect: A strategy for overcoming the PEG dilemma, Adv. Drug Delivery Rev., 63 (2011) 152-160.
[89] H. Hatakeyama, E. Ito, H. Akita, M. Oishi, Y. Nagasaki, S. Futaki, H. Harashima, A pH-sensitive fusogenic peptide facilitates endosomal escape and greatly enhances the gene silencing of siRNA-containing nanoparticles in vitro and in vivo, J. Control. Release, 139 (2009) 127-132.
[90] A.A. Burns, J. Vider, H. Ow, E. Herz, O. Penate-Medina, M. Baumgart, S.M. Larson, U. Wiesner, M. Bradbury, Fluorescent silica nanoparticles with efficient urinary excretion for nanomedicine, Nano Letters, 9 (2008) 442-448.
[91] H.S. Choi, W. Liu, P. Misra, E. Tanaka, J.P. Zimmer, B. Itty Ipe, M.G. Bawendi, J.V. Frangioni, Renal clearance of quantum dots, Nat Biotechnol, 25 (2007) 1165-1170.
[92] K. Yoshida, H. Nagata, H. Hoshi, Uptake of carbon and polystyrene particles by the sinusoidal endothelium of rabbit bone marrow and liver and rat bone marrow, with special reference to multiparticle-pinocytosis, Arch. Histol. Jpn., 47 (1984) 303-317.
[93] C.R. Howlett, M. Dickson, A.K. Sheridan, The fine structure of the proximal growth plate of the avian tibia: vascular supply, J Anat, 139 (Pt 1) (1984) 115-132.
[94] S.M. Moghimi, Exploiting bone marrow microvascular structure for drug delivery and future therapies, Adv. Drug Delivery Rev., 17 (1995) 61-73.
[95] H.-G. Kopp, S.T. Avecilla, A.T. Hooper, S. Rafii, The bone marrow vascular niche: home of HSC differentiation and mobilization, Physiology, 20 (2005) 349-356.
[96] H. Sarin, Physiologic upper limits of pore size of different blood capillary types and another perspective on the dual pore theory of microvascular permeability, J Angiogenes Res, 2 (2010) 2-14.
[97] M. Laroche, P. Chiron, P. Bendayan, M. Degeilh, L. Moulinier, B. Vellas, D. Adoue, H. Boccalon, J. Puget, J.L. Albarede, et al., Fractures of the femoral neck and arterial disease of the lower limbs, Osteoporos Int, 4 (1994) 285.

[98] M. Laroche, I. Ludot, M. Thiechart, J. Arlet, M. Pieraggi, P. Chiron, L. Moulinier, A. Cantagrel, J. Puget, G. Utheza, B. MaziÃ¨res, Study of the intraosseous vessels of the femoral head in patients with fractures of the femoral neck or osteoarthritis of the hip, Osteoporosis International, 5 (1995) 213-217.
[99] J. Arlet, M. Laroche, R. Soler, M. Thiechart, M.T. Pieraggi, B. Mazières, Histopathology of the vessels of the femoral heads in specimens of osteonecrosis, osteoarthritis and algodystrophy, Clinical Rheumatology, 12 (1993) 162-165.
[100] H. Nyangoga, P. Mercier, H. Libouban, M.F. Baslé, D. Chappard, Three-Dimensional Characterization of the Vascular Bed in Bone Metastasis of the Rat by Microcomputed Tomography (MicroCT), PLoS ONE, 6 (2011) e17336.
[101] J. MacDougall, L. Matrisian, Contributions of tumor and stromal matrix metalloproteinases to tumor progression, invasion and metastasis, Cancer and Metastasis Reviews, 14 (1995) 351-362.
[102] K. Ramanlal Chaudhari, A. Kumar, V.K. Megraj Khandelwal, M. Ukawala, A.S. Manjappa, A.K. Mishra, J. Monkkonen, R.S. Ramachandra Murthy, Bone metastasis targeting: a novel approach to reach bone using zoledronate anchored PLGA nanoparticle as carrier system loaded with docetaxel, J Control Release, 158 (2012) 470-478.
[103] G. Sahay, D.Y. Alakhova, A.V. Kabanov, Endocytosis of nanomedicines, J. Control. Release, 145 (2010) 182-195.
[104] S. Xu, B.Z. Olenyuk, C.T. Okamoto, S.F. Hamm-Alvarez, Targeting receptor-mediated endocytotic pathways with nanoparticles: Rationale and advances, Adv. Drug Delivery Rev., 65 (2013) 121-138.
[105] H. Hillaireau, P. Couvreur, Nanocarriers' entry into the cell: relevance to drug delivery, Cell. Mol. Life Sci., 66 (2009) 2873-2896.
[106] J.E. Shea, S.C. Miller, Skeletal function and structure: Implications for tissue-targeted therapeutics, Adv. Drug Delivery Rev., 57 (2005) 945-957.
[107] M.L. Knothe Tate, “Whither flows the fluid in bone?” An osteocyte's perspective, Journal of Biomechanics, 36 (2003) 1409-1424.
[108] W. Wang, D.J. Ferguson, J.M. Quinn, A.H. Simpson, N.A. Athanasou, Biomaterial particle phagocytosis by bone-resorbing osteoclasts, J Bone Joint Surg Br, 79 (1997) 849-856.
[109] H. Palokangas, M. Mulari, H.K. Vaananen, Endocytic pathway from the basal plasma membrane to the ruffled border membrane in bone-resorbing osteoclasts, J Cell Sci, 110 (Pt 15) (1997) 1767-1780.
[110] A. Tautzenberger, L. Kreja, A. Zeller, S. Lorenz, H. Schrezenmeier, V. Mailänder, K. Landfester, A. Ignatius, Direct and indirect effects of functionalised fluorescence-labelled nanoparticles on human osteoclast formation and activity, Biomaterials, 32 (2011) 1706-1714.
[111] K. Väänänen, Mechanism of osteoclast mediated bone resorption--rationale for the design of new therapeutics, Adv. Drug Delivery Rev., 57 (2005) 959-971.
[112] M. Mammen, S.-K. Choi, G.M. Whitesides, Polyvalent interactions in biological systems: implications for design and use of multivalent ligands and inhibitors, Angew. Chem., Int. Ed., 37 (1998) 2754-2794.
[113] H. Pan, M. Sima, P. Kopeckova, K. Wu, S. Gao, J. Liu, D. Wang, S.C. Miller, J. Kopecek, Biodistribution and pharmacokinetic studies of bone-targeting N-(2-hydroxypropyl)methacrylamide copolymer-alendronate conjugates, Mol. Pharm., 5 (2008) 548-558.
[114] S.-W. Choi, J.-H. Kim, Design of surface-modified poly(d,l-lactide-co-glycolide) nanoparticles for targeted drug delivery to bone, J. Control. Release, 122 (2007) 24-30.

[115] H.S. Oberoi, F.C. Laquer, L.A. Marky, A.V. Kabanov, T.K. Bronich, Core cross-linked block ionomer micelles as pH-responsive carriers for cis-diamminedichloroplatinum(II), J. Control. Release, 153 (2011) 64-72.
[116] E.S. Lee, Z. Gao, D. Kim, K. Park, I.C. Kwon, Y.H. Bae, Super pH-sensitive multifunctional polymeric micelle for tumor pHe specific TAT exposure and multidrug resistance, J. Control. Release, 129 (2008) 228-236.
[117] S.I. Thamake, S.L. Raut, Z. Gryczynski, A.P. Ranjan, J.K. Vishwanatha, Alendronate coated poly-lactic-co-glycolic acid (PLGA) nanoparticles for active targeting of metastatic breast cancer, Biomaterials, 33 (2012) 7164-7173.
[118] I. Ozcan, K. Bouchemal, F. Segura-Sanchez, O. Ozer, T. Guneri, G. Ponchel, Synthesis and characterization of surface-modified PBLG nanoparticles for bone targeting: In vitro and in vivo evaluations, J. Pharm. Sci., 100 (2011) 4877-4887.
[119] K.R. Chaudhari, A. Kumar, V.K.M. Khandelwal, A.K. Mishra, J. Monkkonen, R.S.R. Murthy, Targeting efficiency and biodistribution of zoledronate conjugated docetaxel loaded pegylated PBCA nanoparticles for bone metastasis, Adv. Funct. Mater., 22 (2012) 4101-4114.
[120] V. Hengst, C. Oussoren, T. Kissel, G. Storm, Bone targeting potential of bisphosphonate-targeted liposomes: Preparation, characterization and hydroxyapatite binding in vitro, Int. J. Pharm., 331 (2007) 224-227.
[121] D. Wu, M. Wan, Methylene diphosphonate-conjugated adriamycin liposomes: preparation, characteristics, and targeted therapy for osteosarcomas in vitro and in vivo, Biomedical Microdevices, 14 (2012) 497-510.
[122] K. Sou, B. Goins, B.O. Oyajobi, B.L. Travi, W.T. Phillips, Bone marrow-targeted liposomal carriers, Expert Opin. Drug Deliv., 8 (2011) 317-328.
[123] M. Salerno, E. Cenni, C. Fotia, S. Avnet, D. Granchi, F. Castelli, D. Micieli, R. Pignatello, M. Capulli, N. Rucci, A. Angelucci, A. Del Fattore, A. Teti, N. Zini, A. Giunti, N. Baldini, Bone-targeted doxorubicin-loaded nanoparticles as a tool for the treatment of skeletal metastases, Curr. Cancer Drug Targets, 10 (2010) 649-659.
[124] G. Wang, M.E. Babadagli, H. Uludag, Bisphosphonate-derivatized liposomes to control drug release from collagen/hydroxyapatite scaffolds, Mol. Pharm., 8 (2011) 1025-1034.
[125] R. Ikeuchi, Y. Iwasaki, High mineral affinity of polyphosphoester ionomer–phospholipid vesicles, Journal of Biomedical Materials Research Part A, 101A (2012) 318-325.
[126] Z. Zhang, R.D. Ross, R.K. Roeder, Preparation of functionalized gold nanoparticles as a targeted X-ray contrast agent for damaged bone tissue, Nanoscale, 2 (2010) 582-586.
[127] K.A. Gonzalez, L.J. Wilson, W. Wu, G.H. Nancollas, Synthesis and in vitro characterization of a tissue-selective fullerene: vectoring C(60)(OH)(16)AMBP to mineralized bone, Bioorg. Med. Chem., 10 (2002) 1991-1997.
[128] T. Anada, Y. Takeda, Y. Honda, K. Sakurai, O. Suzuki, Synthesis of calcium phosphate-binding liposome for drug delivery, Bioorg. Med. Chem. Lett., 19 (2009) 4148-4150.
[129] G. Wang, N.Z. Mostafa, V. Incani, C. Kucharski, H. Uludağ, Bisphosphonate-decorated lipid nanoparticles designed as drug carriers for bone diseases, Journal of Biomedical Materials Research Part A, 100A (2012) 684-693.
[130] R.D. Ross, R.K. Roeder, Binding affinity of surface functionalized gold nanoparticles to hydroxyapatite, J. Biomed. Mater. Res. A, 99 (2011) 58-66.
[131] S. Georges, C. Ruiz Velasco, V. Trichet, Y. Fortun, D. Heymann, M. Padrines, Proteases and bone remodelling, Cytokine & Growth Factor Reviews, 20 (2009) 29-41.
[132] B. Clarke, Normal bone anatomy and physiology, Clinical Journal of the American Society of Nephrology, 3 (2008) S131-S139.

[133] P. Vaupel, Tumor microenvironmental physiology and its implications for radiation oncology, Seminars in Radiation Oncology, 14 (2004) 198-206.
[134] Y. Bae, N. Nishiyama, K. Kataoka, In Vivo Antitumor Activity of the Folate-Conjugated pH-Sensitive Polymeric Micelle Selectively Releasing Adriamycin in the Intracellular Acidic Compartments, Bioconjugate Chem., 18 (2007) 1131-1139.
[135] M. HrubÃ½, Ä.r. KoÅˆÃ¡k, K. Ulbrich, Polymeric micellar pH-sensitive drug delivery system for doxorubicin, J. Control. Release, 103 (2005) 137-148.
[136] H.S. Yoo, E.A. Lee, T.G. Park, Doxorubicin-conjugated biodegradable polymeric micelles having acid-cleavable linkages, J. Control. Release, 82 (2002) 17-27.
[137] E. Dinand, M. Zloh, S. Brocchini, Competitive reactions during amine addition to cis-aconityl anhydride, Australian Journal of Chemistry, 55 (2002) 467-474.
[138] E.R. Gillies, J.M.J. Fréchet, pH-Responsive copolymer assemblies for controlled release of doxorubicin, Bioconjugate Chem., 16 (2005) 361-368.
[139] Z. Feng, Y. Lai, H. Ye, J. Huang, X.G. Xi, Z. Wu, Poly (γ, L-glutamic acid)-cisplatin bioconjugate exhibits potent antitumor activity with low toxicity: A comparative study with clinically used platinum derivatives, Cancer Science, 101 (2010) 2476-2482.
[140] N. Nishiyama, K. Kataoka, Preparation and characterization of size-controlled polymeric micelle containing cis-dichlorodiammineplatinum(II) in the core, J Control Release, 74 (2001) 83-94.
[141] N. Nishiyama, S. Okazaki, H. Cabral, M. Miyamoto, Y. Kato, Y. Sugiyama, K. Nishio, Y. Matsumura, K. Kataoka, Novel cisplatin-incorporated polymeric micelles can eradicate solid tumors in mice, Cancer Res., 63 (2003) 8977-8983.
[142] H.K. Väänänen, H. Zhao, M. Mulari, J.M. Halleen, The cell biology of osteoclast function, Journal of Cell Science, 113 (2000) 377-381.
[143] Y. Yasuda, J. Kaleta, D. Brömme, The role of cathepsins in osteoporosis and arthritis: Rationale for the design of new therapeutics, Adv. Drug Delivery Rev., 57 (2005) 973-993.
[144] K. Fuller, K.M. Lawrence, J.L. Ross, U.B. Grabowska, M. Shiroo, B. Samuelsson, T.J. Chambers, Cathepsin K inhibitors prevent matrix-derived growth factor degradation by human osteoclasts, Bone, 42 (2008) 200-211.
[145] A.Y. Nosaka, K. Kanaori, N. Teno, H. Togame, T. Inaoka, M. Takai, T. Kokubo, Conformational Studies on the Specific Cleavage Site of Type I Collagen (α-1) Fragment (157–192) by Cathepsins K and L by Proton NMR Spectroscopy, Bioorg. Med. Chem., 7 (1999) 375-379.
[146] C.W. Hsu, R.M. Olabisi, E.A. Olmsted-Davis, A.R. Davis, J.L. West, Cathepsin K-sensitive poly(ethylene glycol) hydrogels for degradation in response to bone resorption, J. Biomed. Mater. Res. A, 98 (2011) 53-62.
[147] H. Pan, J. Liu, Y. Dong, M. Sima, P. Kopečková, M.L. Brandi, J. Kopeček, Release of prostaglandin E1 from N-(2-hydroxypropyl)methacrylamide copolymer conjugates by bone cells, Macromolecular Bioscience, 8 (2008) 599-605.
[148] S.M. Krane, M. Inada, Matrix metalloproteinases and bone, Bone, 43 (2008) 7-18.
[149] T.L. Andersen, M. del Carmen Ovejero, T. Kirkegaard, T. Lenhard, N.T. Foged, J.M. Delaisse, A scrutiny of matrix metalloproteinases in osteoclasts: evidence for heterogeneity and for the presence of MMPs synthesized by other cells, Bone, 35 (2004) 1107-1119.
[150] J.M. Delaisse, T.L. Andersen, M.T. Engsig, K. Henriksen, T. Troen, L. Blavier, Matrix metalloproteinases (MMP) and cathepsin K contribute differently to osteoclastic activities, Microsc Res Tech, 61 (2003) 504-513.

TRAVAUX EXPERIMENTAUX

CHAPITRE II

POLY (γ-BENZYL-L-GLUTAMATE)-PEG-ALENDRONATE MULTIVALENT NANOPARTICLES FOR BONE TARGETING

POLY (γ-BENZYL-L-GLUTAMATE) -PEG-ALENDRONATE MULTIVALENT NANOPARTICLES FOR BONE TARGETING

Laura de Miguel [1], *Magali Noiray*[1], *Georgiana Surpateanu*[2], *Bogdan Iorga* [2] *and Gilles Ponchel*[1] *

[1] Univ. Paris Sud, UMR CNRS 8612, Institut Galien, 92296 Châtenay-Malabry Cedex, France.

[2] UPR 2301, Institut de Chimie des Substances Naturelles, CNRS UPR 2301, Centre de Recherche de Gif-sur-Yvette, 1 Avenue de la Terrasse, 91198 Gif-sur-Yvette, France

*Corresponding author: Gilles Ponchel, Univ. Paris Sud, UMR CNRS 8612, Institut Galien, 92296 Châtenay-Malabry Cedex, France. E-mail: gilles.ponchel@u-psud.fr

Résumé

Le ciblage des nanoparticules aux tissus osseux est une étape importante dans la thérapeutique de maladies squelettiques. L'hydroxyapatite est un composant très spécifique de l'os et donc constitue la cible principale pour conférer des propriétés d' osteotropicité. Des nanoparticules de $PBLG_{10}$-PEG-alendronate (~75 nm) sont préparées par une méthode simple de nanoprécipitation. L'affinité pour les ions calcium (K_{Ca}^{+2}=1.8x10^4 M^{-1}) est évaluée au moyen de la technique de titration calorimétrique isotherme. Leur interaction avec les surfaces de hydroxyapatite (K_{HAP}) est étudiée par fluorescence et estimée à 1.1x10^{10} M^{-1}, ce qui est 4000 fois plus fort que l'interaction monovalente entre l'alendronate et les surfaces de hydroxyapatite préalablement décrit dans la littérature. Les études de modélisation moléculaire suggèrent que le nombre de sites d'union disponibles sur la surface d'hydroxyapatite est en large excès par rapport à ceux qui sont nécessaires pour le recouvrement total de la surface par les nanoparticules décorées avec l'alendronate. L'affinité plus faible envers les ions calcium comparativement à celle envers les surfaces d'hydroxyapatite permettrait aux nanoparticules liées aux ions calcium d'interagir avec l'hydroxyapatite. Cela apporte une compréhension plus profonde des nanoparticules ciblées aux tissus osseux et pourrait potentiellement améliorer leurs propriétés de ciblage.

Abstract

Hydroxyapatite (HAP), a highly specific component of bone tissue, is the main target in order to impart osteotropicity. Bone targeted nanoparticles can increase the strength of the interaction with HAP through multivalency and thus constitute a valuable strategy in the therapeutics of skeletal diseases. $PBLG_{10k}$-*b*-PEG_{6k}-alendronate nanoparticles (~75 nm) were prepared by a simple nanoprecipitation method. The calcium affinity (K_{Ca}^{+2}=1.8x10^4 M^{-1}) of these nanoparticles was evaluated using isothermal titration calorimetry. The multivalent interaction with HAP surfaces (K_{HAP}) was studied by fluorescence and was estimated to be 1.1x10^{10} M^{-1}, which is more than 4000 times stronger than the reported monovalent interaction between alendronate and HAP surfaces. Molecular modeling suggests that the number of binding sites available at the HAP surface is in large excess than what is required for the whole surface coverage by alendronate decorated nanoparticles. The lower calcium affinity of these nanoparticles than for HAP allows calcium bound nanoparticles to interact with HAP, which yields a deeper understanding of bone targeted carriers and could potentially improve their bone targeting properties.

Table of contents graphic

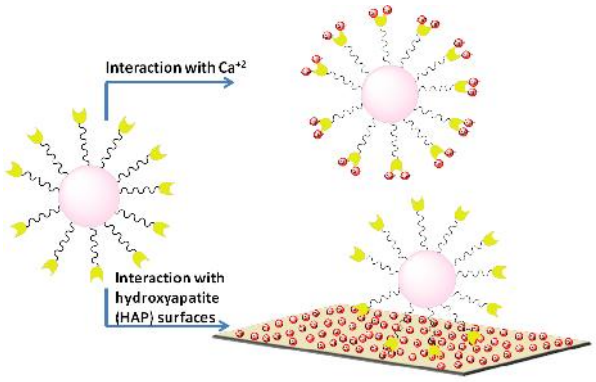

Targeting nanoparticles to bone tissue is an important issue in the therapeutics of skeletal diseases. Hydroxyapatite, a highly specific component of bone tissue is the main target used so as to impart osteotropicity. The aim of this study was to prepare bone targeted nanoparticles derived from poly (γ-

benzyl-glutamate), $PBLG_{10}$-PEG-alendronate, and to evaluate their binding affinity to calcium ions and hydroxyapatite surfaces.

Keywords: bone targeting, nanoparticles, isothermal titration calorimetry, adsorption

1- Introduction

Multivalent interactions, simultaneous binding of multiple ligands into one biological entity are involved in many different biological processes. Once the recognition has been established, the binding strength will depend on the possible number of individual interactions and will be enhanced compared to a single monovalent interaction (Mammen et al., 1998). As a result, site specific drug delivery is expected to increase therapeutic concentrations locally, simultaneously minimizing dose and side effects. For this purpose, nanoparticles can display multivalency through the conjugation of a discrete number of targeting ligands to their surface in order to enhance their target affinity (Carlson et al., 2007; Kiessling et al., 2000).

The design of bone targeted systems is of great importance in the therapeutics of skeletal diseases. HAP, ($Ca_{10}(PO_4)_6(OH)_2$), is specific to bone -except for teeth and pathological calcifications and thus constitutes an ideal target for the design of osteotropic systems. Biphosphonates as well as other molecules such as acidic oligopeptides or tetracyclines have shown to bind effectively to HAP (Wang et al., 2005). Biphosphonate structure presents two phosphonate groups sharing a common carbon atom (P-C-P), which are responsible for the high affinity for HAP; the most important interactions involving the calcium ions of HAP. For a systemically administered system to attain the bone mineralized tissue, it has to cross the blood-bone barrier (Shea and Miller, 2005) including the fenestrated capillaries with pore sizes up to 80 nm (Howlett et al., 1984; Shea and Miller, 2005). Biphosphonates have been largely used to confer osteotropic properties to drugs by conjugation to small molecules (Hirabayashi et al., 2001), to linear macromolecular carriers (Wang et al., 2005), to proteins (Gittens et al., 2005) or to nanoparticles (Park et al., 2003; Ross and Roeder, 2011).

However, only little research on the binding affinities of these systems with bone tissue or HAP has been conducted so far.

In this work we present nanoparticles prepared from poly (γ-benzyl-L-glutamate) (PBLG), a synthetic polypeptide that can adopt rigid α-helix structures and shows biocompatibility and good biodegradability due to the degradable amide bond in its polymeric structure (Oh et al., 1995). Homopolymers and amphiphilic copolymers of PBLG can assemble into small nanoparticles (less than 80 nm in diameter) by a simple nanoprecipitation method as it has been shown in our group (Barbosa et al., 2007).

The aim of this study was to prepare bone targeted nanoparticles under 80 nm derived from PBLG, $PBLG_{10k}$-*b*-PEG_{6k}-alendronate nanoparticles, and to evaluate their binding affinity with HAP crystals and with calcium ions, which are mostly responsible for the interaction with HAP, deepening into the interaction of alendronate with HAP.

2- Materials and Methods

2.1- Materials

DMF extradry Acroseal (99.8 %) and benzylamine Acroseal (+99.5 %) and BLG-NCA were purchased from Acros, and IsoChem respectively and were used as received. TFA (99%) was purchased from Sigma Aldrich. All other regeants were of analytical grade and used directly. MeO-PEG_{5k}-NH_2 ($M_{W\ PEG}$= 5000 g/mol) and α,ω-Bis-NHS-PEG_{6k} ($M_{W\ PEG}$= 6000 g/mol) were purchased from Iris Biotech GmbH. Alendronate was purchased from Chemos GmbH. DCTB and CF_3COOK were purchased from Sigma Aldrich.

Methods

2.2.- Synthesis of PBLG-polymers

Different derivatives of PBLG were synthesized by ring opening polymerization of BLG-NCA: $PBLG_{25k}$-bnz , $PBLG_{10k}$-bnz, $PBLG_{40k}$-*b*-PEG_{5k}, $PBLG_{40k}$-*b*-PEG_{6k}-alendronate, $PBLG_{10k}$-*b*-PEG_{6k} -alendronate and $PBLG_{40k}$-FITC. Briefly, n milimoles of BLG-NCA were weighed in a glove box

under inert atmosphere (argon) and were dissolved in DMF at a concentration of 0.5 M. The solution was stirred for 10 minutes and the initiator, a solution in DMF of benzylamine or previously dried MeO-PEG_{5k}-NH_2 in the case of $PBLG_{40k}$-*b*-PEG_{5k}, was added with an argon-purged syringe. The solution was stirred at 30 °C and bubbled with argon several times during 5 - 7 days. Polymers were obtained by precipitation in cold DEE and dried under vacuum. The evolution of the reaction was controlled by infrared spectroscopy, by following the disappearance of BLG-NCA peaks and the appearance of those of PBLG. A second purification step, consisting of dissolving the precipitate in THF, reprecipitating in cold DEE and drying under vacuum, was performed. For copolymers containing the hydrophilic PEG block or the FITC fluorophore, the purification step also included washing the precipitates three times with MeOH in order to eliminate the excess of unreacted PEG or FITC.

The synthesis of PBLG-*b*-PEG_{6k}-alendronate copolymer was achieved based on a slightly modified carbodiimide chemistry approach (Ozcan et al., 2011) and it is detailed in SI. α,ω-Bis-NHS-PEG_{6k} was dissolved in DMSO and reacted with a solution of alendronate in water with 3.5 equivalents of TEA at a ratio of 1/1.5 overnight at 40 °C (reaction medium DMSO/water 60/40). The reaction was precipitated in a mixture of EtOH/DEE, dialyzed with a membrane of a molecular cut-off of 3500 Da during 72 hours to eliminate unreacted alendronate and lyophilized. A further activation of the COOH groups was conducted in anhydrous DMF, in presence of DCC (5 equivalents) and NHS (5 equivalents), overnight under argon atmosphere at 25°C. After filtration with 0.45 µm filters, it was precipitated in DEE and dried under vacuum. Next, reaction between NHS-PEG-alendronate and the amine groups of the PBLG block, synthesized using the benzylamine as initiator molecule as described above, at a [NHS-PEG-alendronate] /[PBLG] molar ratio of 1.5 was performed in anhydrous DMF at 40 °C for 24 hours. The product was purified by precipitating in DEE and washed three times with MeOH to eliminate the any unreacted PEG. (**Figure 1)**

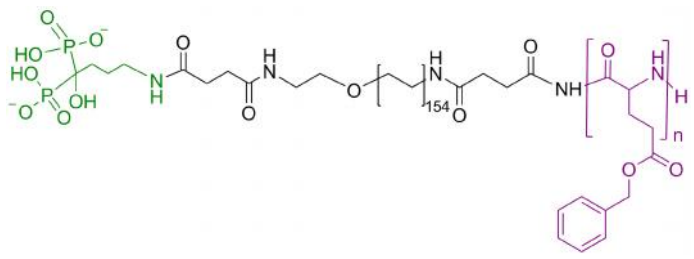

Figure 1: Structure of the PBLG-*b*-PEG_{6k}-alendronate copolymer

For the PBLG-FITC polymers, close to the end of the reaction, a solution containing three times more moles of FITC than of the initiator (benzylamine) was added and after 24 h, PBLG-FITC polymer was obtained by precipitation as described above (Segura-Sanchez et al., 2010) (see SI).

2.3- Characterization of PBLG polymers

2.3.1- Fourier transform infrared spectroscopy (FTIR)

Infrared measurements were performed on a Fourier Transform Perkin-Elmer 1750 infrared spectrometer using the ATR system to confirm the absence of NCA auto-polymerization, to follow the evolution of the polymerization reactions and to determine the secondary structure of the polymers.

2.3.2- Nuclear Magnetic Resonance (NMR)

^{1}H NMR spectra were recorded on a Bruker AC 300 spectrometer. ^{1}H NMR spectra of the polymers were recorded in $CDCl_3$ + 15 % TFA. For the $PBLG_{40k}$-*b*-PEG_{5k} block copolymer, where polymerization initiator was the mPEG-NH_2, the molar mass of the polymer could be determined by integration of the benzyl protons belonging to the PBLG block and the ethylene protons of the PEG block and taking into account the mass of the initiator. For the PBLG-*b*-PEG_{6k}-alendronate copolymers, the efficacy of the reaction between the two blocks could be determined. Phosphorus nuclear magnetic resonance (^{31}P NMR) spectra were recorded on a Bruker AC 300 spectrometer for the PEG-alendronate to quantify the alendronate using KH_2PO_4 as an internal standard.

2.3.3- Matrix-assisted laser desorption/ionization time-of-flight (MALDI-TOF) mass spectrometry

A Voyager DE-STR MALDI-TOF mass spectrometer (AB Sciex, Les Ulis, France), equipped with a 337-nm pulsed nitrogen laser (20 Hz) and an Acqiris® 2 GHz digitizer board, was used for all experiments. Mass spectra were obtained in linear positive ion mode with the following settings: accelerating voltage 20 kV, grid voltage 75 % of accelerating voltage, extraction delay time of 150 ns. The laser intensity was set just above the ion generation threshold to obtain peaks with the highest possible signal-to-noise (S/N) ratio without significant peak broadening. All data were processed using the Data Explorer software package (AB Sciex). DCTB was used as the matrix for MALDI-TOF experiments and CF_3COOK was used as the cationizing agent.

2.4- Nanoparticle preparation and characterization

Nanoparticles were prepared following a modified nanoprecipitation method previously described (Barbosa et al., 2007). Briefly, 5 mL THF solutions of the pure or mixtures of PBLG derivatives were added dropwise to 10 mL water and stirred for 10 minutes. Solvents were evaporated by a standardized protocol under vacuum in the rotavapor at 40 °C. Nanoparticles size and zeta potential were determined by DLS using a Zetasizer 4, Malvern Instruments. Experiments and measurements were always made in triplicate. Nanoparticles were observed by means of TEM at 120 KV with negative staining.

For the alendronate decorated fluorescently labelled nanoparticles, the number of PBLG α-helices forming a nanoparticle was calculated as the ratio between the nanoparticle volume and PBLG α-helix volume. Nanoparticles were considered to be spheres and PBLG α-helices were considered to be rods, whose lengths were calculated by taking into account the projected segment length of a single aminoacid unit (= 0.15 nm), the number of residues, and the diameter of 1.6 nm (Klok et al., 2000).

$$N\alpha\text{helix/np} = \frac{4\,r\text{np}^3}{3(\,0.75\,h\alpha\text{helixA}\,r\alpha\text{helixA}^2 + 0.25\,h\alpha\text{helixB}\,r\alpha\text{helixB}^2)} \quad (1)$$

where $r$np is the radius of nanoparticles obtained from TEM measurements from 100 nanoparticles, rαhelixA and αhelixA are the radius and the length of the PBLG-*b*-PEG-alendronate helices respectively, and rαhelixB, αhelixB are those for the PBLG-FITC helices.

2.5- Multivalent binding affinity for HAP surfaces

2.5.1- *In vitro* HAP binding assay

The multivalent interactions of $PBLG_{10k}$-*b*-PEG_{6k}-alendronate nanoparticles and $PBLG_{40k}$-PEG_{6k}-alendronate nanoparticles with HAP were studied by means of fluorescence. Multifunctional nanoparticles containing a PBLG-derivate and a fluorescent one, PBLG-FITC, at a ratio of 3:1 wt in 0.1 % of poloxamer Pluronic® F 68 were incubated in a HAP suspension in PBS at a pH of 7.4 during 1 and 18 hours. The suspensions were centrifuged at 3000 rpm and were observed under UV light (λ = 365 nm). Pellets were washed three times with 1% poloxamer in PBS at pH 7.4. Supernatants were quantified by a Perkin Elmer Luminescence spectrometer LS 50B at room temperature ($\lambda_{excitation}$=495 nm, $\lambda_{emission}$ =525 nm) in order to determine the amount of nanoparticles bound to HAP. A calibration curve was plotted for each type of nanoparticle.

2.5.2- Binding isotherms

Different concentrations of multifunctional nanoparticles containing $PBLG_{10k}$-*b*-PEG_{6k}-alendronate or $PBLG_{10k}$-bnz, and $PBLG_{40k}$-FITC in 0.1 % of Pluronic® F 68 were incubated in a HAP powder suspension in PBS at a pH of 7.4 during 18 hours and proceeded as described above. Binding isotherms of $PBLG_{10k}$-*b*-PEG_{6k}-alendronate in the presence and absence of $CaCl_2$ (10 equivalents of $CaCl_2$ per equivalent of alendronate, pre-incubated for 3 hours prior to the assay) were plotted as the mass of nanoparticles per mass of HAP added versus the initial nanoparticle concentration. $PBLG_{10k}$-bnz nanoparticles were used as a negative control. Binding isotherms could be described by Langmuir isotherm. Langmuir isotherm assumes an ideal model where adsorption takes place at specific homogenous sites within the adsorbent, no interactions existing between adsorbed molecules and only a monolayer is formed at the maximum adsorption, molecules of adsorbate being only adsorbed on the

free surface of the adsorbant (Langmuir, 1916). The binding data were plotted and expressed in concentration as a function of alendronate, $PBLG_{10k}$-*b*-PEG_{6k}-alendronate copolymer and number of nanoparticles considered as multivalent objects, since a single nanoparticle could present simultaneously many alendronate molecules, all of them being available for interaction with HAP. Data was fitted by the Langmuir linear regression method, as follows:

$$\frac{C}{Q} = \frac{C}{Q_{max}} + \frac{1}{K_{HAP}Q_{max}} \qquad (2)$$

where Q is the mass of alendronate or $PBLG_{10}$-PEG-alendronate copolymer or number of nanoparticles bound per mass of HAP, Q_{max} is the maximum surface binding, K_{HAP} is the multivalent equilibrium binding constant (M^{-1}) and C the initial concentration of nanoparticles. The plot of 1/Q vs 1/C allowed to determine the Q_{max} and the K_{HAP}, expressed either in alendronate, in $PBLG_{10k}$-*b*-PEG_{6k}-alendronate copolymer or in $PBLG_{10k}$-PEG_{6k}-alendronate nanoparticles. The concentration of alendronate available in nanoparticles was calculated taking into account the amount of alendronate estimated by NMR.

When binding data were expressed as a function of the number of particles, the latter was calculated assuming that nanoparticles were spheres and the density of PBLG lyophases available in the literature was taken into account (1.271 g/cm^3) (Shiau and Labes, 1989) as follows:

$$Nnp = \frac{M\text{PBLG}}{d\text{PBLG}\frac{4}{3}\pi r^3} \qquad (3)$$

where MPBLG is the molecular weight of PBLG estimated by MALDI-TOF, dPBLG is the density of PBLG and r^3 is the hydrodynamic radio of $PBLG_{10k}$-*b*-PEG_{6k}-alendronate nanoparticles measured by dynamic light scattering. To calculate the affinity constant (K_{HAP}) in M^{-1} expressed in nanoparticles, the number of Avogadro (N_A) was used.

2.6- Binding affinity for calcium ions

The interaction of alendronate displayed by $PBLG_{10k}$-*b*-PEG_{6k}-alendronate nanoparticles with calcium ions was studied by ITC (Microcal Inc., USA). The cell (1.2 mL) was loaded with the nanoparticle suspension and stirred at 264 rpm by a rotating syringe, which was filled with a 4 mM solution of $CaCl_2$, $PBLG_{10k}$-*b*-PEG_{6k}-alendronate nanoparticle suspensions at 0.3 mM concentration of polymer corresponding to 0.075 mM concentration of alendronate were prepared. The concentration of alendronate in nanoparticles was calculated taking into account the amount of alendronate estimated by NMR. The titration of $PBLG_{10k}$-*b*-PEG_{6k}-alendronate nanoparticles involved 30 injections of 10 µL of the calcium solution during 200 s at an interval of every 600 seconds. Experiments were carried out at 25 °C. Blank nanoparticles, i.e. not containing alendronate groups, were prepared from $PBLG_{10k}$-bnz and $PBLG_{40k}$-*b*-PEG_{5k} and were used as a negative control. A positive control was made with an aqueous solution of PEG-alendronate. As the interaction with calcium ions is a monovalent interaction, the affinity constant was assumed to remain the same for PEG_{6k}-alendronate in solution and when PEG_{6k}-alendronate was inserted at the surface of $PBLG_{10k}$-*b*-PEG_{6k}-alendronate nanoparticles. The affinity constant determined in the PEG-alendronate ITC experiment was obtained constraining the stoichiometry to 1 and it was used to determine the effective stoichiometry of the $PBLG_{10k}$-*b*-PEG_{6k}-alendronate nanoparticles and calcium ions interaction. Additionally, the interaction of an aqueous solution of alendronate with calcium ions was performed and used as a reference.

2.7- Molecular Modeling

The three-dimensional structure of HAP (as a .cif file) was downloaded from the Inorganic Crystal Structure Database (Leventouri et al., 2003) (ICSD, http://icsd.ill.eu/icsd/index.html, code icsd_98873) and manually curated. Packing structures were created with Mercury 3.0 (Macrae et al., 2008) with sizes of 10x10x10 and visualized within Maestro interface from Schrodinger Suite (Schrödinger, 2011).

The three-dimensional structures of alendronate were generated using CORINA v3.44, (CORINA, version 3.44) as individual entities. Alendronates were modeled as zwitterionic molecules, with one negative charge on each phosphonate group and one positive charge on the protonated amino group. A stochastic conformational search, based on Monte Carlo sampling, was employed to generate various conformations, using the Mixed torsional/Low-Mode sampling method in the MacroModel module (Macromodel, 2011) of Schrodinger Suite with improved setup options as follows: the maximum number of steps was set to 10 000, all calculations used 1 000 steps per rotatable bond and an energy cut-off of 42 kJ/mol above the global energy minimum. Redundant conformers were eliminated by imposing a root mean square deviation (RMSD) cutoff of 2.0 Å. Unless otherwise noted, only the lowest energy conformation for each compound was retained. The searches were done using the water continuum model, with standard settings as below: OPLS_2005 force field with supplied charges, dielectric constant 1.0, van der Waals cut-off 8.0 Å, electrostatic cut-off 20.0 Å, and hydrogen bond cut-off 4.0 Å. The conformational search produced a number of 24 unique conformers, for which all possible distances between two oxygen atoms belonging to the bisphosphonate group were measured.

Similar oxygen-oxygen distance measurements were carried out on the exterior surfaces of HAP. The comparison of these two distance data sets showed that four values (4.12 Å, 4.75 Å, 4.80 Å and 5.02 Å) were common to both HAP surfaces and alendronate conformers.

Selected alendronate conformers were inserted on the HAP surface using the matching oxygen-oxygen distances identified earlier, the biphosphonate moiety facing the HAP surface and the amino-containing positive end stretched in the opposite direction. Various HAP-alendronate complexes were designed, in accordance with the global symmetry of the HAP exterior surfaces and with the biphosphonate coordination states in alendronate. Steric clashes within the complexes were removed by energy minimization using Schrödinger's Maestro framework, with all HAP atoms frozen in order to keep the intact crystal structure. Visual inspection of the resulting HAP-alendronate complexes using PyMol (DeLano, 2006) showed that the amino-alkyl substituent in alendronate is mainly

oriented vertically on the HAP surface. Larger HAP-alendronate complexes (10 x 10 x 10) were then built by extending the crystal network on both surfaces using symmetry rules.

3- Results

3-1 Synthesis and characterization of PBLG polymers

Polymerization reactions were followed by FTIR. The complete disappearance of the anhydride signals at ~1850 cm^{-1},~1775 cm^{-1} ,~920 cm^{-1} corresponding respectively to the C^5=O and C^2= O and C–O–C of the anhydride confirms the completion of the polymerization reaction (see SI). Polymers were characterized by NMR, FTIR, and MALDI-TOF. FTIR spectra of all polymers show an α-helix secondary structure, characterized by the amide I, amide II, and amide III at ~1655 cm^{-1} ,~1550 cm^{-1} and ~1260 cm^{-1} respectively (Barbosa et al., 2007; Cauchois et al., 2013; Segura-Sanchez et al., 2010). A critical DP_n of 18 was established above which the α-helix structure is increasingly favored versus the β-sheet secondary structure (Papadopoulos et al., 2004). In the present study, the minimal DP_n of the synthesized polymers was 38, and as a result they were only composed of α helical secondary structures (**Table 1).**

Table 1: Molar mass of the polymers determined by ^{1}H NMR and MALDI-TOF

PBLG-polymers	DP_n [a]	DP_n [b]	M_n (g/mol)	PI[c]
$PBLG_{25k}$-bnz	136	106[c]	23407[c]	1.13
$PBLG_{10k}$-bnz	45	38[c]	8431[c]	1.16
$PBLG_{40k}$-*b*-PEG_{5k}	228	156[c] 235[d]	39366[c] 56465[d]	1.23
$PBLG_{40k}$-*b*-PEG_{6k} -alendronate	228	190[c]	42415[c]	1.17
$PBLG_{10k}$-*b*-PEG_{6k} -alendronate	45	38[c]	8711[e]	-
$PBLG_{40k}$-FITC	228	163[c]	36155[c]	1.14

(a) theoretical; (b) of the PBLG block; (c)determined by Maldi-TOF; (d) determined by NMR; (e) determined from the PBLG10k-bnz

Differences between theoretical and the experimental DP_n determined by the MALDI-TOF technique and between DP_n established for $PBLG_{40k}$-PEG_{5k} by NMR and MALDI-TOF, suggest that

MALDI-TOF technique underestimated the molar mass of polymers, probably due to the molar mass discrimination effect (Favier et al., 2004). Alendronate content in PBLG-*b*-PEG-alendronate was estimated by ^{31}P NMR (see SI) and ^{1}H NMR, quantifying the efficacy of the reactions. It was found that 3.6 % of $PBLG_{40k}$-PEG_{6k}-alendronate copolymer chains contained a molecule of alendronate whereas that of 5.3 % for the $PBLG_{10k}$- PEG_{6k}-alendronate copolymer chains.

3.2- Characterization of nanoparticles

Nanoparticles prepared from one or from a mixture of different PBLG derivates could be easily obtained by a simple nanoprecipitation method without the use of any additional surfactants. In all cases, nanoparticles were characterized by a size under 80 nm with a narrow size distribution and thus nanoparticles were likely to pass through the bone-blood barrier and reach the bone tissue. They all showed a negative zeta potential, which varied depending on the polymer or polymer mixtures. The more negative zeta potential of $PBLG_{10k}$-*b*-PEG_{6k}-alendronate nanoparticles could be attributed to the presence of alendronate, which holds two negative charges at pH 7.9. **(Table 2)**

Table 2: Size and Zeta potential of nanoparticles determined by DLS

Nanoparticles	Size (nm) ± SD [a]	Polydispersity Index	ζ Potential (meV) ± SD
$PBLG_{25k}$-bnz	58 ±0.4	0.14	-29 ± 1.3
$PBLG_{10k}$-bnz	70 ± 0.3	0.13	-23 ± 1.4
$PBLG_{40k}$-*b*-PEG_{5k}	52 ± 2.8	0.15	-24 ± 0.5
$PBLG_{40k}$-*b*-PEG_{6k}-alendronate	57 ± 1.7	0.16	-27 ± 0.8
$PBLG_{10k}$-*b*-PEG_{6k}-alendronate	76 ± 1.3	0.17	-34 ± 1.2
$PBLG_{25k}$-bnz: $PBLG_{40k}$-FITC 3:1	68 ± 2.1	0.17	-18 ± 1.3
$PBLG_{10k}$-bnz: $PBLG_{40k}$-FITC 3:1	56 ± 1.2	0.16	-17 ± 0.9
$PBLG_{40k}$-*b*-PEG_{5k}: $PBLG_{40k}$-FITC 3:1	52 ±1.1	0.13	-20 ± 1.0
$PBLG_{40k}$-*b*-PEG_{6k}-alendronate: $PBLG_{40k}$-FITC 3:1	63 ± 1.3	0.12	-20 ± 1.6
$PBLG_{10k}$-*b*-PEG_{6k}-alendronate: $PBLG_{40k}$-FITC 3:1	69 ± 0.5	0.15	-38 ± 1.2

$PBLG_{10k}$-*b*-PEG_{6k}-alendronate: $PBLG_{40k}$-FITC 3:1 pre-incubated with $CaCl_2$	70 ± 0.8	0.18	-16 ± 1.2

Nanoparticles prepared from the $PBLG_{10k}$-bnz and $PBLG_{10k}$-*b*-PEG_{6k}-alendronate, and their mixtures with $PBLG_{40k}$-FITC in a 3:1 proportion, presented rather a spherical form, as revealed by the TEM images, whereas it can be observed that nanoparticle shape became increasingly ellipsoidal as the molar mass of the PBLG increased (Cauchois et al., 2013), as shown also for $PBLG_{25k}$-bnz nanoparticles and $PBLG_{40k}$-*b*-PEG_{6k}-alendronate (see SI).

Calculations suggested that on an average each individual fluorescently labelled $PBLG_{10k}$-b-PEG_{6k} -alendronate nanoparticle could be formed by the self-assembly of approximately 1100 α-helix chains and thus, approximately 60 molecules of alendronate were present on each nanoparticle. For fluorescently labelled $PBLG_{40k}$-*b*-PEG_{6k} -alendronate nanoparticles, each individual nanoparticle could contain approximately 190 α-helix chains and thus the number of alendronate molecules per nanoparticle was estimated to be around 7. Thus, it is observed that the molecular weight of the PBLG block had a considerable influence in the number of ligands theoretically available for interactions with HAP. Both the high solubility of alendronate in water combined with the rigidity of the auto-assembling PBLG blocks favors the localization of the alendronate molecules on the nanoparticle surface.

3.3- Multivalent binding affinity for HAP

In vitro HAP binding assay

The multivalent interaction of $PBLG_{10k}$-*b*-PEG_{6k} -alendronate nanoparticles with HAP was studied by means of fluorescence to determine if alendronate decorated nanoparticles could bind to HAP surfaces. It is a multivalent interaction because each nanoparticle is decorated with multiple alendronate molecules on its surface, which interact at multiple sites with one HAP surface with

various calcium ions available on its structure. This assay revealed the effective binding of alendronate nanoparticles to HAP (**Figure 2).**

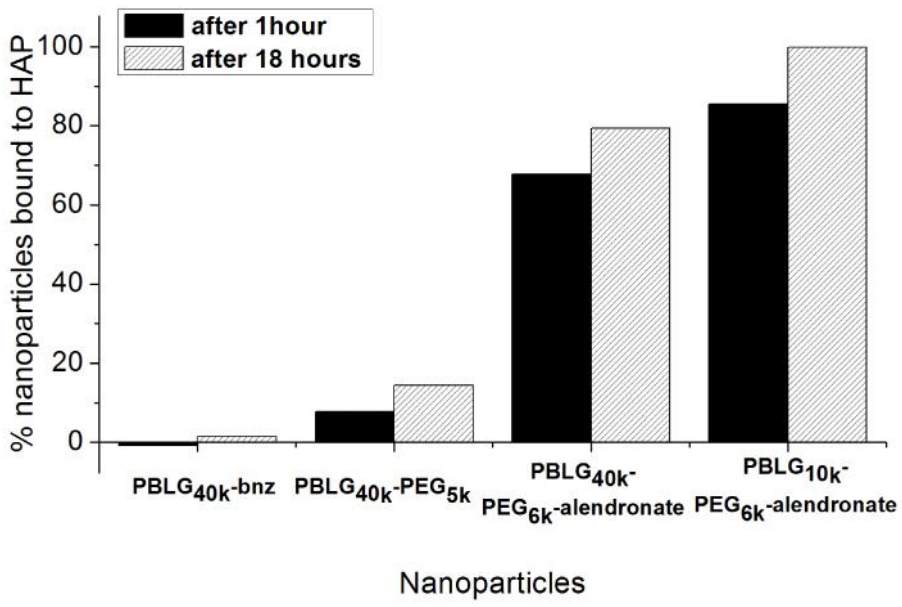

Figure 2: Degree of binding expressed in percentage of nanoparticles bound to HAP for $PBLG_{40k}$-*b*-PEG_{6k} -alendronate nanoparticles and $PBLG_{10k}$-*b*-PEG_{6k}-alendronate nanoparticles after 1 and 18 hours compared to $PBLG_{25k}$-bnz and $PBLG_{40k}$-*b*-PEG_{5k} nanoparticles. Nanoparticles at a concentration of 1.5 mg/mL in 0.1 % Pluronic® F 68 were incubated with 0.4 g of HAP suspension in PBS buffer.

$PBLG_{10k}$-*b*-PEG_{6k}-alendronate nanoparticles, decorated with approximately 60 molecules of alendronate per nanoparticle, could bind totally to HAP after 18 hours whereas for $PBLG_{40k}$-*b*-PEG_{6k}-alendronate nanoparticles, which contained around 7 molecules of alendronate per nanoparticle, HAP bound particles were of about 80%. Control nanoparticles showed no binding in the case of $PBLG_{25k}$-bnz nanoparticles. In the case of $PBLG_{40k}$-*b*-PEG_{5k} nanoparticles, a non specific interaction was observed, as shown by the 20 % of HAP bound nanoparticles after 18 hours.

The binding of alendronate decorated nanoparticles to HAP was a kinetic process, as described already for alendronate (Leu et al., 2006) and other molecules (Kandori et al., 2000; Moreno et al., 1984; Rill

et al., 2009), Indeed it was a rapid process since 85 % of $PBLG_{10k}$-*b*-PEG_{6k}-alendronate nanoparticles were already bound after one hour, which was similar but slightly quicker than previously observed for biphosphonate-tagged gold nanoparticles (Ross and Roeder, 2011).

Binding Isotherms

The multivalent interaction between $PBLG_{10k}$-*b*-PEG_{6k}-alendronate nanoparticles and HAP was estimated from binding isotherms experiments. Binding isotherms of $PBLG_{10k}$-*b*-PEG_{6k}-alendronate and calcium pre-incubated $PBLG_{10k}$-*b*-PEG_{6k}-alendronate nanoparticles were studied and compared to $PBLG_{10k}$-bnz nanoparticles, used as a negative control.

No differences were observed between the binding isotherm for $PBLG_{10k}$-*b*-PEG_{6k}-alendronate in presence or in absence of calcium ions **(Figure 3)**.

Both followed the Langmuir model. This could suggest that calcium ions in solution could be easily exchanged with calcium ions belonging to the HAP structure. The plot of C/Q vs C expressed in alendronate, in polymer and in nanoparticles using a Langmuir model exhibited correlation coefficients R^2 of 0.99, where Q_{max} and K_{HAP} could be determined and are shown in table 4. (**Table 3)**

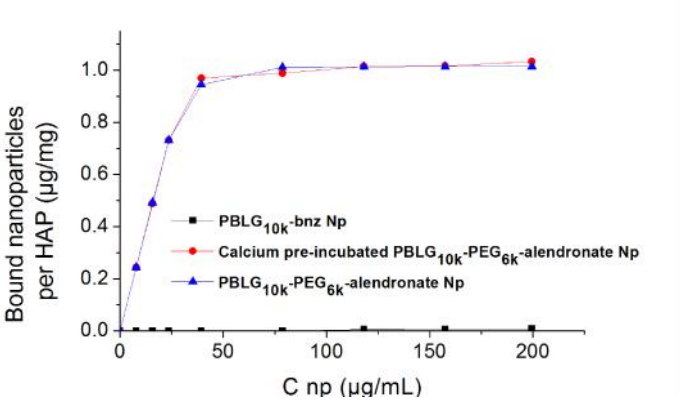

Figure 3: Binding isotherms of $PBLG_{10k}$-*b*-PEG_{6k}-alendronate nanoparticles and calcium pre-incubated $PBLG_{10k}$-*b*-PEG_{6k}-alendronate nanoparticles with HAP in PBS pH 7.4 vs $PBLG_{10k}$-bnz nanoparticles. Experimental data were fitted to a Langmuir model using the equation 1.

Table 3: The binding parameters of $PBLG_{10k}$-*b*-PEG_{6k}-alendronate nanoparticles for HAP determined by the Langmuir model using the Langmuir linear regression method

Np $PBLG_{10k}$-*b*-PEG_{6k}-alendronate	R^2	Q_{max} (moles/g HA)	K_{HAP} (M^{-1})
Expressed in alendronate	0.99	$4.4x10^{-9}$	$1.6x10^{7}$
Expressed in polymer $PBLG_{10k}$-*b*-PEG_{6k}-alendronate	0.99	$7.1x10^{-9}$	$9.6x10^{7}$
Expressed in nanoparticles	0.99	$6.4x10^{-12}$	$1.1x10^{10}$

Not surprisingly, calcium pre-incubated $PBLG_{10k}$-*b*-PEG_{6k}-alendronate nanoparticles had a less negative zeta potential (from -26.7 meV to -16.2 meV), which did not affect nanoparticle interaction with HAP. This supports the fact that the interaction of nanoparticles were driven by the alendronate targeting moiety, and not by the zeta potential.

3.4- Binding affinity for calcium ions by isothermal titration calorimetry

ITC experiments were carried out to determine the affinity of the interaction between the alendronate molecules in $PBLG_{10k}$-*b*-PEG_{6k}-alendronate nanoparticles and calcium ions, as it is the most important interaction involved in the interaction of alendronate with HAP. $PBLG_{10k}$-*b*-PEG_{6k}-alendronate nanoparticles clearly showed a specific interaction with calcium ions that was not seen for negative control nanoparticles. Such interaction resulted in exponentially decreasing heats of interactions while adding calcium ions to the nanoparticle suspension. A positive control with PEG_{6k}-alendronate in solution was performed so as to mimic the type of interaction occurring with nanoparticles, since alendronate conjugation with PEG chains (see figure 1) was likely to differ from that observed with free alendronate molecules. Alendronate on its zwitteronic form is known to form 2:1 complexes with calcium ions (Fernandez et al., 2003). However, alendronate moiety in PEG_{6k}-alendronate in solution or exposed on nanoparticle surface had two negative charges, where it could be depicted that interaction with Ca^{2+} would form a 1:1 complex. Interactions between alendronate, PEG_{6k}-alendronate in solution and $PBLG_{10k}$-*b*-PEG_{6k}-alendronate nanoparticles with calcium ions had similar thermodynamic parameters (ΔH and ΔS), which confirmed that the interaction involved was likely to

be similar. All interactions were entropically driven and could be described by a one-site model. **(Figure 4)**

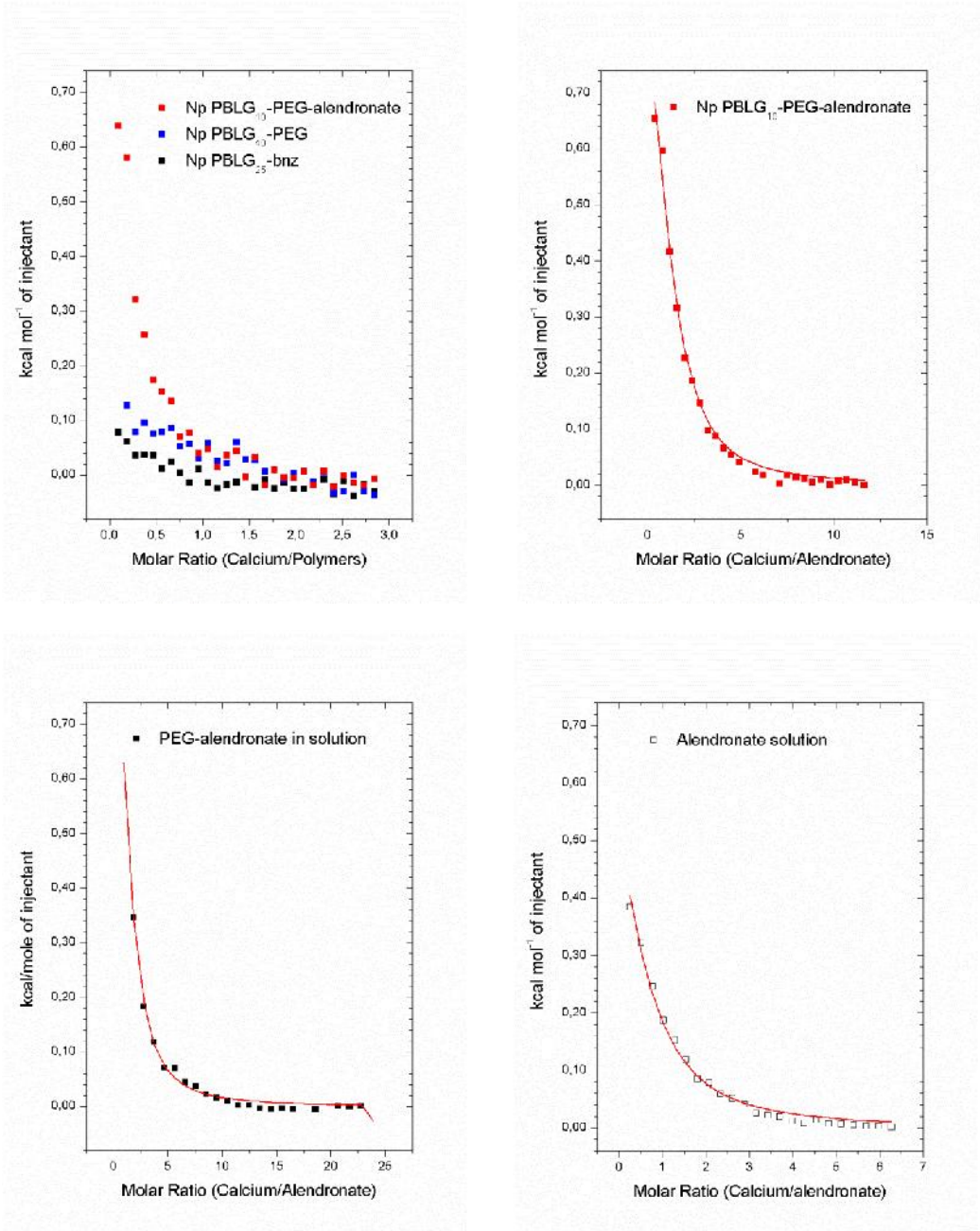

Figure 4: Typical ITC integrated heat data profiles obtained from the binding interaction of $CaCl_2$ with: (a) (up-left) Nanoparticles (Np) $PBLG_{10k}$-*b*-PEG_{6k}-alendronate vs Np $PBLG_{25k}$-bnz and Np $PBLG_{40k}$-*b*-PEG_{6k}; (b) (up-right) Np $PBLG_{10k}$-*b*-PEG_{6k}-alendronate (c) (down-left) PEG_{6k}-alendronate solution (d) (down-right)alendronate solution.

Interactions were strong, as suggested by the binding constants (K_{Ca}^{+2}), and slightly stronger for the 1:1 complex alendronate calcium (in PEG_{6k}-alendronate and $PBLG_{10k}$-*b*-PEG_{6k}-alendronate nanoparticles) than for the 2:1 complex (in calcium- alendronate solution). The heat signal variations were weaker in the case of the titration of $PBLG_{10k}$-*b*-PEG_{6k}-alendronate nanoparticles due to the limited concentration of alendronate, but were still exploitable. The stoichiometry for $PBLG_{10k}$-*b*-PEG_{6k}-alendronate nanoparticles and calcium interaction was found to be 1,04 indicating that all molecules of alendronate were exposed on the nanoparticle surface and available to interact with calcium ions. **(Table 4)**

Table 4 : Binding parameters for $PBLG_{10k}$-*b*-PEG_{6k}-alendronate nanoparticles and for PEG_{6k}-alendronate and alendronate in solution with calcium ions determined by isothermal titration calorimetry.

	Alendronate	PEG_{6k}-alendronate	$PBLG_{10k}$-*b*-PEG_{6k}-alendronate nanoparticles
Chi^2/DoF	99	90	238
Stoichiometry, N	0.5[a]	1.0[a]	1.0 ± 0,05[b]
$K_{Ca}^{+2}(M^{-1})$[c]	$1.8x10^4 \pm 7\ x10^2$	$1,8x10^4 \pm 1.7x10^3$	$1,8x10^4$
ΔH (kcal mol^{1})	$11x10^2 \pm 34$	$16x10^2 \pm 36$	$13x10^2 \pm 57$
ΔS (cal deg^{-1} mol^{-1})	23	25	24

[a]imposed stoichiometry for calculations. [b]calculated stoichiometry using the experimental affinity constant determined for PEG_{6k}-alendronate in solution. [c]expressed in alendronate concentration.

3.5- Analysis of alendronate complexation at HAP-surfaces by molecular modeling

Molecular modeling has been used to investigate the possibilities of interactions of alendronate moieties with the two surfaces of HAP crystals. Four modes of interaction of alendronate molecules with HAP surfaces 1 and 2 were identified as shown in figure 5. The alendronate interacts with HAP not only by chelation of calcium ions but also by hydrogen bonds with oxygen atoms from the crystalline structure. The distances between the oxygen atoms of alendronate in the selected conformers are compatible with the same distances in the HAP structure, which allows for an optimal

interaction between these two entities. These oxygen-oxygen interatomic distances are of 4.12, 4.80 and 5.02 Å respectively for Models 1, 2 and 3 on Face 1, and of 4.75 Å for Model 4 on Face 2 **(Figure 5).**

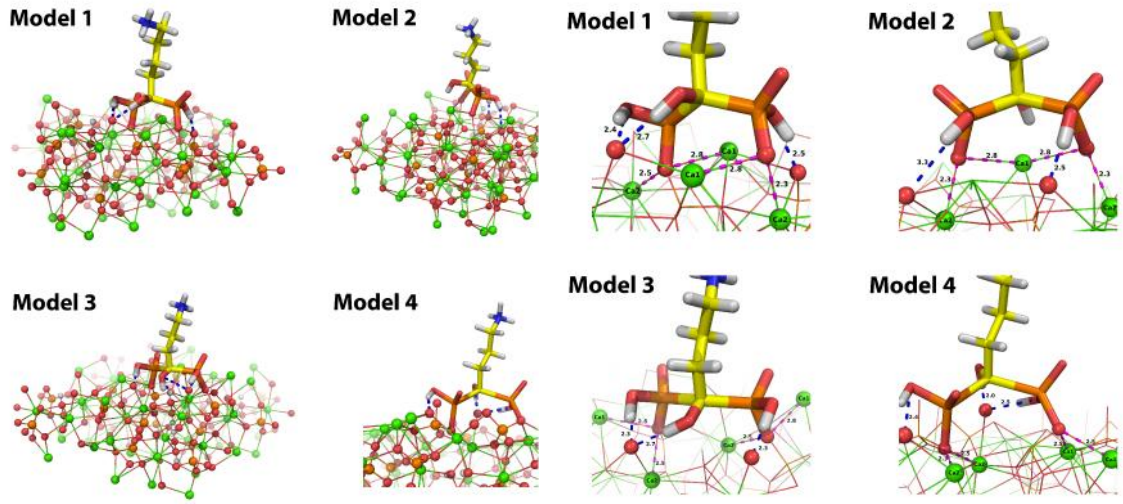

Figure 5: HAP-Alendronate complexes on face 1 (Model 1, 2, 3) and on face 2 (Model 4)

For Model 1, two calcium atoms coordinated by oxygen are situated at 2.48 and 2.83 Å from the first atom and respectively at 2.52 and 2.83 Å from the second oxygen on HAP surface. For Model 2, distances of 2.81 Å are measured between the oxygen atoms responsible for binding and the common calcium ion. Two others calcium ions coordinate these oxygen atoms and are found at 2.33 Å. According to Model 3, the binding of alendronate is mediated by two calcium ions that coordinate oxygen, within distances of 2.32 and 2.74 Å for the first oxygen and 2.58 and 2.89 Å for the second. Alendronate coordination on HAP's face 2 involves oxygen atoms positioned at a distance of 4.75 Å. These atoms are coordinated with two calcium ions, positioned at 2.50 and 2.30 Å from the first, and at 2.50 Å from the second oxygen.

The alendronate interaction with HAP is enhanced by the interaction between the three -OH groups of alendronate with the crystalline structure: two hydrogen bonds for Model 2 and three hydrogen bonds for the other models. The areas of external surfaces of HAP were measured in order to determine the specific surface for the interaction with alendronate and for comparison with the

experimental data. The HAP structure that we generated contains 1000 units (10x10x10 units from the crystal cell) with areas of 9427 Å² for the first surface (face 1) and 7544 Å² for the second (face 2) (see SI). According to our models, a number of 121 to 132 alendronate molecules can theoretically interact with the first face (corresponding to interatomic oxygen-oxygen distances of 4.80 Å, 5.02 Å and 4.12 Å). Similarly, up to 110 alendronate molecules can interact with the second surface (face 2), corresponding to the oxygen-oxygen distance of 4.75 Å (see SI).

4- Discussion

The design of efficient bone targeted delivery systems depends on many aspects, an important one being the affinity of the drug carriers to their target. Self-assembly of amphiphilic copolymers to form nanoparticles represents a convenient way to display multiple targeting units to their surface, likely to result in multivalent interactions with their targets. Multivalent interactions occur frequently in nature and are known to be much more stronger than corresponding monovalents interactions (Mammen et al., 1998).

PBLG copolymers have been selected for preparing bone targeted nanoparticles due to an attractive set of other characteristics including their biocompatibility and degradability. Ring opening polymerization was found to be convenient to obtain copolymers with low polymolarity index (PI <1.3). In order to attain bone, HAP targeting has been the selected strategy as it is highly specific of bone tissue, existing only also in teeth and pathological calcifications. Alendronate has been successfully coupled to PBLG copolymers which could self-assemble to form small nanoparticles so as to impart bone osteotropicity.

For bone-targeted nanoparticles to reach bone tissue, a prolonged time of circulation is required. The small hydrodynamic diameter of the nanoparticles (50-75 nm, depending on the composition) was likely to favor a prolonged bloodstream circulation (Alexis et al., 2008). In order to avoid premature clearance by the reticuloendothelial system, pegylation of nanoparticles is a preferred method (Owens I and Peppas, 2006). The hydrophilicity and flexibility of the surface PEG chains is widely used to

prevent the adsorption of opsonins and the subsequent phagocytosis and clearance by the reticuloendothelial system. Thus, a PEG above 5 kDa, MeO-PEG_{5k}-NH_2,was selected to synthesize $PBLG_{40k}$-*b*-PEG_{5k} block copolymer. To ensure that molecules of alendronate could be exposed and available on the surface, NHS-PEG_{6k}-NHS was chosen for the synthesis of the bone-targeting copolymer both as a spacer and to confer stealth properties to the bone-targeted nanoparticles.

As previously reported by our group, PBLG blocks adopt α-helix structures resulting in quite rigid rods able to self-assemble and to form the core of nanoparticles. Nanoparticles made from PBLG-*b*-PEG_{6k}-alendronate copolymers had a core-shell structure, where the flexible PEG chains would form an external flexible hydrophilic shell, while the rigidity of the hydrophobic PBLG block would mechanically favor alendronate presentation on the particle surface.

First, the ability of alendronate decorated nanoparticle to effectively bind to HAP was checked by a fluorescence method. The possibility of assembling different PBLG-derivates to form multifunctional nanoparticles was previously reported by our group (Martinez-Barbosa et al., 2009) and it was confirmed with this assay, where each $PBLG_{10k}$-*b*-PEG_{6k}-alendronate nanoparticle displayed at the same time its fluorescent and its bone binding property. It can be inferred from this experiment that the binding between $PBLG_{10k}$-*b*-PEG_{6k}-alendronate nanoparticles and $PBLG_{40k}$-*b*-PEG_{6k}-alendronate nanoparticles with HAP is a specific interaction, not driven by the negative zeta potential of nanoparticles. The absence of binding for $PBLG_{10k}$-bnz nanoparticles allowed us to conclude that the affinity of $PBLG_{10k}$-*b*-PEG_{6k}-alendronate nanoparticles for HAP is due to the alendronate moiety and to exclude the differences in shape, evidenced by the TEM.

Next, the affinity between $PBLG_{10k}$-*b*-PEG_{6k}-alendronate nanoparticles and the HAP surface was studied by adsorption isotherms. Multivalent interactions are known to enhance the affinity compared to its corresponding monovalent interaction (Kiessling et al., 2006; Mammen et al., 1998). The multivalent affinity constant for $PBLG_{10k}$-*b*-PEG_{6k}-alendronate nanoparticles (K_{HAP}) expressed in alendronate was more than 5 times stronger compared to the monovalent interaction between

alendronate and HAP reported value in the literature (Nancollas et al., 2006). It was almost 4000 times more if the multivalent affinity constant was expressed in terms of nanoparticle concentrations. This is in agreement with the previous works which showed that multivalent interactions are 4 to 9500 times stronger than the corresponding monovalent ones, the highest enhancements seen for weaker intrinsic affinities (Tassa et al., 2010).

Affinity binding was also studied in presence of calcium ions in solution since the main interaction between the alendronate and HAP is known to involve the calcium ions of the HAP crystalline stucture. Interestingly, it was shown that calcium-bound nanoparticles could still bind to HAP structures with the same affinity as in absence of calcium ions.

Then, interaction of $PBLG_{10k}$-*b*-PEG_{6k}-alendronate nanoparticles with calcium ions was studied by ITC. The interaction with calcium ions, K_{Ca}^{+2}, determined by ITC was of $1.8x10^4$ M^{-1} which is 900 times weaker than the multivalent interaction of $PBLG_{10k}$-*b*-PEG_{6k}-alendronate nanoparticles with HAP (K_{HAP} =$1.6x10^7$ M^{-1}) estimated from binding isotherm. This enhanced affinity of alendronate nanoparticles for HAP in comparison with calcium ions in solution explains why calcium pre-incubated $PBLG_{10k}$-*b*-PEG_{6k}-alendronate nanoparticles can still bind to HAP surfaces, this being a competition which is favorable to HAP. After intravenous administration of nanoparticles, they are confronted to physiological concentrations of calcium ions in the blood. Interestingly, this would imply that even if nanoparticles could interact with calcium ions present in the bloodstream or physiological fluids, this would be reversible and would not affect their interaction with the mineral matrix of the bone tissue due to higher affinity to HAP.

Finally, molecular modelling studies were performed so as to determine the interactions involving alendronate and HAP. Although the most important interactions between alendronate and HAP involves the coordination of the calcium ions of HAP, the interactions involving alendronate/calcium ions and alendronate/ HAP crystalline structure were not the same since in addition hydrogen bonding involving the alendronate and the HAP structure are established (see figure 5). The theoretical models

developed in this work for the interaction of alendronate with the HAP surface are important in evidencing the detailed structural determinants of this interaction, at atomic level, and allow the rational analysis of the experimental data showing a good affinity of PBLG nanoparticles for the bone tissue. According to molecular modeling data, the theoretical number of free alendronate molecules that can interact with a HAP surface unit of 95 nm^2 or 75 nm^2 was of 132 and 110 respectively, depending on the crystal face. Experimentally, depending on the molecular weight of the PBLG block, the number of alendronate decorating molecules could be considerably varied. However, irrespective of the situation, binding sites available at HAP surface were in excess compared to the number of alendronate available at nanoparticle surface. For example, in the case of the $PBLG_{10k}$-*b*-PEG_{6k}-alendronate nanoparticles (about 60 alendronate per nanoparticle) only a reduced fraction of these alendronate moieties was likely to interact with HAP surface due to nanoparticle size (ranging from 52 to 76 nm in size). Therefore, it could be concluded that numerous sites at the surface of HAP crystals were available for interactions with alendronate molecules compared to the number of interactions necessary in the case of alendronate decorated nanoparticles, which is obviously favorable for their binding to HAP crystals included in bone matrix.

5- Conclusion

Bone-targeted multifunctional alendronate nanoparticles which showed strong affinity for HAP, one major component of bone extracellular matrix, could be easily prepared. The binding isotherm for $PBLG_{10k}$-PEG_{6k}-alendronate nanoparticles with HAP surfaces suggested that multivalency of the nanoparticles resulted in 4000 fold stronger interactions with HAP compared the monovalent interaction with free alendronate molecules. The molecular modeling studies yielded a deep insight into the possible interactions of alendronate with HAP. These interactions could be considerably enhanced by the ability of the nanoparticles to develop specific multivalent interactions with HAP, via calcium binding as well as hydrogen bonding. In this case, it was suggested that steric hindrance due to the size of the nanoparticles resulted in a very number of HAP binding sites involved in the

interaction, which favors a very strong interaction between alendronate and HAP. Finally, the 900 fold lower affinity of the nanoparticles for free calcium ions compared to HAP allowed calcium bound nanoparticle to interact with HAP. This is favorable to maintain the targeting specificity of the nanoparticles and yields a deeper understanding of bone targeted nanoparticle in the body.

Acknowledgements

This work has benefited from the facilities and expertise of the Platform for Transmission Electronic Microscopy of IMAGIF (Centre de Recherche de Gif - www.imagif.cnrs.fr)". We gratefully acknowledge the european postgraduate program from "La Caixa" Foundation for the financial support.

References

Alexis, F., Pridgen, E., Molnar, L.K., Farokhzad, O.C., 2008. Factors affecting the clearance and biodistribution of polymeric nanoparticles. Mol. Pharm. 5, 505-515.

Barbosa, M.E.M., Montembault, V., Cammas-Marion, S., Ponchel, G., Fontaine, L., 2007. Synthesis and characterization of novel poly(γ-benzyl-L-glutamate) derivatives tailored for the preparation of nanoparticles of pharmaceutical interest. Polym. Int. 56, 317-324.

Carlson, C.B., Mowery, P., Owen, R.M., Dykhuizen, E.C., Kiessling, L.L., 2007. Selective tumor cell targeting using low-affinity, multivalent interactions. ACS Chem. Biol. 2, 119-127.

Cauchois, O., Segura-Sanchez, F., Ponchel, G., 2013. Molecular weight controls the elongation of oblate-shaped degradable poly(γ-benzyl-l-glutamate)nanoparticles. Int. J. Pharm. 452, 292-299.

CORINA, version 3.44. Molecular networks GmbH, http://www.molecular-networks.com ed. Erlanger, Germany.

DeLano, S., 2006. The pymol molecular graphic system, version 0.99. Palo Alto, CA.

Favier, A., Ladavière, C., Charreyre, M.-T., Pichot, C., 2004. MALDI-TOF MS investigation of the RAFT polymerization of a water-soluble acrylamide derivative. Macromolecules 37, 2026-2034.

Fernandez, D., Vega, D., Goeta, A., 2003. Alendronate zwitterions bind to calcium cations arranged in columns. Acta Crystallogr. C 59, m543-545.

Gittens, S.A., Bansal, G., Zernicke, R.F., Uludag, H., 2005. Designing proteins for bone targeting. Adv. Drug Delivery Rev. 57, 1011-1036.

Hirabayashi, H., Sawamoto, T., Fujisaki, J., Tokunaga, Y., Kimura, S., Hata, T., 2001. Relationship between physicochemical and osteotropic properties of bisphosphonic derivatives: rational design for osteotropic drug delivery system (ODDS). Pharm Res 18, 646-651.

Howlett, C.R., Dickson, M., Sheridan, A.K., 1984. The fine structure of the proximal growth plate of the avian tibia: vascular supply. J Anat 139 (Pt 1), 115-132.

Kandori, K., Fudo, A., Ishikawa, T., 2000. Adsorption of myoglobin onto various synthetic hydroxyapatite particles. Phys. Chem. Chem. Phys. 2, 2015-2020.

Kiessling, L.L., Gestwicki, J.E., Strong, L.E., 2000. Synthetic multivalent ligands in the exploration of cell-surface interactions. Curr Opin Chem Biol 4, 696-703.

Kiessling, L.L., Gestwicki, J.E., Strong, L.E., 2006. Synthetic multivalent ligands as probes of signal transduction. Angew. Chem., Int. Ed. 45, 2348-2368.
Klok, H.-A., Langenwalter, J.F., Lecommandoux, S.b., 2000. Self-assembly of peptide-based diblock oligomers. Macromolecules 33, 7819-7826.
Langmuir, I., 1916. The constitution and fundamental properties of solids and liquids. Part I. Solids. J. Am. Chem. Soc 38, 2221-2295.
Leu, C.-T., Luegmayr, E., Freedman, L.P., Rodan, G.A., Reszka, A.A., 2006. Relative binding affinities of bisphosphonates for human bone and relationship to antiresorptive efficacy. Bone 38, 628-636.
Leventouri, T., Bunaciu, C.E., Perdikatsis, V., 2003. Neutron powder diffraction studies of silicon-substituted hydroxyapatite. Biomaterials 24, 4205-4211.
Macrae, C.F., Bruno, I.J., Chisholm, J.A., Edgington, P.R., McCabe, P., Pidcock, E., Rodriguez-Monge, L., Taylor, R., van de Streek, J., Wood, P.A., 2008. Mercury CSD 2.0 - new features for the visualization and investigation of crystal structures. J. Appl. Crystallogr. 41, 466-470.
Macromodel, 2011. version 9.9, Schrödinger. LLC, New York, NY.
Mammen, M., Choi, S.-K., Whitesides, G.M., 1998. Polyvalent interactions in biological systems: implications for design and use of multivalent ligands and inhibitors. Angew. Chem., Int. Ed. 37, 2754-2794.
Martinez-Barbosa, M.E., Cammas-Marion, S., Bouteiller, L., Vauthier, C., Ponchel, G., 2009. PEGylated degradable composite nanoparticles based on mixtures of PEG-b-poly(gamma-benzyl L-glutamate) and poly(gamma-benzyl L-glutamate). Bioconjug. Chem. 20, 1490-1496.
Moreno, E., Kresak, M., Hay, D., 1984. Adsorption of molecules of biological interest onto hydroxyapatite. Calcif. Tissue Int. 36, 48-59.
Nancollas, G.H., Tang, R., Phipps, R.J., Henneman, Z., Gulde, S., Wu, W., Mangood, A., Russell, R.G.G., Ebetino, F.H., 2006. Novel insights into actions of bisphosphonates on bone: Differences in interactions with hydroxyapatite. Bone 38, 617-627.
Oh, I., Oh, J., Cho, C., Lee, K., 1995. Biodegradability of poly(γ-benzyl L-glutamate)/poly(ethylene oxide) /poly(γ-benzyl L-glutamate) block copolymer in mice. Arch. Pharmacal Res. 18, 8-11.
Owens I, D.E., Peppas, N.A., 2006. Opsonization, biodistribution, and pharmacokinetics of polymeric nanoparticles. Int. J. Pharm. 307, 93-102.
Ozcan, I., Bouchemal, K., Segura-Sanchez, F., Ozer, O., Guneri, T., Ponchel, G., 2011. Synthesis and characterization of surface-modified PBLG nanoparticles for bone targeting: In vitro and in vivo evaluations. J. Pharm. Sci. 100, 4877-4887.
Papadopoulos, P., Floudas, G., Klok, H.A., Schnell, I., Pakula, T., 2004. Self-assembly and dynamics of poly(gamma-benzyl-l-glutamate) peptides. Biomacromolecules 5, 81-91.
Park, Y.J., Nah, S.H., Lee, J.Y., Jeong, J.M., Chung, J.K., Lee, M.C., Yang, V.C., Lee, S.J., 2003. Surface-modified poly(lactide-co-glycolide) nanospheres for targeted bone imaging with enhanced labeling and delivery of radioisotope. J. Biomed. Mater. Res. A 67, 751-760.
Rill, C., Kolar, Z.I., Kickelbick, G., Wolterbeek, H.T., Peters, J.A., 2009. Kinetics and thermodynamics of adsorption on hydroxyapatite of the [160Tb] terbium complexes of the bone-targeting ligands DOTP and BPPED. Langmuir 25, 2294-2301.
Ross, R.D., Roeder, R.K., 2011. Binding affinity of surface functionalized gold nanoparticles to hydroxyapatite. J. Biomed. Mater. Res. A 99, 58-66.
Schrödinger, 2011. Suite 2011:Maestro ; version 9.2, in: LLC, N.Y. (Ed.).
Segura-Sanchez, F., Montembault, V., Fontaine, L., Martinez-Barbosa, M.E., Bouchemal, K., Ponchel, G., 2010. Synthesis and characterization of functionalized poly(gamma-benzyl-L-glutamate) derivates and corresponding nanoparticles preparation and characterization. Int J Pharm 387, 244-252.

Shea, J.E., Miller, S.C., 2005. Skeletal function and structure: Implications for tissue-targeted therapeutics. Adv. Drug Delivery Rev. 57, 945-957.
Shiau, C.C., Labes, M.M., 1989. Correlation of pitch with concentration and molecular weight in poly(.gamma.-benzyl glutamate) lyophases. Macromolecules 22, 328-332.
Tassa, C., Duffner, J.L., Lewis, T.A., Weissleder, R., Schreiber, S.L., Koehler, A.N., Shaw, S.Y., 2010. Binding affinity and kinetic analysis of targeted small molecule-modified nanoparticles. Bioconjug. Chem. 21, 14-19.
Wang, D., Miller, S.C., Kopecková, P., Kopecek, J., 2005. Bone-targeting macromolecular therapeutics. Adv. Drug Delivery Rev. 57, 1049-1076.

Supporting information

POLY (γ-BENZYL-L-GLUTAMATE) -PEG-ALENDRONATE MULTIVALENT NANOPARTICLES FOR BONE TARGETING

Laura de Miguel [1], *Magali Noiray*[1], *Georgiana Surpateanu*[2], *Bogdan Iorga* [2] *and Gilles Ponchel*[1]*

[1] Univ. Paris Sud, UMR CNRS 8612, Institut Galien, 92296 Châtenay-Malabry Cedex, France.

[2] UPR 2301, Institut de Chimie des Substances Naturelles, CNRS UPR 2301, Centre de Recherche de Gif-sur-Yvette, 1 Avenue de la Terrasse, 91198 Gif-sur-Yvette, France

*Corresponding author: Laura de Miguel, Univ. Paris Sud, UMR CNRS 8612, Institut Galien, 92296 Châtenay-Malabry Cedex, France. Tel: 0033 1 46 83 57 12 Fax: 0033 1 46 83 57 12 E-mail: laura.de-miguel@u-psud.fr

1. Chemical synthesis of PBLG-PEG$_{6k}$-alendronate

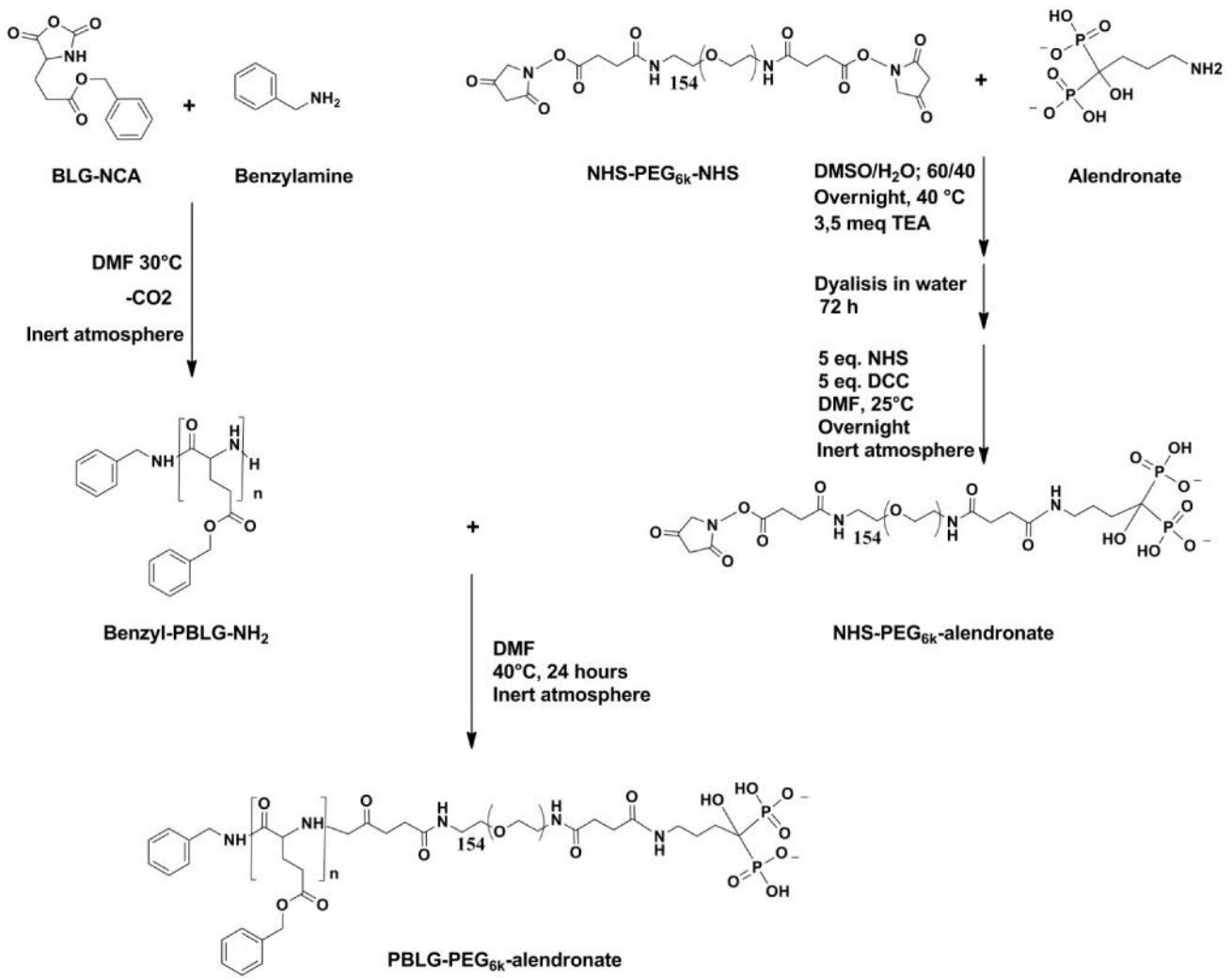

Figure S1: Chemical pathway for the synthesis of PBLG-PEG$_{6k}$-alendronate

2. Chemical synthesis of PBLG$_{40k}$ -FITC

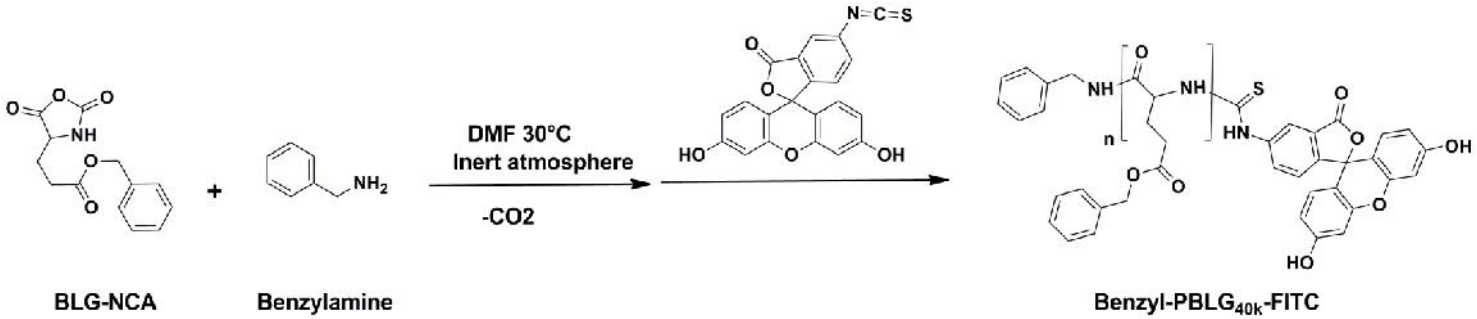

Figure S2: Chemical pathway for the synthesis of PBLG$_{40k}$-FITC

3. Typical FTIR spectrum of a PBLG derivate polymerization

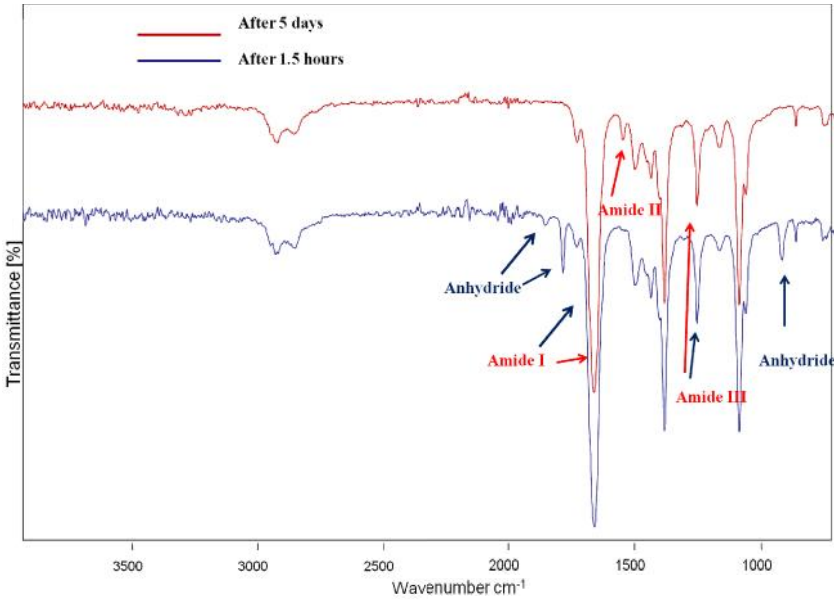

Figure S3: Typical infrared spectrum of a PBLG derivate polymerization after 1.5 hours (below) and 5 days (above)

4. ^{31}P NMR quantification of alendronate in PEG_{6k} -alendronate

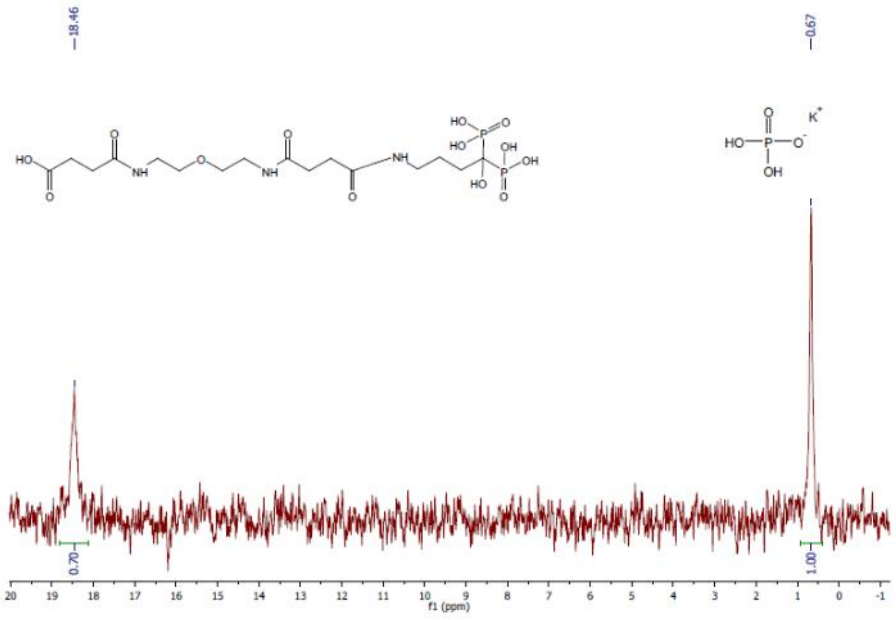

Figure S4: ^{31}P NMR quantification of alendronate contained in PEG_{6k}-alendronate in D_2O using a solution of KH_2PO_4 in D_2O as a reference standard

5. ^{1}H NMR spectrum of PBLG-PEG$_{6k}$-alendronate

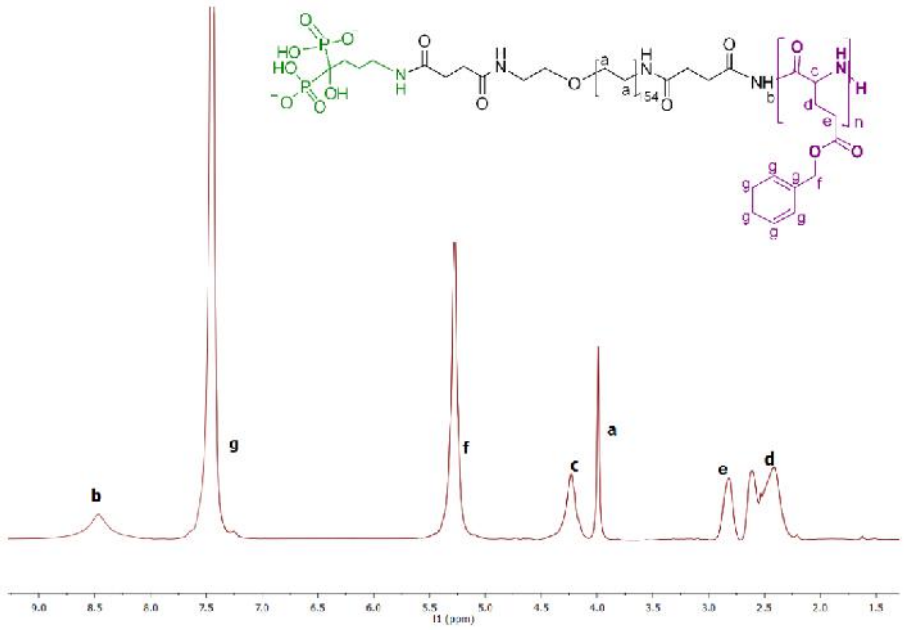

Figure S5: ^{1}H NMR spectrum of PBLG-PEG$_{6k}$-alendronate in $CDCl_3$ 15 % TFA

6. Typical MALDI-TOF spectrum of a PBLG-derivate

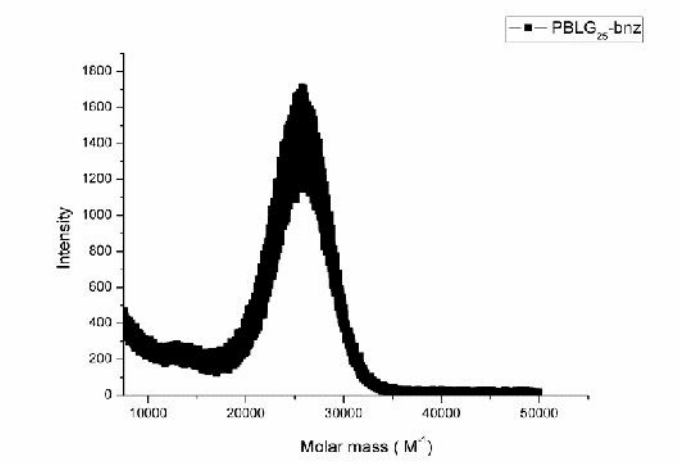

Figure S6: Typical MALDI-TOF spectrum of a PBLG-derivate, here shown for PBLG$_{25k}$-bnz

7. TEM images of different PBLG derivate nanoparticles

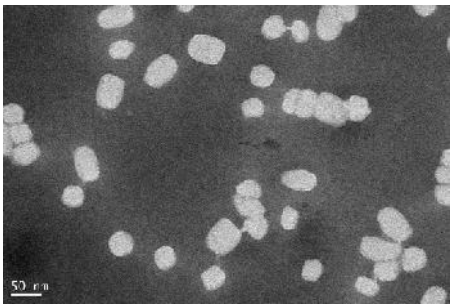

$PBLG_{25k}$-bnz

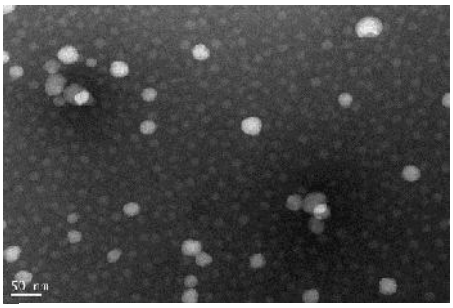

$PBLG_{10k}$-PEG_{6k}-alendronate

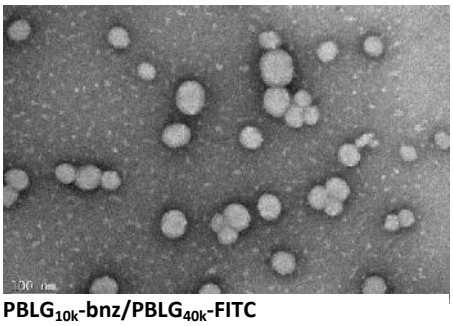

$PBLG_{10k}$-bnz/$PBLG_{40k}$-FITC

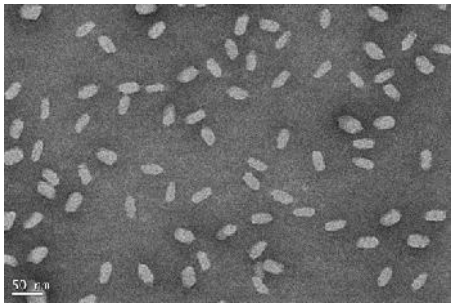

$PBLG_{40k}$-PEG_{6k}-alendronate/ $PBLG_{40k}$-FITC

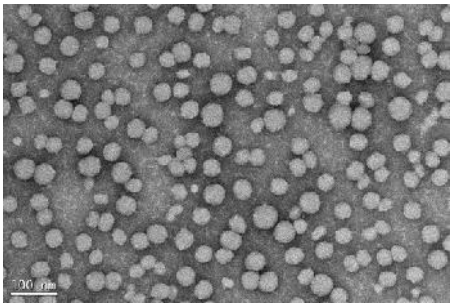

$PBLG_{10k}$-PEG_{6k}-alendronate/$PBLG_{40k}$-FITC

Figure S7: TEM images of different PBLG derivate nanoparticles

6. Analysis of alendronate complexation at HAP-surfaces by molecular modeling

The analysis of HAP edifices(fig. 6.1) reveals the existence of two dissimilar surfaces, the first having a rhomb shape (Face1) and the latter having a parallelepiped shape that correspond to the two lateral external surfaces (Face2). Modifications were made on both surfaces by removing the external layer containing calcium atoms, in order to make the oxygen atoms from the crystal structure available for direct interaction with alendronate bisphosphonates. Relative distances between all oxygen atoms on HAP surface were measured and compared with the corresponding distances in alendronate conformers.

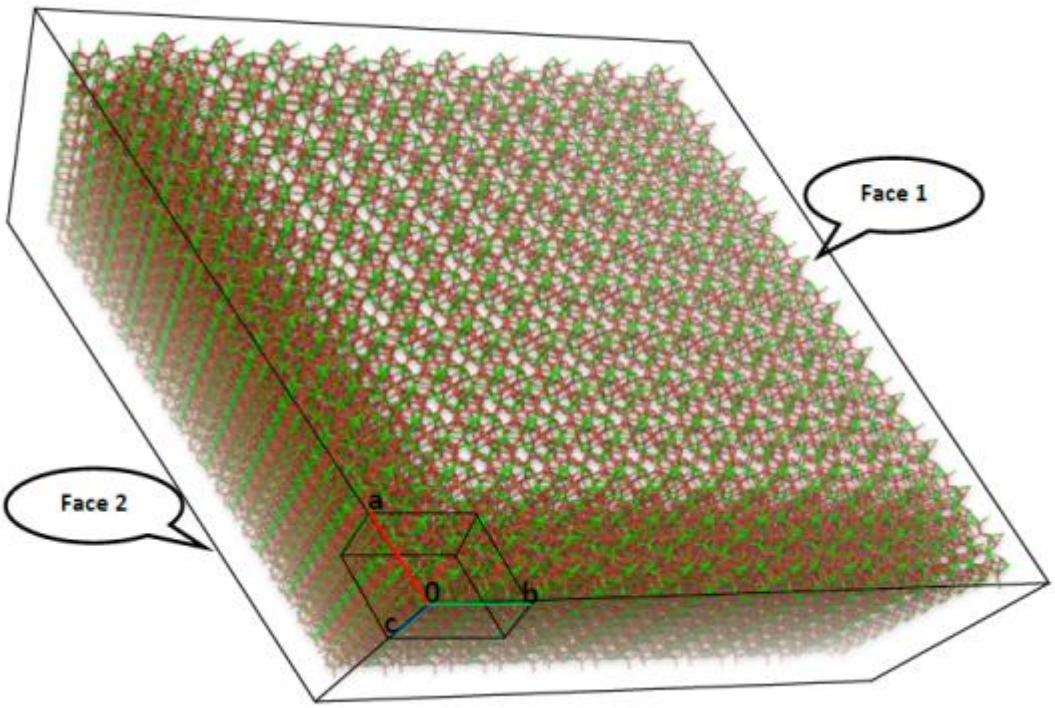

Figure S8: HAP building block showing the two dissimilar surfaces: face 1 and face 2 having a rhomb and a parallelepiped shape, respectively.

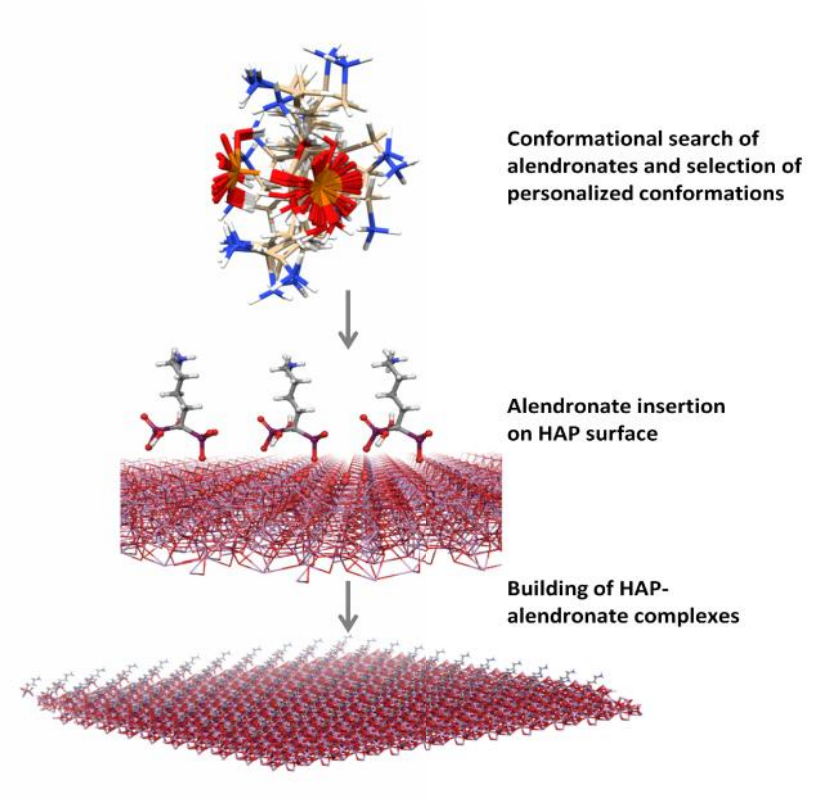

Figure S9: Conformational search protocol and building of HAP-alendronate complexes

The areas of external surfaces of HAP were measured, in order to determine the specific surface for the interaction with alendronate and for comparison with experimental data. The HAP structure that we generated contains 1000 units (10x10x10 units from the crystal cell) with areas of 9427 Å² for the first surface (face 1) and 7544 Å² for the second (face 2). According to our models, a number of 121 to 132 alendronate molecules can theoretically interact with the first face (corresponding to interatomic oxygen-oxygen distances of 4.80 Å, 5.02 Å and 4.12 Å). Similarly, up to 110 alendronate molecules can interact with the second surface (face 2), corresponding to the oxygen-oxygen distance of 4.75 Å as shown in fig. 6.3.

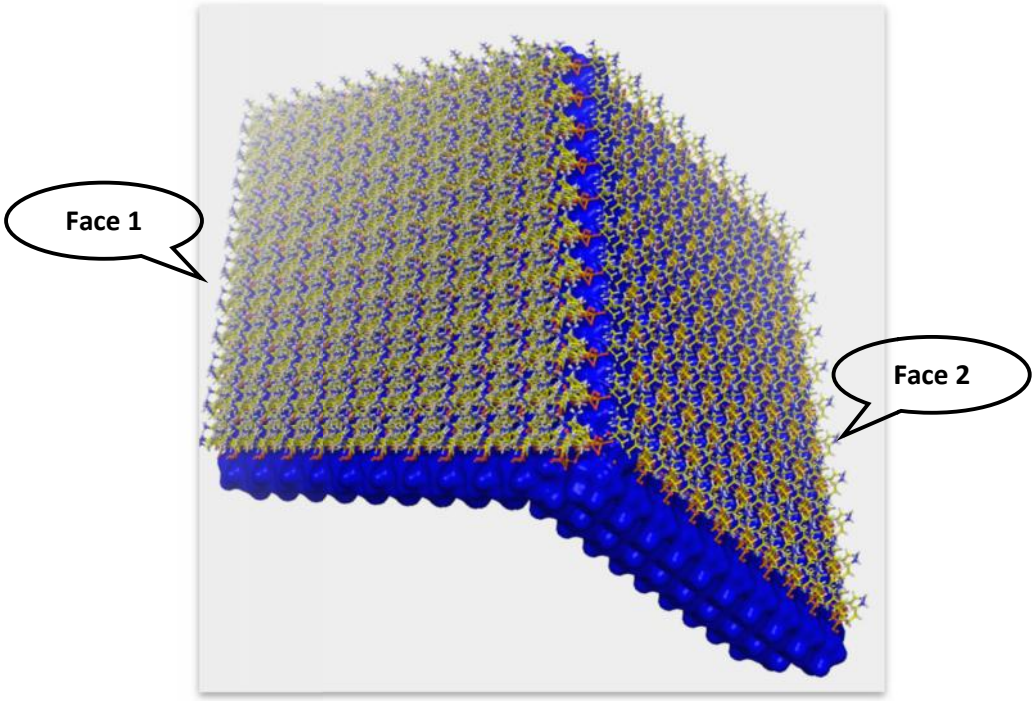

Figure S10: Alendronate interaction with HAP surfaces

CHAPITRE III:

OSTEOTROPIC POLY

(γ-BENZYL-L-GLUTAMATE)

CO-POLY(GLUTAMIC ACID)

NANOPARTICLES FOR CISPLATIN

DELIVERY

OSTEOTROPIC POLY(γ- BENZYL-L-GLUTAMATE) CO POLY(GLUTAMIC ACID) NANOPARTICLES FOR CISPLATIN DELIVERY

Laura de Miguel[1], Iuliana Popa[1], Magali Noiray[1], Eric Caudron[2,3], Ludovica Arpinati[1], Didier Desmaele[1], Gerardo Cebrián-Torrejón[4], Antonio Doménech-Carbó[4] and Gilles Ponchel*[1].

[1] Institut Galien Paris-Sud, Paris-Sud University, Chatenay-Malabry, France, CNRS, UMR 8612, 5 rue Jean Baptiste Clément, Chatenay-Malabry, France

[2] Hôpital Européen Georges Pompidou (AP-HP), Service de Pharmacie, Paris, France

[3] Paris Sud Analytical Chemistry Group, School of Pharmacy, Paris-Sud University, 5 rue Jean Baptiste Clément, Châtenay-Malabry, France

[4] Departament de Química Analítica, Facultat de Química, Universitat de València, Dr. Moliner 50, 46100 Burjassot, Valencia, Spain

*Corresponding author: Gilles Ponchel, Univ. Paris Sud, UMR CNRS 8612, Institut Galien, 92296 Châtenay-Malabry Cedex, France. E-mail: gilles.ponchel@u-psud.fr

Graphical Abstract

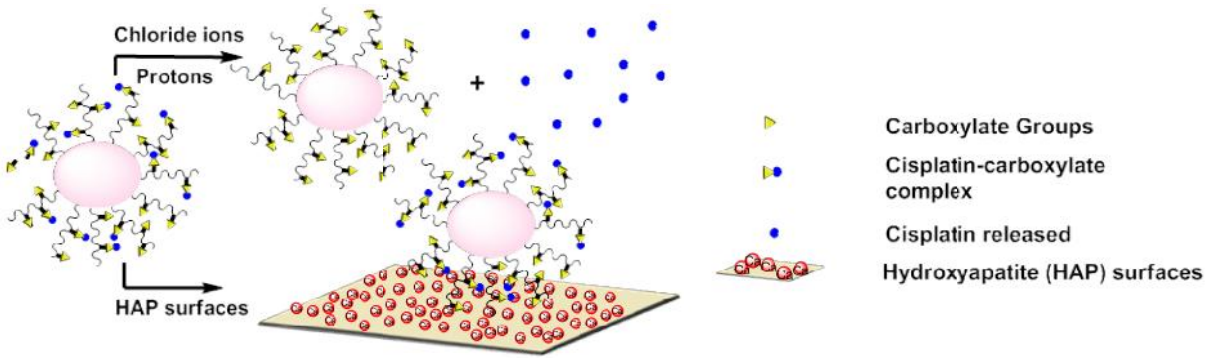

Resumé

Les cancers de la prostate et du sein ont une tendance élevée à métastaser dans l'os et représentent deux causes majeures de mortalité par cancer. Des nanoparticules ciblées aux tissus osseux ayant une taille ~50 nm et des propriétés anticancéreuses ont été préparées à partir du copolymère amphiphile poly (glutamate de benzyle)-poly (acide glutamique) (PBLG-*b*-PGlu) par une méthode simple de nanoprécipitation. Les nanoparticules PBLG-*b*-PGlu ont permis la complexation du cisplatine avec un

taux d'association élevé de 6.2 ± 0.23 % (p/p). La libération du cisplatine était déclenchée par des concentrations physiologiques d' ions chlorures et était parfaitement maîtrisée durant une période de 14 jours selon un cinétique d'ordre quasi zéro. Les nanoparticules cisplatine PBLG-*b*-PGlu ont montré de façon simultanée des propriétés *in vitro* de ciblage osseux par des chaînes PGlu, mises en évidence dans une expérience *in vitro* avec de l'hydroxyapatite et des nanoparticules fluorescentes. Finalement, elles ont montré un effet cytotoxique dans trois lignées cellulaires de cancer de la prostate pouvant potentiellement métastaser dans l'os. Ces propriétés suggèrent une utilité potentielle des nanoparticules cisplatine PBLG-*b*-PGlu comme vecteurs pour le traitement de métastases osseuses dérivées de cancer de la prostate.

Abstract

Prostate and breast cancers, two of the leading causes of death by cancer, have a high tendency to metastasize to bone. Bone targeted nanoparticles of ~50 nm in size with anticancer properties were successfully prepared from the amphiphilic copolymer poly(γ-benzyl-glutamate)-poly(glutamic acid) (PBLG-*b*-PGlu) by a simple nanoprecipitation method. PBLG-*b*-PGlu nanoparticles could complex cisplatin with a high drug loading content of 6.2 ± 0.23 % (w/w). Cisplatin release was triggered by physiological concentrations of chloride ions and was perfectly controlled during a 14 day period according to an almost zero order kinetics. Simultaneously, cisplatin-loaded PBLG-*b*-PGlu nanoparticles showed *in vitro* bone targeting properties mediated by the poly(glutamic acid) (PGlu) moiety, as evidenced in an *in vitro* hydroxyapatite binding assay using fluorescent nanoparticles. Finally, they were shown to exert a cytotoxic effect in three prostate cancer cell lines that potentially metastasize to bone. These properties suggest the potential utility of cisplatin-loaded PBLG-*b*-PGlu nanoparticles as carrier systems for the treatment of bone metastases derived from prostate cancer.

Keywords: bone targeting, cisplatin, cancer, nanoparticles, poly(benzylglutamate), poly(glutamic acid)

1- Introduction

The skeleton is the preferred metastatic site for breast and prostate cancers, which constitute the second leading causes of cancer death in women and in men [1]. Many other cancers, such as lung, renal, melanoma and multiple myeloma can also develop skeletal metastasis. Metastatic bone disease results in metabolic complications such as hypercalcaemia, fractures, bone pain and spinal cord compression and it is associated with a bad prognosis of the disease [2]. Chemotherapy is generally poorly efficient and therapeutic alternatives, including chirurgical removal of metastasis, can be foreseen in some situations, although it is not possible in many patients due to their general health conditions and/or multiple dissemination.

Cisplatin is used for the treatment of different types of cancer, such as ovarian, testicular, bladder, cervical, head and neck, small cell lung cancer and esophageal [3]. It is also used in combined chemotherapy for advanced prostate cancer. However, its biodistribution properties should be improved: cisplatin has a very short half life in the bloodstream due to glomerular excretion [4] and its use is limited due to several side effects, the most threatening ones being neurotoxicity, nephrotoxicity and ototoxicity [4, 5]. Moreover, cisplatin has showed minimal efficacy against some types of cancer due to the development of resistances [6, 7].

To increase cisplatin therapeutic efficacy and to circumvent side effects, much research has been focused on the development of targeted polymeric drug delivery systems [8]. Cisplatin has two chloride groups that can be replaced by a variety of groups, such as carboxylates in low chloride concentration medium. The good leaving property of carboxylates makes the metal complex reversible, such property being used for the design of drug carrier systems. Therefore, much research has been devoted to the development of macromolecular systems containing carboxylate groups so as to form reversible complexes with cisplatin including polymer systems [9-11] and micellar forming copolymers [9-13].

Site specific drug delivery would allow to attain therapeutic concentrations locally, therefore reducing side effects and the dose administered. Nanomedicine plays a major role in tissue specific drug delivering. A lot of research has been focused on active targeting of cancer cells as a way of improving treatment. Bone targeting drug delivery approach is a promising way of enhancing drug time of residence within the bone affected by cancer and thus of increasing its therapeutic effect.

Herein, we report the preparation of bone targeted nanoparticles derived from an amphiphilic PBLG-*b*-PGlu copolymer that can self-assemble into nanoparticles by a simple nanoprecipitation method. Preformed PBLG-*b*-PGlu nanoparticles can then easily associate cisplatin via a coordinate bond and show good bone targeting properties using hydroxyapatite (HAP) as an *in vitro* model. Cisplatin (CDDP) from PBLG-*b*-PGlu nanoparticles is released in a sustained manner in a phosphate buffer saline (PBS) medium to induce a cytotoxic effect on prostate cancer cell lines that constitute cellular models for bone metastases [14].

2-Materials and Methods

2.1-Materials

Dimethylformamide (DMF) (99.8 %) Extradry Acroseal and cisplatin (CDDP) were purchased from Acros, γ-benzyl-L-glutamate-N-carboxylic anhydride (BLG-NCA) was provided by IsoChem and used as received. Hexylamine (puriss ≥99.5%), trifluoroacetic acid (TFA) (99 %), palladium on carbon (Pd/C), deuterated chloroform ($CDCl_3$) and blue trypan were provided by Sigma Aldrich. Dialysis membranes were purchased from Carlroth, (Spectra Por). 1 mL microdialyzers used for *in vitro* drug release experiments were bought from Orange Scientific. $PGlu_{3000}$ and $PGlu_{30000}$ were purchased from Alamanda Polymers. PC-3 were kindly provided by the Institut Curie (Paris, France) and LNCaP and DU-145 were obtained from American Type Culture Collection (ATCC). CellTiter 96® aqueous one solution cell ([3-(4,5-dimethylthiazol-2-yl)-5-(3-carboxymethoxyphenyl)-2-(4 sulfophenyl)-2H-tetrazolium, inner salt) (MTS) proliferation assay was purchased from Promega. Double stranded

deoxyribonucleic acid sodium salt from salmon testes (ds-DNA) was purchased for Sigma Aldrich and used as received.

2.2- Synthesis of PBLG-*b*-PGlu copolymer

A poly(γ-benzyl-L-glutamate)-block-poly(glutamic acid) (PBLG-*b*-Pglu) copolymer was synthesized by a modified method previously described [15]. Briefly, the synthetic approach consisted of preparing a hydrophilic PGlu derivate, which was further used as a macroinitiator for the synthesis of the hydrophobic PBLG block. The synthetic approach for the synthesis of this copolymer is shown in Figure 1.

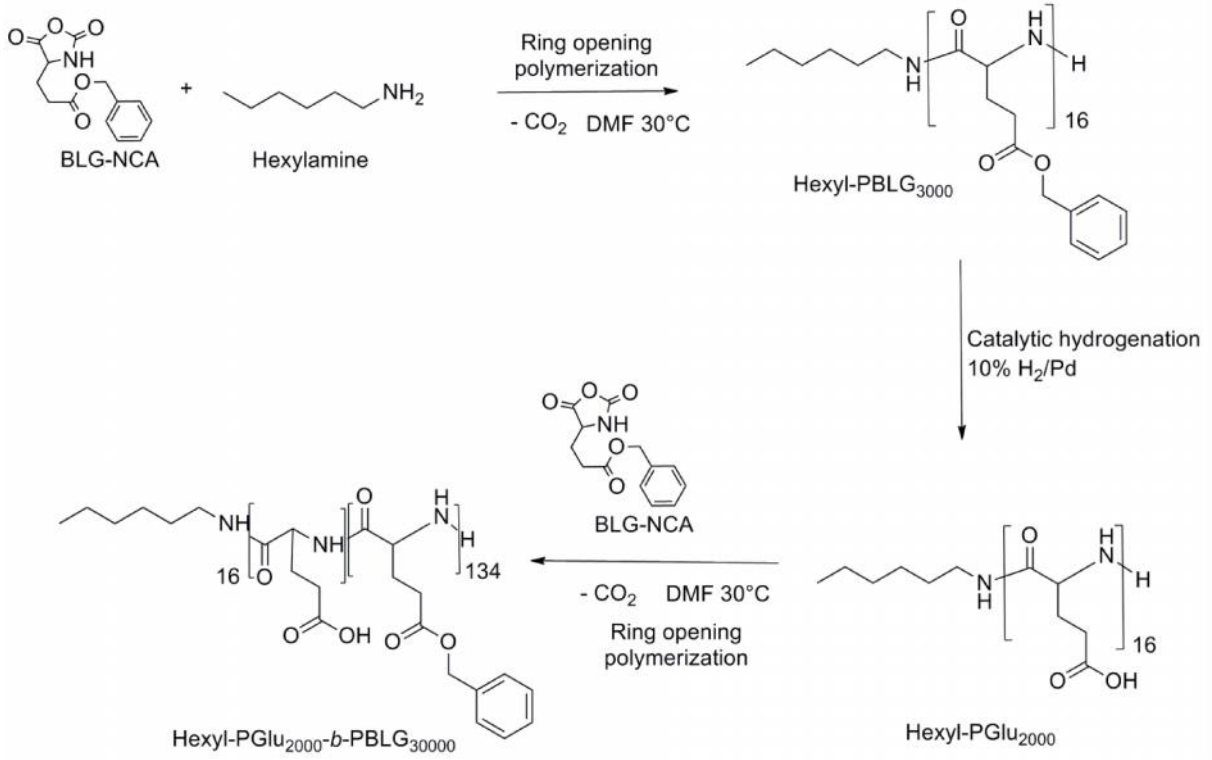

Figure 1: Synthetic scheme for PBLG-*b*-PGlu copolymer

2.2.1- Synthesis of hexyl-PBLG

Firstly, $PBLG_{3000}$ polymer was synthesized by ring opening polymerization of γ-benzyl-L-glutamate-N-carboxylic anhydride (BLG-NCA). Briefly, 3.9 g of BLG-NCA were weighed in a glove box under inert atmosphere (argon) and were dissolved in DMF at a concentration of 0.5 M. The solution was

stirred for 10 minutes and the initiator, a DMF solution of hexylamine at a concentration of 0.037 M, was added with an argon-purged syringe. The solution was stirred at 30 °C during 5 days. Then, the mixture was poured into a large excess of cold diethyl ether (DEE) and the precipitate filtered and dried under vacuum. The extent of the reaction was controlled by infrared analysis, by checking the disappearance of BLG-NCA bands and the appearance of the PBLG ones. A second purification step, dissolving the precipitate in tetrahydrofuran (THF) and reprecipitating in DEE and drying it under vacuum was made. This polymer was analyzed by proton nuclear magnetic resonance (^{1}H NMR) in $CDCl_3$ + 15 % TFA and its molecular weight could be determined in function of the relative intensities of the benzyl groups of the PBLG and of the methylene protons belonging to the hexylamine.

2.2.2- Debenzylation of hexyl-PBLG

The benzyl groups of the hexyl-PBLG polymer were eliminated by catalytic hydrogenation. Briefly, 1.6 g of hexyl-PBLG were dissolved in 27 mL of anhydrous DMF and 10 % of Pd/C was added to the solution. After purging three times with argon, the reaction mixture was stirred for 3 days at room temperature under overpressure of hydrogen (4 mbar). Then, the solution was centrifuged at 25°C, 4000 rpm for 10 minutes and was further filtered over 0.22 µm filters in order to eliminate the Pd/C (black). It was then precipitated into a large excess of DEE, filtered and the precipitate dried under vacuum at 40°C overnight. The reaction product was analyzed by ^{1}H NMR in deuterated dimethyl sulfoxide (DMSO (d_6)).

2.2.3- Ring opening polymerization of BLG-NCA using hexyl-PGlu as a macroinitiator

Secondly, synthesis of PBLG-*b*-PGlu was achieved by ring opening polymerization of BLG-NCA. Briefly, 1.8 g of BLG-NCA mg were dissolved in anhydrous DMF at a concentration of 0.5 M. The solution was stirred for 10 minutes and the initiator, a DMF solution of hexyl-PGlu at a concentration of 0.0031 M, was added with an argon-purged syringe. The solution was stirred at 30 °C during 7 days. Then, the mixture was poured into a large excess of cold DEE and the precipitate filtered and

dried over vacuum. A second purification step, involving dissolution in THF/MeOH 75/25 and reprecipitation into cold DEE, filtration and drying over vacuum was made. The evolution of the reaction was controlled by infrared analysis, by checking the disappaerance of BLG-NCA bands and the appearance of the PBLG ones. This polymer was analyzed by

^{1}H NMR in $CDCl_3$ + 15 % TFA and its molecular weight was determined by size exclusion chromatography (SEC).

2.3- Synthesis of other PBLG derivates

PBLG-bnz and PBLG-dansyl were synthesized by a ring opening polymerization of BLG-NCA in the conditions described above using benzylamine and dansylcadaverine respectively as initiators. For the PBLG-dansyl, purification also included a washing step with methanol (MeOH).

2.4- Characterization of PBLG copolymers

2.4.1- Fourier transform infrared spectroscopy (FTIR)

FTIR spectra of the polymers were performed on a Fourier Transform Perkin-Elmer 1750 spectrometer using the attenuated total reflection system (ATR) to confirm the absence of NCA auto-polymerization, to follow the evolution of the polymerization reactions and to study the secondary structure of the polymers.

2.4.2- Proton nuclear magnetic resonance (^{1}H NMR)

^{1}H NMR spectra of polymers were recorded on a Bruker AC 300 MHz spectrometer in $CDCl_3$ + 15% TFA for PBLG polymers and in deuterated dymethylsufoxide (DMSO d_6). The role of the TFA is to disrupt α-helix that PBLG polymers adopt in chloroform, rendering them in a random coil conformation [16].

2.4.3- Size exclusion chromatography (SEC)

SEC was used to determine the molecular weight of PBLG-*b*-PGlu. The SEC system was equipped with two PLgel 5µm MIXED-D (7,5mm ID x 30,0cm L) and a PLgel 5µm guard column (guard column 7,5mm ID x 5,0 cm L), a refractive index detector (Jasco 1530-RI) and a UV detector (Jasco 875-UV). DMF with 1g/L of lithium bromide (LiBr) was used as a diluent at a flow of 0.8 ml/min at 80°C and linear polystyrene samples were used as calibration standards.

2.5- Nanoparticle preparation

PBLG-*b*-PGlu nanoparticles were prepared following a novel nanoprecipitation method. Briefly,7.5 mg of the PBLG-*b*-PGlu copolymer were dissolved in THF/MeOH 75/25 at 40 °C at a concentration of 0.1 nM without magnetic stirring. Once dissolved, they were added by dripping to an aqueous solution containing two equivalents of sodium hydroxyde (NaOH) per equivalent of COOH and stirred for 10 minutes. Solvents were eliminated by a standardized protocol under vacuum in the rotavapor at 40 °C. Nanoparticles size and ζ potential were determined by dynamic light scattering (DLS) at 25 °C (Zetasizer 4, Malvern Instruments) after dialysis with a SpectraPor membrane (molecular weight cut off 3000 Da) during 24 hours to eliminate the NaOH. PBLG-*b*-PGlu nanoparticle size and ζ potential were measured before and after cisplatin association. Nanoparticles were observed by means of a Transmission Electron Microscopy (TEM) at 120 KV (MET JEOL 1400) with phosphotungstic acid as a negative coloration agent. Measurements of the longitudinal and axial radius of 100 nanoparticles were made on TEM photos using Image J.

2.6- PBLG-*b*-PGlu nanoparticle interaction with cisplatin by isothermal titration calorimetry (ITC)

Interaction of PBLG-*b*-PGlu nanoparticles with cisplatin was studied by ITC (Microcal.Inc.USA). The cell was loaded with PBLG-*b*-PGlu nanoparticles at a molar concentration of polymer of 0.042 mM and a molar concentration of COO^- groups of 0.68 mM. The nanoparticle suspension was placed in the measurement cell (approx. 1.3 mL) and stirred at 112 rpm by the syringe, which was filled with an aqueous solution of cisplatin at a concentration of 0.8 mM. The titration of PBLG-*b*-PGlu

nanoparticles involved a first injection of 5 µL followed by 27 injections of 10 µL during 20 s each 300 seconds. Experiments were carried out at 37 °C. PBLG-bnz nanoparticles, not containing COO^- groups, were used as a negative control.

2.7- Cisplatin association to PBLG nanoparticles

Cisplatin was dissolved in water at a concentration of 1 mg/mL and reacted with silver nitrate ($AgNO_3$) in a 1/1 [$AgNO_3$/CDDP] molar ratio to form the aqueous complex. The solution was kept in dark overnight at room temperature under gentle stirring. The presence of AgCl precipitates confirmed the reaction [9, 11, 17]. Next, centrifugation of the reaction mixture at 10000 rpm for 10 minutes and supernatant filtration over 0.22 µm filters was made in order to eliminate AgCl precipitates. The content of cisplatin was measured by atomic absorption spectroscopy (AAS) (Varian® SpectrAA 220Z) as detailed in Supplementary Data (SD).

A first approach consisting of encapsulating the aqueous soluble poly(glutamic acid)-cisplatin complex (PGlu-CDDP) in PBLG-bnz nanoparticles was assayed. PGlu-CDDP complex was obtained after reaction of PGlu with aqueous cisplatin at a [CDDP/ COO^-] ratio of 0.2, in dark for 48 hours at 25°C, under gentle stirring. Unreacted cisplatin was purified by a further dialysis (SpectraPor membrane, molecular weight cut off 1000 Da) during 24 hours and cisplatin content measured by AAS. Two different molecular weight of PGlu were assayed:3000 g/mol and 30000 g/mol. Next, the PGlu-CDDP complex was encapsulated in PBLG-bnz nanoparticles by the nanoprecipitation method described above, where the aqueous complex was dissolved in the aqueous phase. PBLG-bnz nanoparticles were further filtered with 1µm filter and centrifuged at 20000 rpm for 1 hour at 4°C. Cisplatin loading content was quantified by AAS as the difference between total cisplatin and remaining cisplatin in the filter and supernatant.

A second approach consisting of complexing aqueous cisplatin to the carboxylate groups of the preformed PBLG-*b*-PGlu nanoparticles was assayed. Firstly, the kinetics of the reaction of cisplatin

with PBLG-*b*-PGlu nanoparticles at a [CDDP/COO^-] ratio of 1.25 was followed over time. A purification step by dialysis with a SpectraPor membrane (molecular weight cut off 3000 Da) was performed during 24 hours. The cisplatin content in the nanoparticles was determined by AAS. Secondly, PBLG-*b*-PGlu nanoparticles at a [COO^-] of 0.86 mM were incubated under gentle stirring with the cisplatin aqueous complex solution at different [CDDP/ COO^-] feed ratios ranging from 0 to 1.56 and reacted for 60 hours in dark to form the complex between the hydrophilic chains of PGlu and CDDP. Purification and analysis were made as described above. Cisplatin-loaded PBLG-*b*-PGlu nanoparticles were prepared at a ratio [CDDP/ COO^-] = 1.25 as described above for further experiments. Drug loading content (mg of loaded cisplatin/mg of polymer * 100) and association efficiency (mg of loaded cisplatin/mg of initial cisplatin * 100) were determined by AAS and expressed in percentage.

2.8- *In vitro* cisplatin release

In vitro cisplatin release from the cisplatin-loaded PBLG-*b*-PGlu nanoparticles was studied by the dialysis method in a 0.01 M phosphate buffer saline (PBS pH 7.4) containing 0.138 M of NaCl and in distilled MilliQ water at 37 °C. Briefly, 0.950 mL of a PBLG-*b*-PGlu nanoparticle suspension at a concentration of 0.75 mg/mL and containing 0.1 % of Pluronic F 68 were introduced in the 1 mL microdialyzers and dialyzed against 15 mL of medium using dialysis membranes with a molecular weight cut off of 3500 Da. The solution outside the microdialyzers was sampled at defined periods and replaced with fresh medium. Cisplatin release was measured by AAS. Experiments were carried out by triplicate. Control release experiments with a cisplatin solution in the conditions described above were also carried out.

2.9- *In vitro* hydroxyapatite (HAP) binding assay

Multifunctional nanoparticles containing the fluorescent PBLG-dansyl polymer and the osteotropic PBLG-*b*-PGlu copolymer, loaded with cisplatin at a ratio [CDDP]/[COO^-]= 1.25 and containing 0.1 % of poloxamer (Pluronic® F68, BASF) were incubated in a HAP (0.4 g/mL) suspension in PBS at a pH

of 7.4 at 25 °C during 24 hours. The suspensions were centrifuged at 5000 rpm for 5 minutes, washed three times with poloxamer 1% in PBS 7.4 and observed under UV light at 365 nm. Supernatants were quantified by a Perkin Elmer Luminescence spectrometer LS 50B at room temperature ($\lambda_{excitation}$ =340 nm . $\lambda_{emission}$ = 472 nm) so as to determine the amount of nanoparticles not bound to HAP.

2.10- Interaction of cisplatin released from PBLG-*b*-PGlu nanoparticles with DNA

The capability of cisplatin released from nanoparticles to interact with DNA has been evidenced by electrochemistry. 2 mL of a cisplatin loaded PBLG-*b*-PGlu nanoparticle suspension at a concentration of 1.5 mg/mL were incubated in PBS (pH 7.4) during 1 week in the presence of an excess of double stranded DNA (dsDNA). A positive control was performed with a 0.2 mM cisplatin solution. Electrochemical experiments were performed at 298±1 K in a thermostated cell with a CH I660 equipment. A BAS MF2012 glassy carbon working electrode (GCE) (geometrical area 0.071 cm^2), a platinum wire auxiliary electrode and an Ag/AgCl (3M NaCl) reference electrode were used in a conventional three-electrode arrangement. 0.10 M potassium phosphate buffer (pH 7.0) and PBS (pH 7.4), deaerated by argon bubbling during 15 min, were used as supporting electrolytes.

2.11- *In vitro* cytotoxicity studies

The cytotoxic effect of free cisplatin, PBLG-*b*-PGlu nanoparticles and cisplatin-loaded PBLG-*b*-PGlu nanoparticles was studied in three different prostate cancer cell lines, PC-3, DU-145 and LNCaP by the MTS cell viability assay 48 and 72 hours after exposure. PC-3, DU-145 and LNCaP were grown in RPMI 1640 (BE 12−702 F, Lonza) supplemented with 10% (v/v) heat-inactivated fetal bovine serum (Lonza), penicillin (100 UI/mL), and streptomycin (100 µg/mL). Cells were maintained in a 95% humidified atmosphere of 5% CO2 at 37 °C. Cells were seeded in 96-well plates (5.5 10^3 cells per well) and were pre-incubated during 48 hours. Then, cisplatin, PBLG-*b*-PGlu nanoparticles and cisplatin-loaded PBLG-*b*-PGlu nanoparticles at different concentrations were added and after 48 or 72 hours 20 µL of MTS solution per well were added. Viable cells were quantified by recording the UV

absorbance at 492 nm using a plate reader multi-well scanning spectrophotometer (Labsystems Multiskan MS). Cytotoxicity was also followed by the blue trypan exclusion assay. Briefly, fresh media was replaced by trypsine 0.25 % EDTA and once cells were in suspension trypan blue was added. Cells were counted through a hemacytometer (Kova slides).

3- Results and discussion

3.1-Synthesis and characterization of PBLG polymers

Characteristic peaks were identified for hexyl-PBLG polymer in ^{1}H NMR (see SD). The degree of polymerization (DP_n) could be determined in function of the relative intensities of the benzyl groups of the PBLG and of the methylene protons belonging to the hexylamine and it was found to be 16 (see SD). The debenzylation reaction is driven to completion as confirmed by the absence of the benzyl and aromatic protons peaks (see SD). ^{1}H NMR spectrum of the PBLG-*b*-PGlu copolymer is shown below (figure 2).

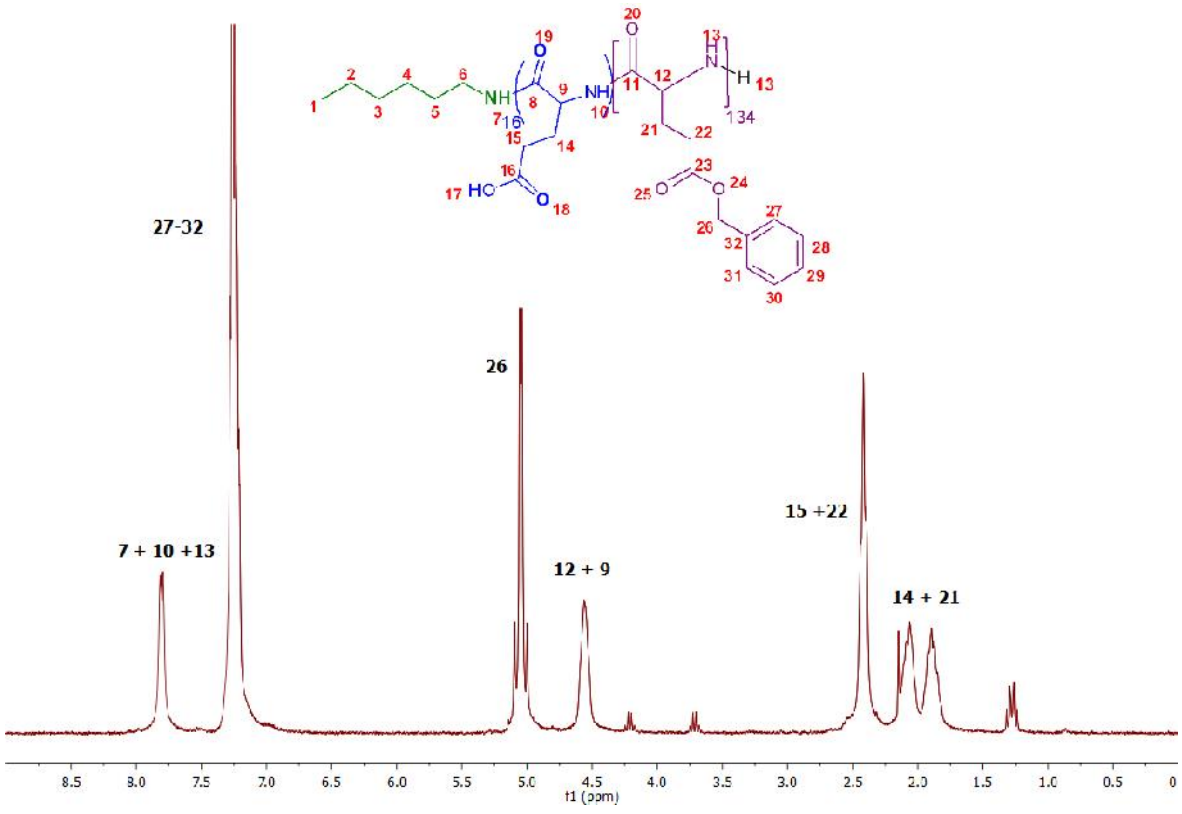

Figure 2: ^{1}H NMR spectrum of PBLG-*b*-PGlu in $CDCl_3$ + 15% TFA

Infrared study of PGlu polymer, which presented a DP_n of 16, revealed a majority of α-helices with a minor existence of β-sheets, evidenced by a shoulder at 1628 cm^{-1} (see SD). This is in coherence with the reported secondary structures for PBLG polymers with a DP_n <18 [18] and for PGlu oligomers (see SD) [19]. Carboxylic acids from PGlu were in the protonated state as evidenced by the band at 1710 cm^{-1}. PBLG-*b*-PGlu copolymer presented an α-helix structure, as shown by the amide I amide II and amide III bands at ~1655cm^{-1}, ~1550 cm^{-1} and ~1260 cm^{-1} respectively and the ester C=O band at ~1735 cm^{-1} (see SD) [20-22].

Table 1: Experimental molecular weights of the PBLG polymers determined by SEC. (a) DP_n of the PBLG block

PBLG polymers	M_n (g/mol)	PI
PBLG-*b*-PGlu	24436	1.7
PBLG-bnz	31727	1.1
PBLG-dansyl	25944	1.1

3.2- Nanoparticle preparation

The preparation of novel PBLG-*b*-PGlu nanoparticles was achieved by a new nanoprecipitation method, modified from a previously described one [20]. The use of NaOH was essential for nanoparticle preparation since it ionized the carboxylate groups of the hydrophilic PGlu block, avoiding nanoparticle aggregation. DLS measurements suggested that the nanoparticles had a hydrodynamic diameter in the range of 50 nm and a very negative ζ potential, as a result of the ionised carboxylate groups, which enhanced the nanoparticle stability. Accurate size measurements from TEM images revealed that nanoparticles presented an ellipsoidal form with an aspect ratio of 1.33 and an actual size of 37 ± 7 nm x 27 ± 6 nm, with no significant changes in the morphology and size after cisplatin coordination.

Table 2: Size and ζ potential determined by DLS of PBLG-derivate and PBLG-*b*-PGlu nanoparticles prepared at different [CDDP]/[COO^-] ratios

Nanoparticles	Size (nm) ± SD [a]	Polydispersity Index ± SD [a]	ζ Potential (meV) ± SD [a]	Drug loading content[b] (w/w%)
PBLG-bnz	57 ± 1.1	0.17 ± 0.073	-37 ± 2.5	0
PBLG-dansyl	58 ± 0.91	0.12 ± 0.0077	-45 ± 1.5	
PBLG-*b*-PGlu nanoparticles	53 ± 0.11	0.13 ± 0.010	-37 ± 2.4	0
After CDDP loading at [CDDP]/[COO^-] ratio				
0.3	52 ± 0.61	0.22 ± 0.075	-36 ± 2.5	0.36
0.5	49 ± 1.1	0.15 ± 0.049	-34 ± 0.3	0.62
0.8	49 ± 0.12	0.17 ± 0.0071	-34 ± 0.81	2.3
1.0	51 ± 0.53	0.12 ± 0.0089	-32 ± 2.2	5.3
1.2	50 ± 0.31	0.12 ± 0.0077	-35 ± 0.74	5.9
1.6	51 ± 0.33	0.15 ± 0.0084	-33 ± 1.3	8.3

[a] (n=3) [b] CDDP content determined by AAS expressed as mass of associated CDDP per mass of nanoparticles (% w/w)

Nanoparticles might exhibit a core-shell structure, where the inner hydrophobic core is formed by the stacking of quite rigid α-helices of the PBLG blocks and the outer shell by the hydrophilic PGlu chains. PGlu chain conformation is known to be dependent on pH. At acidic pH (<4.3-4.9) the side chains are protonated [23] and can adopt an α-helix conformation whereas when side chains are charged (pH>5), electrostatical repulsion between the side chains induces a random coil conformation [24-26]. The pH of nanoparticle suspensions was 7.9, above the pK for PGlu and thus carboxylate groups were ionized, which avoided nanoparticle aggregation. Therefore, PGlu should adopt a random coil conformation and should be forming the outer hydrophilic flexible shell. Metal interactions can have a significant impact on the secondary structures of PGlu [27]. Cisplatin coordination to the COO^-

groups could lead to an enhancement of the α-helical conformation, as it has been previously reported for other metals [28]. However, infrared spectroscopy and circular dichroism studies showed an α-helical conformation, with absence of random coils. Further studies should be necessary to fully understand the conformation adopted by the PGlu block in the PBLG-*b*-PGlu copolymer and nanoparticles and the influence of pH and cisplatin coordination.

3.3- Cisplatin association to PBLG nanoparticles

Once PBLG-*b*-PGlu colloidal suspensions were obtained, cisplatin was associated to the preformed PBLG-*b*-PGlu nanoparticles through incubation with an aqueous cisplatin solution, which is most appropriate for complex formation due to better leaving group properties of hydroxide/water molecules compared to chloride ions.

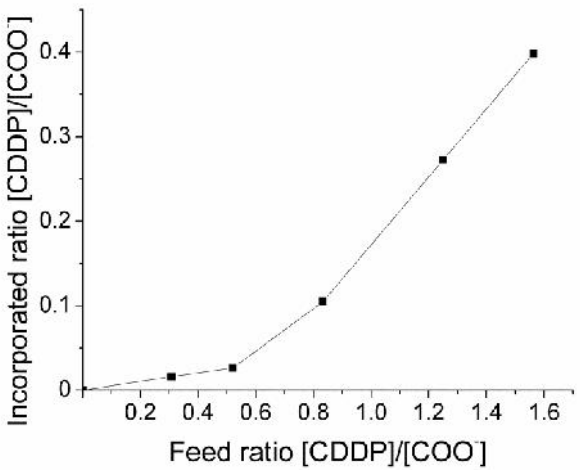

Figure 3: [CDDP]/[COO^-] incorporated ratio to the PBLG-*b*-PGlu nanoparticles at different [CDDP]/[COO^-] feed ratios.

DLS measurements showed that nanoparticles size remained constant (~50 nm) before and after cisplatin association. As shown in figure 3, the incorporated ratio increased almost linearly when the [CDDP]/[COO^-] feed ratio increased from 0.6 to 1.6, suggesting no saturation in this range of concentration ratios. It can be estimated that the core-shell structure was maintained for cisplatin-

loaded PBLG-*b*-PGlu nanoparticles, since remaining negative electric charges could still exist on the PGlu chains after cisplatin coordination as shown by figure 3.

However, shell cross-linking could be foreseen considering that cisplatin can bind up to two COO^- groups born by two adjacent PGlu chains. Cisplatin can form complexes with poly(carboxylates) groups where one or two carboxylates could be complexed to cisplatin. The 1.25 [CDDP]/[COO^-] feed ratio was chosen for further experiments where the [CDDP]/[COO^-] incorporated ratio was of 0.27, which was considered to be a good balance between cisplatin loading and nanoparticle stability. At the 0.27 incorporated ratio, free COO^- groups which are not coordinated to cisplatin remained ionized and enhanced the colloidal stability of nanoparticle suspension.

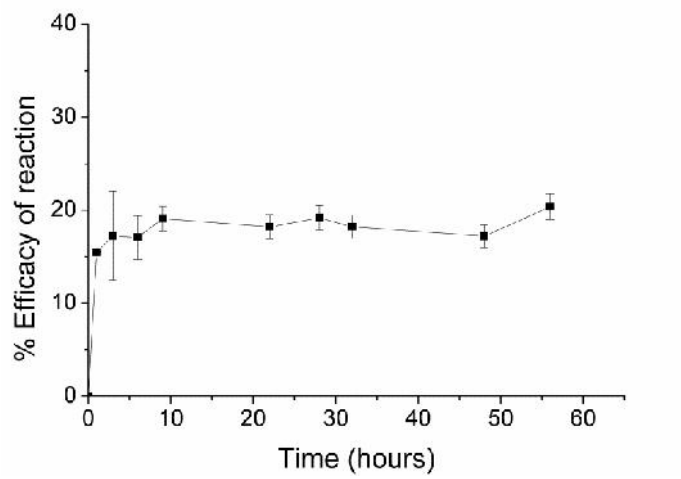

Figure 4: Kinetics of the reaction of PBLG-*b*-PGlu nanoparticles with aqueous cisplatin at a [CDDP]/[COO^-] ratio of 1.25.

Therefore, nanoparticle suspensions were stable for a prolonged period of time (up to several months) and did not exhibit aggregation or precipitation behaviour. The kinetics of the reaction of the carboxylates on the outer shell of the PBLG-*b*-PGlu nanoparticles and aqueous cisplatin was followed (figure 4). Although usual reaction times to form cisplatin-polycarboxylate complex have been reported as 24 hours [30], 48 hours and 72 hours (for cisplatin-P(Asp or Glu)-PEG micelles whose formation is driven by the formation of cisplatin-polymer complexes), reaction of PBLG-*b*-PGlu

nanoparticles with aqueous cisplatin was much more rapid and was almost completed in few hours. These results are in coherence with the reaction kinetics of cisplatin with PEG-P(Asp) copolymer shown for similar poly(glutamic acid) chain lengths [12].

3.4- PBLG-*b*-PGlu nanoparticle interaction with cisplatin by ITC

ITC experiments were conducted to study the interaction between PBLG-*b*-PGlu nanoparticles and cisplatin.

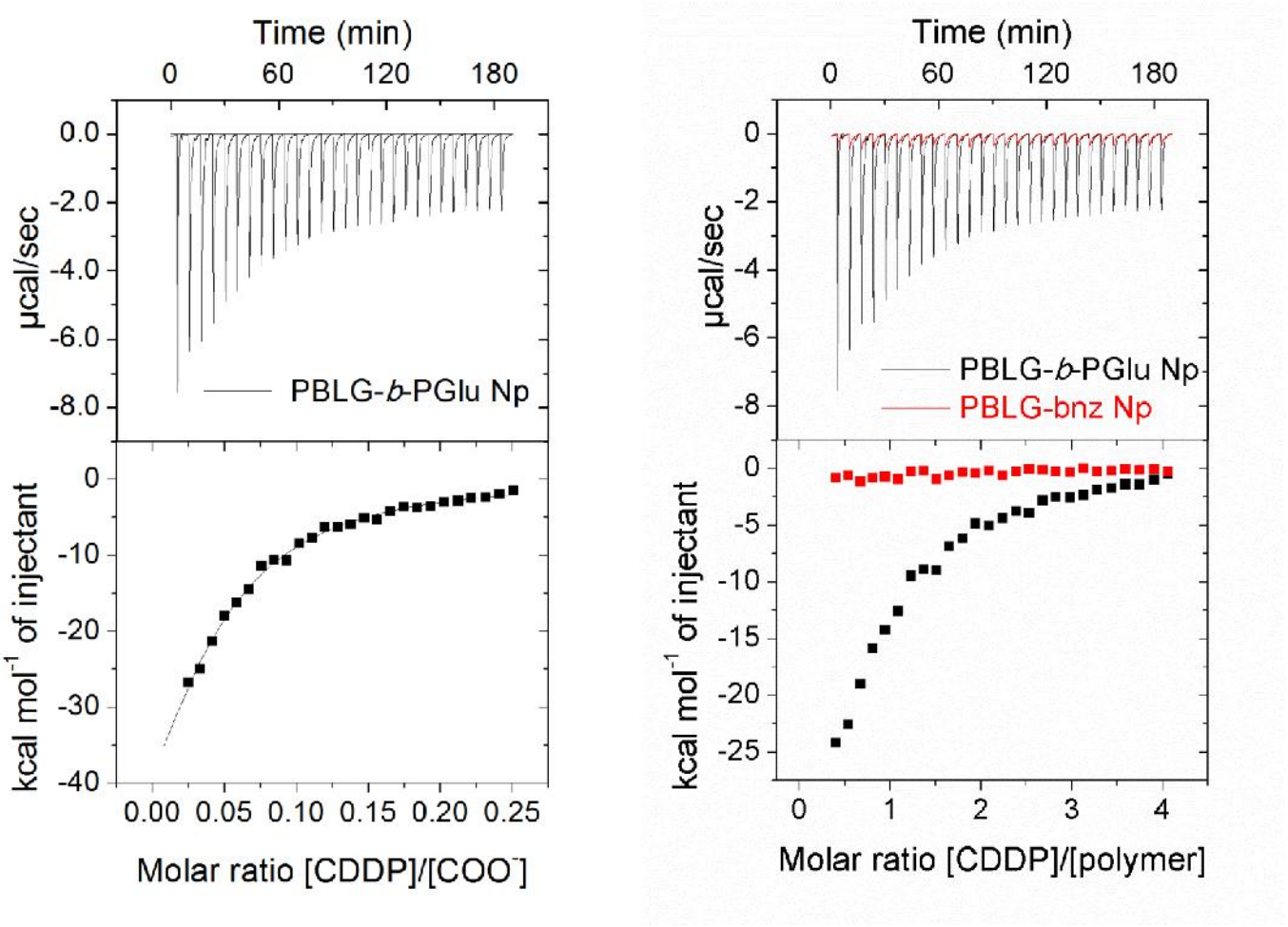

Figure 5: Typical ITC raw data and integrated heat data profiles obtained from the interaction of cisplatin at 0.8 mM with PBLG-*b*-PGlu nanoparticles at [COO^-] of 0.68 mM and compared to the negative control PBLG-bnz nanoparticles.

As shown in figure 5, an interaction that did not exist for control PBLG-bnz nanoparticles, which could be considered as the core of the PBLG-*b*-PGlu nanoparticles, was found. The effect of the 1.5 %

of NaOH used for nanoparticle preparation was checked and was found to be negligible. Heats measured during ITC experiments are the sum of different processes implied during cisplatin association to nanoparticles, including possible polymer conformation changes [31].

Cisplatin contains two chloride ligands that can be replaced by the carboxylate groups belonging to the PBLG-*b*-PGlu nanoparticle shells. At low [CDDP]/[COO^-] ratios, as in the conditions of the experiment, a stoichiometry of two COO^- per CDDP could be favoured. Carboxylate-metal complexes could occur between cisplatin and carboxylate groups belonging to the same or an adjacent PGlu chain, inducing conformational changes that could induce heat variations. Therefore, the heat measured included both cisplatin binding to the carboxylate groups and possible conformation changes of the PGlu chains induced by it.

3.5- Cisplatin loading content

Since cisplatin is a water soluble and hydrophilic molecule, direct cisplatin encapsulation into the PBLG nanoparticles was not assayed. PBLG-*b*-PGlu complex encapsulation in PBLG-bnz nanoparticles using two different molecular weights of PGlu, 3000 g/mol and 30000 g/mol, was found to be negligible, with drug loadings of 0.066 ± 0.11 % and of 0.18 ± 0.30 % respectively and drug encapsulation efficiencies of 1.9 ± 3.4 % and 6.4 ± 9.8 %. Since PGlu has a polypeptide backbone as the nanoparticle forming PBLG-bnz polymer, interactions between these two similar chains could have been expected. However, this was not the case. As explained above, the approach implying the complexation of cisplatin to the carboxylate groups of preformed PBLG-*b*-PGlu nanoparticles was much more successful and revealed to be simple in view of scaling up the preparation process. The initial ratio [CDDP/COO^-] was adjusted to 1.25 to have an optimal balance between stability and cisplatin association. In these conditions, drug loading content was found to be 6.2 ± 0.23 % with a drug association efficacy of 16 ± 0.58 %.

3.6- *In vitro* cisplatin release

Cisplatin release was triggered by chloride ions. In presence of chloride ions, cisplatin-loaded PBLG-*b*-PGlu nanoparticles released cisplatin in a sustained manner with a remarkable absence of initial burst under physiological conditions (figure 6). The absence of a burst effect suggests that cisplatin was mainly associated to nanoparticles through complexation to the carboxylate groups and not physically entrapped. An almost linear release profile was obtained suggesting an almost zero order kinetics on the whole range. Remarkably, cisplatin was completely released from the PBLG-*b*-PGlu nanoparticles, more than 90 % was released after 14 days. Cisplatin release from nanoparticles was slow; less than 10 % and 50% of cisplatin was released after 24 hours and 7 days respectively. It is striking to compare cisplatin association and release kinetics from the PBLG-*b*-PGlu nanoparticles, the latter being much slower. These differences can be attributed to the fact that cisplatin association to PGlu and cisplatin release in presence of chloride ions are two distinct chemical reactions.

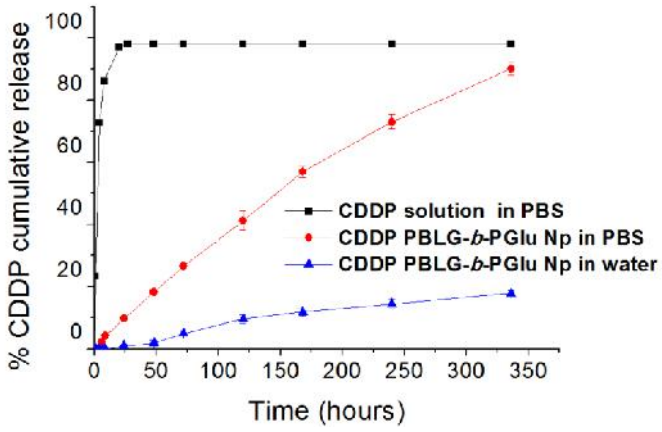

Figure 6: *In vitro* cisplatin release from a cisplatin solution and from cisplatin-loaded PBLG-*b*-PGlu nanoparticles in 0.01 M PBS (pH 7.4) containing 0.138 M of NaCl and in water.

As previously reported in the literature, the presence of chloride ions is essential for cisplatin release due to a ligand exchange reaction where chloride ions would substitute the Glu residues from the PBLG-*b*-PGlu nanoparticle, due to good leaving properties of Glu residues [12]. Other ions such as

acetates or phosphates can also play a minor role in the release of cisplatin. An enhanced cisplatin release from carboxylate complex at mild acidic pH involving the protons has also been reported [32]. However, contrarily to what has been previously described in the literature for cisplatin-carboxylate complexes [9, 11, 17] and cisplatin-loaded micelles [12, 13], release of cisplatin in distilled water medium did take place, although it was considerably reduced, since less than 2 % and only 20 % of the initial dose was released after 48 hours and 14 days respectively.

3.7- *In vitro* HAP binding assay

An *in vitro* HAP binding assay showed a total binding for cisplatin-loaded PBLG-*b*-PGlu and fluorescently labelled (33% of PBLG-dansyl and 66% of PBLG-*b*-PGlu) nanoparticles (figure 7). HAP binding property was driven by the PGlu block polymer and not by the PBLG or dansyl moiety as evidenced by the absence of binding of the negative control PBLG-dansyl nanoparticles.

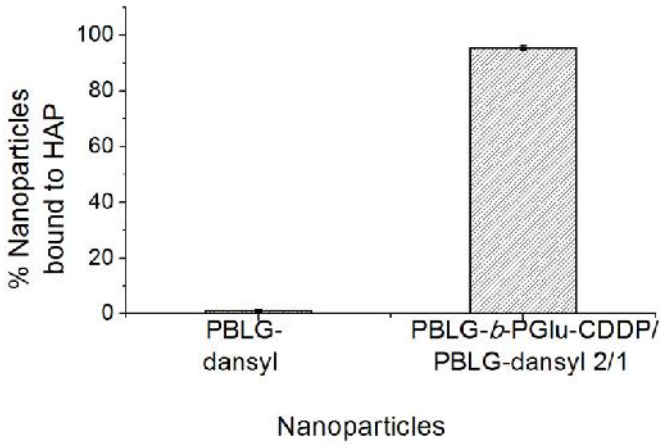

Figure 7: Degree of HAP binding expressed in percentage of nanoparticles bound to HAP. PBLG-dansyl nanoparticles and cisplatin-loaded PBLG-*b*-PGlu/PBLG-dansyl nanoparticles at a concentration of 1.5 mg/mL in 0.1 % poloxamer were incubated with 0.4 g of HAP suspension in PBS during 1 hour.

Indeed, oligomers of glutamic acid have been shown to have both *in vitro* and *in vivo* affinity to bone matrix and HAP respectively [33] and it has been used to provide drugs with osteotropic properties [34]. In the case of cisplatin-loaded PBLG-*b*-PGlu nanoparticles, the complexation of cisplatin to

carboxylate groups at a [CDDP]/[COO^-] ratio of 1.25 did not affect their bone binding properties, likely due to the free carboxylate groups remaining available for interactions. Besides, cisplatin could also be involved in HAP binding [35].

3.8- Interaction of cisplatin released from PBLG-*b*-PGlu nanoparticles with DNA

Adduct formation between DNA and platinum derivates is responsible for their cytotoxic activity. An electrochemical technique has been used in order to assess the capability of platinum species to interact with DNA after being progressively released from cisplatin-loaded PBLG-*b*-PGlu nanoparticles. Indeed, electrochemical detection techniques can be conveniently used to monitor cisplatin interactions with DNA [36]. Voltammograms for cisplatin-loaded PBLG-*b*-PGlu nanoparticles incubated with PBS in presence and absence of a DNA solution were different (figure 8).

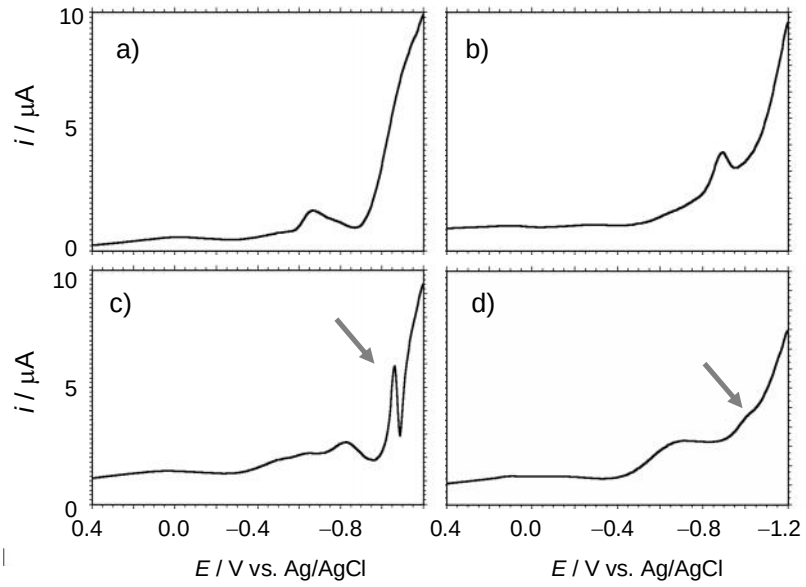

Figure 8: Square wave voltammetry (SWVs) for a) cisplatin solutions in phosphate buffer (pH 7.0); b) cisplatin-loaded PBLG-*b*-PGlu nanoparticles in phosphate buffer; c) free cisplatin diluted in PBS (pH 7.4) and incubated with DNA for 24 hours d) cisplatin loaded PBLG-*b*-PGlu nanoparticles previously incubated in PBS for 5 days and with DNA for 24 hours. Potential scan initiated at +0.4 V in the negative

direction; potential step increment 4 mV; square wave amplitude 25 mV; frequency 5 Hz. Arrows indicate the DNA-bound cisplatin signal.

The response of free cisplatin with DNA in phosphate buffer was performed as a positive control. The voltammograms in figure 8 showed intense peaks at -1.10 V, corresponding to the interaction of free cisplatin with DNA. The peak observed at -0.45 V in the case of free cisplatin (figure 8a and 8b) could be attributed to the adsorption of cisplatin to the electrode surface. Further voltamogramms in figure 8c and 8d suggested that the cisplatin released from the cisplatin-loaded PBLG-*b*-PGlu nanoparticles during PBS incubation was able to interact with the DNA strands similarly to free cisplatin.

3.9- *In vitro* cytotoxicity assay

The *in vitro* cytotoxic activity of cisplatin-loaded PBLG-*b*-PGlu nanoparticles has been determined in three different prostate cancer cell lines that have the potential to metastasize to bone [14]. As inferred from figure 9, which corresponds to the MTS assay, PBLG-*b*-PGlu nanoparticles exhibited no or very low toxicity for PC-3 and DU 145 cell lines whereas for LNCaP cell line they were not toxic under 25 μM. The MTS assay revealed a dose-dependent response on all three cell lines. Lower cytotoxicity was observed for cisplatin-loaded PBLG-*b*-PGlu nanoparticles than for free cisplatin, which was also confirmed by the blue trypan assay (see SD). This might be related to the fact that cisplatin is coordinated to PBLG-*b*-PGlu nanoparticles and is slowly released. This lower cytotoxicity has already been reported for other cisplatin carboxylate coordination complexes within a wide range of cancer cell lines. Therein, their IC_{50} values were between 6-15 times higher than those of free cisplatin, this low toxicity not compromising the antitumour activity [11, 28]. Cytotoxicity of cisplatin-loaded PBLG-*b*-PGlu nanoparticles appeared to be enhanced with time as suggested by the 48 and 72 hours IC_{50} values. This suggests an elapsed time for nanoparticles to be cytotoxic either through cell internalisation or cisplatin release in the vicinity. Once distributed to bone and due to the bone binding properties of the PGlu ligand, nanoparticles could remain in the bone tumour vicinity, and thus they

could constitute drug reservoirs for sustained cisplatin release for the treatment of skeletal malignancies.

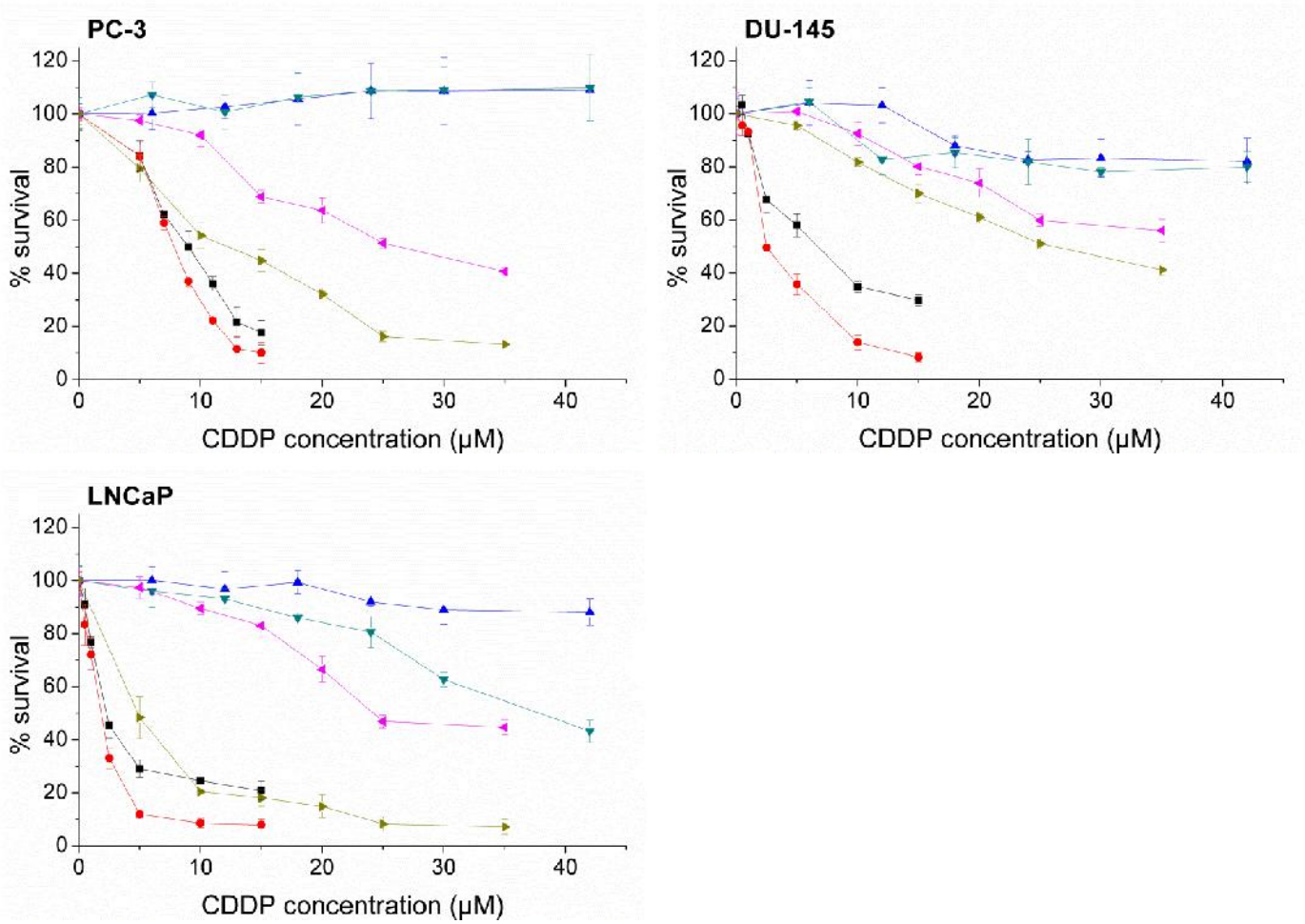

Figure 9: *In vitro* cytotoxicity profiles of free cisplatin, cisplatin-loaded PBLG-*b*-PGlu nanoparticles and PBLG-*b*-PGlu nanoparticles after 48 and 72 hours after exposure determined by the MTS assay. ■cisplatin 48 hours; ● cisplatin 72 hours; ▲ PBLG-*b*-PGlu np 48 hours; ▼ PBLG-*b*-PGlu np 72 hours; ◄ PBLG-*b*-PGlu -CDDP np 48 hours; ► PBLG-*b*-PGlu-CDDP np 72 hours.

Table 3: IC_{50} values for free cisplatin and cisplatin-loaded PBLG-*b*-PGlu nanoparticles after 48 and 72 hours after exposure determined by the MTS assay

Cell line		IC_{50} (µM) 48 hours	IC_{50} (µM) 72 hours
PC-3	Cisplatin	8,7	7,8
	Cisplatin-PBLG-*b*-PGlu np	25	13
DU-145	Cisplatin	5,8	2,6
	Cisplatin-PBLG-*b*-PGlu np	>35	26
LNCaP	Cisplatin	2,3	1,7
	Cisplatin-PBLG-*b*-PGlu np	24	4,8

4- Conclusion

We report the synthesis of novel PBLG-*b*-PGlu nanoparticles with the dual functionality of bone targeting and efficient cisplatin loading and controlled release. PBLG-*b*-PGlu nanoparticles could complex high cisplatin payloads (6.2 % w/w) without affecting stability and released it in a very sustained way, triggered by chloride ions, in order to produce cytotoxic effects in three different prostate cancer cell lines that could potentially metastasize to bone.

Simultaneously, cisplatin-loaded PBLG-*b*-PGlu nanoparticles showed very efficient hydroxyapatite binding suggesting potential for *in vivo* bone targeting. Therefore, *in vivo* drug residence time into or in the vicinity of the bone tumour could be potentially enhanced. Favourably, sustained cisplatin release from these nanoparticles may help to prolong cytotoxic effects, making them promising carriers for the treatment of bone metastases derived from prostate cancers.

Acknowledgements

This work has benefited from the facilities and expertise of the Platform for Transmission Electronic Microscopy of IMAGIF (Centre de Recherche de Gif - www.imagif.cnrs.fr). We gratefully

acknowledge the european postgraduate program from "Ibercaja Foundation" for the financial support. We thank Dr Silvia Mazzaferro for the SEC analyses.

References

[1] R. Siegel, D. Naishadham, A. Jemal, Cancer statistics, 2012, CA. Cancer J. Clin., 62 10-29.

[2] R.E. Coleman, Metastatic bone disease: clinical features, pathophysiology and treatment strategies, Cancer Treat. Rev., 27 (2001) 165-176.

[3] B. Desoize, C. Madoulet, Particular aspects of platinum compounds used at present in cancer treatment, Crit. Rev. Oncol. Hematol., 42 (2002) 317-325.

[4] V. Pinzani, F. Bressolle, I. Johanne Haug, M. Galtier, J.P. Blayac, P. Balmès, Cisplatin-induced renal toxicity and toxicity-modulating strategies: a review, Cancer Chemother. Pharmacol., 35 (1994) 1-9.

[5] F.P. Harmers, W.H. Gispen, J.P. Neijt, Neurotoxic side-effects of cisplatin, Eur. J. Cancer, 27 (1991) 372-376.

[6] R.F. Ozols, Ovarian cancer: new clinical approaches, Cancer Treat. Rev., 18 Suppl A (1991) 77-83.

[7] G. Giaccone, Clinical perspectives on platinum resistance, Drugs, 59 (2000) 9-17.

[8] M. Galanski, B.K. Keppler, Searching for the magic bullet: anticancer platinum drugs which can be accumulated or activated in the tumor tissue, Anticancer Agents Med. Chem., 7 (2007) 55-73.

[9] W. Zhu, Y. Li, L. Liu, W. Zhang, Y. Chen, F. Xi, Biamphiphilic triblock copolymer micelles as a multifunctional platform for anticancer drug delivery, Journal of Biomedical Materials Research Part A, 96A 330-340.

[10] E. Gianasi, M. Wasil, E.G. Evagorou, A. Keddle, G. Wilson, R. Duncan, HPMA copolymer platinates as novel antitumour agents: in vitro properties, pharmacokinetics and antitumour activity in vivo, Eur. J. Cancer, 35 (1999) 994-1002.

[11] H. Ye, L. Jin, R. Hu, Z. Yi, J. Li, Y. Wu, X. Xi, Z. Wu, Poly(gamma-L-glutamic acid) cisplatin conjugate effectively inhibits human breast tumor xenografted in nude mice, Biomaterials, 27 (2006) 5958-5965.

[12] N. Nishiyama, M. Yokoyama, T. Aoyagi, T. Okano, Y. Sakurai, K. Kataoka, Preparation and characterization of self-assembled polymer metal complex micelle from cis-dichlorodiammineplatinum(II) and poly(ethylene glycol)-poly(L-aspartic acid) block copolymer in an aqueous medium, Langmuir, 15 (1998) 377-383.

[13] N. Nishiyama, K. Kataoka, Preparation and characterization of size-controlled polymeric micelle containing cis-dichlorodiammineplatinum(II) in the core, J Control Release, 74 (2001) 83-94.

[14] H. Yonou, T. Yokose, T. Kamijo, N. Kanomata, T. Hasebe, K. Nagai, T. Hatano, Y. Ogawa, A. Ochiai, Establishment of a novel species- and tissue-specific metastasis model of human prostate cancer in humanized non-obese diabetic/severe combined immunodeficient mice engrafted with human adult lung and bone, Cancer Res., 61 (2001) 2177-2182.

[15] N. Higashi, T. Koga, M. Niwa, Helical superstructures from a poly(γ-benzyl-l-glutamate)−poly(l-glutamic acid) amphiphilic diblock copolymer: monolayer formation on water and its specific binding of amino acids, Langmuir, 16 (2000) 3482-3486.

[16] J.S. Crespo, S. Lecommandoux, R. Borsali, H.A. Klok, V. Soldi, Small-angle neutron scattering from diblock copolymer poly(styrene-d_8)-b-poly(γ-benzyl l-glutamate) solutions: rod−coil to coil−coil transition, Macromolecules, 36 (2003) 1253-1256.

[17] Z. Feng, Y. Lai, H. Ye, J. Huang, X.G. Xi, Z. Wu, Poly (gamma, L-glutamic acid)-cisplatin bioconjugate exhibits potent antitumor activity with low toxicity: a comparative study with clinically used platinum derivatives, Cancer Sci., 101 2476-2482.

[18] P. Papadopoulos, G. Floudas, H.A. Klok, I. Schnell, T. Pakula, Self-assembly and dynamics of poly(gamma-benzyl-l-glutamate) peptides, Biomacromolecules, 5 (2004) 81-91.

[19] M. Rinaudo, A. Domard, Circular dichroism studies on alpha-L-glutamic acid oligomers in solution, J. Am. Chem. Soc, 98 (1976) 6360-6364.

[20] M.E.M. Barbosa, V. Montembault, S. Cammas-Marion, G. Ponchel, L. Fontaine, Synthesis and characterization of novel poly(γ-benzyl-L-glutamate) derivatives tailored for the preparation of nanoparticles of pharmaceutical interest, Polym. Int., 56 (2007) 317-324.

[21] F. Segura-Sanchez, V. Montembault, L. Fontaine, M.E. Martinez-Barbosa, K. Bouchemal, G. Ponchel, Synthesis and characterization of functionalized poly(gamma-benzyl-L-glutamate) derivates and corresponding nanoparticles preparation and characterization, Int J Pharm, 387 (2010) 244-252.

[22] T. Buffeteau, E. Le Calvez, S. Castano, B. Desbat, D. Blaudez, J. Dufourcq, Anisotropic optical constants of α-helix and β-sheet secondary structures in the infrared J. Phys. Chem. B, 104 (2000) 4537-4544.

[23] S. Nilsson, W. Zhang, Helix-coil transition of a titrating polyelectrolyte analyzed within the Poisson-Boltzmann cell model: effects of pH and salt concentration, Macromolecules, 23 (1990) 5234-5239.

[24] D.S. Olander, A. Holtzer, Stability of the polyglutamic acid alpha helix, J. Am. Chem. Soc, 90 (1968) 4549-4560.

[25] A. Holtzer, R.B. Hawkins, The state of aggregation of α-helical poly(l-glutamic acid) in aqueous salt solutions, J. Am. Chem. Soc, 118 (1996) 4220-4221.

[26] T. Kimura, S. Takahashi, S. Akiyama, T. Uzawa, K. Ishimori, I. Morishima, Direct Observation of the Multistep Helix Formation of Poly-l-glutamic Acids, J. Am. Chem. Soc, 124 (2002) 11596-11597.

[27] D. Bhattacharyya, J.A. Hestekin, P. Brushaber, L. Cullen, L.G. Bachas, S.K. Sikdar, Novel poly-glutamic acid functionalized microfiltration membranes for sorption of heavy metals at high capacity, J. Membr. Sci., 141 (1998) 121-135.

[28] Y. Wang, Y.C. Chang, Synthesis and conformational transition of surface-tethered polypeptide: poly(l-lysine), Macromolecules, 36 (2003) 6511-6518.

[29] H. Uchino, Y. Matsumura, T. Negishi, F. Koizumi, T. Hayashi, T. Honda, N. Nishiyama, K. Kataoka, S. Naito, T. Kakizoe, Cisplatin-incorporating polymeric micelles (NC-6004) can reduce nephrotoxicity and neurotoxicity of cisplatin in rats, Br. J. Cancer, 93 (2005) 678-687.

[30] B. Schlechter, A. Neumann, M. Wilchek, R. Arnon, Soluble polymers as carriers of cis-platinum, J. Control. Release, 10 (1989) 75-87.

[31] P.Y. Chou, H.A. Scheraga, Calorimetric measurement of enthalpy change in the isothermal helix–coil transition of poly-L-lysine in aqueous solution, Biopolymers, 10 (1971) 657-680.

[32] A. Vonarbourg, C. Passirani, P. Saulnier, J.-P. Benoit, Parameters influencing the stealthiness of colloidal drug delivery systems, Biomaterials, 27 (2006) 4356-4373.

[33] T. Sekido, N. Sakura, Y. Higashi, K. Miya, Y. Nitta, M. Nomura, H. Sawanishi, K. Morito, Y. Masamune, S. Kasugai, K. Yokogawa, K.-I. Miyamoto, Novel drug delivery system to bone using acidic oligopeptide: pharmacokinetic characteristics and pharmacological potential, J. Drug Targeting, 9 (2001) 111-121.

[34] J. Ishizaki, Y. Waki, T. Takahashi-Nishioka, K. Yokogawa, K.-i. Miyamoto, Selective drug delivery to bone using acidic oligopeptides, J. Bone Miner. Metab., 27 (2009) 1-8.

[35] A. Barroug, M.J. Glimcher, Hydroxyapatite crystals as a local delivery system for cisplatin: adsorption and release of cisplatin in vitro, J. Orthop. Res., 20 (2002) 274-280.

[36] S. Krizkova, V. Adam, J. Petrlova, O. Zitka, K. Stejskal, J. Zehnalek, B. Sures, L. Trnkova, M. Beklova, R. Kizek, A suggestion of electrochemical biosensor for study of platinum(II)-DNA interactions, Electroanalysis, 19 (2007) 331-338.

Supplementary data

OSTEOTROPIC POLY(γ- BENZYL-L-GLUTAMATE) CO POLY(GLUTAMIC ACID) NANOPARTICLES FOR CISPLATIN DELIVERY

Laura de Miguel[1], Iuliana Popa[1], Magali Noiray[1], Eric Caudron[2,3], Ludovica Arpinati[1], Didier Desmaele[1], Gerardo Cebrián-Torrejón[4], Antonio Doménech-Carbó[4] and Gilles Ponchel*[1].

[1] Institut Galien Paris-Sud, Paris-Sud University, Chatenay-Malabry, France, CNRS, UMR 8612, , 5 rue Jean Baptiste Clément, Chatenay-Malabry, France

[2] Hôpital Européen Georges Pompidou (AP-HP), Service de Pharmacie, Paris, France

[3] Paris Sud Analytical Chemistry Group, School of Pharmacy, Paris-Sud University, 5 rue Jean Baptiste Clément, Châtenay-Malabry, France

[4] Departament de Química Analítica, Facultat de Química, Universitat de València, Dr. Moliner 50, 46100 Burjassot, Valencia, Spain

*Corresponding author: Gilles Ponchel, Univ. Paris Sud, UMR CNRS 8612, Institut Galien, 92296 Châtenay-Malabry Cedex, France. E-mail: gilles.ponchel@u-psud.fr

1. ^{1}H NMR spectra of polymers

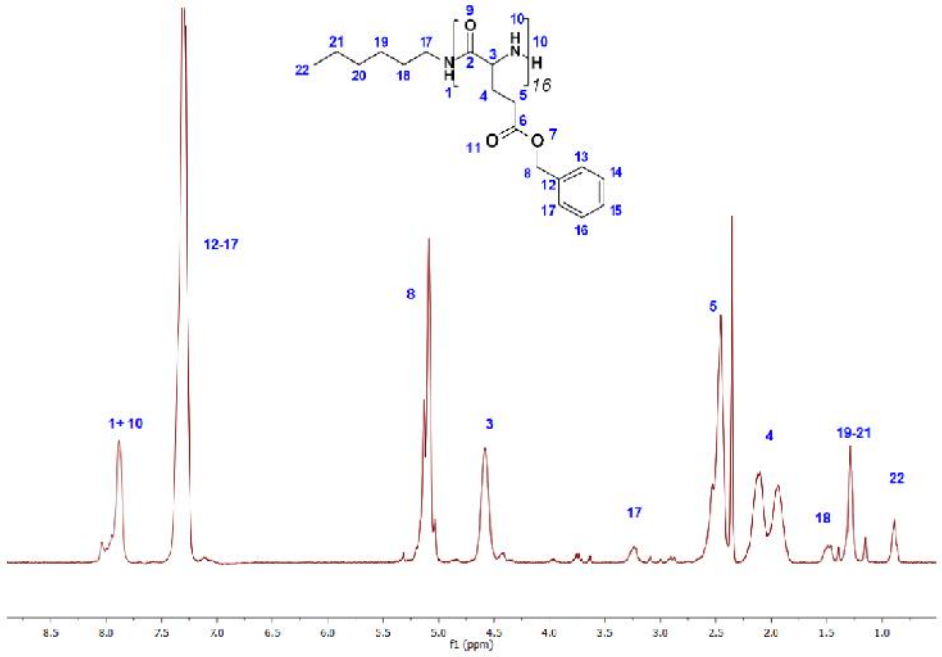

Figure 1: ^{1}H NMR spectrum of hexyl-PBLG polymer

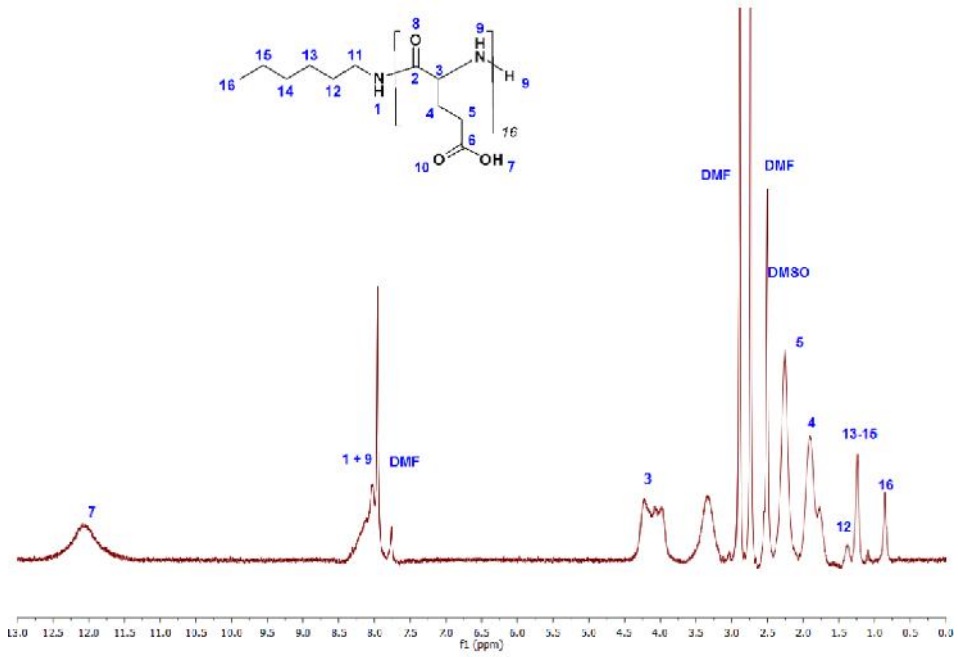

Figure 2:^{1}H NMR spectrum of hexyl-PGlu polymer

2. FTIR spectra of polymers

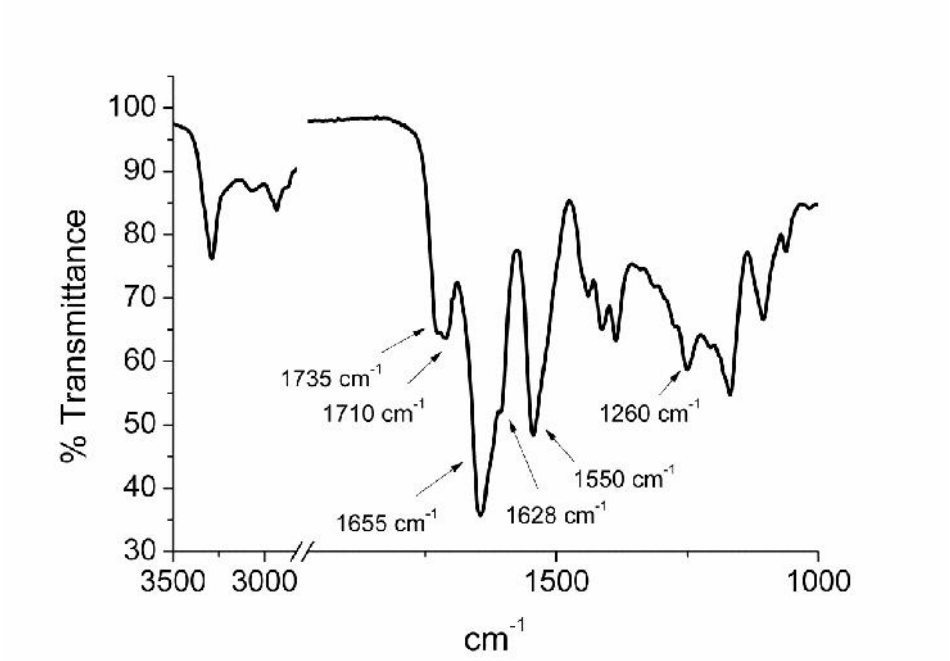

Figure 3: FTIR spectrum of solid-state hexyl-PGlu polymer

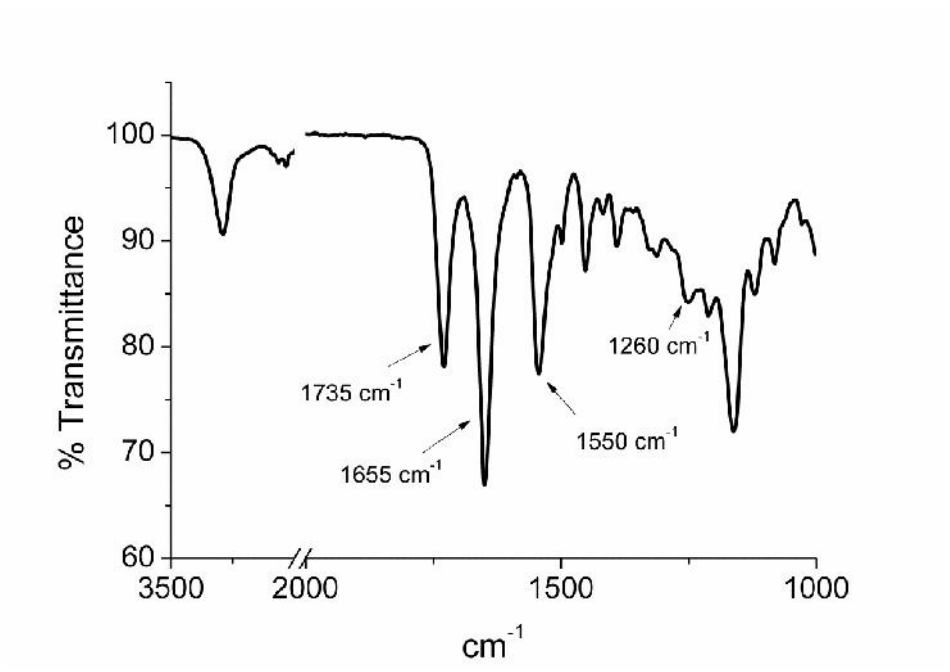

Figure 4: FTIR spectrum of solid-state PBLG-*b*-PGlu copolymer

3. TEM images of PBLG-*b*-PGlu nanoparticles

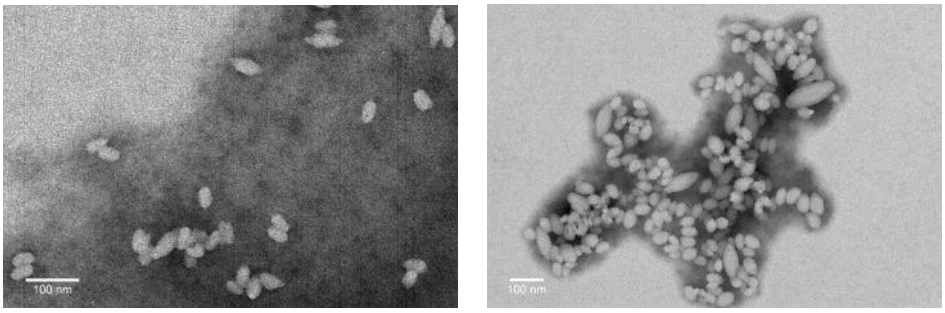

Figure 5: TEM images at 120 kV of PBLG-*b*-PGlu nanoparticles using 1% phosphotungstic acid as negative coloration; left: before cisplatin loading; right: after cisplatin loading

4. AAS for cisplatin determination

Table 1: Detailed procedure of the GFAAS heating program

Step	Furnace Temperature(°C)	Ramp Time (s)	Hold Time (s)	Internal Gas Flow ($L.min^{-1}$)	
1	40	0	0.1	3	Drying
2	120	55	0	3	
3	600	10	5	3	
4	1300	5	5	3	Ashing
5	1300	0	0.5	0	
6	2700	0.9	2	0	Atomizing
7	2850	1	0	3	Cleaning
8	40	22	0	3	

The instrument used for AAS was a Varian® SpectrAA graphic furnace AA spectrophotometer (model 200Z) (GFAAS) (Australia) with Zeeman background correction and equipped with an

adapted autosampler, an ultrAA® platinum lamp and a pyrolytically coated graphite tube (Varian® partition tubes (coated)-GTA). A platinum hollow-cathode lamp was used as radiation source at 265.9 nm with a slit width of 0.5 nm. Lamp current was set at 10.0 mA. Volume of automatic sample injection was 20 µL; internal Ar flow rate was 3 $L.min^{-1}$ and was stopped during atomizing. Details of the GFAAS heating program are listed in table 1.

5. Blue trypan exclusion assay

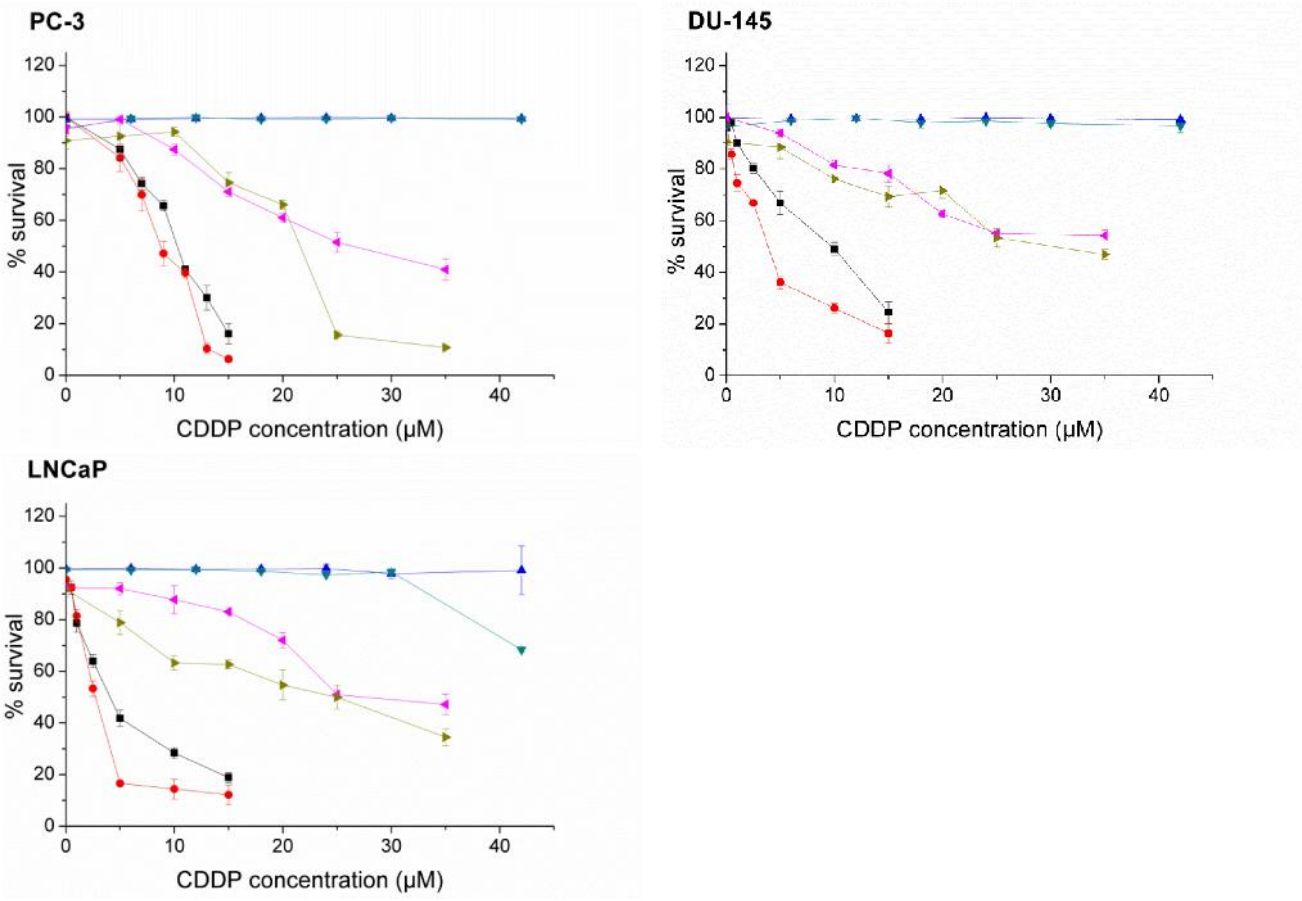

Figure 6: *In vitro* cytotoxicity profiles obtained by the blue trypan exclusion assay of free cisplatin, cisplatin-loaded PBLG-*b*-PGlu nanoparticles and PBLG-*b*-PGlu nanoparticles after 48 and 72 hours after exposure determined by the MTS assay. ■cisplatin 48 hours; ● cisplatin 72 hours; ▲ PBLG-*b*-PGlu np 48 hours; ▼ PBLG-*b*-PGlu np 72 hours; ◄ PBLG-*b*-PGlu-CDDP np 48 hours; ► PBLG-*b*-PGlu-CDDP np 72 hours.

CHAPITRE IV:

BONE TARGETED

CISPLATIN-COMPLEXED

PBLG-PGLU NANOPARTICLES:

AN ELECTROCHEMICAL APPROACH

BONE TARGETED CISPLATIN-COMPLEXED PBLG-*b*-PGLU NANOPARTICLES: AN ELECTROCHEMICAL APPROACH

Laura de Miguel[1**], Gerardo Cebrián-Torrejón[2**], Eric Caudron[3,4], Ludovica Arpinati[1], Antonio Doménech-Carbó[2*] and Gilles Ponchel[1*].

[1] Institut Galien Paris-Sud, Paris-Sud University, Châtenay-Malabry, France, CNRS, UMR 8612, 5 rue Jean Baptiste Clément, Châtenay-Malabry, France.

[2] Departament de Química Analítica, Facultat de Química, Universitat de València, Dr. Moliner 50, 46100 Burjassot, Valencia, Spain.

[3] Paris Sud Analytical Chemistry group, School of Pharmacy, Paris-Sud University, 5 rue Jean Baptiste Clément, Châtenay-Malabry, France.

[4] Hôpital Européen Georges Pompidou (AP-HP), Service de Pharmacie, Paris, France

*Corresponding authors:

Antonio Doménech-Carbó, Facultat de Química, Universitat de València, Dr. Moliner 50, 46100 Burjassot, Valencia, Spain. e-mail: antonio.domenech@uv.es.

Gilles Ponchel, Univ. Paris Sud, UMR CNRS 8612, Institut Galien, 92296 Châtenay-Malabry Cedex, France. e-mail: gilles.ponchel@u-psud.fr.

** Authors contributed equally to this work.

Graphical Abstract

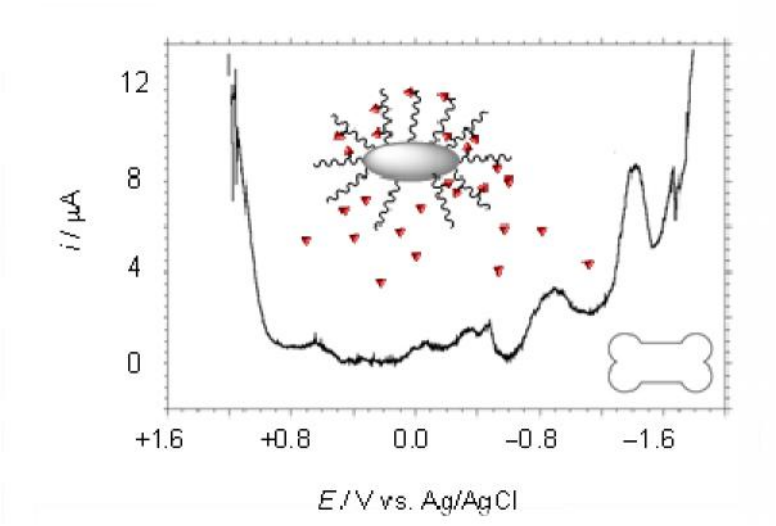

Résumé

La voltammétrie a été mise en œuvre afin de caractériser à pH voisin de la neutralité et en présence d'ions des nanoparticules multifonctionnelles de poly(L-glutamate de γ-benzyle)-poly(acide glutamique) conçues pour le ciblage des tissus osseux. L'affinité de ces nanoparticules pour l'hydroxyapatite, c'est-à-dire la composante minérale majoritaire de l'os, a été réalisée grâce à la décoration de la surface des particules par des chaînes de poly(acide glutamique). Des signaux voltammétriques significativement différents ont permis de mettre en évidence l'association du cisplatine aux nanoparticules et d'établir sa cinétique de libération, en concordance avec les expériences de spectroscopie d'absorption atomique. La fixation des nanoparticules à l'hydroxyapatite a été évaluée par marquage en fluorescence des nanoparticules et a été confirmée par la technique d'électrochimie. En conclusion, la méthode électrochimique permet de confirmer les données obtenues par les méthodes de caractérisation par absorption atomique et fluorescence, tout en apportant des informations complémentaires

Abstract

The voltammetric response of different processes concerning cisplatin-complexed (γ-benzyl-L-glutamate)-*b*-poly(glutamic acid) derivate nanoparticles with bone targeting properties was studied in aqueous electrolytes and at biological pH. Bone targeting properties were achieved by targeting hydroxyapatite, the major mineral component of bone, by decorating the nanoparticles with poly (glutamic acid) chains. Significant differences in the cisplatin-centered voltammetric signals allowed to monitor cisplatin association to nanoparticles as well as release kinetics from them, in agreement with the data generated by atomic absorption spectroscopy experiments. *In vitro* hydroxyapatite binding assay was performed by using fluorescencently labelled nanoparticles and was further confirmed by electrochemistry, using the voltammetry method previously developed for microspheres. Electrochemistry revealed as a very useful tool which provides with complementary information to that obtained by atomic absorption spectroscopy and fluorescence techniques.

Keywords: electrochemistry; bone targeted nanoparticles; cisplatin; hydroxyapatite

1- Introduction

Cisplatin is a cytotoxic metallodrug used for the treatment of different types of cancers, such as ovarian, testicular, bladder, cervical, small cell lung cancer, esophageal, head and neck [1]. The main target accounting for the cytotoxic action of cisplatin is DNA [2], although other non-DNA targets are also involved [3]. However, its use is highly limited due to several strong side effects, the most threatening ones being neurotoxicity, nephrotoxicity and ototoxicity [4, 5].

In order to circumvent side effects and to increase the therapeutic activity, research has been focused in the development of cisplatin targeted nanoparticle carrier systems. Cisplatin structure allows chemical modifications, due to the presence of two chlorides that can be replaced by a wide variety of chemical groups, such as carboxylate units and such property being used for the design of drug carrier systems [6, 7]. The good leaving properties of carboxylate group converts the metal complex reversible, allowing the release of cisplatin from the carrier.

Electrochemical methods are very sensitive, easy to handle and inexpensive tools for drug detection. In the cisplatin (cis-dichlorodiamineplatinum (II), $[Pt^{II}(NH_3)_2Cl_2]$), the platinum can be electrochemically reduced to Pt^0 and this voltammetric response can be employed to determine its concentration, complexation and to monitor its role in biochemical processes [8-10].

In this work, multifunctional cisplatin-complexed poly(γ-benzyl-L-glutamate) block poly(glutamic acid) (PBLG-*b*-PGlu) derivate nanoparticles where the metallodrug is coordinated to the carboxylate groups of the poly(glutamic acid) and possessing bone targeting properties were prepared. Bone targeting properties were achieved by targeting hydroxyapatite (HAP), the major mineral component of bone. Poly(glutamic acid) (PGlu) block was used to target HAP, since acidic oligopeptides have shown *in vitro* and *in vivo* bone affinity and they have been used to provide drugs with osteotropic properties [11]. Association of cisplatin to PBLG-*b*-PGlu derivate nanoparticles, cisplatin release from them and bone targeting properties were studied. A multiple electrochemical approach combining

conventional solution-phase voltammetry and voltammetry of microparticles approaches [12-14], allowed to monitor these three processes. Electrochemical tools are proposed as innovative tools for monitoring properties of active targeting metal containing nanoparticles providing complementary information to the results obtained by other techniques.

2- Materials and Methods

2.1- Materials

Cisplatin, phosphate buffer saline (PBS) and hydroxyapatite (HAP) were purchased from Acros and Sigma, respectively. All reagents were of analytical grade and used directly. Dialysis membranes were purchased from Carlroth, (Spectra Por). 1 mL microdialyzers used for *in vitro* drug release experiments were bought from Orange Scientific. The glassy carbon working electrode (GCE) was purchased to BAS MF2012.

2.2- Atomic absorption spectroscopy (AAS) detection

Cisplatin content of the nanoparticles was quantified by AAS. Details of the instrument and heating program used are found in Supplementary Information (SI).

2.3- Electrochemical detection

Electrochemical experiments were performed at 298±1 K in a thermostated cell with CH I660 equipment. A BAS MF2012 glassy carbon working electrode (GCE) (geometrical area 0.071 cm^2), a platinum wire auxiliary electrode and an Ag/AgCl (3M NaCl) reference electrode were used in a conventional three-electrode arrangement. 0.10 M aqueous potassium phosphate buffer (pH 7.0) and PBS (pH 7.4), optionally dearated by bubbling Argon during 15 min, were used as supporting electrolytes. Blank experiments were conducted in ca. 1 mM cisplatin solutions. For *in vitro* HAP binding assay, a different electrochemical strategy, previously developed for microspheres has been adaptated to nanoparticles such as described in section 2.7.

2.4- Preparation of multifunctional poly(γ-benzyl-L-glutamate) (PBLG) nanoparticles

PBLG copolymers were obtained by a ring opening polymerization (ROP) procedure previously described. Multifunctional nanoparticles based either only on PBLG-*b*-PGlu copolymer or from a mixture of this and poly(γ-benzyl-L-glutamate) block poly(ethylene glycol) (PBLG-*b*-PEG) were prepared following a novel nanoprecipitation method. Briefly, different proportions of the copolymer PBLG-*b*-PGlu and PBLG-*b*-PEG were dissolved in tetrahydrofuran/methanol 75/25 (THF/MeOH) at 40 °C at a concentration of 0.1 nM without magnetic stirring. Once dissolved, they were added by dripping to an aqueous solution containing two equivalents of sodium hydroxide (NaOH) per equivalent of carboxylic acid (COOH) contained in the PGlu block and stirred for 10 min. Solvents were eliminated by a standardized protocol under vacuum in the rotavapor at 40 °C. Nanoparticles size and ζ potential before and after incubation with cisplatin were determined by dynamic light scattering (DLS) at 25 °C (Zetasizer 4, Malvern Instruments). Morphological characterization of nanoparticles was performed by means of transmission electron microscopy (TEM) at 120 kV (TEM JEOL 1400) after negative coloration with phosphotungstic acid 1% w/w. Measurements of the longitudinal and axial diameter of 100 nanoparticles of each type were made on TEM photos using Image J.

2.5- Cisplatin association to PBLG-*b*-PGlu and PBLG-*b*-PGlu/PBLG-*b*-PEG nanoparticles

Cisplatin was associated to preformed nanoparticles prepared from PBLG-*b*-PGlu or PBLG-*b*-PEG or from a mixture of them at different proportions. Cisplatin-complexed PBLG-*b*-PGlu/PBLG-*b*-PEG nanoparticles were prepared at [CDDP/COO^-] ratios of 0.8 and 1 and reacted for 60 h in dark to form the complex between the carboxylate groups of PGlu block and cisplatin. A purification step by dialysis (membrane of a molecular weight cut off size of 3000 Da, SpectraPor) was performed during 24 h. The cisplatin content in the nanoparticles was determined by AAS.

The electrochemical response of cisplatin and cisplatin-complexed PBLG-*b*-PGlu/PBLG-*b*-PEG nanoparticles was studied. PBLG-*b*-PGlu/ PBLG-*b*-PEG nanoparticles were incubated with cisplatin at a ratio of [CDDP/COO^-] = 1 in the conditions described above. A cisplatin solution of 4 mM was

used as a positive control. PBLG-benzyl (PBLG-bnz) nanoparticles, not containing COO^- substituents, were incubated with cisplatin as described and used as a negative control. No purification step was done. The electrochemical response was achieved diluting each sample in 1 mL of aqueous phosphate buffer (pH=7).

2.6- *In vitro* drug release from cisplatin-complexed PBLG-*b*-PGlu nanoparticles

In vitro cisplatin release from the PBLG-*b*-PGlu nanoparticles was studied by the dialysis method in a 0.01 M PBS at pH 7.4 containing 0.138 M of NaCl and in distilled MilliQ water at 37 °C. Briefly, 0.950 mL of nanoparticles at a concentration of 0.75 mg/mL containing 0.1% of Pluronic® F 68 were introduced in 1 mL microdialyzers and dialyzed against 15 mL of medium using dialysis membranes with a molecular weight cut off of 3500 Da. The solution outside the microdialyzers was sampled at defined periods and replaced with fresh medium. The release of cisplatin was measured by AAS.

The cisplatin loading content is expressed as the mg of loaded cisplatin with respect to 100 mg of the PBLG-*b*-PGlu nanoparticle forming copolymer.

The electrochemical response of cisplatin-complexed PBLG-*b*-PGlu nanoparticles in aqueous phosphate buffer (pH=7) was studied diluting 1 mL of the nanoparticles solution with 1 mL of PBS (pH=7.4) and 1 mL of water respectively for 5 days.

2.7- *In vitro* HAP binding assay

Fluorescently-labelled bone targeted nanoparticles containing the fluorescent PBLG-dansyl, and an osteotropic PBLG derivate, PBLG-*b*-PGlu copolymer in 0.1 % of Pluronic® F 68 were incubated in 3 mL of PBS containing 0.4 g of HAP at a pH of 7.4 during 24 hours at 25°C. The suspensions were centrifuged at 5000 rpm for 5 minutes, washed three times with Pluronic® F 68 1% / PBS 7.4 1/1 and observed under UV light at 365 nm. Supernatants were quantified by a Perkin Elmer Luminescence spectrometer LS 50B at room temperature ($\lambda_{excitation}$ = 340 nm . $\lambda_{emission}$ = 472 nm) to determine the amount of nanoparticles not bound to HAP.

For the electrochemical detection, a different strategy, based on a voltammetric methodology originally proposed for microparticles was used [12, 15]. This methodology has been previously used to study nanoparticle systems [16]. Microparticulate deposits of HAP on GCE were prepared by evaporation of suspensions (1 mg/mL) of the solid in ethanol (EtOH). Blank experiments were performed with HAP. Briefly, 1 ml of monofunctional cisplatin-complexed PBLG-*b*-PGlu nanoparticles were diluted in 1 ml of phosphate buffer and their electrochemical responses were studied.

3- Results and discussion

3.1- Nanoparticle characterization

Different osteotropic monofunctional and multifunctional nanoparticles were prepared, as well as other non osteotropic ones that were used as controls.

Table 1: Morphological characterization of multifunctional PBLG nanoparticles by TEM

Nanoparticles	$D_{longitudinal}$ (nm) ± SD [a]	D_{axial} (nm) ± SD[a]	Aspect ratio	$D_{equivalent}$ (nm)
$PBLG_{25}$-bnz	34 ± 8.8	26 ± 5.7	1.6	39
PBLG-*b*-PGlu/PBLG-*b*-PEG 100/0	37 ± 7.4	27 ± 5.9	1.3	34
PBLG-*b*-PGlu/ PBLG-*b*-PEG 80/20	41 ± 6.4	26 ± 5.3	1.6	35
PBLG-*b*-PGlu/ PBLG-*b*-PEG 60/40	40 ± 7.8	24 ± 5.1	1.5	35
PBLG-*b*-PGlu/ PBLG-*b*-PEG 40/60	40 ± 6.6	28 ± 5.1	1.4	36
PBLG-*b*-PGlu/ PBLG-*b*-PEG 20/80	36 ± 7.42	23 ± 4.3	1.6	31
PBLG-*b*-PEG	39.6 ± 2.6	23 ± 2.6	1.7	29
After CDDP association				
PBLG-*b*-PGlu/PBLG-*b*-PEG 100/0	39 ± 8.1	28 ± 5.9	1.3	35
PBLG-*b*-PGlu/ PBLG-*b*-PEG 80/20	48 ± 6.7	34 ± 5.5	1.4	43
PBLG-*b*-PGlu/ PBLG-*b*-PEG 60/40	40 ± 7.8	27 ± 4.8	1.6	34
PBLG-*b*-PGlu/ PBLG-*b*-PEG 40/60	41 ± 5.2	27 ± 5.2	1.5	36
PBLG-*b*-PGlu/ PBLG-*b*-PEG 20/80	37 ± 5.2	26 ± 4.6	1.4	33

The nanoprecipitation method using previously synthesised PBLG copolymers allowed the preparation of nanoparticles of with an oblate morphology and a relatively small size, with an equivalent diameter less than ~40 nm and an aspect ratio of 1.3 to 1.7 as evidenced by the TEM measurements. No significant changes in size were seen after cisplatin association to the nanoparticles. DLS experiments were routinely performed to confirm nanoparticle formation during the preparation process (see Supplementary Information).

3.2- Association of cisplatin to PBLG-*b*-PGlu and PBLG-*b*-PGlu/PBLG-*b*-PEG nanoparticles

Cisplatin association experiments showed the capability of multifunctional nanoparticles prepared from mixtures of PBLG-*b*-PGlu/PBLG-*b*-PEG copolymers in different proportions to associate cisplatin (Figure 1).

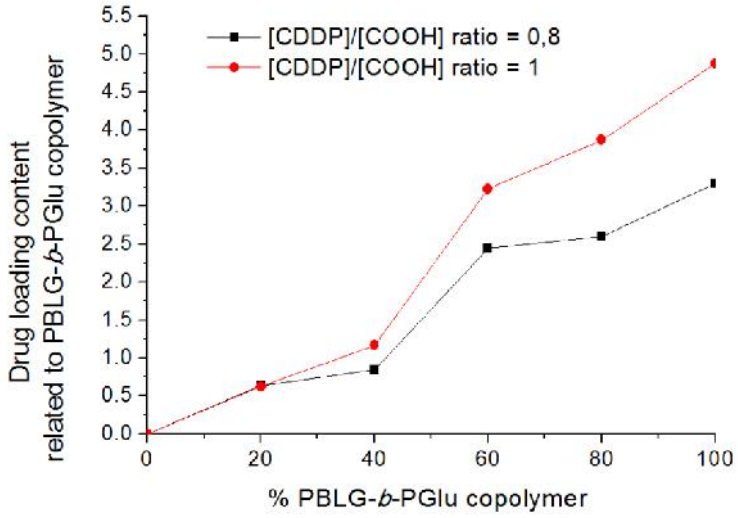

Figure 1: Cisplatin loading content related to PBLG-*b*-PGlu copolymer of different PBLG-*b*-PGlu/PBLG-*b*-PEG nanoparticles incubated at [CDDP/COO^-] ratios of 0.8 and 1.

Cisplatin association has been tested at two [CDDP/COO^-] ratios, but cisplatin loading contents trends were similar. Interestingly, there was an important increase of nearly three times in the cisplatin loading content when the proportion of the nanoparticle forming polymer PBLG-*b*-PGlu passed from

40% to 60% w/w in the final composition of the nanoparticles. Indeed, cisplatin was more efficiently associated when the proportion of the PBLG-*b*-PGlu copolymer was predominant (beyond 60% w/w) over the PBLG-*b*-PEG one. This could be related to the arrangements of the PGlu and PEG chains within the nanoparticles or to a possible steric hindrance of PGlu chains in presence of other PEG chains.

The electrochemical experiments were performed with cisplatin-complexed PBLG-*b*-PGlu nanoparticles using cisplatin and PBLG-bnz nanoparticles as positive and negative controls, respectively. Figure 2 shows such voltammetric responses for cisplatin solutions and cisplatin-complexed PBLG-*b*-PGlu nanoparticles in phosphate buffer (pH 7.0).

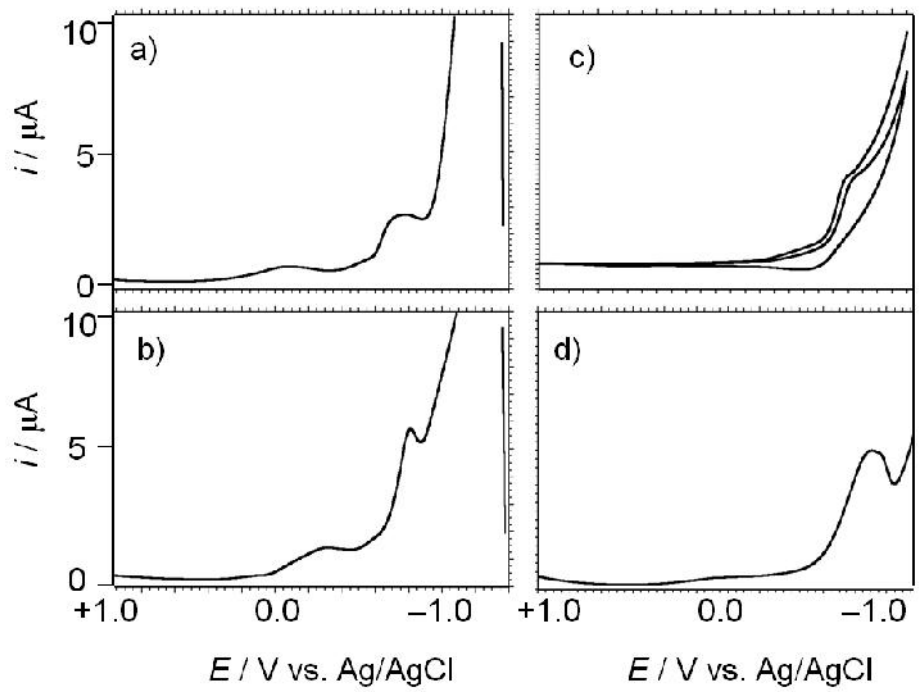

Figure 2. Voltammograms of: a) cisplatin; b) cisplatin-complexed PBLG-*b*-PGlu nanoparticles; c, d) PBLG-bnz nanoparticles in phosphate buffer (pH 7.0). a, b ,d) Square wave voltammograms initiated at +1.25 V in the negative direction; potential step increment 4 mV; square wave amplitude 25 mV; frequency 5 Hz. c) Cyclic voltammogram, potential scan rate 20 mV/s.

For cisplatin, two cathodic waves at −0.20 and −0.80 V vs. Ag/AgCl were recorded. For cisplatin-complexed PBLG-*b*-PGlu nanoparticles, the response was similar but both signals became enhanced in height and slightly shifted towards more negative potentials (−0.40 and −0.85 V), the second wave now defining a sharp-shaped peak. As frequently occurring for nanoparticles functionalized with electroactive motifs, the voltammetric response was dominated by the signals of such species anchored to the nanoparticles [17, 18]. The peak potential shift suggested that cisplatin was coordinated to the PBLG-*b*-PGlu copolymer while the peak current enhancement could be attributed to the increase of the effective concentration of cisplatin due to its association to the nanoparticle system. In the case of PBLG-bnz nanoparticles similar features to free cisplatin were obtained, confirming the absence of interaction between the cisplatin and PBLG-bnz nanoparticles. Experiments for monofunctional cisplatin-complexed PBLG-*b*-PGlu nanoparticles (see figure 3a), produced voltammograms with a cathodic peak at −0.75 V, which could be attributed to cisplatin reduction involving prior de-complexation from PBLG-*b*-PGlu nanoparticles. Experiments for the multifunctional cisplatin-complexed PBLG-*b*-PGlu /PBLG-*b*-PEG nanoparticles at a proportion of 40/60 yielded a similar voltammetric response (see figure 3b), but the signal became significantly decreased (notice the different current scale in figures 3a,b) while an additional wave at −0.20 V appeared. This wave increased linearly on increasing frequency, a characteristic of adsorption-mediated voltammetric signals [18-20] and also increased with decreasing PBLG-*b*-PGlu/PBLG-*b*-PEG ratios. These features suggested that cisplatin was effectively bound to PGlu and, under this binding situation, was available for electrochemical reduction. For multifunctional PBLG-*b*-PGlu/PBLG-*b*-PEG nanoparticles, the presence of PEG was responsible for adsorption-mediated peak at −0.20 V, cisplatin was indeed coordinated to the PGlu block although to a much lesser extent, as evidenced by the significantly decreased signal at −0.75 V. These results confirmed the more effective coordination of cisplatin to PBLG-*b*-PGlu nanoparticles compared to PBLG-*b*-PGlu/PBLG-*b*-PEG nanoparticles 40/60 in coherence with the AAS measurements.

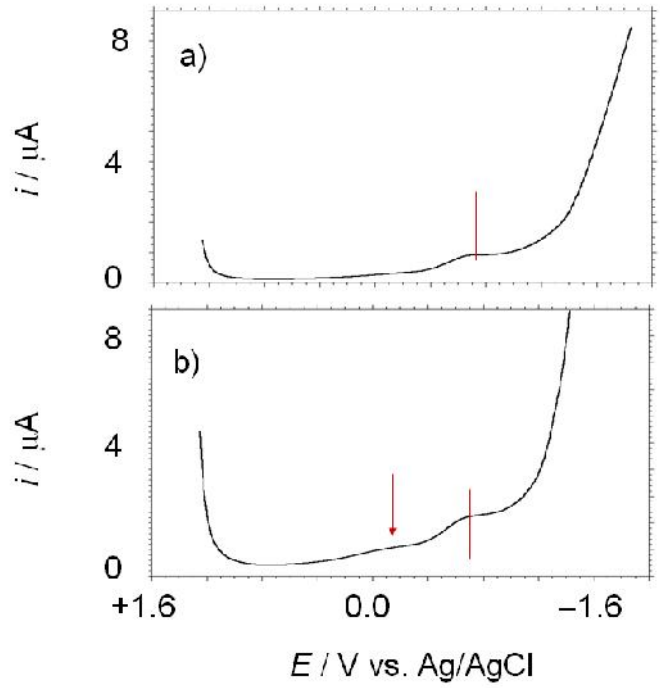

Figure 3. Square wave voltammograms of: a) cisplatin-complexed PBLG-*b*-PGlu (100% PBLG-*b*-PGlu) nanoparticles and b) cisplatin-complexed PBLG-*b*-PGlu/PBLG-*b*-PEG nanoparticles 40/60 in phosphate buffer (pH 7.0). Potential scan initiated at +1.25 V in the negative direction; potential step increment 4 mV; square wave amplitude 25 mV; frequency 5 Hz.

3.3- *In vitro* cisplatin release from PBLG-*b*-PGlu nanoparticles

In vitro cisplatin release from PBLG-*b*-PGlu nanoparticles was studied by the dialysis method during 15 days. After 5 days, cisplatin release in PBS medium was incomplete and significantly higher than in water medium as shown by figure 4. Indeed, chloride ions are known to play a major role in cisplatin release from PBLG-*b*-PGlu nanoparticles since they act as nucleophile groups that would replace carboxylate groups via ligand exchange reaction and due to the good leaving properties of carboxylates[7]. Acidic pH has also shown to play a role in cisplatin release [21]. This role of chloride ions accounted for the enhanced cisplatin release in PBS medium compared to water medium. These

results are in coherence with other cisplatin-carboxylate complexes and micelles previously reported[6, 7, 22].

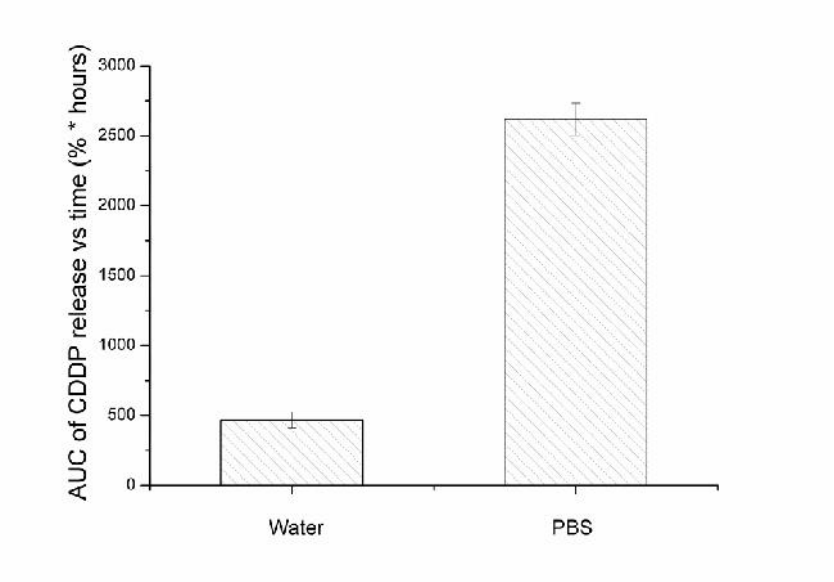

Figure 4. *In vitro* cisplatin release after 5 days from cisplatin-complexed PBLG-*b*-PGlu nanoparticles in water and in 0.01 M PBS medium (pH 7.4) containing 0.138 M of NaCl. The *in vitro* release is expressed as area under the cisplatin release curve related with the time (% * h).

The voltammetric responses obtained for cisplatin-complexed PBLG-*b*-PGlu release experiments in water and in PBS were different as shown in figure 5. In PBS release medium, two peaks at −0.60 and −1.20 V appeared. The first one could be attributed to the released cisplatin and the second one to the reduction of cisplatin associated to PBLG-*b*-PGlu nanoparticles, respectively. In water, only one cathodic peak at −0.85 V was recorded. This peak was attributable to the reduction of cisplatin associated to the PBLG-*b*-PGlu nanoparticle and thus no cisplatin was released in these conditions (figure 5). These results confirmed the effective cisplatin release from the PBLG-*b*-PGlu nanoparticles induced by the PBS medium in contrast with the absence of significant cisplatin release when the experiment is conducted in water. Although PBS medium introduces an electrostatic barrier

disfavouring the cisplatin reduction, there is no inhibition of the electrochemical activity of the drug, and cisplatin release is promoted by the PBS.

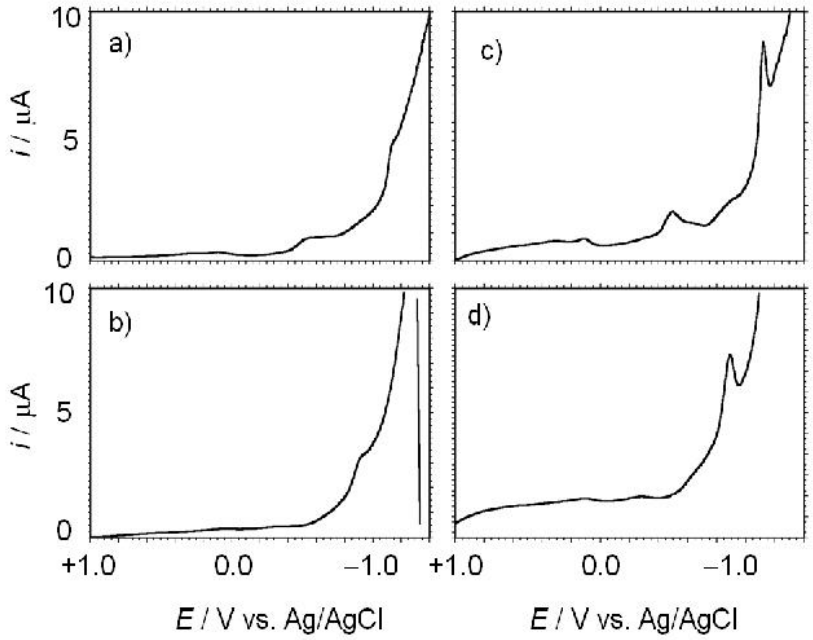

Figure 5. a, b) square wave voltammograms and c, d) their respective deconvolution of: a, c) cisplatin-complexed PBLG-*b*-PGlu and incubated with a PBS (pH 7.4) solution, b, d) cisplatin-complexed PBLG-*b*-PGlu and incubated with phosphate buffer (pH 7.0). Potential scan initiated at +1.25 V in the negative direction; potential step increment 4 mV; square wave amplitude 25 mV; frequency 5 Hz.

3.4- *In vitro* HAP binding assay

HAP is the major mineral component of bone and accounts for 50-70 % of the bone extracellular matrix. The *in vitro* HAP binding assay showed a total binding for fluorescently labelled cisplatin-complexed PBLG-*b*-PGlu nanoparticles as shown in figure 6. This HAP binding property was driven by the PGlu block and not by the PBLG or dansyl moiety as evidenced by the absence of binding of PBLG-dansyl nanoparticles. Moreover, cisplatin could also be involved in the adsorption onto HAP, as it has been previously reported [23]. There are several osteotropic moieties such as biphosphonates, acidic oligopeptides and tetracycline analogs [24]. The discovery that acidic non collagenous salivary

proteins could bind HAP with high affinity [25] and the identification of glutamic acid rich sequences as the responsible moieties for this binding opened the way to the use of acidic oligopeptides as bone targeting moieties. Indeed, oligoglutamic acid such as oligoaspartates and oligoglutamates have been shown to have affinity to HAP *in vitro* and to bone *in vivo* and they have been used to provide drugs with osteotropic properties [11].

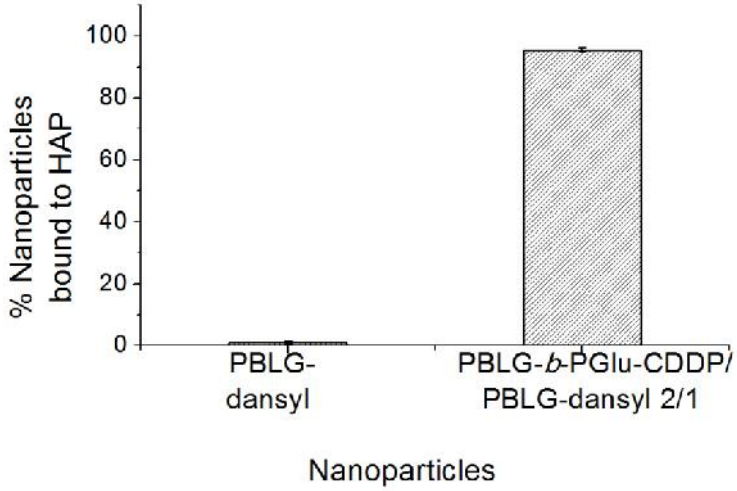

Figure 6: Degree of binding expressed in percentage of nanoparticles bound to HAP for PBLG-dansyl and cisplatin-complexed PBLG-*b*-PGlu/PBLG-dansyl 2/1 nanoparticles after 18 h. Nanoparticles at a concentration of 1.5 mg/mL in 0.1% Pluronic® F 68 were incubated in 3 mL of PBS containing 0.4 g of HAP at 25 °C.

Electrochemical monitoring of *in vitro* HAP binding assay was performed using the voltammetry of microparticles approach, a solid-state electrochemical methodology developed by Scholz et al. which provides information on solid materials attached to inert electrodes in contact with suitable electrolytes [12, 13]. Using this technique, previously used for nanoparticulate system studies [16], the voltammetric response of fluorescently-labelled cisplatin-complexed PBLG-*b*-PGlu nanoparticles

attached to HAP was studied. Square wave voltammetry was used as a detection mode because of the inherently high sensitivity of this technique and its reluctance to undergo capacitive distortions [18]. Voltammograms for cisplatin-complexed PBLG-*b*-PGlu associated to HAP showed two main cathodic peaks at −0.90 and −1.40 V, as can be seen in Fig. 7a. The peak at −0.90 V can be assigned to the reduction of cisplatin directly released from the PBLG-*b*-PGlu nanoparticles due to the use of the PBS medium and the peak at −1.40 corresponds to the reduction of cisplatin complexed to the PBLG-*b*-PGlu nanoparticles that are bound to the HAP. Such peaks are slightly shifted to more negative potentials relative to those recorded at PBLG-*b*-PGlu nanoparticles solution. It appears that attachment to HAP results in negative potential shifts, in particular, for the reduction of released cisplatin, possibly due to the formation of cisplatin adsorbates on the HAP.

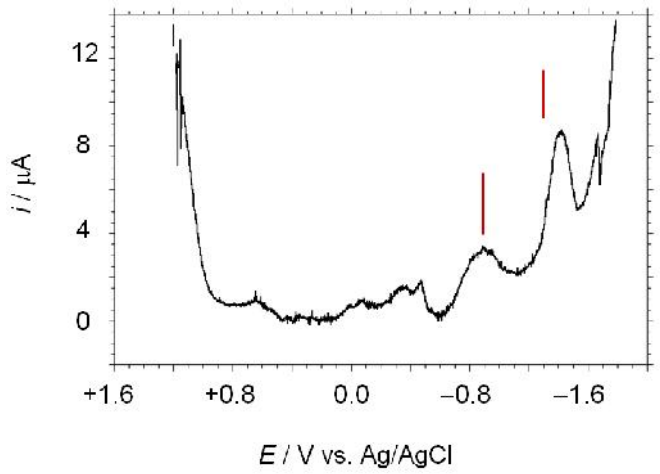

Figure 7. Square wave voltammograms for films on GCE of NPs associated to HAP using: cisplatin-complexed PBLG-*b*-PGlu nanoparticles and immersed in 0.10 M phosphate buffer (pH 7.0) after subtraction of the blank voltammogram for HAP-modified GCE. Potential scan initiated at +1.25 V in the negative direction; potential step increment 4 mV; square wave amplitude 25 mV; frequency 5 Hz

These results can be interpreted combining the theoretical model proposed by Lovric, Scholz, Oldham et al. [26-29] on the electrochemistry of ion-insertion solids with modelling for complexes associated to

microporous and mesoporous inorganic supports [30-34] The essential idea is that the observed electrochemical signals results from the superposition of the processes due to different topological redox isomers; i.e., electroactive guest molecules located in different sites of the inorganic host. This is schematized in figure 8, where at least four different electrochemical pathways can be associated to the previously described voltammetric features: reduction of 'free' cisplatin adsorbed on the electrode surface (A), reduction of cisplatin-complexed to PBLG-*b*-PGlu derivate nanoparticles (B), reduction of HAP-adsorbed cisplatin-complexed to PBLG-*b*-PGlu nanoparticles (C) and reduction of HAP-adsorbed cisplatin (D).

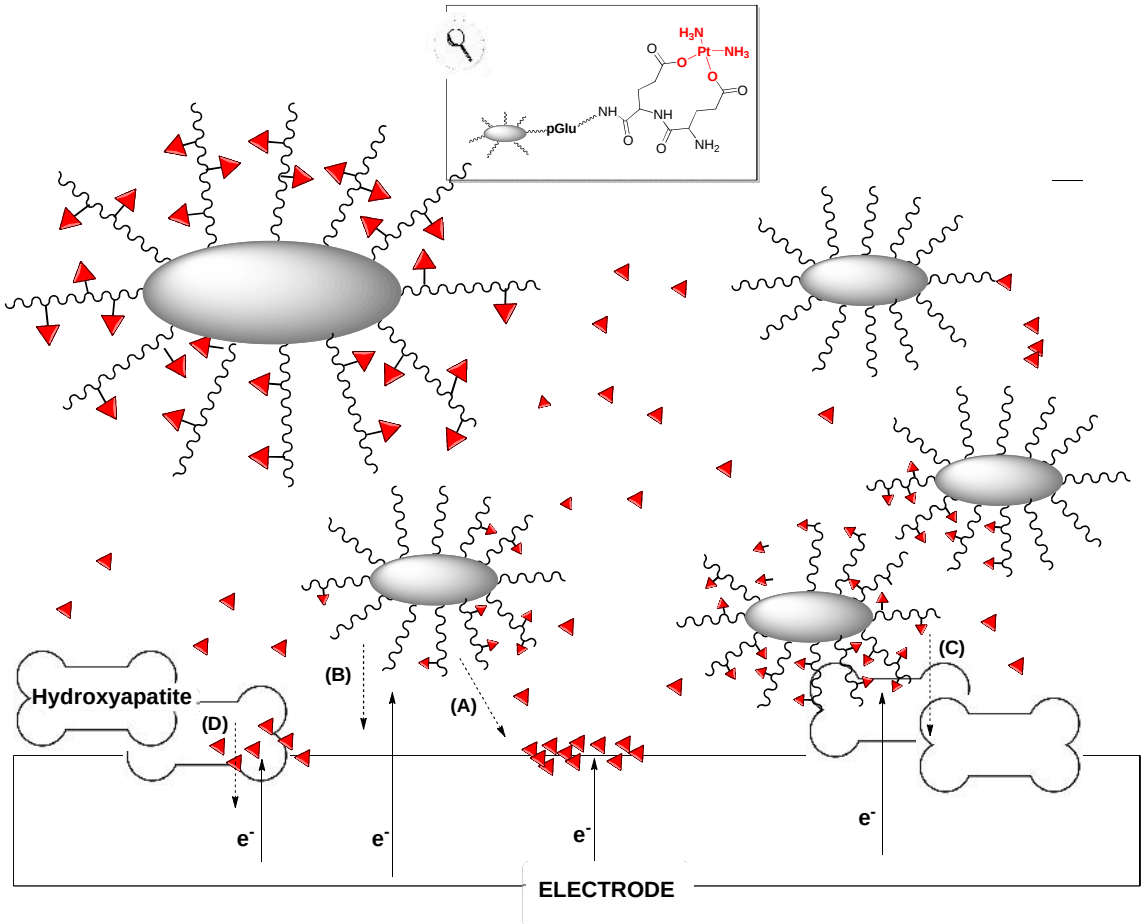

Figure 8. Scheme for the different electrochemical processes involved in the voltammetry of cisplatin-complexed PBLG-*b*-PGlu nanoparticles and associated or not to HAP.

According to the above set of results, voltammetric techniques not only confirmed the interaction of cisplatin-complexed PBLG-*b*-PGlu nanoparticles with the HAP but provided further information, being able to distinguish free cisplatin from cisplatin associated to the PBLG-*b*-PGlu nanoparticle and bound to the HAP.

4- Conclusion

In this work, multifunctional bone targeted nanoparticles derived from PBLG-*b*-PGlu and PBLG-*b*-PEG copolymers were prepared. The cisplatin association, release and bone targeting properties were studied by AAS and fluorescence techniques and were confirmed by electrochemical methodologies. Interestingly, cisplatin association was significantly effective only when the proportion of the PBLG-*b*-PGlu copolymer was predominant over the PBLG-*b*-PEG one and this was confirmed by both electrochemistry and AAS experiments. Moreover, both techniques showed that cisplatin release from PBLG-*b*-PGlu nanoparticles was enhanced by the chloride containing PBS medium, as compared to water. Finally, HAP binding of fluorescently labelled PBLG-*b*-PGlu nanoparticles could be shown by both fluorescence and the voltammetry of microparticles approach. In conclusion, electrochemical techniques showed to be innovative tools for the study of cisplatin-complexed PBLG-*b*-PGlu derivate nanoparticles which provided further information about the different existing platine species.

Acknowledgements

The authors acknowledge the european postgraduate program from "Ibercaja" Foundation and the Spanish “I+D+I MEC” project CTQ2011-28079-CO3-02, supported by ERDF funds, for the financial support. This work has benefited from the facilities and expertise of the Platform for Transmission Electronic Microscopy of IMAGIF (Centre de Recherche de Gif - www.imagif.cnrs.fr)”.

References

[1] Desoize B, Madoulet C. Particular aspects of platinum compounds used at present in cancer treatment. Crit Rev Oncol Hematol. 2002;42:317-25.

[2] Jamieson ER, Lippard SJ. Structure, Recognition, and Processing of Cisplatin DNA Adducts. Chem Rev. 1999;99:2467-98.

[3] Wang K, Lu J, Li R. The events that occur when cisplatin encounters cells. Coord Chem Rev. 1996;151:53-88.

[4] Harmers FP, Gispen WH, Neijt JP. Neurotoxic side-effects of cisplatin. Eur J Cancer. 1991;27:372-6.

[5] Pinzani V, Bressolle F, Johanne Haug I, Galtier M, Blayac JP, Balmès P. Cisplatin-induced renal toxicity and toxicity-modulating strategies: a review. Cancer Chemother Pharmacol. 1994;35:1-9.

[6] Zhu W, Li Y, Liu L, Zhang W, Chen Y, Xi F. Biamphiphilic triblock copolymer micelles as a multifunctional platform for anticancer drug delivery. Journal of Biomedical Materials Research Part A.96A:330-40.

[7] Nishiyama N, Yokoyama M, Aoyagi T, Okano T, Sakurai Y, Kataoka K. Preparation and characterization of self-assembled polymer metal complex micelle from cis-dichlorodiammineplatinum(II) and poly(ethylene glycol)-poly(L-aspartic acid) block copolymer in an aqueous medium. Langmuir. 1998;15:377-83.

[8] Mebsout F, Kauffmann JM, Patriarche GJ. Electrochemical behaviour of cis-platin at carbon paste and platinum electrodes. J Pharm Biomed Anal. 1988;6:441-8.

[9] Krizkova S, Adam V, Petrlova J, Zitka O, Stejskal K, Zehnalek J, et al. A suggestion of electrochemical biosensor for study of platinum(II)-DNA interactions. Electroanalysis. 2007;19:331-8.

[10] Petrlova J, Potesil D, Zehnalek J, Sures B, Adam V, Trnkova L, et al. Cisplatin electrochemical biosensor. Electrochim Acta. 2006;51:5169-73.

[11] Kasugai S, Fujisawa R, Waki Y, Miyamoto K, Ohya K. Selective drug delivery system to bone: small peptide (Asp)6 conjugation. J Bone Miner Res. 2000;15:936-43.

[12] Scholz F, Meyer B. Voltammetry of solid microparticles immobilized on electrode surfaces. New York1998.

[13] Scholz F, Schröder R, Gulabowski R. Electrochemistry of inmobilized particles and droplets. Berlin: Springer; 2005.

[14] Doménech-Carbó A, Labuda F, Scholz F. Electroanalytical chemistry for the analysis of solids: Characterization and classification (IUPAC Technical Report) Pure Appl Chem. 2013:609-32.

[15] Schröder U, Oldham KB, Myland JC, Mahon PJ, Scholz F. Modelling of solid state voltammetry of immobilized microcrystals assuming an initiation of the electrochemical reaction at a three-phase junction. J Solid State Electrochem. 2000;4:314-24.

[16] Doménech-Carbó A, Coronado E, Díaz P, Ribera A. Solid-State Electrochemical Method for Determining Core and Shell Size in Pd@PdO Nanoparticles. Electroanalysis. 2010;22:293-302.

[17] Murray RW. Nanoelectrochemistry: metal nanoparticles, nanoelectrodes, and nanopores. Chem Rev. 2008;108:2688-720.

[18] Alghamdi AH, Belal FF, Al-Omar MA. Square-wave adsorptive stripping voltammetric determination of danazol in capsules. J Pharm Biomed Anal. 2006;41:989-93.

[19] Mirceski V, Komorsky-Lovric S, M L. Square wave Voltammetry-Theory and Applications-. Berlin-Heidelberg: Springer; 2007.

[20] Yan J-L. Determinationation of kanamycin by square-wave cathodic adsorptive stripping voltammetry. Russ J Electrochem. 2008;44:1334-8.

[21] Xia Y, Wang Y, Wang Y, Tu C, Qiu F, Zhu L, et al. A tumor pH-responsive complex: Carboxyl-modified hyperbranched polyether and cis-dichlorodiammineplatinum(II). Colloids and Surfaces B: Biointerfaces. 2011;88:674-81.

[22] Ye H, Jin L, Hu R, Yi Z, Li J, Wu Y, et al. Poly(gamma-L-glutamic acid) cisplatin conjugate effectively inhibits human breast tumor xenografted in nude mice. Biomaterials. 2006;27:5958-65.

[23] Barroug A, Glimcher MJ. Hydroxyapatite crystals as a local delivery system for cisplatin: adsorption and release of cisplatin in vitro. J Orthop Res. 2002;20:274-80.

[24] Low SA, Kopeček J. Targeting polymer therapeutics to bone. Adv Drug Delivery Rev. 2012;64:1189-204.

[25] Fujisawa R, Kuboki Y. Preferential adsorption of dentin and bone acidic proteins on the (100) face of hydroxyapatite crystals. Biochim Biophys Acta. 1991;1075:56-60.

[26] Lovrić M, Scholz F. A model for the propagation of a redox reaction through microcrystals. J Solid State Electrochem. 1997;1:108-13.

[27] Lovrić M, Hermes M, Scholz F. The effect of the electrolyte concentration in the solution on the voltammetric response of insertion electrodes. J Solid State Electrochem. 1998;2:401-4.

[28] Oldham KB. Voltammetry at a three-phase junction. J Solid State Electrochem. 1998;2:367-77.

[29] Lovrić M, Scholz F. A model for the coupled transport of ions and electrons in redox conductive microcrystals. J Solid State Electrochem. 1999;3:172-5.

[30] Bessel CA, Rolison DR. Topological Redox Isomers: Surface Chemistry of Zeolite-Encapsulated Co(salen) and [Fe(bpy)3]2+ Complexes. The Journal of Physical Chemistry B. 1997;101:1148-57.

[31] Bessel CA, Rolison DR. Electrocatalytic Reactivity of Zeolite-Encapsulated Co(salen) with Benzyl Chloride. J Am Chem Soc. 1997;119:12673-4.

[32] Doménech A, Formentín P, García H, Sabater MJ. On the Existence of Different Zeolite-Associated Topological Redox Isomers. Electrochemistry of the Y Zeolite-Associated Mn(Salen)N3 Complex. The Journal of Physical Chemistry B. 2002;106:574-82.

[33] Doménech A. Model for Solid State Voltammetry of Zeolite-Associated Species. The Journal of Physical Chemistry B. 2004;108:20471-8.

[34] Doménech A, García H, Casades I, Esplá M. Electrochemistry of 6-Nitro-1‘,3‘,3‘-trimethylspiro[2H-1-benzopyran-2,2‘-indoline] Associated with Zeolite Y and MCM-41 Silicates. Light-Driven Site-Selective Electrocatalytic Effect on N,N,N‘,N‘,-Tetramethylbenzidine Oxidation. The Journal of Physical Chemistry B. 2004;108:20064-75.

Supplementary information

BONE TARGETED CISPLATIN-COMPLEXED PBLG-*b*-PGLU NANOPARTICLES: AN ELECTROCHEMICAL APPROACH

Laura de Miguel[1**], Gerardo Cebrián-Torrejón[2**], Eric Caudron[3,4], Ludovica Arpinati[1], Antonio Doménech-Carbó[2*] and Gilles Ponchel[1*].

[1] Institut Galien Paris-Sud, Paris-Sud University, Chatenay-Malabry, France, CNRS, UMR 8612, 5 rue Jean Baptiste Clément, Chatenay-Malabry, France.

[2] Departament de Química Analítica, Facultat de Química, Universitat de València, Dr. Moliner 50, 46100 Burjassot, Valencia, Spain.

[3] Paris Sud Analytical Chemistry group, School of Pharmacy, Paris-Sud University, 5 rue Jean Baptiste Clément, Châtenay-Malabry, France.

[4] Hôpital Européen Georges Pompidou (AP-HP), Service de Pharmacie, Paris, France

*Corresponding authors:

Antonio Doménech-Carbó ,Facultat de Química, Universitat de València, Dr. Moliner 50, 46100 Burjassot, Valencia, Spain. e-mail: antonio.domenech@uv.es.

Gilles Ponchel, Univ. Paris Sud, UMR CNRS 8612, Institut Galien, 92296 Châtenay-Malabry Cedex, France. e-mail: gilles.ponchel@u-psud.fr.

** Authors contributed equally to this work.

1. AAS for cisplatin determination

The instrument used for atomic absorption measurements was a Varian® SpectrAA GFAAS (Australia) graphic furnace AA spectrophotometer (model 200Z) with Zeeman background correction and equipped with an adapted autosampler, an ultrAA® platinum lamp and a pyrolytically coated graphite tube (Varian® partition tubes (coated)-GTA, Part No. 63-100012-00). A platinum hollow-cathode lamp was used as radiation source at 265.9 nm with a slit width of 0.5 nm. Lamp current was set at 10.0 mA. The volume of automatic sample injection was 20 µL; the internal Argon flow rate was 3 L.min-1 and was stopped during atomizing. Details of the GFAAS heating program are listed in table 1.

Table 1: Detailed heating program for AAS

Step	Furnace Temperature (°C)	Ramp Time (s)	Hold Time Time (s)	Internal Gas Flow ($L.min^{-1}$)	
1	40	0	0.1	3	Drying
2	120	55	0	3	
3	600	10	5	3	
4	1300	5	5	3	Ashing
5	1300	0	0.5	0	
6	2700	0.9	2	0	Atomizing
7	2850	1	0	3	Cleaning
8	40	22	0	3	

2. TEM images of nanoparticles

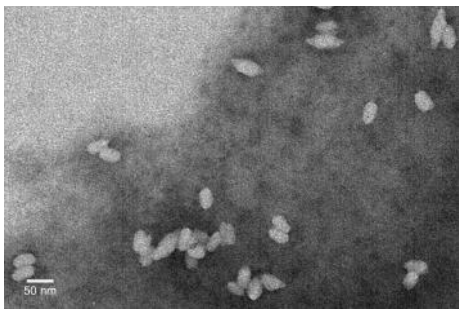

PBLG-*b*-PGlu/PBLG-*b*-PEG 100/0

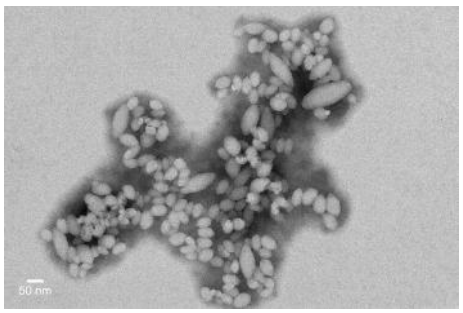

CDDP-PBLG-*b*-PGlu/PBLG-*b*-PEG 100/0

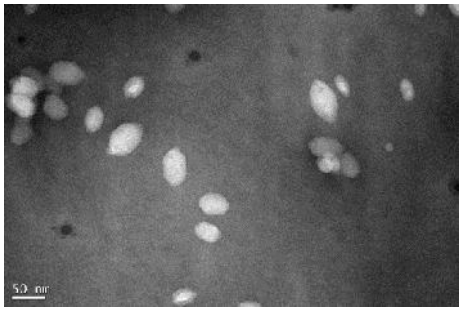

PBLG-*b*-PGlu/PBLG-*b*-PEG 80/20

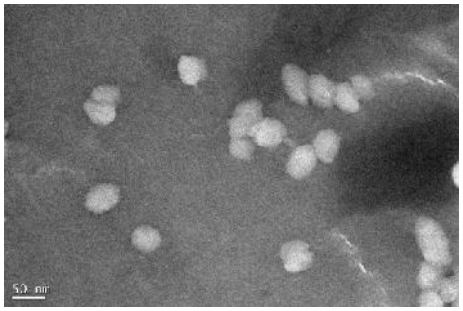

CDDP-PBLG-*b*-PGlu/PBLG-*b*-PEG 80/20

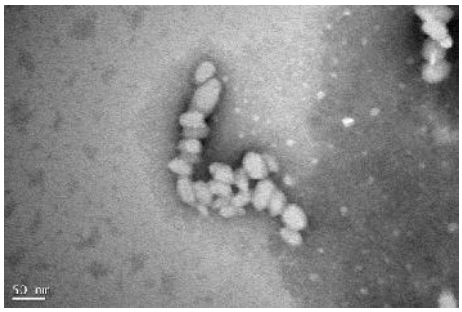

PBLG-*b*-PGlu/PBLG-*b*-PEG 60/40

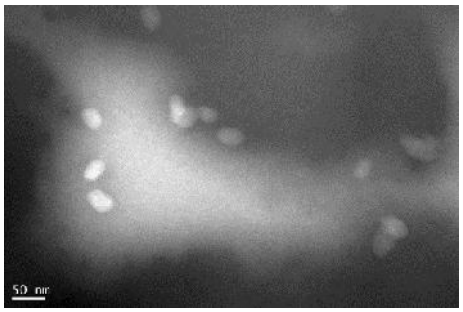

CDDP-PBLG-*b*-PGlu/PBLG-*b*-PEG 60/40

PBLG-*b*-PGlu/PBLG-*b*-PEG 40/60

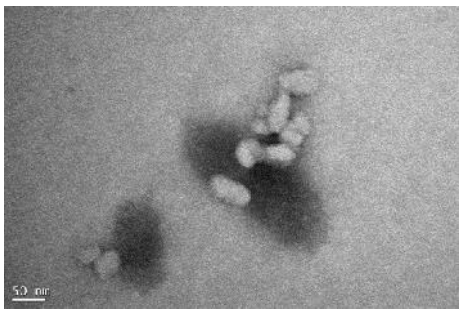

CDDP-PBLG-*b*-PGlu/PBLG-*b*-PEG 40/60

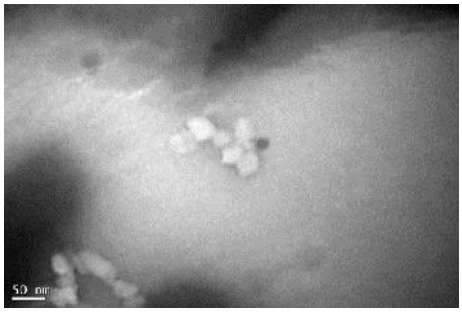

PBLG-*b*-PGlu/PBLG-*b*-PEG 20/80

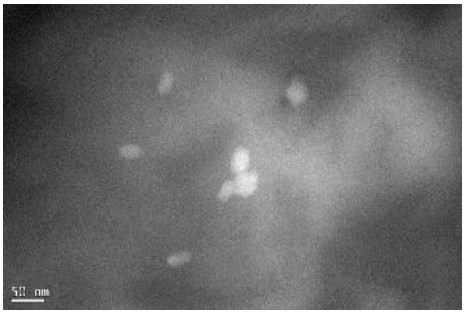

CDDP-PBLG-*b*-PGlu/PBLG-*b*-PEG 20/80

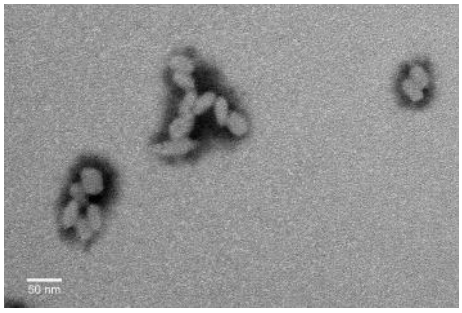

PBLG-*b*-PGlu/PBLG-*b*-PEG 0/100

Figure 1: TEM images obtained at 120 kV of nanoparticles obtained from PBLG-*b*-PGlu/PBLG-*b*-PEG at different proportions.

3. DLS characterization of nanoparticles

Table 2: Characterization of PBLG-derivate nanoparticles by DLS

Nanoparticles	Size (nm) ± SD [a]	PI ± SD (nm)	ζ Potential (meV) ± SD [a]
PBLG-bnz	47 ± 1.1	0.16 ± 0.0081	-37 ± 2.5
PBLG-dansyl	58 ± 0.9	0.12 ± 0.0077	-45 ± 1.5
PBLG-*b*-PGlu/PBLG-*b*-PEG 100/0	53 ± 0.82	0.13 ± 0.010	-46 ± 0.20
PBLG-*b*-PGlu/ PBLG-*b*-PEG 80/20	45 ± 0.45	0.14 ± 0.0012	-49 ± 2.48-
PBLG-*b*-PGlu/ PBLG-*b*-PEG 60/40	39 ± 0.26	0.099 ± 0.011	-45 ± 0.78
PBLG-*b*-PGlu/ PBLG-*b*-PEG 40/60	51 ± 0.39	0.13 ± 0.0005	-48 ± 2.08
PBLG-*b*-PGlu/ PBLG-*b*-PEG 20/80	38 ± 0.78	0.16 ± 0.0016	-48 ± 0.44
PBLG-*b*-PEG	38 ± 1.7	0.13 ± 0.005	-31 ± 0.86
After CDDP complexing			
PBLG-*b*-PGlu/PBLG-*b*-PEG 100/0	53 ± 1.7	0.13 ± 0.016	-39 ± 0.66
PBLG-*b*-PGlu/ PBLG-*b*-PEG 80/20	45 ± 0.74	0.14 ± 0.025	-50 ± 4.6
PBLG-*b*-PGlu/ PBLG-*b*-PEG 60/40	45 ± 1.4	0.15 ± 0.013	-43 ± 0.47
PBLG-*b*-PGlu/ PBLG-*b*-PEG 40/60	56 ± 0.82	0.16 ± 0.023	-49 ± 8.6
PBLG-*b*-PGlu/ PBLG-*b*-PEG 20/80	49 ± 0.31	0.17 ± 0.013	-44 ± 1.2

CHAPITRE V:

OSTEOTROPICITY AND MICRODISTRIBUTION IN BONES OF SELF-ASSEMBLED MULTIFUNCTIONAL POLY(BENZYLGLUTAMATE) NANOPARTICLES

OSTEOTROPICITY AND MICRODISTRIBUTION IN BONES OF SELF-ASSEMBLED MULTIFUNCTIONAL POLY(BENZYLGLUTAMATE) NANOPARTICLES

Laura de Miguel [1],Christine Charrueau[2], Michel-Francis Bureau[3], Pierre J Marie[4], and Gilles Ponchel[1]*

[1] Univ. Paris Sud, UMR CNRS 8612, Institut Galien, 92296 Châtenay-Malabry Cedex, France.

[2] Univ Paris Descartes, Laboratoire de Pharmacie Galénique, EA4466, Sorbonne Paris Cité, 75270 Paris Cedex 06, France

[3] Unité de Pharmacologie Chimique et Génétique et d'Imagerie UMR 8151 CNRS / U1022 INSERM

[4] Laboratory of Osteoblast Biology and Pathology, UMR-606 Inserm et Université Paris Diderot, Sorbonne Paris Cité, Paris, France

*Corresponding author: Gilles Ponchel, Univ. Paris Sud, UMR CNRS 8612, Institut Galien Paris Sud, 92296 Châtenay-Malabry Cedex, France. E-mail: gilles.ponchel@u-psud.fr

Keywords: hydroxyapatite, bone, nanoparticles, biphosphonates, poly(amino acid).

Résumé

Des nanoparticules multifonctionnelles ont été obtenues par auto-assemblage de polymères issus d'une minilibrairie de dérivés du poly(glutamate de benzyle) (PBLG). Ces nanoparticules ont été conçues de manière à cibler l''hydroxyapatite, car il s'agit d'un composant très spécifique de l'os. Pour cela, une série de nanoparticules décorées par deux ligands de l'hydroxyapatite, l'alendronate et/ou le poly(acide glutamique) a été préparée par une méthode versatile de nanoprécipitation, ce qui a permis la modulation précise des propriétés d'attachement *in vitro* à l'hydroxyapatite. Des études de distribution conduites *in vivo* dans la structure complexe de l'os ont montré que certains types de nanoparticules pouvaient s'accumuler à différents degrés dans ce tissu, sans relation directe avec la présence de ligands ostéotropes. En revanche, l'examen de la microdistribution dans la structure complexe de l'os a montré que la présence d'alendronate ou de poly(acide glutamique) en surface des nanoparticules

favorisait leur immobilisation sur les surfaces minéralisées osseuses, en accord avec les études *ex vivo* de fixation sur l'os. Grâce à leur ostéotropicité et à la possibilité de les adresser précisément dans l'os, ces nanoparticules multifonctionnelles constituent donc des vecteurs prometteurs pour le traitement de maladies squelettiques.

Abstract

Bone targeted polymeric nanoparticles may be a valuable option in view of the treatment of different skeletal diseases. Multifunctional osteotropic nanoparticles were obtained by the self-assembly of poly(gamma-benzyl-L-glutamate) derivates, which could be decorated by alendronate and/or poly(glutamic acid) moieties intended for hydroxyapatite targeting. The nanoparticles were prepared by a versatile nanoprecipitation method which allowed precise tuning of *in vitro* hydroxyapatite binding properties. *In vivo* studies showed that both osteotropic and non osteotropic nanoparticles could attain bone tissues, be distributed into the bone and bound to mineralised bone surfaces, in coherence with *ex vivo* bone binding results. Detailed microdistribution studies showed for alendronate nanoparticles and poly(glutamic acid) ones an enhanced *in vivo* bone binding, constituting promising carriers for the treatment of skeletal diseases.

1-Introduction

Bone diseases such as osteoporosis, Paget's diseases, osteopenia, osteogenesis imperfecta or bone cancer constitute an increasingly major public health problem in our society**.** As an example of this, it is estimated that in 2020 more than one of two Americans over 50 years will risk or actually develop osteoporosis in any part of the skeleton [1]**.**

Active targeting nanoparticles have attracted much attention during the last decade, as a way of increasing drug delivery to the target reducing side effects. Various approaches can be foreseen in view of increasing specific delivery. In the case of cancers various approaches attempt to target the over expressing receptors of tumor vasculature or cells. However, these receptors do in fact exist in healthy cells and vasculature, driving to not so specific distributions in the body [2] and only few

approaches are based on the targeting of truly specific targets. Bone, composed of 50-70% of hydroxyapatite, ($Ca_{10}(PO_4)_6(OH)_2$), which is specific of bone tissue and is only present also in teeth and pathological calcifications, offers a highly specific target for the engineering of nanoparticles. The targeting of nanoparticles to bone extracellular matrix is a promising emerging approach [3-5] where nanoparticles could constitute a drug reservoir for intra tissue delivery.

There are several identified bone targeting moieties, among which biphosphonates and acidic oligopeptides have been largely used to impart drug osteotropicity [6]. Biphosphonate compounds are analogous of the endogenous pyrophosphate, where the labile P-O-P linkage has been substituted by the hydrolysis resistant P-C-P structure. The O-P-C-P-O backbone is responsible for the strong affinity of calcium ions. Acidic rich domains of bone acidic non collagenous proteins were identified and opened the way to the use of acidic oligopeptides, such as $(Asp)_6$ and $(Glu)_6$, as bone targeting moieties [7]. Both binding moieties have been shown to have differential *in vitro* and *in vivo* bone binding properties [8].

Here, we report the development of a library of osteotropic poly(benzylglutamate) (PBLG) polymers that self-assemble to produce a series of novel bone targeted nanoparticles with tuned surface properties. *In vitro* bone binding properties could be modulated depending on the osteotropic ligand attached to nanoparticles. Bone histological and microdistribution studies showed that alendronate and poly(glutamic acid) PBLG decorated nanoparticles could reach the mineralized surfaces. They showed good *in vivo* long-term bone binding for five types of nanoparticles with alendronate and poly(glutamic acid) PBLG nanoparticles being the most promising carriers for intra-tissue controlled drug release in long-term therapeutics of bone skeletal diseases.

2- Materials and Methods

2.1- Materials

Dimethylformamide (DMF) (99.8 %) Extradry Acroseal and cisplatin were purchased from Acros, γ-benzyl-L-glutamate-N-carboxyanhydride (BLG-NCA) was provided by IsoChem and used as

received. Trifluoroacetic acid (TFA) (99 %), dansylcadaverin (≥99%), hexylamine (puriss ≥99.5%), Palladium on carbon (Pd/C) were provided by Sigma Aldrich. All other reagents used were of analytical grade. α-N-hydroxysuccinimide-ω- alkyne-poly(ethylene glycol) (NHS-PEG-alkyne) (M_w=3000 Da) and α-azide-ω-amine poly(ethylene glycol) (N_3-PEG-NH_2) (M_w= 3317 Da) were bought from Iris Biotech and Rapp Polymers respectively and dried overnight under vacuum at 40 °C prior to use.

2.2- Synthesis of poly(γ-benzyl-L-glutamate) (PBLG) polymers

2.2.1- General polymerization procedure

A mini library of polymers based on a constant PBLG block has been prepared by ring opening polymerization of the corresponding N-carboxyanhydride (NCA). Polymerization reactions were carried out under inert pure argon atmosphere. Briefly, 1.5 g of BLG-NCA were weighed in a glove box under inert atmosphere (pure argon) and were dissolved in DMF at a concentration of 0.5 M . The solution was stirred for 10 minutes and a solution of the initiator in DMF was added with an argon-purged syringe. The solution was stirred at 30 °C during 5-7 days. Then, the mixture was poured into a large excess of cold diethylether (DEE) and the precipitate filtered and dried under vacuum. The extent of the reaction was controlled by infrared analysis, by checking the disappearance of BLG-NCA and the appearance of the PBLG bands. Polymers were analyzed by proton nuclear magnetic resonance (^{1}H NMR) in $CDCl_3$ 15 % trifluoroacetic acid (TFA) and for the PBLG-*b*-PEG copolymers molecular weight of the PBLG block could be determined in function of the relative intensities of the benzyl groups of the PBLG and the ethylene protons of the PEG.

2.2.2- Synthesis of PBLG-*b*-PEG-alendronate

The synthesis of PBLG-*b*-PEG-alendronate was achieved by a combination of ring-opening polymerization initiated by N_3-PEG_{3k}-NH_2 (M_w= 3317 Da), click chemistry with an alendronate-

PEG_{3k}-alkyne block and carbodiimide approach to synthesize the alendronate-PEG-alkyne block. The chemical scheme is detailed in Supplementary Data**.**

The synthesis of alendronate-PEG-alkyne block was achieved in the following conditions. Briefly, 2 mmoles of alendronate trihydrate were dissolved in 30 mL of water with 3.5 meq of triethylamine (TEA) and added to 0.2 mmoles of NHS-PEG-alkyne. The reaction mixture was stirred at 50 °C overnight and rotavapor was used to remove TEA. The solution was dialyzed with dialyze membranes of molecular cut off of 3500 Da over 72 hours and lyophilized to obtain a white powder. The structure of alendronate-PEG-alkyne block was confirmed by ^{1}H NMR. The presence of alendronate was confirmed and quantified by ^{31}P NMR and by phosphorus elemental analysis.

Synthesis of N_3-PEG-PBLG block was achieved by ring opening polymerization using a DMF solution of N_3-PEG_{3k}-NH_2 (Mw= 3317 Da) at a concentration of 4.4 mM as initiator as described in section 2.2.1 and its molecular weight was determined by ^{1}H NMR in deuterated chloroform ($CDCl_3$) + 15 % TFA, using the relative intensities of the protons belonging to the benzylic groups of the PBLG and the ethylenic protons of the PEG. Click reaction between azido-PEG-PBLG and alendronate-PEG-alkyne was performed in DMF at 55 °C for 72 hours. In a typical experiment azido-PEG-PBLG (2 µmol) and alendronate-PEG-alkyne (10 µmol, 5 equiv) were dissolved in 1 mL of anhydrous DMF. The mixture was stirred for 10 minutes and degassed prior to the addition of a DMF solution containing pentamethyldiethylenetriamine (PMDETA) (10 equiv) and copper(I) bromide (CuBr) (5 equiv). The block copolymer was recovered by precipitation in water after a dialysis purification step against water during 5 days (SpectraPor, molecular weight cut off: 12-14000 Da) to remove the excess of alendronate-PEG-alkyne, and was lyophilized. The efficacy of the click reaction was determined by ^{1}H NMR based on the relative intensities of the protons belonging to the benzylic groups of the PBLG and the ethylenic protons of the PEG

2.2.3- Synthesis of PBLG-*b*-poly(glutamic acid) (PBLG-*b*-PGlu) copolymer

A PBLG-*b*-PGlu copolymer was synthesized by a modified method previously described [9]. The synthetic scheme for this copolymer is detailed in SD.

First, $PBLG_{3k}$-bnz was synthesized by ring opening polymerization of γ-benzyl-L-glutamate-N-carboxylic anhydride (BLG-NCA) as previously described in section 2.2. This polymer was analyzed and its molecular weight determined by ^1H NMR in $CDCl_3$ + 15 % TFA by using the ratio of the integrations of the peaks corresponding to CH_3-NH_2 from hexylamine and benzylic peaks from PBLG, respectively.

Then, the benzylic groups were eliminated by catalytic hydrogenation. Briefly, 1.6 mg of hexyl-PBLG were dissolved in 27 mL of anhydrous DMF and 10 % of Pd/C was added to the solution. After purging three times with argon, the reaction mixture was stirred for 3 days at room temperature under overpressure of hydrogen (4 mbar). Then, the solution was centrifuged at 25 °C, 4000 rpm for 10 minutes and was further filtered over 0.22 μm filters in order to eliminate the Pd(black). It was then precipitated into a large excess of DEE, filtered and the precipitate dried in under vacuum at 40°C overnight. The completion of the reaction was analyzed by ^1H NMR in deuterated dimethyl sulfoxide (DMSO (d_6)).

Finally, the synthesis of PBLG-*b*-PGlu was achieved by ring opening polymerization of γ-benzyl-L-glutamate-N-carboxylic anhydride (BLG-NCA) as described in section 2.2. using a solution of hexyl-PGlu in DMF at a concentration of 3,1 mM as an initiator.

2.2.4- Synthesis of PBLG-dansyl

The synthesis of PBLG-dansyl was achieved by ring polymerization of γ-benzyl-L-glutamate-N-carboxylanhydride (BLG-NCA) using dansylcadaverin as an initiator. The polymerization reaction was made in the conditions described above. The resulting product was further washed three times with methanol (MeOH).

2.2.5- Synthesis of other PBLG-derivates

The synthesis of PBLG-benzyl (PBLG-bnz), PBLG- fluorescein isothiocyanate (PBLG-FITC) and PBLG-*b*-PEG was achieved as previously described [10] and following the general method described in section 2.1.

2.3- Characterization of PBLG copolymers

2.3.1- Nuclear magnetic resonance (NMR)

^{1}H NMR spectra were recorded on a Bruker AC 300 spectrometer in $CDCl_3$ + 15% TFA. The role of the acid is to disrupt helix, rendering PBLG in a random coil conformation.

2.3.2- Fourier transform infrared spectroscopy (FTIR)

FTIR spectra of the polymers were performed on a Fourier Transform Perkin-Elmer 1750 infrared spectrometer using an attenuated total reflection system (ATR) to confirm the absence of NCA auto-polymerization, to follow the evolution of the polymerization reactions and to study the secondary structure of the polymers.

2.3.3- Size exclusion chromatography (SEC)

Size exclusion chromatography (SEC) was used to determine the molar mass of PBLG-*b*-PGlu. SEC system was equipped with two PLgel 5µm MIXED-D (7.5mm ID x 30.0cm L) and a PLgel 5µm guard column (guard column 7.5mm ID x 5.0cm L), a refractive index detector (Jasco 1530-RI) and a UV detector (Jasco 875-UV). DMF with 1g/L of LiBr was used as a diluent at a flow of 0.8 ml/minute and linear polystyrene samples were used as calibration standards.

2.3.4- Quantification of alendronate in PBLG-*b*-PEG-alendronate

Quantitative NMR spectroscopy using coaxial inserts containing monopotassium phosphate (KH_2PO_4) solution as a reference standard was used to quantify the concentration of alendronate in alendronate-PEG-alkyne. Details of the methods can be found in SD. Phosphorus elemental analysis of

alendronate-PEG-alkyne was also performed. The alendronate content in PBLG-*b*-PEG-alendronate was determined considering the efficacy of the click reaction yielded by ^{1}H NMR.

2.4- Nanoparticle preparation

Nanoparticles were prepared following nanoprecipitation method previously described in our group either single or different mixtures of PBLG copolymers, with varying ratios (expressed in wt%). Briefly, 7.5 mg of the different PBLG derivates were dissolved in 2.5 mL of tetrahydrofuran (THF)/MeOH 75/25 at 40 °C without magnetic stirring. Once dissolved they were added by dripping to an aqueous solution containing two equivalents of sodium hydroxide (NaOH) per equivalent of carboxylic acid (COOH) and magnetically stirred for 10 minutes. Solvents were eliminated by a standardized protocol under vacuum at 40 °C and nanoparticles were added with poloxamer (Pluronic® F68) to a final concentration of 0.1 % .

2.5- Morphological characterization of nanoparticles

Nanoparticle size and zeta potential were determined by dynamic light scattering (DLS) using a Zetasizer 4 (Malvern Instruments). Nanoparticles were observed by means of a Transmission Electron Microscopy (TEM) at 120 kV after negative coloration. 3µL of the diluted nanoparticle suspension were deposited on a formvarcarbon film previously coated on a copper grid of 400 meshes and phosphotungstic acid 1% w/w used as a negative coloration staining.

2.6- Nanoparticle interaction with hydroxyapatite (HAP)

2.6.1- *In vitro* HAP binding assay

One mL of multifunctional nanoparticles containing a fluorescent PBLG derivate, PBLG-dansyl, and an osteotropic PBLG derivate in poloxamer (Pluronic® F68) 0.1 % w/v were incubated in 3 mL of phosphate buffer saline (PBS) containing 0.4 g of HAP at a pH of 7.4 during 18 hours at 25 °C. The suspensions were centrifuged at 5000 rpm for 5 minutes, washed and vortexed three times with poloxamer 1% in PBS 7.4 and observed under UV light at 365 nm. Supernatants were quantified by a

Perkin Elmer Luminescence spectrometer LS 50B at room temperature ($\lambda_{excitation}$ =340 nm . $\lambda_{emission}$ = 472 nm) so as to determine the amount of nanoparticles not bound to HAP.

2.6.2- Kinetics binding assay

0.25 mL of multifunctional nanoparticles containing a fluorescent PBLG derivate, PBLG-dansyl, and an osteotropic PBLG derivate in poloxamer (Pluronic® F 68) 0.1 % w/v were incubated in 0.75 mL of PBS containing 0.1 g of HAP at a pH of 7.4 at 25 °C different times. Suspensions were centrifuged at 5000 rpm for 5 minutes and washed three times with poloxamer 1% in PBS 7.4 with the subsequent centrifugation step. Supernatants were quantified as described in section 2.6.1.

2.6.3- pH- dependent dissociation of nanoparticle-HAP complexes

Nanoparticle-HAP complexes were washed with poloxamer 1% /PBS 1/1 at several consecutive pH 5.5, 4.5 and 3.5, three times for each pH, centrifuged at 5000 rpm for 5 minutes and supernatants obtained were quantified as described in section 2.6.1.

2.7- Bone binding assay

Femurs were obtained from specific pathogen-free BALB/cByJ mice and were embedded in ethanol/water 70/30 and stored for two weeks prior to use. 3 mL of multifunctional nanoparticle suspensions containing a fluorescent PBLG derivate, PBLG-FITC, and a PBLG derivate in 0.1 % of poloxamer (Pluronic® F 68) were incubated with one femur overnight at 37 °C under rotary stirring. Nanoparticles were removed and femurs were washed three times with poloxamer 1%. Images were acquired using a CCD camera (Apogée Alta U 47). The images were analyzed with the public-domain ImageJ software (US National Institutes of Health, Bethesda, MD). The average fluorescence intensity was determined for each bone diaphysis using the same threshold settings (low threshold: 400, high threshold: 20,000). Data are reported as the average channel fluorescence of bone diaphysis and expressedas relative units after background subtraction.

2.8- *In vivo* distribution studies

Male, 5-week-old, specific pathogen-free BALB/cByJ mice were purchased from Charles River Laboratories. Mice were kept in accordance with the institutional guidelines of the French Ethical Committee. Xylenol orange tetrasodium was injected subcutaneously at a dose of 40 mg/Kg in order to label bone formation sites. Three days after, 200 µL of the different nanoparticle suspensions at a concentration of 4.3 mg/mL, labelled with FITC, containing 0.2 % of poloxamer 188, and diluted in 0.9% wt NaCl, were injected via the tail vein and animals were euthanized by intraperitoneal injection of sodium pentobarbital after 24 hours and 5 days (n=3 for each group).

Ex vivo fluorescence imaging

Liver, spleen, femurs and kidneys were extracted after euthanasia of the animals for isolated organ imaging to estimate the tissue distribution of the fluorescently labelled nanoparticles with a CCD camera (Photon Imager, Biospace). The fluorescence intensity was quantified using M3Vision 2.2.1 (Biospace Lab) after determination of regions of interest for each organ. Results were expressed as photon per steradian per second per square centimeter (ph/sr/s/cm^2).

Histological studies

For fluorescence analysis, the left femurs were excised for undecalcified tissue embedding. Briefly, bones were fixed in 70% ethanol and dehydrated progressively in graded concentrations of ethanol and embedded in methyl methacrylate. 10 µm sections were obtained with a Leica microtome (SM2500S) (Wetzlar, Germany) and the distribution pattern of PBLG-derivate nanoparticles was analyzed under microscopy (Microvision). Bone formation surfaces labelled with the different PBLG-FITC nanoparticles were quantified by the Parfitt method [11] in both cortical and trabecular bones. The simple labelled surfaces (FITC-Nanoparticles) and the double labelled surfaces (Xylenol orange and FITC-Nanoparticles) were quantified with respect to the total bone using the objective eyepiece Leitz intergratepaltte II.

3- Results and discussion

3.1- Synthesis and characterization of PBLG polymers

Several PBLG polymers bearing different functionalities could be synthesized by ring opening polymerization. Two osteotropic copolymers bearing alendronate or poly(glutamic acid) were synthesized. Alendronate belongs to the family of biphosphonates and with poly(glutamic acid) are well known to have affinity to HAP and have been used to impart osteotropicity to drugs [12-15]. The synthesis of PBLG-*b*-PEG-alendronate copolymer was achieved by a combination of carbodiimide and click chemistry. Alendronate content was quantified by a combination of NMR and elemental analysis and it could be estimated that 31% of the PBLG-*b*-PEG-alendronate polymeric chains contained an alendronate molecule. PBLG-*b*-PGlu copolymer could be synthesized by a living polymerization approach. The PGlu block was composed of 16 repetitive units of glutamic acid, as estimated by ^{1}H NMR and theoretically 100 % of PBLG-*b*-PGlu chains contained a PGlu macromolecule. Structures were characterized by ^{1}H NMR and infra-red spectroscopy. Molar masses were estimated using SEC as shown in table 1. Detailed procedures and characterization of the PBLG copolymers are described in SD.

PBLG-polymers	DP_n [a, b,]	Mn(g/mol)[c]	PI[c]	DP_n [c]
PBLG-bnz	136	31727	1.14	144
PBLG-dansyl	91	25944	1.10	117
PBLG-*b*-PEG	228	65513	1.27	276
PBLG-*b*-PGlu	137	24436	1.75	102
PBLG-*b*-PEG-alendronate	228	52816	1.54	214
PBLG-FITC	228	52647	1.17	238

Table 1: Molecular weight (Mn), degree of polymerization (DP_n) and polymolarity index (PI) of the polymers (a): theoretical (b): of the PBLG block (c): determined by SEC

3.2- Morphological characterization of nanoparticles

PBLG polymers were shown to self-assemble into nano-objects following a simple nanoprecipitation method previously described in our group. Interestingly, different PBLG polymers could assemble to form multifunctional nanoparticles, where surface properties could be precisely tuned.

Nanoparticles	$D_{longitudinal}$ (nm) ± SD [a]	D_{axial} (nm) ± SD[a]	Aspect ratio	$D_{equivalent}$ (nm) ± SD
PBLG-dansyl [a]	43 ± 8.6	32 ± 6.5	1.4	39 ± 7.3
PBLG-bnz [a]	53 ± 10	34 ± 5.1	1.6	46 ± 8.5
PBLG-*b*-PEG [a]	41 ± 7.2	25 ± 3.5	1.6	35 ± 5.1
PBLG-*b*-PEG-alendronate [a]	43 ± 5.3	29 ± 4.3	1.5	37 ± 4.2
PBLG-*b*-PGlu [a]	46 ± 10	34 ±5.0	1.4	41 ± 7.8
PBLG-*b*-PEG-alendronate/ PBLG-*b*-PGlu (1/3) [a,c]	44 ± 8.4	32 ± 5.1	1.4	39 ± 6.6
PBLG-*b*-PEG/ PBLG-*b*-PGlu (1/3) [a,d]	48 ± 9.1	30 ± 4.6	1.6	41 ± 6.7
PBLG-bnz [b]	66 ± 19	31 ± 5	2.1	51 ± 11
PBLG-*b*-PEG [b]	51 ± 13	26 ± 4	2.0	41 ± 8.0
PBLG-*b*-PEG-alendronate [b]	48 ± 9	31 ± 5	1.6	41 ± 6
PBLG-*b*-PGlu [b]	62 ± 20	32 ± 7	1.9	49 ± 13
PBLG-*b*-PEG-alendronate/ PBLG-*b*-PGlu (1/3) [b,c]	58 ± 16	30 ± 6.5	1.9	46 ± 10
PBLG-*b*-PEG/ PBLG-*b*-PGlu (1/3) [b,d]	62 ± 19	32 ± 6	1.9	50 ± 12

Table 2: Morphological data obtained by TEM measurements of nanoparticles (n= 100). a: nanoparticles containing 33% w/w of the PBLG-dansyl derivate except for PBLG-dansyl nanoparticles which contained 100 % of it. b; nanoparticles containing 25 % w/w of the PBLG-FITC derivate. c; ratio w/w PBLG-*b*-PEG/PBLG-*b*-PGlu. c; ratio PBLG-*b*-PEG-alendronate/PBLG-*b*-PGlu

Nanoparticles presented an oblate spheroid form with aspect ratio ranging from 1.4 to 2.1 and their longitudinal diameter being smaller than 70 nm (Table 2). Different osteotropic monofunctional and multifunctional nanoparticles were prepared as well as other non osteotropic nanoparticles, as controls.

3.3- *In vitro* HAP binding

The *in vitro* HAP binding assay (Figure 1) showed the capability of alendronate and poly(glutamic acid) to impart HAP binding ability to nanoparticles. Hence, the four types of nanoparticles containing an osteotropic ligand could bind specifically to HAP whereas no binding occur for the negative control nanoparticles, not bearing an osteotropic ligand except for bnz nanoparticles where ~ 20 % of binding appears, which might be attributed to non specific binding.

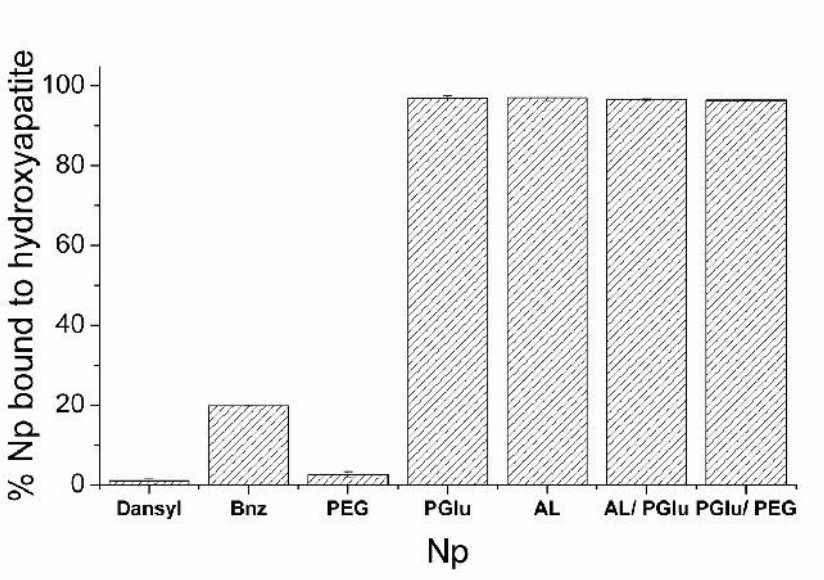

Figure 1: Degree of binding expressed in percentage of nanoparticles bound to HAP after 18 hours. Nanoparticles at a concentration of 1.5 mg/mL in 0.1 % w/v poloxamer were incubated with 0.4 g of HAP suspension in 3 mL of PBS buffer (n=3).

Probably, the efficiency of binding depends on the efficiency of the binding ligand presentation on the nanoparticle surface. This is likely to be very effective due to the rigidity of the assembled PBLG

hydrophobic block, which makes unlikely the hindrance of hydrophilic moieties in the core of the particles, but on the contrary induces their exposure onto nanoparticle surface (see chapter II).

The kinetics binding assay (Figure 2) showed a rapid binding with a full binding for the four types of osteotropic nanoparticles after 2 hours. At shorter times, differential kinetics were observed depending on the osteotropic ligand, with the following decreasing rate of binding: alendronate > alendronate/poly(glutamic acid) > poly(glutamic acid) > poly(glutamic acid)/PEG nanoparticles. After 10 minutes, less than 55% poly(glutamic acid)/PEG nanoparticles, ~65% poly(glutamic acid) and alendronate/poly(glutamic acid) nanoparticles and more than 80% alendronate nanoparticles were bound to HAP. Nanoparticles binding to HAP is a time dependent process, as it has been already described in the literature for alendronate and other osteotropic molecules [12, 16, 17]

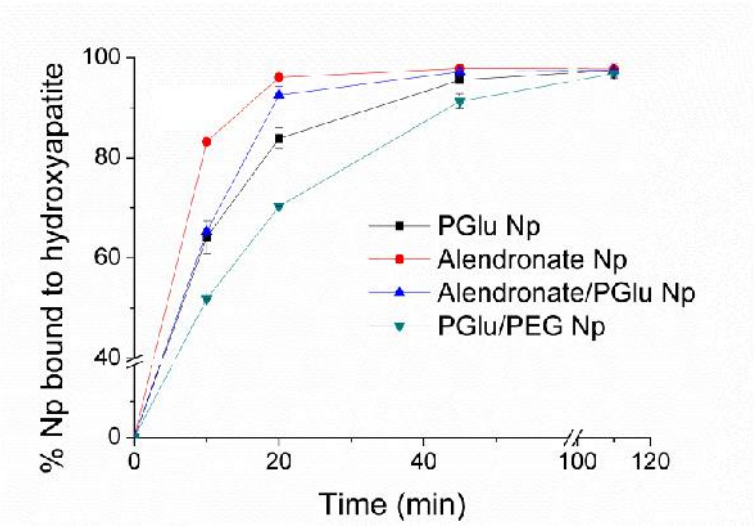

Figure 2: Binding kinetics of nanoparticles to HAP (n=3).

The possible desorption of HAP-bound nanoparticles was studied at different acidic pH (Figure 3) since the pH in the resorption lacunae is known to be acidic [18] and localized acidification, without implying a true resorption, has been suggested to cause the release of bone bound biphosphonate. [19].

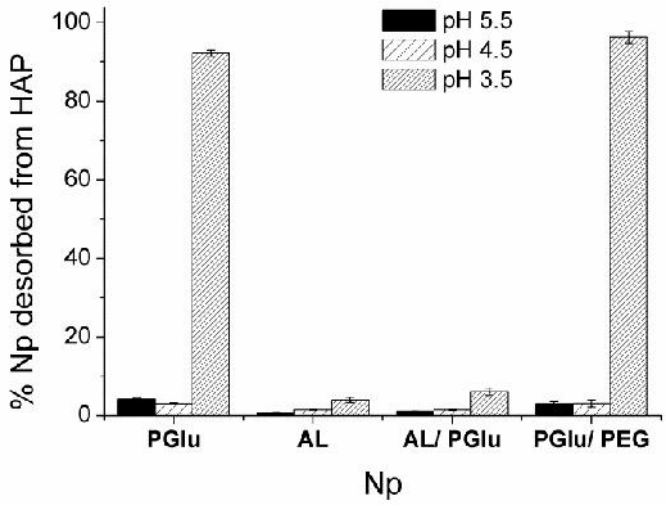

Figure 3: Desorption of the different HAP-bound nanoparticles at the following consecutive pH: 5.5, 4.5 and 3.5 (n=3).

Desorption from HAP was negligible at pH 5.5 and 4.5 whatever the type of nanoparticle. However, at pH 3.5, nearly 100 % of poly (glutamic acid) and poly (glutamic acid)/PEG nanoparticles were desorbed whereas alendronate and alendronate/ poly (glutamic acid) nanoparticles resisted to desorption. This assay also shows the differential HAP binding of alendronate and poly(glutamic acid) decorated nanoparticles. Both kinetics and desorption studies suggest that for mixed alendronate/ poly (glutamic) nanoparticles, it is the alendronate moiety which displays the HAP binding. *In vitro* bone dissociation studies for alendronate (in the molecular state) have shown that 50% of alendronate molecules are released at a pH of 3.5 [20]. In the present case, no desorption was observed for alendronate nanoparticles. This difference can be attributed to the multivalency of alendronate nanoparticles, which present several molecules of alendronate per nanoparticle, which is known to increase dramatically the binding affinities (see chapter 2), as shown more specifically in the present case for HAP at this pH. Finally, desorption from mineral is an important property that could be influence the *in vivo* interaction within bone microenvironment. Obviously, once attained the mineralized bone surfaces, the duration of their retention would depend on the balance between

attachment and detachment, which is likely to affect further their microdistribution. Desorption from mineral is an important property that influences *in vivo* interaction within bone microenvironment. Once bound to bone, nanoparticles if they are prone to detachment, could more easily interact with bone cells and they would be expected to have less skeletal retention [21].

3.4- *Ex vivo* bone binding assay

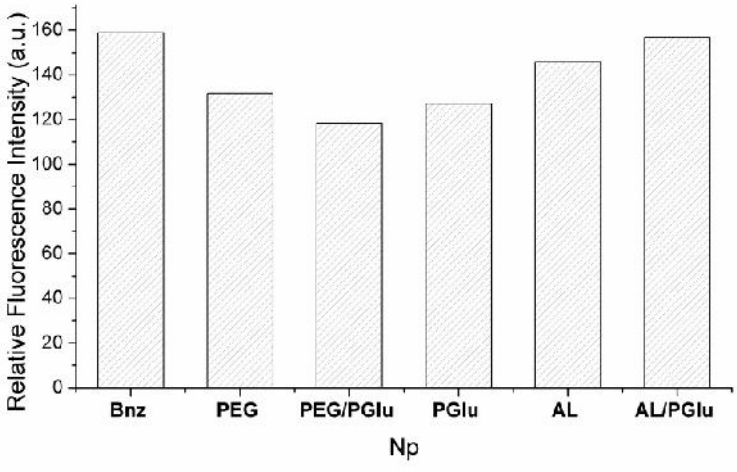

Figure 4: Bone binding of the different PBLG-derivate nanoparticles using BALB/c femurs and determined by fluorescence quantification.

Ex vivo bone binding studies were performed to determine the ability of nanoparticles to bind to the bone (Figure 4). Surprisingly, all types of PBLG-derivate nanoparticles, osteotropic and non osteotropic ones, where found to bind to bone. Bone is composed of 50-70% mineralised matrix, 20-40% organic matrix, 5-10% water and 5% of lipids. The mineral phase consists of impure HAP crystals whereas the organic matrix is mainly constituted of (~85-90%) type I collagen and also other collagenous proteins and non collagenous proteins [22]. Moreover, synthetic and biological HAP are

different in terms of hydroxylation degree, carbonate substitution and crystal size [23]. In view of the results, it seems that PBLG nanoparticles themselves have an intrinsic affinity for bone mineral.

3.5- *In vivo* biodistribution studies

Nanoparticles ability to attain bone was determined by their biodistribution profile, which depends on both anatomo-physiological characteristics of the organism and physico-chemical nanoparticle characteristics. *Ex vivo* organ imaging using fluorescently labelled nanoparticles (25% of the PBLG-FITC) was employed to estimate nanoparticles biodistribution in healthy mice following intravenous administration. Figure 5 shows the biodistribution of the several types of nanoparticles 24 hours and 5 days post-administration.

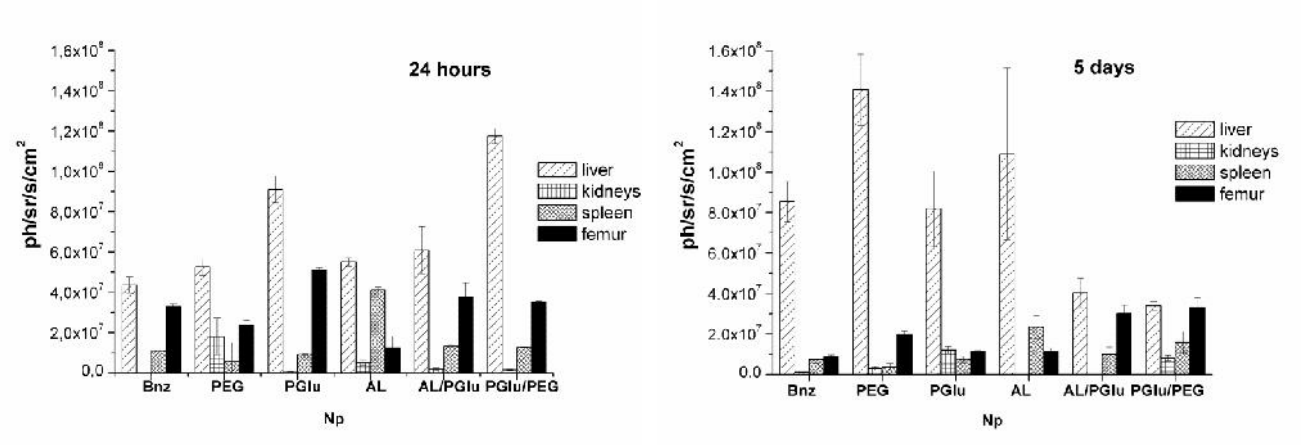

Figure 5: Quantification of the fluorescence distributed in the organs 24 hours and 5 days after intravenous administration of PBLG-derivate nanoparticles (n=3).

Nanoparticles were highly distributed to liver with different behaviours depending on the type of nanoparticle. This behaviour is expected as the avoidance of the capture of nanoparticles by the reticuloendotelial system (RES) is often difficult to achieve and due to the larger fenestrations of the liver vasculature, that allows a transvascular flow up to 280 nm in mice [24]. Interestingly, the amount of Bnz, PEG and AL nanoparticles distributed to liver increased between 1 and 5 days post-

administration, suggesting a prolonged circulation in the bloodstream (i.e. stealth effect) whereas for PGlu/PEG and AL/PGlu nanoparticles it diminished, suggesting a possible elimination by the Kuppfer cells. No change was observed for PGlu nanoparticles. Nanoparticles were also considerably distributed to bone, as evidenced by the bone/liver ratio, which ranges from 0.71-0.10 depending on the type of nanoparticles and time. After 24 hours, the fluorescence intensity in bone decreased as follows: PGlu> AL/PGlu> Bnz > PGlu/PEG> PEG> AL nanoparticles. After 5 days, the order was different, being PGlu/PEG> AL/PGlu> PEG> PGlu> AL> Bnz.

For all nanoparticles the fluorescence intensity in bone diminished with time probably due to the elimination by macrophages; the slightest diminution was seen for AL nanoparticles. This considerable distribution to bone is likely to be due to the role of bone marrow as a RES organ. It is known that the endothelium of bone marrow can remove non-endogenous macromolecules by phago-endocytosis and upon transvascular release or spill over, be found in the interstitial bone marrow space [24, 25]. Although less attention has been devoted to the bone marrow as a RES organ, some studies have stressed its importance in the uptake of surface-modified nanoparticles [26]. It has been shown that some poloxamer-coated nanoparticles could be highly distributed to bone marrow [27]. Nanoparticles should be stealth and small enough (around 60 nm) so as to be able to avoid liver RES capture and be able to be endo-phagocytosed by the bone marrow endothelium [24]. In the present experiments and whatever the type of PBLG nanoparticles, their size was smaller than 60 nm and an adsorbed poloxamer-coating was added to render the nanoparticles stealth or bring to perfection the coating of the nanoparticle surfaces with PEG blocks (where used), allowing the endo-phagocytosis by the bone marrow endothelium. Logically, osteotropic ligands did not enhance accumulation in bone since it is the capability of nanoparticles to be endo-phagocytosed by bone marrow endothelial cells which would be the bottleneck to their delivery to mineral surfaces and finally would determine their concentration in bone. In addition, bone mineralised surfaces are not readily next to the vessels.

The present method was limited since quantification of nanoparticles was performed on the whole bone and it did not allow distinguishing between distribution in the bone marrow from that in the mineralized bone. Once nanoparticles have attained the bone microenvironment, there are still important barriers to overcome so that they can attain bone mineralized tissue. Bone marrow contains a large number of cells and is the site of production of $4.9\ 10^{11}$ cells per day as well as the site for homing stem cells from the circulation [28]. Bone marrow produces stromal and hematopoietic cells, including monocytes, granulocytes and bone marrow macrophages which are involved in the clearance of nanoparticles [29]. In order to efficiently attain bone mineralized surfaces, nanoparticles should penetrate through the bone marrow avoiding internalisation by these numerous cells. For this purpose, stealthiness is again favourable. Once nanoparticles bound, nanoparticle desorption, if existing, might also be considered. Nanoparticles more prone to detachment could interact more likely with bone cells and could be more easily eliminated from the skeleton.

Bone histological experiments were therefore implemented so as to determine which type of nanoparticle could attain more efficiently bone mineralized tissue and bone formation surfaces (specifically labelled with xylenol orange) (Figure 6). Histological studies by fluorescence microscopy revealed that most nanoparticles could attain mineralised tissue and remained bound to it (Figure 6).
Among them, alendronate nanoparticles were the most efficient nanoparticles in attaining bone mineralized tissue at both 24 hours and 5 days even if they showed the lowest biodistribution to overall bone. This could be in part due to the rapid bone binding kinetics, as evidenced by the HAP binding assay. In trabecular bone after 5 days, PGlu nanoparticles were bound to mineralized surfaces almost at the same degree as the alendronate ones. Bnz and PEG nanoparticles, although they lack an active bone targeting moiety, could effectively bind to bone mineralized surfaces, in coherence with the bone binding assay. Surprisingly, AL/PGlu nanoparticles, although they are found in the bone and despite the efficient *in vitro* HAP and bone binding characteristics, did not appear to be able to bind to bone mineralized surfaces *in vivo*.

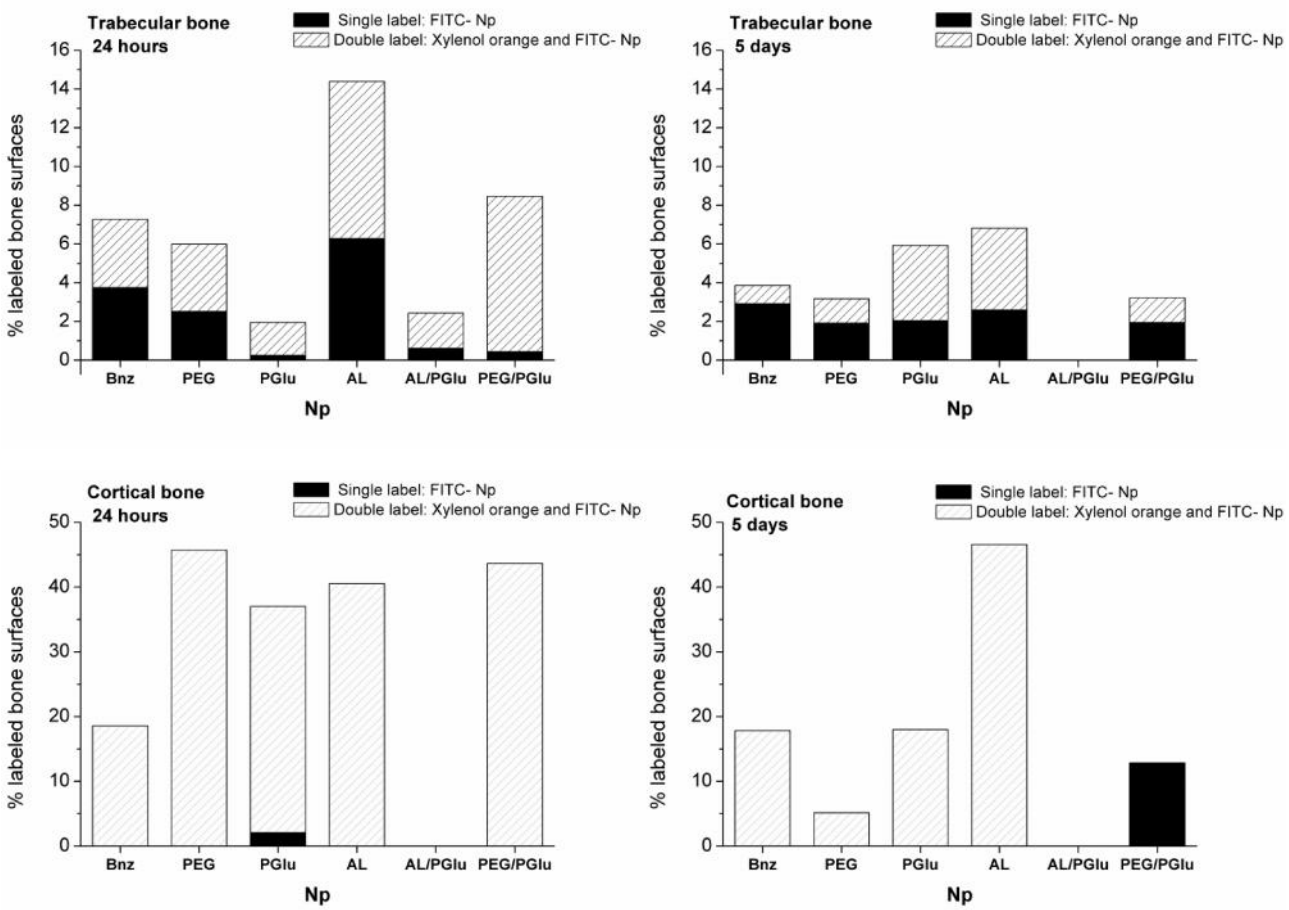

Figure 6: Histological semi-quantitative study of the single and double labelled mineralizing bone surfaces in femurs 24 hours and 5 days after intravenous administration of PBLG-derivate nanoparticles. Single labelled surfaces corresponds to fluorescently-labelled FITC nanoparticles (FITC-Np) whereas double labelled surfaces corresponds to surfaces labelled with both the bone formation marker xylenol orange and the fluorescently-labelled FITC nanoparticles (FITC-Np).

This might result from the complex multifactorial *in vivo* kinetic processes involved as indicated above. This study underlines the difficulty to extrapolate results obtained with *in vitro* and *ex vivo* methods to the in vivo fate of nanoparticles intended for bone targeting as others have evidenced [30]

4- Conclusions

We have prepared a series of bone-targeted multifunctional PBLG nanoparticles with tuned bone targeting properties. *In vitro* HAP binding properties could be controlled by precise modulation of the

type and amount of osteotropic moiety born on their surface and only nanoparticles bearing a bone targeting moiety could bind to HAP. *In vivo* studies showed that all types of nanoparticles could also be distributed to bone. Logically, biodistribution into the bone was not enhanced by the osteotropic moieties since it is determined by the capability of trafficking and being endocytosed by bone marrow endothelial cells. Most types of nanoparticles could attain bone surface and remain bound to it as shown by the histological studies, exhibiting different microdistribution patterns. Among all, alendronate nanoparticles showed enhanced *in vivo* bone binding, both in cortical and trabecular bone and 1 and 5 days after injection. However, no benefit has been obtained from the combination of both alendronate and glutamic acid on the nanoparticles. Binding of alendronate nanoparticles at mineralizing surfaces may have a high potential for the long-term therapeutics of skeletal diseases.

Acknowledgements

We gratefully acknowledge the european postgraduate program from "Caja Madrid Foundation" for the financial support. We thank Dr Morvan for her help with the quantitative with the quantitative ^{31}P NMR spectroscopy. This work has benefited from the facilities and expertise of the Platform for Transmission Electronic Microscopy of IMAGIF (Centre de Recherche de Gif - www.imagif.cnrs.fr)". We are grateful to Silvia Mazzaferro for the SEC analysis. We thank the Animal Platform of the School of Pharmacie, Paris-Sud University. We thank Miss Cynthia Gillet for her valuable help with the TEM image acquisitions. We thank Dr Julia Brun and Alice Gaudin for her kindly help with femur extraction and animal experiments respectively and Mrs Caroline Marty for her help with the histological studies.

References

[1] Bone health and osteoporosis: a report of the surgeon general. Office of the surgeon general (US); 2004.

[2] Zhang X-Q, Xu X, Bertrand N, Pridgen E, Swami A, Farokhzad OC. Interactions of nanomaterials and biological systems: Implications to personalized nanomedicine. Adv Drug Delivery Rev. 2012;64:1363-84.

[3] Zhang G, Guo B, Wu H, Tang T, Zhang BT, Zheng L, et al. A delivery system targeting bone formation surfaces to facilitate RNAi-based anabolic therapy. Nat Med. 2012;18:307-14.

[4] Thamake SI, Raut SL, Gryczynski Z, Ranjan AP, Vishwanatha JK. Alendronate coated poly-lactic-co-glycolic acid (PLGA) nanoparticles for active targeting of metastatic breast cancer. Biomaterials. 2012;33:7164-73.

[5] Ramanlal Chaudhari K, Kumar A, Megraj Khandelwal VK, Ukawala M, Manjappa AS, Mishra AK, et al. Bone metastasis targeting: a novel approach to reach bone using zoledronate anchored PLGA nanoparticle as carrier system loaded with docetaxel. J Control Release. 2012;158:470-8.

[6] Ishizaki J, Waki Y, Takahashi-Nishioka T, Yokogawa K, Miyamoto K-i. Selective drug delivery to bone using acidic oligopeptides. J Bone Miner Metab. 2009;27:1-8.

[7] Fujisawa R, Wada Y, Nodasaka Y, Kuboki Y. Acidic amino acid-rich sequences as binding sites of osteonectin to hydroxyapatite crystals. Biochim Biophys Acta. 1996;1292:53-60.

[8] Wang D, Miller SC, Shlyakhtenko LS, Portillo AM, Liu XM, Papangkorn K, et al. Osteotropic peptide that differentiates functional domains of the skeleton. Bioconjug Chem. 2007;18:1375-8.

[9] Higashi N, Koga T, Niwa M. Helical superstructures from a poly(γ-benzyl-l-glutamate)−poly(l-glutamic acid) amphiphilic diblock copolymer: monolayer formation on water and its specific binding of amino acids. Langmuir. 2000;16:3482-6.

[10] Segura-Sanchez F, Montembault V, Fontaine L, Martinez-Barbosa ME, Bouchemal K, Ponchel G. Synthesis and characterization of functionalized poly(gamma-benzyl-L-glutamate) derivates and corresponding nanoparticles preparation and characterization. Int J Pharm. 2010;387:244-52.

[11] Parfitt AM, Drezner MK, Glorieux FH, Kanis JA, Malluche H, Meunier PJ, et al. Bone histomorphometry: Standardization of nomenclature, symbols, and units: Report of the asbmr histomorphometry nomenclature committee. J Bone Miner Res. 1987;2:595-610.

[12] Leu C-T, Luegmayr E, Freedman LP, Rodan GA, Reszka AA. Relative binding affinities of bisphosphonates for human bone and relationship to antiresorptive efficacy. Bone. 2006;38:628-36.

[13] Bauss F, Esswein A, Reiff K, Sponer G, Muller-Beckmann B. Effect of 17beta-estradiol-bisphosphonate conjugates, potential bone-seeking estrogen pro-drugs, on 17beta-estradiol serum kinetics and bone mass in rats. Calcif Tissue Int. 1996;59:168-73.

[14] Sekido T, Sakura N, Higashi Y, Miya K, Nitta Y, Nomura M, et al. Novel drug delivery system to bone using acidic oligopeptide: pharmacokinetic characteristics and pharmacological potential. J Drug Targeting. 2001;9:111-21.

[15] Kasugai S, Fujisawa R, Waki Y, Miyamoto K, Ohya K. Selective drug delivery system to bone: small peptide (Asp)6 conjugation. J Bone Miner Res. 2000;15:936-43.

[16] Rill C, Kolar ZI, Kickelbick G, Wolterbeek HT, Peters JA. Kinetics and thermodynamics of adsorption on hydroxyapatite of the [160Tb] terbium complexes of the bone-targeting ligands DOTP and BPPED. Langmuir. 2009;25:2294-301.

[17] Kandori K, Fudo A, Ishikawa T. Adsorption of myoglobin onto various synthetic hydroxyapatite particles. Phys Chem Chem Phys. 2000;2:2015-20.

[18] Baron R, Neff L, Louvard D, Courtoy PJ. Cell-mediated extracellular acidification and bone resorption: evidence for a low pH in resorbing lacunae and localization of a 100-kD lysosomal membrane protein at the osteoclast ruffled border. J Cell Biol. 1985;101:2210-22.

[19] Rogers MJ, Gordon S, Benford HL, Coxon FP, Luckman SP, Monkkonen J, et al. Cellular and molecular mechanisms of action of bisphosphonates. Cancer. 2000;88:2961-78.

[20] Sato M, Grasser W, Endo N, Akins R, Simmons H, Thompson DD, et al. Bisphosphonate action. Alendronate localization in rat bone and effects on osteoclast ultrastructure. J Clin Invest. 1991;88:2095-105.

[21] Nancollas GH, Tang R, Phipps RJ, Henneman Z, Gulde S, Wu W, et al. Novel insights into actions of bisphosphonates on bone: Differences in interactions with hydroxyapatite. Bone. 2006;38:617-27.

[22] Marks Jr SC, Odgren PR, John PB, Lawrence G. Raisz and Gideon A. Rodan A2 - John P. Bilezikian LGR, Gideon AR. Chapter 1 - Structure and development of the skeleton. Principles of bone biology (second edition). San Diego: Academic press; 2002. p. 3-15.

[23] Leventouri T. Synthetic and biological hydroxyapatites: Crystal structure questions. Biomaterials. 2006;27:3339-42.

[24] Sarin H. Physiologic upper limits of pore size of different blood capillary types and another perspective on the dual pore theory of microvascular permeability. J Angiogenes Res. 2010;2:2-14.

[25] Moghimi SM. Exploiting bone marrow microvascular structure for drug delivery and future therapies. Adv Drug Delivery Rev. 1995;17:61-73.

[26] Sou K. Advanced drug carriers targeting bone marrow, recent advances in novel drug carrier systems In: (Ed.) PADS, editor.2012.

[27] Moghimi SM, Porter CJH, Illum L, Davis SS. The effect of poloxamer-407 on liposome stability and targeting to bone marrow: comparison with polystyrene microspheres. Int J Pharm. 1991;68:121-6.

[28] Yin T, Li L. The stem cell niches in bone. The Journal of Clinical Investigation. 2006;116:1195-201.

[29] Gibaud S, Demoy M, Andreux JP, Weingarten C, Gouritin B, Couvreur P. Cells involved in the capture of nanoparticles in hematopoietic organs. J Pharm Sci. 1996;85:944-50.

[30] Kirpotin DB, Drummond DC, Shao Y, Shalaby MR, Hong K, Nielsen UB, et al. Antibody targeting of long-circulating lipidic nanoparticles does not increase tumor localization but does increase internalization in animal models. Cancer Res. 2006;66:6732-40.

Supplementary Data

OSTEOTROPICITY AND MICRODISTRIBUTION IN BONES OF SELF-ASSEMBLED MULTIFUNCTIONAL POLY(BENZYLGLUTAMATE) NANOPARTICLES

Laura de Miguel [1],Christine Charrueau[2], Michel-Francis Bureau[3], Pierre J Marie[4], and Gilles Ponchel[1]*

[1] Univ. Paris Sud, UMR CNRS 8612, Institut Galien, 92296 Châtenay-Malabry Cedex, France.

[2] Univ Paris Descartes, Laboratoire de Pharmacie Galénique, EA4466, Sorbonne Paris Cité, 75270 Paris Cedex 06, France

[3] Unité de Pharmacologie Chimique et Génétique et d'Imagerie UMR 8151 CNRS / U1022 INSERM

[4] Laboratory of Osteoblast Biology and Pathology, UMR-606 Inserm et Université Paris Diderot, Sorbonne Paris Cité, Paris, France

*Corresponding author: Gilles Ponchel, Univ. Paris Sud, UMR CNRS 8612, Institut Galien Paris Sud, 92296 Châtenay-Malabry Cedex, France. E-mail: gilles.ponchel@u-psud.fr

1. PBLG-*b*-PEG-AL copolymer: synthesis and characterization

1.1. Synthesis scheme for PBLG-*b*-PEG-alendronate

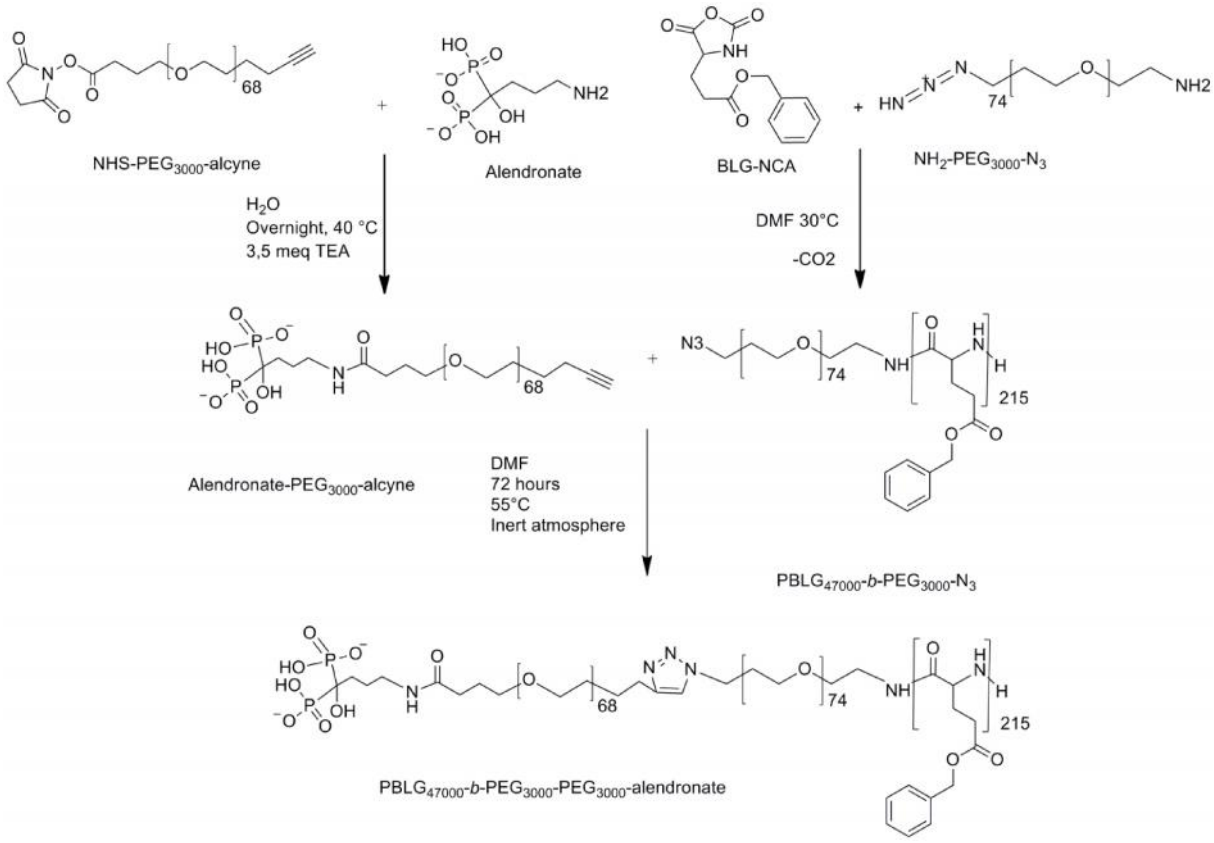

1.2. Quantitative ^{31}P NMR spectroscopy in alendronate-PEG-alkyne

Quantification of alendronate in alendronate-PEG-alkyne was performed by a previously described method with the use of coaxial inserts containing a KH_2PO_4 solution as a reference standard [1]. Because the specific condition for quantitative NMR that both the sample and the reference occupy the same volume is violated, a first experiment was done so as to introduce a correction factor in function of the ratio of volumes of both tubes, the insert and NMR sample tube. Values of volume reference/volume tube (Vr/V_T) were evaluated using two potassium phosphate solutions of same concentration but differing in hydrogen ion concentration and thus in observed ^{31}P chemical shift. To prepare two potassium phosphate solutions of concentration as close as possible, a stock solution of

KH_2PO_4 at a 0.1 g/mL concentration was prepared. Into a 5 mL flask, 2 mL of this solution, 1 mL of deuterium oxide and 0.4 mL of NaOH 25% were added and diluted with water up to 5 mL. This constituted the basic solution, confirmed by its basic pH of 13 where the form PO_4^{-3} is predominant and the ^{31}P chemical shift is observed at 6.29 ppm. The acid solution of pH 5.5, was prepared identically but without the addition of NaOH, where the predominant form is KH_2PO_4 and the observed shift is at 1.26 ppm. To determine the Vr/V_T ratio, they were analyze by quantitative NMR where the basic solution was contained in the NMR tube and the KH_2PO_4 solution was introduced in the coaxial insert tube (see Figure 1). Experiments were done by quadruplicate.

To determine alendronate concentration in the alkyne-PEG-alendronate macromolecule, and thus the efficacy of the reaction, a water solution of alkyne-PEG-alendronate macromolecule was analyzed by quantitative NMR using as a standard reference a solution of KH_2PO_4 in the coaxial insert (see figure 2). The relaxation times of both molecules were also checked prior to the experiment. The concentration of alendronate was calculated with the following equation

$$C_t = C_r\, I_t\, V_r / V_t\, I_r$$

where C_t and C_r are the concentrations of the tube and reference, respectively I_t and I_r, the intensities of the phosphorus signal of the tube and reference, respectively.

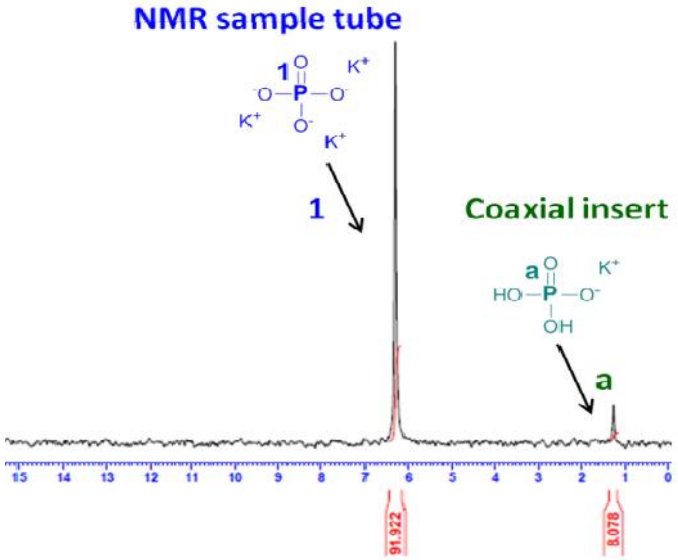

Figure 1: ^{31}P NMR spectrum for the correction factor calculation. In the NMR sample tube, a basic solution containing PO_4^{-3} and in the coaxial insert a mild acidic solution containing KH_2PO_4 at the same concentration.

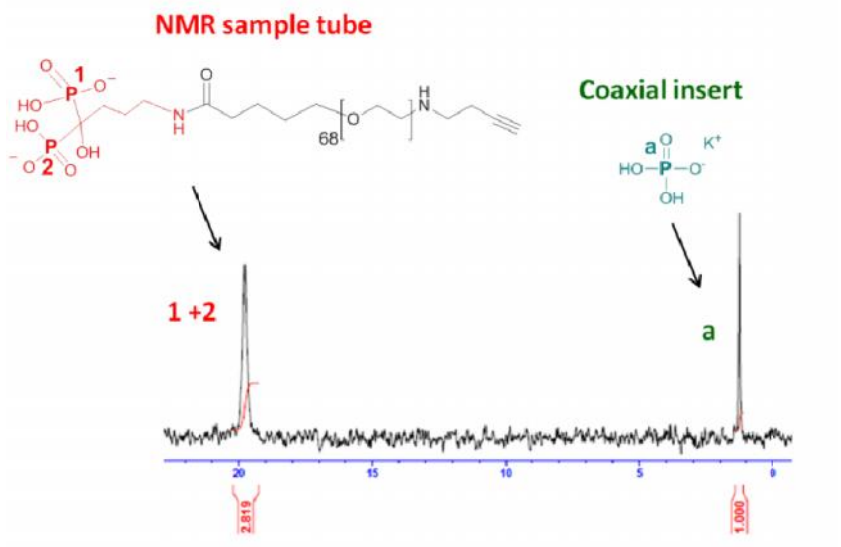

Figure 2: ^{31}P NMR spectrum for the quantification of alendronate in alendronate-PEG-alkyne using a mild acidic solution containing KH_2PO_4 in the coaxial insert as a reference standard.

1.3. Quantification of alendronate in PBLG-*b*-PEG-alendronate

The quantitative NMR spectroscopy determined a phosphorus concentration of 31 mM and therefore the efficacy of the reaction between alkyne-PEG-NHS and alendronate was found to be of 67 %. The phosphorus concentration determined by elemental analysis was 1.40% and yielded an efficacy of reaction of 71 %. The efficacy of the reaction between alkyne-PEG-alendronate and N_3-PEG-PBLG was found to be 46% and therefore 31 %. of the $PBLG_{50}$-*b*-PEG-alendronate polymeric chains were estimated to contain an alendronate molecule.

1.4. ^{1}H NMR of PBLG-*b*-PEG-alendronate

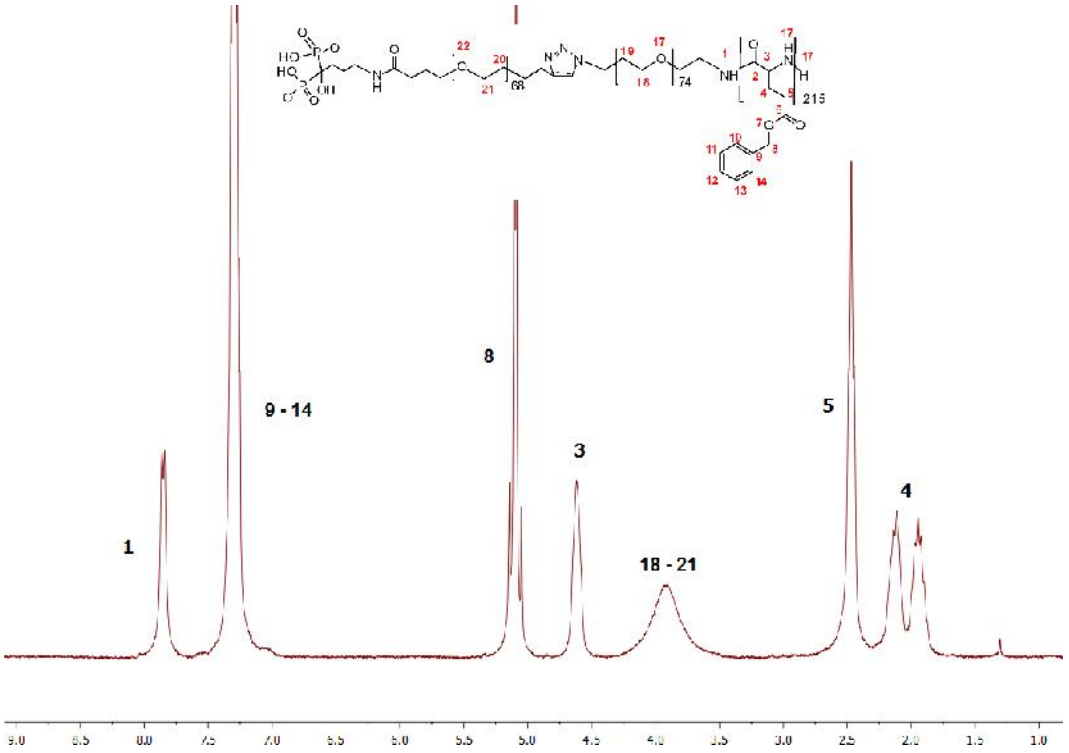

Figure 3: ^{1}H NMR of PBLG-*b*-PEG-alendronate

2. PBLG-*b*-PGlu copolymer: synthesis and characterization

2.1. Synthesis scheme of PBLG-*b*-PGlu

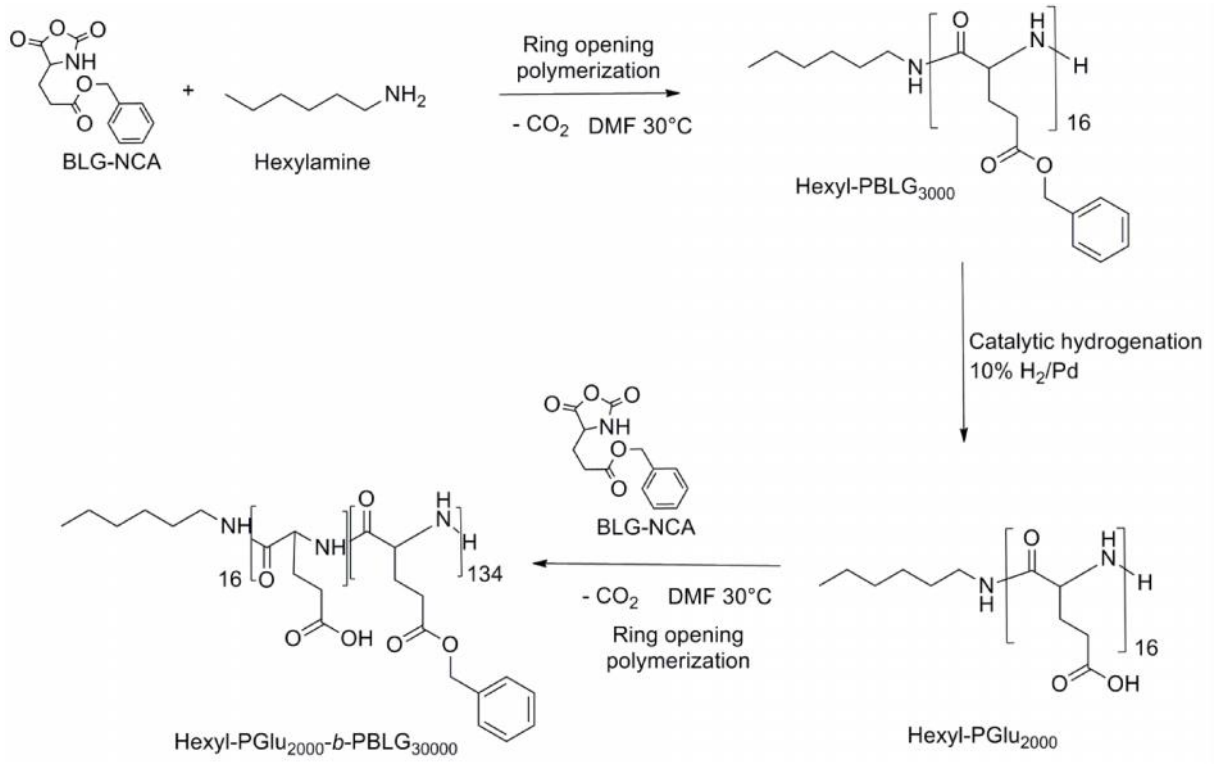

2.2. ^{1}H NMR of PBLG-*b*-PGlu

Characteristic peaks were identified for hexyl- PBLG polymer. The molar mass of the polymer could be determined by integration of the benzyl protons belonging to the PBLG block and the CH_3 protons of the hexylamine. The completion of the debenzylation reaction was checked by the absence of the pics corresponding to the benzyl and aromatic protons. NMR spectra of the PBLG-*b*-PGlu copolymer is shown below (see figure 4)**.**

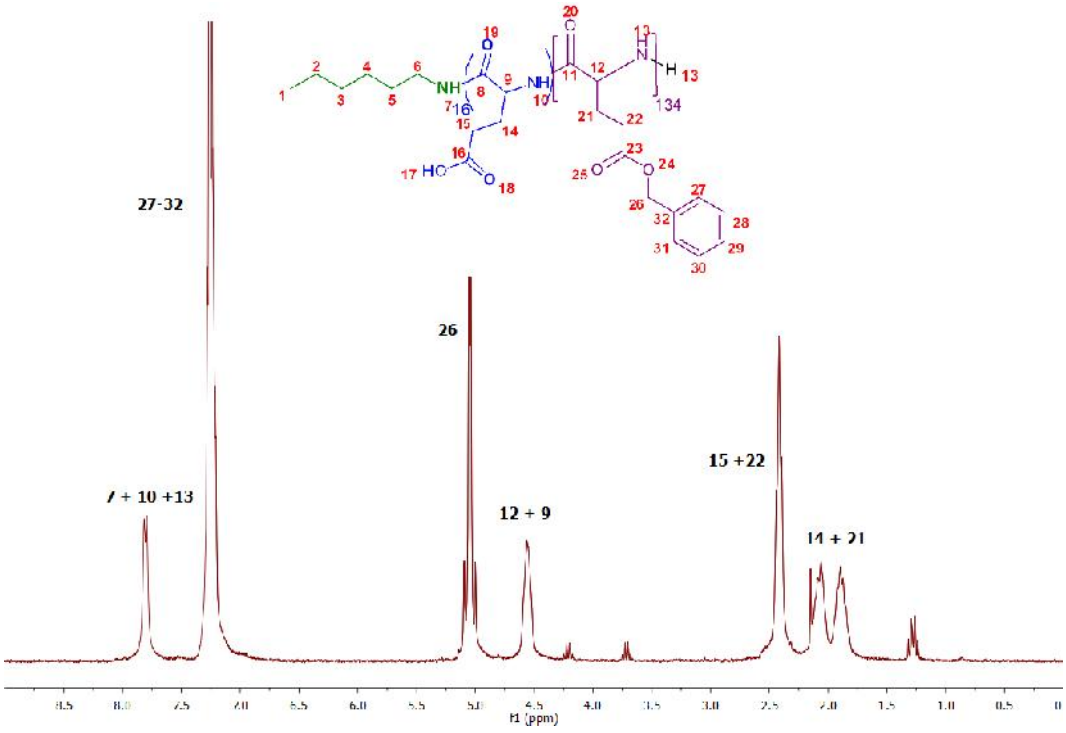

Figure 4: ^{1}H NMR of PBLG-*b*-PGlu

3. TEM images of nanoparticles

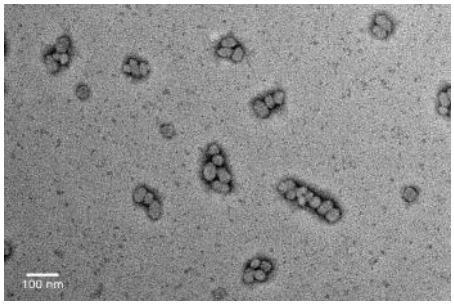

PBLG-bnz/PBLG-dansyl

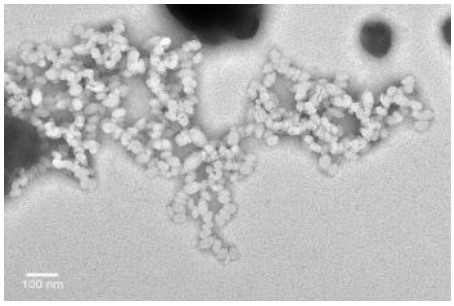

PBLG-*b*-PEG/PBLG-dansyl

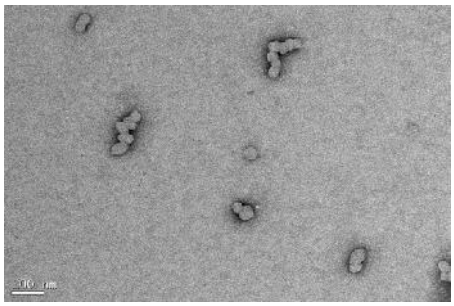

PBLG-dansyl

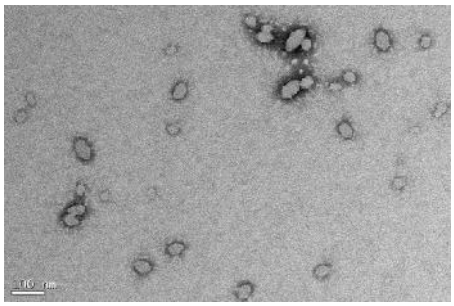

PBLG-*b*-PGlu/ PBLG-dansyl

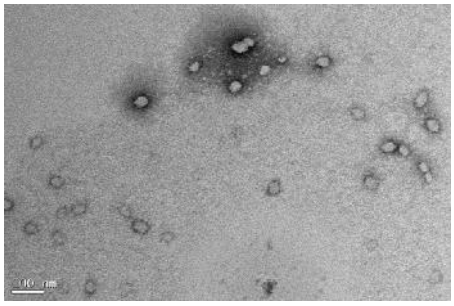

PBLG-*b*-PEG-alendronate/PBLG-dansyl

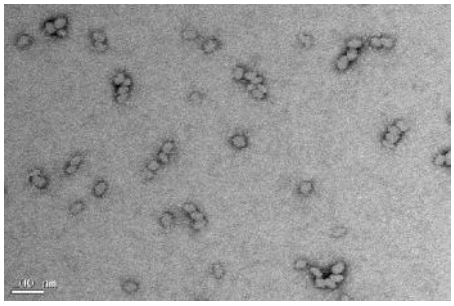

PBLG-*b*-PGlu/PBLG-*b*-PEG/PBLG-dansyl

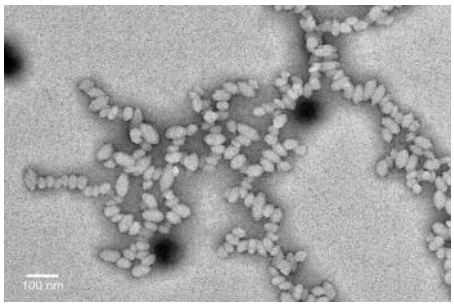

PBLG-*b*-PEG-alendronate/PBLG-*b*-PGlu/PBLG-dansyl

Figure 5: TEM images obtained at 120 kV and 20000 X screen magnification of nanoparticles containing 33% w/w of the PBLG-dansyl polymer except for PBLG-dansyl nanoparticles which contain 100 % w/w of this derivate.

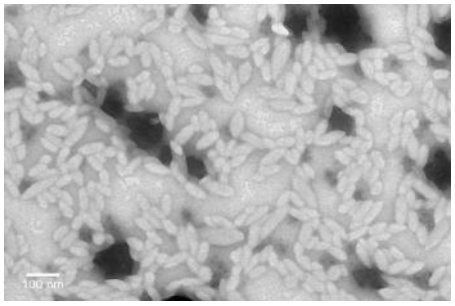

PBLG-bnz/PBLG-FITC

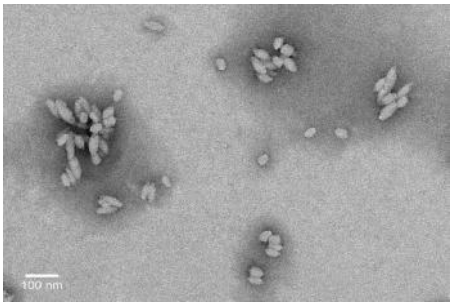

PBLG-*b*-PEG/PBLG-FITC

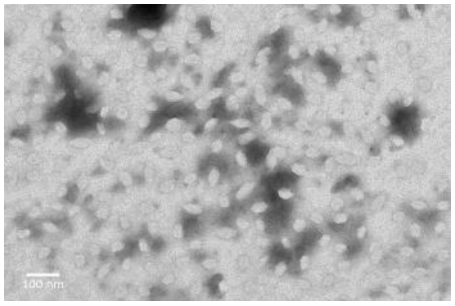

PBLG-*b*-PEG-alendronate/PBLG-FITC

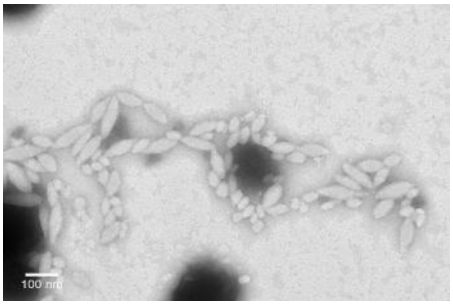

PBLG-*b*-PGlu/PBLG-FITC

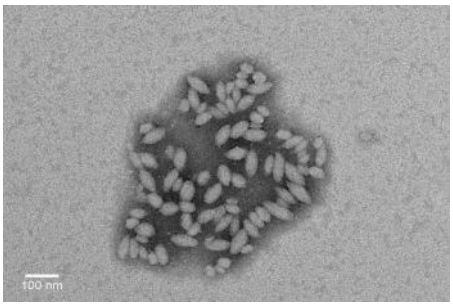

PBLG-*b*-PEG-alendronate/PBLG-*b*-PGlu/PBLG-FITC

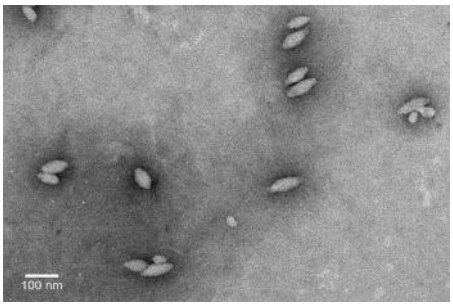

PBLG-*b*-PGlu/PBLG-*b*-PEG/PBLG-FITC

Figure 6: TEM images obtained at 120 kV and 20000 X screen magnification of nanoparticles containing 33% w/w of the PBLG-FITC polymer.

4. Bone histological images 24 hours and 5 days after IV administration of nanoparticles

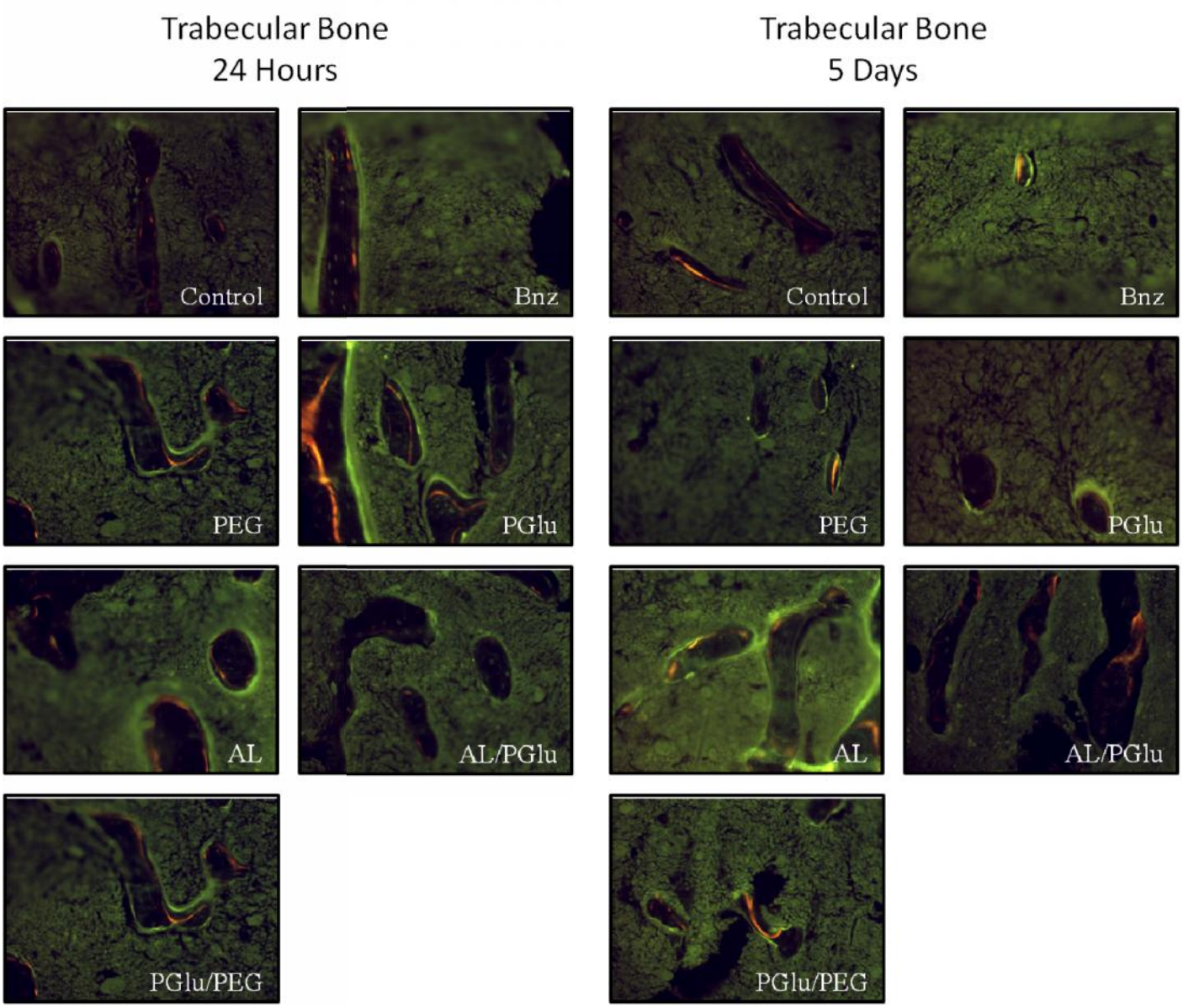

Figure 7: Bone histological images under fluorescent microscopy of trabecular bone of femurs after 24 hours (left) and 5 days (right) after IV administration of the FITC-labelled nanoparticles and further undecalcified tissue embedding and inclusion procedure in methyl methacrylate**.**

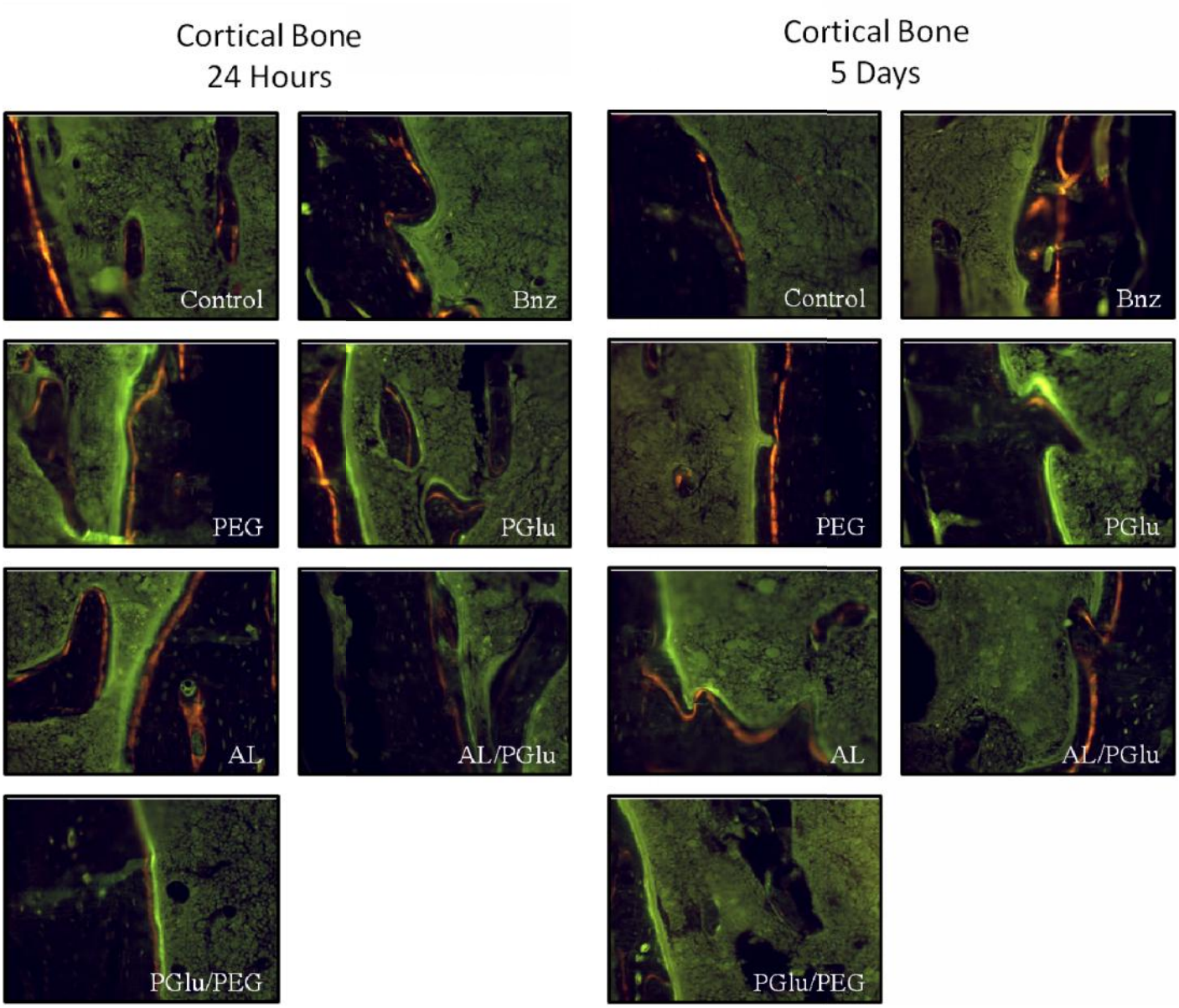

Figure 8: Bone histological images under fluorescent microscopy of cortical bone of femurs after 24 hours (left) and 5 days (right) after IV administration of the FITC-labelled nanoparticles and further undecalcified tissue embedding and inclusion procedure in methyl methacrylate

References

[1] Henderson TJ. Quantitative NMR Spectroscopy Using Coaxial Inserts Containing a Reference Standard: Purity Determinations for Military Nerve Agents. Anal Chem. 2001;74:191-8.

CHAPITRE VI:

GENERAL DISCUSSION

GENERAL DISCUSSION

1- Introduction

Nanomedicine, which is the application of the nanotechnology to medicine, is promising for the development of theranostic tools. The use of nanomedicine for cancer can improve current therapeutic treatments; over two dozen nanotechnology based therapeutics have been approved for clinical use by the FDA and more being in clinical trials [1].

A major attention has been devoted to active targeting of cancer over the past few years. The need for safer treatments with enhanced efficacy are desired. The goal of this approach is to deliver specifically the cytotoxic treatment to the malignant cells avoiding side effects in the healthy tissue and cells. In order to achieve this goal, different targeting approaches can be designed such as nanoparticles targeting cancer angiogenesis, cancer cell proliferation markers or cancer cells themselves.

The skeleton is the third most common sites of metastasis. Prostate and breast cancer, which are leading causes of cancer death, have a high tendency to metastasize to bone, and constitute more than 80% of cases of metastatic bone diseases. Bone metastases are infrequently silent and are associated with a high morbidity involving pain, hypercalcemia, spinal cord compression or fractures. Although no prevalence figures for people affected by bone metastases exist, it is estimated that more than 350.000 people in the United States die with bone metastases and thus there is an important need for the development of effective treatments [2, 3].

Anatomy and physiology of bone tissues is complex in nature making difficult to design an efficient targeting system. Indeed, we are demanding not only affinity for the target but also specificity, which means that no interactions with other targets should occur during the distribution process following delivery.

The objective of this work was to design multifunctional nanoparticles derived from poly (benzylglutamate) (PBLG) that could attain bone tissue and remain bound for a prolonged time period in order to ensure intra-bone time-controlled delivery of anticancer drug. In this way, nanoparticles could constitute anticancer drug reservoirs for long-term skeletal cancer treatments.

For this purpose, a small library of various PBLG copolymers bearing different functionalities have been synthesised. We succeeded in assembling them into various proportions to form multifunctional nanoparticles, whose bone binding affinity was evaluated *in vitro*, *ex vivo* and *in vivo*. An anticancer agent was successfully associated to the nanoparticles in view of a bone anticancer application. This discussion is divided into different sections and deals with the different steps needed to achieve these bone targeted nanoparticles, from copolymer synthesis, nanoparticle preparation and *in vitro* characterization of bone binding properties and anticancer agent association to *in vivo* binding efficacy.

2- Synthesis of a mini-library of polymers with different functionalities

In order to prepare multifunctional nanoparticles, we proceeded to the synthesis of a mini-library of PBLG polymers bearing various functionalities. These copolymers were intended to be self-assembled together to form multifunctional nanoparticles. Polymerizations were achieved by ring opening polymerization (ROP) of the α-aminoacid N-carboxyanhydrides (NCAs). It can basically proceed by two main routes, the amine mechanism and the activated monomer mechanism. The amine mechanism is a ROP where an amine attacks the carbonyl of a NCA molecule and in absence of side reactions the polymer grows linearly with monomer conversion. Activated monomer mechanism consists of the deprotonation of a NCA molecule, which becomes a nucleophilic molecule which in turn initiates the polymerization by attacking the carbonyl of another NCA. It is important to remark that both mechanisms can occur and can switch back and forth during a polymerization, one being the side reaction for the other one. The nucleophilicity/basicity ratio of the initiating molecule will influence

the preponderance of one or the other polymerization mechanism. Primary amines, being more nucleophilic than basic, are good initiators in general for NCA polymerizations so as to proceed by the normal amine mechanism. One inherent problem of conventional NCA polymerizations is that there is no control on the reactivity of the growing polymer chain end and thus they are subjected to a variety of side reactions. In order to circumvent such side reactions, developments have been made. Developments in ROP includes the use of zerovalent metal complexes as initiators of well controlled ROP that produce polypeptides with narrow chain length distributions PI < 1.2 and controlled molecular weights. However, the active propagating species are generated from the first NCA monomer and therefore no functionalities can be attached to polymers by this method [4]. Alternatively, functionalized precursors of amido-amidate nyckelacycles, that are transformed into NCA initiators have been successfully synthesised. They allow to obtain C-ending functionalized polymers [5]. Other recent developments include variations of the conditions of the reaction (temperature and vacuum) as it is discussed below.

In this work, polymerization reactions were carried out by ROP of γ-benzyl-L-glutamate-N-carboxylic anhydride (BLG-NCA) using primary amines as initiators without the use of any zerovalent metal complexes. Optimising the conditions for polymerizations would have been interesting, above all for the PBLG-*b*-PGlu initiated by the PGlu-NH_2 that gave a too large polymolarity index. However, due to technical difficulties, analyses with steric exclusion chromatography (SEC) could be only done months after the synthesis and thus optimization could not be efficiently performed. Different polymers bearing several functionalities are presented below.

PBLG-bnz

Different batches of PBLG-bnz with various molecular weights were synthesised using benzylamine, a primary amine, as an initiator. These polymerizations were well controlled as indicated by the comparison between theoretical and experimental molecular weightes and the low polymolarity

indexes obtained by MALDI-TOF and SEC (For PBLG-bnz of a theoretic molecular weight of 30000 Da: PI_{SEC} = 1.14 and $PI_{MALDI-TOF=}$ 1.13).

PBLG-*b*-PEG

PBLG-*b*-PEG copolymers were prepared in view of conferring stealth properties to nanoparticles by the introduction of PEG chains onto their surface. Different batches of $PBLG_{50k}$-*b*-$PEG_{\mathbf{5k}}$ of 50000 g/mol of molecular weight were synthesised. The molecular weight of the PEG block was chosen to be 5000 Da since in general terms it seems to be an appropriate length so as to reduce the adsorption of opsonins [6]. Reaction was initiated by methoxy-PEG-NH_2 and yielded polymers of a relatively low polymolarity (PI_{SEC} = 1.27 and $PI_{MALDI-TOF=}$ 1.23)

PBLG-*b*-PEG-alendronate

In order to provide nanoparticles with bone targeting properties, a PBLG copolymer bearing a biphosphonate moiety was synthesised. In order to immobilize nanoparticles onto the bone, hydroxyapatite (HAP) was chosen as a possible binding target. HAP is the main mineral component that accounts for 50-70 % of the extracellular matrix. Within the body, HAP is very specific to bone, although it is also found in teeth and pathological calcifications. There are some molecules that have affinity for HAP such as tetracyclines, tetracycline derivates, biphosphonates, acidic oligomers or poly(malonic acids). Among these compounds, biphosphonates are the most widely used drugs for the therapeutics of skeletal diseases such as osteoporosis, metastatic bone disease or Paget's disease. Biphosphonates are chemically stable analogues of inorganic pyrophosphate and it is the P-C-P moiety which is responsible for their binding to HAP [7]. Among them, alendronate was chosen since it has a primary amine on its structure and was therefore appropriate for coupling reactions with a PBLG block. Different coupling strategies were assayed.

PBLG-*b*-PEG-alendronate *synthesised by the carbodiimide coupling approach*

Two copolymers of different molar masses were prepared by a carbodiimide coupling approach: $PBLG_{50k}$-*b*-PEG_{6k}-alendronate and $PBLG_{10k}$-*b*-PEG_{6k}-alendronate. To ensure that molecules of alendronate could be exposed and available on nanoparticle surface, NHS-PEG_{6k}-NHS was chosen for the synthesis of the bone-targeting copolymers both as a spacer and to confer stealth properties to the bone-targeted nanoparticles.

In order to synthesise an alendronate bearing polymer, the carbodiimide approach had been previously carried out successfully in our group. However, many technical problems were encountered during this synthetic approach. This approach was not optimal due to the use of an homofunctional linker, NHS-PEG_{6k}-NHS, that limits to 1 the [alendronate]/[NHS-PEG_{6k}-NHS] molar ratio in the reaction between them so as to try to prevent the reaction of two molecules of alendronate with this linker. Modifications were made to the original method proposed by Ozcan et al. [8], including elimination of unreacted free alendronate and further activation of the carboxylate group. However, this latter step might have provoked the activation of the phosphonate groups of the alendronate molecule, which leaded finally to the formation of star-shaped polymers, which had to be eliminated with a further purification process.

In spite of all the technical difficulties encountered during the chemical synthesis, bone targeted nanoparticles could be obtained and were shown to display bone targeting properties using the HAP as an *in vitro* model (see section 4). However, the low efficacy of this coupling reaction, (only 5,3 % of the $PBLG_{10k}$-*b*-PEG_{6k}-alendronate chains beared an alendronate group) added technical difficulties to further physico-chemical experiments carried out to determine the binding affinity with the divalent calcium ions by isothermal titration calorimetry (ITC). These difficulties prompted us to look for an alternative coupling method.

PBLG-*b*-PEG-alendronate ***synthesised by a combination of click chemistry and carbodiimide coupling approach***

Due to the unsuitability of the coupling reaction pathway described above and despite the obtaining of bone targeted nanoparticles, a new chemical synthetic approach was carefully designed involving the click chemistry and carbodiimide approach. Two copolymers of different molar mass were prepared by click chemistry: $PBLG_{17k}$-*b*-PEG_{6k}-alendronate and $PBLG_{50k}$-*b*-PEG_{6k}-alendronate. For further clarification we will refer to this latter copolymer as alendronate PBLG copolymer (click). The length of the PEG spacer was chosen to be of 6000 Da, similar to the one in the carbodiimide approach.

The use of an heterobifunctional linker, NHS-PEG_{3k}-alkyne, allowed us to improve the efficacy of the reaction between alendronate and NHS-PEG_{3k} -alkyne since the [alendronate]/[NHS-PEG_{3k} -alkyne] molar ratio could be enormously increased. The click chemistry reaction of PBLG-PEG_{3k} -N_3 and alendronate-PEG_{3k}-alkyne proceeded with a high efficacy of reaction. The overall efficacy of both reactions resulted in the fact that among the $PBLG_{50k}$-*b*-PEG_{6k}-alendronate chains, 69% were actually PBLG-*b*-PEG chains (15% $PBLG_{50k}$-*b*-PEG_{6k} and 54 % $PBLG_{50k}$-*b*-PEG_{3k}) and 31 % consisted of $PBLG_{50k}$-*b*-PEG_{6k}-alendronate chains. Polymeric chains bearing an alendronate molecule in the $PBLG_{50k}$-*b*-PEG_{6k}-alendronate (click) were almost six times more abundant than for the $PBLG_{10k}$-*b*-PEG_{6k}-alendronate (carbodimide) and more than 8.5 times higher if compared to the similar molecular weight copolymer, $PBLG_{50k}$-*b*-PEG_{6k}-alendronate (carbodimide). Due to initial technical difficulties in the synthesis of $PBLG_{50k}$-*b*-PEG-alendronate, a lower molecular weight PBLG block, namely $PBLG_{17k}$-*b*-PEG_{6k}-N_3 was synthesised. Efforts were made to evidence the azide functionality of the block $PBLG_{17k}$-*b*-PEG_{3k}-N_3 by infrared spectroscopy techniques at 2100 cm^{-1} and its disappearance after reaction with alendronate-PEG_{3k}-alkyne. However, even with this shorter polymer, this band could not be seen, probably due to the too high polymer molecular weight per azide group.

PBLG-*b*-PGlu

Poly(glutamic acid) (PGlu) was chosen as a block with a double functionality. Firstly, bone affinity of glutamic acid oligomers is largely known [9]. Secondly, its ability to complex metals, including cisplatin, has been considered as a mean of associating such derivates and thus conferring anticancer properties to the nanoparticles.

$PBLG_{25K}$-*b*-$PGlu_{2k}$ polymerization was initiated by a hydrophilic $PGlu_{2k}$-NH_2 block previously synthesised by us by a ROP of NCA and a further debenzylation by catalytic hydrogenation. The method of debenzylation was chosen so as to reduce any possible polymer degradation and so as to favour the presence of protonated carboxylic acids and to avoid carboxylate ions in the $PGlu_{2k}$-NH_2 block. Such a polymerization has been previously described [10]. However, it was not a well controlled polymerization as depicted from the PI_{SEC}= 1.75. Efforts to obtain a MALDI-TOF spectrum in various conditions were made but were unsuccessful. Despite this large polymolarity, nanoparticles were rather homogeneous and not more polydisperse than nanoparticles made from other PBLG-derivates.

In order to reduce polymolarity and side reactions, various alternatives for the polymerization reaction are available such as the use of zerometal complexes or the use of low temperatures (0°C degrees) [11] or a combination of low temperature and low pressure [12]. Problems associated to the purity of PGlu-NH_2 and to the availability of the amine in the initiator molecule $PGlu_{2k}$-NH_2 might also account for this lack of control. Polymerizations carried out at 25 °C are known to proceed with diverse side reactions which result in several end-groups, a common being the pyrrolidone ring [12]. Besides, the effect of the catalytic hydrogenation reaction on these issues should be studied.

PBLG derivates with fluorescence properties

PBLG-dansyl:

A PBLG-dansyl fluorescent polymer was synthesised in view of preparing multifunctional fluorescently labelled nanoparticles for *in vitro* experiments. The synthesis of PBLG-dansyl was achieved by ROP of BLG-NCA using dansylcadaverin as an initiator. Dansylcadaverin has a primary amine on its structure and no anions or groups that could interfere with the polymerization.

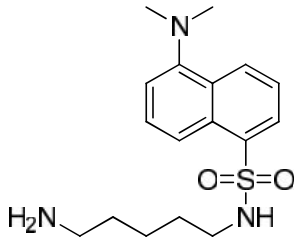

Figure 1: Structure of dansylcadaverin

As evidenced by MALDI-TOF (M_n of 19880 g/mol and PI of 1.15) and SEC (M_n of 25900 g/mol and PI of 1.1) results, the synthesis was well controlled, which evidenced the good suitability of the initiator. The initial molecular weight of PBLG-dansyl was chosen to be 22000 g/mol. It has a lower molecular weight compared to the initially established one at 50000 g/mol. This was chosen to increase the number of fluorophore molecules per gram of polymer and thus the fluorescence detection.

PBLG-rhodamine

Efforts were made to synthesise a PBLG derivate bearing a rhodamine molecule to prepare rhodamine-labelled nanoparticles. In order to achieve this goal, a ring opening polymerization of NCA was carried out using a derivate of rhodamine possessing on its structure a secondary amine, rhodamine piperazine, as showed below. This rhodamine derivate has been synthesised and provided by Dr B. Le Droumaguet and Dr. J. Nicolas. However, even if this polymerization has been previously reported [13], nanoparticles from this derivate could not be successfully achieved in our case. It is

likely that problems encountered through the polymerization reaction were due to the use of a secondary amine as an initiator having a counter-ion on its structure, which led to an heterogeneous PBLG-rhodamine derivate that precipitated partially during the nanoprecipitation step.

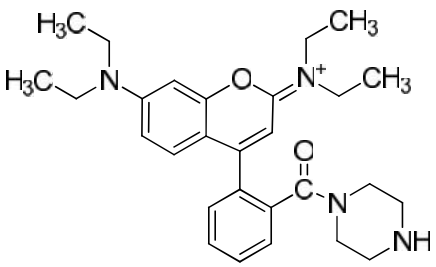

Figure 2: Structure of the rhodamine-piperazine initiator for the attempt of PBLG-rhodamine synthesis

PBLG-FITC

A PBLG-FITC fluorescent polymer has been previously synthesised in our group and was directly used. Its chemical synthesis has been carefully designed using fluorescein isothiocyanate (FITC), an electrophilic group, as a chain terminating agent, as it has been previously shown [14]. Fluorescein isothiocyanate isomer I (FITC), was introduced into the polymer structure by ending a ROP initiated by benzylamine. This strategy allowed the functionalization of the N-terminal ends and the preparation of a PBLG-FITC polymer with a well controlled molecular weight and a narrow polymolarity index ($PI_{MALDI-TOF}$ = 1.14 and PI_{SEC}=1.18).

Miscellaneous

Regarding the polymer molecular weight characterization technique, it is important to remark the great concern that exists: only the ^{1}H NMR technique in the case of the copolymers PBLG-*b*-PEG can give an accurate molecular weight of the degree of polymerization but no polymolarity index is provided. Molecular weight data obtained from both SEC and MALDI-TOF were obtained with experimental errors, as shown in Table 1.

Table 1: Molecular weight data of different PBLG polymers

PBLG-polymers	DP_n[a]	M_n (g/mol)	PI[b]	M_n[c] (g/mol)	PI[c]
$PBLG_{10k}$-bnz	45	8431[c]	1.16	-	-
$PBLG_{25k}$-bnz	136	23407[c]	1.13	31727	1.14
$PBLG_{50k}$-bnz	228	39690	1.1	-	-
$PBLG_{40k}$-*b*-PEG_{5k}	228	39366[c] 56465[d]	1.23	65513	1.27
$PBLG_{40k}$-*b*-PEG_{5k}	228	34512[c] 50425[d]	1.22	-	-
$PBLG_{40k}$-*b*-PEG_{6k} -alendronate (carbodiimide)	228	42415[c]	1.17	-	-
$PBLG_{10k}$-*b*-PEG_{6k} -alendronate (carbodiimide)	45	8711[e]	-	-	-
$PBLG_{25K}$-*b*-$PGlu_{2k}$	137	-	-	24436	1.75
$PBLG_{20k}$-dansyl	91	19786[c]	1.19	25944	1.10
$PBLG_{40k}$-FITC	228	36155[c]	1.14	52647	1.17
$PBLG_{17k}$-*b*-PEG_{6k} -alendronate (click)	78	-	-	34171	1.17
$PBLG_{50k}$-*b*-PEG_{6k} -alendronate (click)	228	-	-	52816	1.54

(a) theoretical; (b) determined by MALDI-TOF; (c) determined by SEC; (d) determined by NMR; (e) determined from $PBLG_{10k}$-bnz

The MALDI-TOF technique has been reported to underestimate the molecular weight of polymers, probably due to the molecular weight discrimination effect during ionization/desorption processes [15, 16] whereas the SEC measurements, lacking of an appropriate standard for the rod-like PBLG polymer led to an overestimation of the molecular weight as reported by other authors [17].

3- Preparation of multifunctional nanoparticles

As shown in table 2, various types of multifunctional nanoparticles were prepared by nanoprecipitation of the different polymers issued from the library described above, either alone or as mixtures of two or more polymers. Because of the presence of the constant PBLG block, it was expected that these different polymers could self-associate together, without segregation phenomena. From a practical point of view, the nanoprecipitation protocol was modified in order to be able to prepare nanoparticles containing the $PBLG_{25k}$-*b*-$PGlu_{2k}$ copolymer.

$PBLG_{25k}$-*b*-$PGlu_{2k}$ nanoparticles

The previous nanoprecipitation method carried out in our group consisted in the nanoprecipitation in water of a THF solution containing the PBLG derivate. A novel nanoprecipitation method allowed the preparation of $PBLG_{25k}$-*b*-$PGlu_{2k}$ nanoparticles. This method consisted of dissolving $PBLG_{25k}$-*b*-$PGlu_{2k}$ copolymer in THF/MeOH 75/25 at 40 °C and precipitating it in water containing two equivalents of NaOH per equivalent of COOH contained in the PGlu moiety. The presence of NaOH was essential so as nanoparticles did not aggregate. In absence of NaOH, nanoparticles aggregated presumably through the formation of hydrogen bonds between adjacent nanoparticles. The aggregation of nanoparticles was macroscopically appreciable as shown in figure 3 and confirmed by dynamic light scattering (DLS) measurements, which yielded 150 nm objects while transmission electron microscopy (TEM) measurements showed very small nanoparticles (typically 24 x 17 nm in size with an aspect ratio of 1.4). Nanoparticles prepared in the basic nano-precipitating medium were 34 x 27 nm in size with an aspect ratio of 1.3.

Figure 3: $PBLG_{25k}$-*b*-$PGlu_{2k}$ nanoparticle suspensions prepared from the novel nanoprecipitation method: left: in presence of sodium hydroxide; right: in absence of sodium hydroxide

Table 3: Size measured by TEM and DLS of $PBLG_{25k}$-*b*-$PGlu_{2k}$ nanoparticles prepared in absence and presence of NaOH.

Nanoparticles	TEM			DLS
$PBLG_{25k}$-*b*-$PGlu_{2k}$	$D_{longitudinal}$ (nm)	D_{axial} (nm)	Aspect ratio	Size (nm)
In absence of NaOH	34	27	1.4	150
In presence of NaOH	24	17	1.3	50

$PBLG_{25k}$-*b*-$PGlu_{2k}$/PBLG derivate nanoparticles

Multifunctional nanoparticles obtained by the mixture of $PBLG_{25k}$-*b*-$PGlu_{2k}$ copolymer and another PBLG derivate could be obtained by the same nanoprecipitation method described above. The amount of NaOH was adjusted to two equivalents of NaOH per equivalent of COOH, which was optimal and did not provoke the precipitation of the other PBLG copolymers. For the $PBLG_{17k}$-*b*-PEG_{6k}-AL (click) copolymer, the nanoprecipitation method had to be modified due to the solubility problems encountered in THF/MeOH 75/25. So as to be able to prepare multifunctional nanoparticles together with the $PBLG_{25k}$-*b*-$PGlu_{2k}$ copolymer, the nanoprecipitation method needed DMF for dissolving the different polymers before nanoprecipitation in water and further elimination of the DMF by dialysis.

Nanoparticle stabilization

In presence of ions and biological media, all types of nanoparticles precipitated, except those obtained only from the $PBLG_{25k}$-*b*-$PGlu_{2k}$ copolymer, which were further stabilized by the electrostatic repulsion among the negatively charged carboxylate groups. In order to render nanoparticles stable in ion containing and thus biological media, nanoparticles had to be stabilised with poloxamer. The use of pluronic F68 ® in large excess at a concentration of 66 % (% w/w per PBLG polymer mass) resulted in the obtaining of stable nanoparticles in physiological media.

4- Hydroxyapatite (HAP) binding nanoparticles

Alendronate and acidic oligopeptides are well known for their affinity to bone and have been used to impart osteotropicity to many drugs [18, 19]. A small library of nanoparticles with modulated HAP affinity were prepared from the alendronate copolymer (carbodiimide and click), poly(glutamic acid) copolymer, a combination of them or a combination of non osteotropic and osteotropic polymers. The nanoprecipitation technique was found to be a versatile tool to modulate precisely nanoparticle surfaces, being able to modulate HAP targeting properties as well. It was likely that the efficient presentation of the HAP targeting ligands was also favoured by the rigidity of the PBLG block, since hindrances of these hydrophilic moieties inside the hydrophobic nanoparticle core were not likely to occur.

First, alendronate decorated nanoparticles were prepared from the alendronate copolymer $PBLG_{10k}$-*b*-PEG_{6k} -alendronate (carbodiimide) and interaction with HAP and divalent calcium ions was studied. Interestingly, experiments showed that calcium-bound nanoparticles can still bind to HAP with the same affinity, confirming that calcium is displaced and not interfering with HAP binding. This yields a deeper understanding of potential *in vivo* fate of bone targeted nanoparticles.

Nanoparticles decorated with either alendronate or/and poly(glutamic acid) prepared from $PBLG_{50k}$-*b*-PEG_{6k} -alendronate (click) or/and $PBLG_{25K}$-*b*-$PGlu_{2k}$ copolymers showed differential targeting properties, as shown by both the kinetics and desorption *in vitro* HAP assays. Interestingly, for nanoparticles containing both osteotropic ligands, alendronate and PGlu, a low percentage of the alendronate copolymer (click) (ratio alendronate/PGlu polymer of 0.34) was enough so that the alendronate moieties, and not the poly(glutamic acid) were responsible for HAP binding.

Alendronate and acidic oligopeptides are known to present differential bone binding properties. *In vitro* HAP binding affinity for the acidic oligopeptides $(L\text{-}Asp)_6$ or $(L\text{-}Glu)_6$ was found to be in the order of ~ 10^2 lower than for the biphosphonates [20, 21]. This lower affinity could result in more

chemical desorption and less skeletal retention but at the same time to more penetration into the osteocyte network. Moreover, some studies with osteotropic HPMA polymers have shown differential *in vitro* and *in vivo* interaction between alendronate and $(Asp)_6$, $(Asp)_6$ being distributed preferentially to bone resorption sites whereas alendronate would be distributed to both formation and resorption sites. This could be due to the lower affinity of $(Asp)_6$ to HAP and to a more dependent binding on HAP crystallinity, which is higher for resorption sites rather than for the newly formed bone.

Influence of cisplatin on hydroxyapatite (HAP) binding properties

Interaction of cisplatin-loaded $PBLG_{25k}$-*b*-$PGlu_{2k}$ nanoparticles with HAP differed from $PBLG_{25k}$-*b*-$PGlu_{2k}$ nanoparticles free of cisplatin (see section 5 for cisplatin association to nanoparticles). In terms of kinetics, the presence of cisplatin fastened the HAP binding reaction whereas the desorption assay revealed an intermediate desorption degree of $PBLG_{25k}$-*b*-$PGlu_{2k}$-cisplatin nanoparticles. This is not surprising since cisplatin is known to interact with HAP in such a manner that its release from HAP is very slow and dependent on the chloride concentration [22, 23]. Therefore we could hypothesize that the cisplatin involvement in HAP binding could account for the faster kinetics and for the lower release of cisplatin-$PBLG_{25k}$-*b*-$PGlu_{2k}$ nanoparticles at pH 3.5 compared to $PBLG_{25k}$-*b*-$PGlu_{2k}$ nanoparticles. In a coherent way, alendronate/PGlu-cisplatin nanoparticles displayed similar binding properties as the alendronate ones.

Comparison of hydroxyapatite(HAP) binding properties of alendronate PBLG nanoparticles (carbodiimide) and (click)

Both alendronate nanoparticles obtained either from $PBLG_{10k}$-*b*-PEG_{6k}-alendronate (carbodiimide), synthesised by a double carbodiimide approach or from $PBLG_{50k}$-*b*-PEG_{6k}-alendronate (click) obtained by a combined carbodiimide and click approach showed total binding to HAP, the kinetics being much quicker for nanoparticles obtained from $PBLG_{50k}$-*b*-PEG_{6k}-alendronate (click). This could be attributed to the increased number of alendronate molecules per polymer chains, although other

factors such as aspect ratio, number of chains per nanoparticle or different degree of steric hindrance caused by the different length of PEG could be involved and should be further studied.

***Ex vivo* bone binding properties**

Ex vivo bone binding experiments using fluorescently labelled nanoparticles showed differences compared to the *in vitro* HAP binding assay. It revealed that all types of nanoparticles (osteotropic and non-osteotropic ones) presented similar bone binding.

Some hypotheses could explain this discrepancy between *in vitro* and *in vivo* experiments. First of all, bone is composed not only by HAP, the major component of the mineralised tissue (50-70%), but also by an organic phase consisting mainly of collagen type I and other proteins [24] to which nanoparticles could also bind. Secondly, it has to be considered that synthetic and biological HAPs differ substantially since biological HAPs have multiple substitutions and deficiencies at all ionic sites. For example, cortical biological HAP contains 20 % hydroxyl groups compared to the stoichiometric HAP [25], and carbonates substitutions (4-6% in weight) for the phosphate ion are present in biological HAP.

Whether the observed amount of fluorescent nanoparticles bound to bone was high enough to be considered as actually reflecting an interaction between nanoparticles and bone and whether the stabilizing poloxamer could influence this interaction are the first questions to be solved. If we consider that an interaction exist between poloxamer coated PBLG nanoparticles and bone, several questions arise to understand the nature of this interaction, any of which would require further experiments to confirm them.

Considering the nanoparticle, what is this interaction due to? Is it due to the poloxamer, to the PBLG itself or more probably to complex interactions involving several components? Considering the bone structure, is this interaction due to the biological HAP (whose composition and structure are different from that of synthetic HAP) or rather due to the organic proteic components or other of bone

or more likely to a combination of all of them? It could be not be ruled out that among these complex interactions, peptide-protein interactions between type I collagen, which is constituted by three polypeptide chains forming a triple-helix, and the poly(benzylglutamate) could also be involved. Further experiments to explore interactions of nanoparticles with these components, and also with collagen, which is the most abundant non mineralized component of the bone, would be necessary.

Moreover, a lot of research has been conducted on the adsorption of proteins onto the HAP structures. Protein adsorption is known to be dependent on many factors such as surface charge, composition (i.e. Ca/P ratio) or HAP crystallinity [26]. Some essential aminoacids have been shown to bind to poorly crystallized HAP [27]. Moreover HAP chromatography is a common well-known method for the separation of mitochondrial proteins [28]. In an elegant study, a library of peptides were screened for interaction with human tooth. The authors discovered that peptides, free of acidic aminoacid sequences did display affinity for teeth (and differently for dentin and enamel), opening a new insight into the mechanisms involved in interactions with biomineral surfaces [29].

5- Bone binding nanoparticles for bone cancer applications: associating an anticancer agent to PBLG derivate nanoparticles

When designing nanomedicines, whatever their nature, drug association is generally a challenge concerning the need to associate and to vehicle sufficient drug amounts to the target, to trigger and control the release kinetics. Different approaches have been foreseen during this work in order to associate an anti-cancer drug to the bone binding nanoparticles.

5.1- pH labile polymeric prodrug

Cancers are known to present a mild extracellular pH due to an increased metabolic activity of cancerous cells, which exports H^+ to the extracellular space via a Na^+/H^+ exchanger. Thus, the pH in cancer extracellular space was found to be 6.60-6.98 in various tumours [30]. Secondly, if

nanoparticles are interacting and endocytosed by cells, they encounter acidic pH, since early endosomes present a pH ranging from 6.0-6.8 while lysosomes are more acidic (pH 5.2-4.5) [31].

Moreover, in the specific case of bone, in the resorption lacunae created by osteoclasts, it exists an acidic microenvironment, where pH is approximately 4-4.5 [32] since osteoclasts secrete protons through the ruffled border via direct pumping or by fusions of acidic vesicles extracellularly into the resorption lacunae that will dissolve the mineral content of the matrix, the HAP [33].

Taking advantage of these specific pH conditions, several pH labile linkers such as hydrazone, acetal, have been described and used to deliver drugs from prodrugs depending on acidic pH. Efforts to make a pH-sensitive polymeric prodrug of gemcitabine were made. Cis- aconityl was chosen as a pH labile linker between the PBLG-derivate polymer and the anticancer drug gemcitabine.

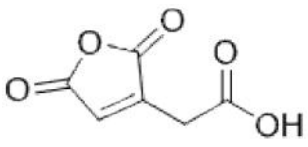

Figure 4: Structure of cis-aconityl anhydride

However, it might not be an optimal approach since cis-aconityl prodrugs have shown an incomplete release probably due to the formation of a trans isomer that cannot be cleaved [34]. Numerous conditions were assayed to couple cis-aconityl anhydride and gemcitabine. Reaction studies using the aniline as a model drug led us to conclude that this approach was not feasible likely due to the low nucleophilicity of the gemcitabine. The pH labile polymeric prodrug approach was therefore discarded.

5.2- Paclitaxel physical entrapment

A first approach for physically associating an anticancer agent, paclitaxel, to PBLG nanoparticles was assayed. Paclitaxel is an antineoplasic agent that belongs to the family of taxanes, and that has

been approved by the FDA for some types of cancers, including prostate and breast cancers. These two types of cancer have both a high incidence of bone metastasis with 73% and 68% occurrences found respectively at post-mortem studies [35]. Two methods for physically entrapping paclitaxel were tested using $PBLG_{50k}$-bnz as the nanoparticle forming polymer since whatever the nanoparticle type, the PBLG block remained constant and formed the hydrophobic core.

First, a tetrahydrofuran (THF) solution of paclitaxel and $PBLG_{50k}$-bnz polymer was precipitated in water in view to form paclitaxel-loaded nanoparticles. No controlled release was achieved by this method: 82.5% of total paclitaxel was released within 90 minutes. A second strategy implementing a cosolvency method using 1/10 dichloromethane(DCM)/THF instead of THF was tested in view of delaying the release kinetics. Paclitaxel and PBLG-bnz polymer were dissolved in 1/10 DCM/THF and further precipitated in water. However, no improvement in the control of paclitaxel release was achieved: 86% of total paclitaxel was released within the first 70 minutes.

In both methods paclitaxel was not efficiently encapsulated but probably rather adsorbed onto the surface of nanoparticles or forming nanocrystals (that maybe could have been evidenced by TEM within the nanoparticle suspension) since no control on the release of paclitaxel from nanoparticles was achieved. In any case, the impossibility to obtain satisfying release kinetics evidenced the failure of this strategy.

5.3- Cisplatin association

Cisplatin (Figure 4) is an antineoplasic agent used for the treatment of different types of cancers, such as ovarian, testicular, bladder, cervical, head and neck, esophageal and small cell lung cancers [36]. It is also used in combined chemotherapy for advanced prostate cancer. Cisplatin is rapidly distributed throughout the whole body upon administration and thus gives rise to side effects such as the nephro, neuro, oto and hepatotoxicity among others, as well as to drug resistance. In order to improve its pharmacokinetics and reduce side effects, many efforts have been focused on the

development of nanoparticulate carriers, some of them undergoing preclinical or clinical development, such as Prolindac®, LipoPlatin® or Nanoplatin® [37-39]. Cisplatin has the following structure:

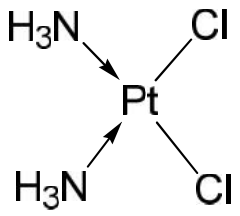

Figure 5: Structure of cisplatin

Due to its aqueous solubility and considering the hydrophobicity of the core of the PBLG nanoparticles, cisplatin encapsulation into these nanoparticles was not investigated due to the poor expected results.

5.3.1- Cisplatin-PGlu complex encapsulation

Cisplatin-PGlu complexes were prepared and attempts to physically encapsulate these complexes in PBLG nanoparticles were made. The similarity in the structure of poly(glutamic acid) and poly(benzylglutamate), two polypeptides, was expected to favour its encapsulation. However, this was not the case and the encapsulated payload was found to be negligible.

5.3.2- Cisplatin association to preformed $PBLG_{25k}$-b-$PGlu_{2k}$ nanoparticles

A novel approach was conceived to associate cisplatin to preformed bone targeted $PBLG_{25k}$-*b*-$PGlu_{2k}$ nanoparticles through cisplatin complexation to the carboxylates of the PGlu block. These nanoparticles were able to associate cisplatin with a drug loading content of approximately 6 % when a [CDDP]/ [COO^-] ratio of 1.25 was used. It would be very interesting to deepen into the mechanism of interaction of cisplatin with $PBLG_{25k}$-*b*-$PGlu_{2k}$ nanoparticles. At higher [CDDP]/ [COO^-] ratios, the 1:1 stoichiometry is thought to be more favoured vs the 1:2 one than at lower [CDDP]/ [COO^-] ratios, but both can occur. In the case of 1:2 stoichiometry, it could be interesting to study if intra-chain and inter-chain crosslinking could be possible, which one would be favoured and the effect of shell-

crosslinking on nanoparticle properties. Theoretical chemistry studies and molecular modelling could be useful to deepen into this issue. Regarding cisplatin release, this was surprisingly slow in a PBS media with absence of any burst release. This type of almost zero order release kinetics confirmed that cisplatin is coordinated to the carboxylate groups of PGlu and not physically entrapped in the nanoparticle PBLG core. As it has been previously stated in the literature, the presence of chloride ions is essential for cisplatin release from PGlu complexes due to a ligand exchange reaction where chloride ions would substitute the Glu residues from the $PBLG_{25k}$-*b*-$PGlu_{2k}$ nanoparticle, due to good leaving properties of Glu residues [40]. Other ions such as acetates or phosphates are also likely to play a minor role in cisplatin release. Moreover, the release of cisplatin from carboxylate complexes have been shown to be enhanced in mild acidic pH [41]. It should be studied in the case of cisplatin $PBLG_{25k}$-*b*-$PGlu_{2k}$ nanoparticles how the pH affects the cisplatin release. The release of small amounts of cisplatin in distilled water medium was observed but was very slow compared to the one in physiological medium. However, others have found no release at all for cisplatin complex [42-44] and cisplatin-loaded micelles [40, 45]. The possible role of impurities or hypothetically poloxamer (although *a priori* it should not be involved) should be studied. Cisplatin release from $PBLG_{25k}$-*b*-$PGlu_{2k}$ nanoparticles is mainly dependent on the concentration of chloride ions. The proton concentration has been also shown to play a role as it has been previously commented above. In the case of bone targeting nanoparticles for the therapeutics of bone cancer, this is important in two ways.

First, cancers, due to an enhanced metabolic activity of cancer cells are known to present a mild acidic extracellular pH (pH 6.60-6.98 in various tumours) [30] and nanoparticles if endocytosed encounter an acidic pH.

Secondly, in the case that nanoparticles bind to the bone mineralized surface and remain there, the osteoclast mediated resorption could induce the release of cisplatin. Osteoclast pump chloride ions into the resorption lacunae creating an acidic microenvironment with a high concentration in chloride. It

might happen that in these conditions the release of cisplatin could be enhanced. Further experiments should be done so as to confirm these hypothesis:

5.3.3- Cisplatin association to PBLG$_{25k}$-b-PGlu$_{2k}$ / PBLG$_{40k}$-*b*-PEG$_{5k}$ *nanoparticles*

Cisplatin association studies carried out with multifunctional nanoparticles made of different proportions of PBLG$_{25k}$-*b*-PGlu$_{2k}$/PBLG$_{40k}$-*b*-PEG$_{5k}$ showed that such nanoparticles had to be formed by at least 60% of PBLG$_{25k}$-*b*-PGlu$_{2k}$ so as to be able to complex cisplatin in significant quantities. It was observed that nanoparticles made from 40% of PBLG$_{25k}$-*b*-PGlu$_{2k}$ could hardly complex cisplatin. This was likely due to the steric hindrance caused by the PEG chains that makes more difficult or inhibits cisplatin access to the carboxylate groups. It could also be related to the fact that in the assembling of PBLG$_{25k}$-*b*-PGlu$_{2k}$/PBLG$_{40k}$-*b*-PEG$_{5k}$ nanoparticles, the chains of PBLG$_{25k}$-*b*-PGlu$_{2k}$ are not adjacent anymore but intercalate between the other PBLG$_{40k}$-*b*-PEG$_{5k}$ chains; this might influence cisplatin complexation. Molecular modelisation studies as stated above would be of high utility to yield deeper insight into this issue. Also, similar experiments of associating cisplatin to nanoparticles made from different proportions of PBLG$_{25k}$-*b*-PGlu$_{2k}$ and a PBLG derivate not containing PEG chains might contribute to clarify this issue.

5.3.4- In vitro antitumor properties

Aquation or hydrolysis of cisplatin in the body is a preliminary step before adduct formation with DNA, which are partly responsible for the cytotoxic effect of the drug.

It results from a series of equilibria, depending on the concentration of water and chloride ions, as shown in figure 6. In extracellular fluids, where the concentration of chloride is above 100 mM, the hydrolysis of cisplatin is not favoured and it mainly remains on its neutral state. Once it has entered cells, where the chloride concentration is between 2-30 mM, hydrolysis or aquation of cisplatin occurs, one or two chlorides being replaced by water molecules, forming the cationic mono and diaquacisplatin, $[Pt(H_2O)Cl(NH_3)_2]^+$ and $[Pt(H_2O)_2(NH_3)_2]^{2+}$, which are very reactive towards

nucleophilic centers, including DNA, RNA and proteins, mainly because of the good leaving properties of water.

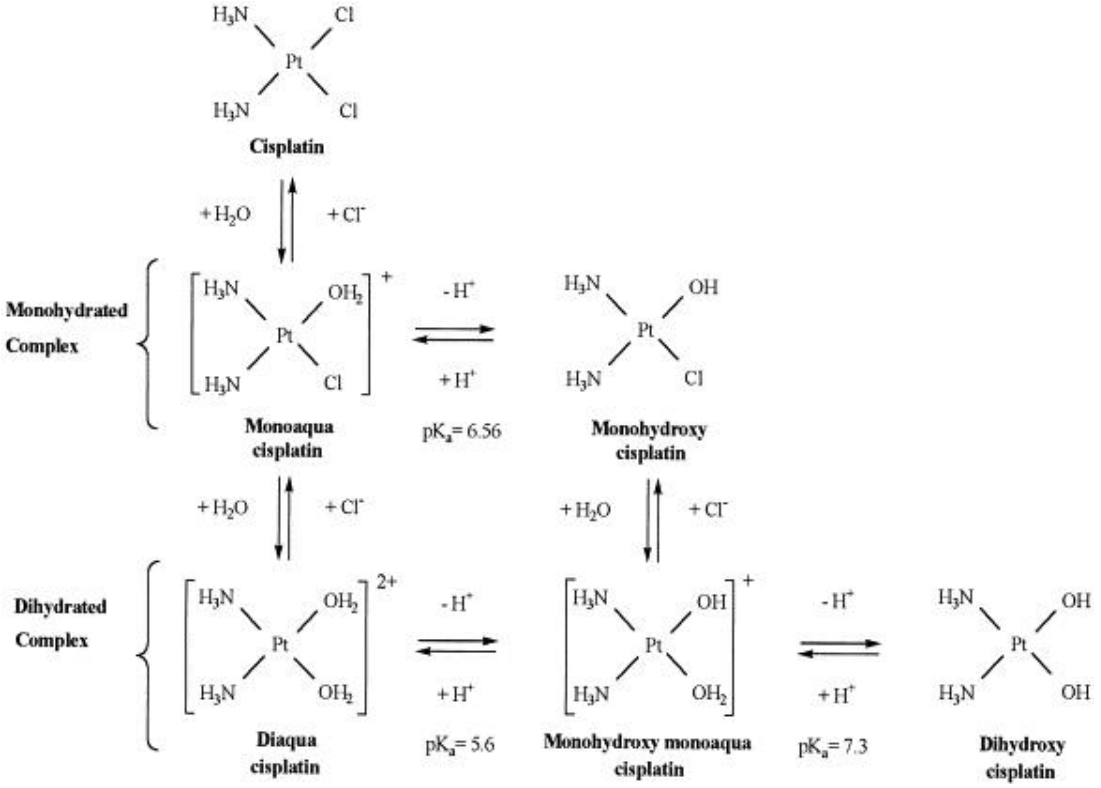

Figure 6: Species resulting of the hydrolysis of cisplatin**.** Adapted from [46].

The interaction with DNA involves reaction with the N7 atoms of the imidazole rings of guanine and adenosine. It is believed that the hydrolysis reaction is the rate limiting step for DNA binding. Monoadducts are first formed when one chloride is substituted by one water molecule. Most of the monoadducts (90%) subsequently react to form bifunctional adducts, most of them being intrastrand rather than interstrand crosslinks. The most abundant intrastrand crosslink has been shown to be 1,2-intrastrand crosslinks involving two adjacent guanines. Adducts involving DNA-protein crosslinks have also been reported [47-49].

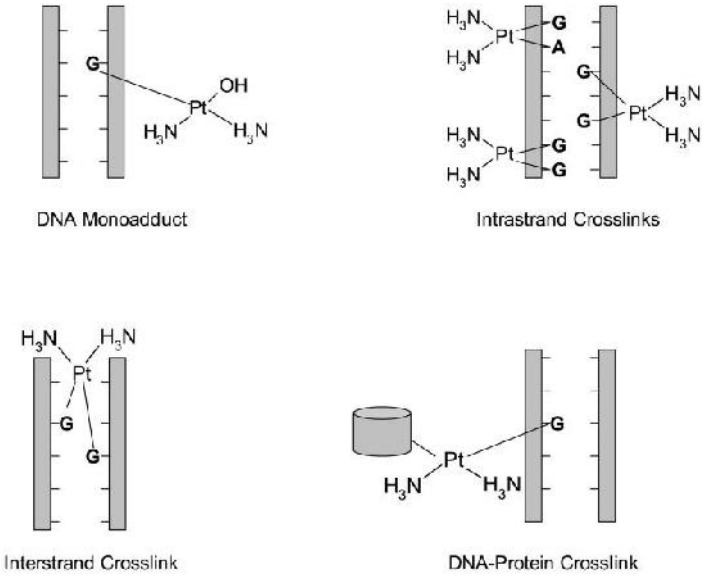

Figure 7: Platinating species adducts on DNA**.** Figure adapted from [47].

The cytotoxic mechanism of cisplatin involves the binding of cisplatin to DNA and non-DNA targets inducing cell death through apoptosis and/or necrosis [50]. The cytotoxicity of cisplatin-loaded PBLG-PGlu nanoparticles was evaluated by two methods: MTS test and trypan blue exclusion assay in three different cell lines that have the potential to metastasize to bone [51]. Cisplatin-loaded $PBLG_{25k}$-*b*-$PGlu_{2k}$ nanoparticles exhibited less cytotoxicity compared to cisplatin in solution whatever the experimental method used. The IC_{50} of cisplatin-loaded $PBLG_{25k}$-*b*-$PGlu_{2k}$ nanoparticles was 2-11 times higher than for cisplatin solution. Differences were observed depending on the testing methods, trypan blue determining higher IC_{50} as reported by other authors [52, 53]. Other methods to evaluate cytotoxicity based on ATP or DNA measurements would be useful to determine which is the most accurate method in our experimental conditions (type of cells, treatment). Interestingly, blank PBLG-PGlu nanoparticles were hardly toxic.

As evidenced by electrochemistry experiments, the platin species released from nanoparticles previously incubated in PBS were able to interact with DNA. At a sodium chloride (NaCl) aqueous concentration of 0.150 mM these species consist probably mainly of cisplatin, although a small

fraction exists as mono(aqua) species [54]. This mono(aqua) species can interact with DNA. Cisplatin bound to DNA will shift the equilibrium, generating more monoaqua species that are able to interact with DNA. It could also occur a slow interaction with dichlorodiamineplatinum (II) via a ligand exchange mechanism. These two mechanisms are considered to account for the interaction of extracellular cisplatin with the head groups of the phospholipids of the membranes [55]. Another hypothesis would be the direct interaction of the cisplatin born by the $PBLG_{25k}$-*b*-$PGlu_{2k}$-cisplatin nanoparticles and that would be in equilibrium with the released cisplatin since in addition carboxylate groups are good leaving groups.

5.3.5- Protection of cisplatin associated to $PBLG_{25k}$-b-$PGlu_{2k}$ nanoparticles during transport in blood and extra-cellular fluids

Once administered in the body, cisplatin is readily attacked by proteins with exchange of one or two chloride to form protein-cisplatin complexes. Approximately, one day after rapid intravenous administration, 65-98 % of platinum in blood plasma is protein bound, particularly to those proteins containing thiol groups such as albumin [56]. This results in reduced concentrations of freely diffusible drug to the tumoral cells and thus reduced therapeutic efficacy. Further, it contribute to some side effects. In order to reduce protein binding and thus side effects, Pt(IV) prodrugs are promising alternatives [57, 58]. Pt (IV) is more inert than Pt (II) thus avoiding more efficaciously interaction with proteins and others and thus side reactions. This Pt (IV) prodrugs can be reduced extra or intracellularly (ideally) to Pt(II), taking advantage of the reducing tumour environment, and could interact with DNA [59].

Interestingly, it can be speculated that cisplatin association to $PBLG_{25k}$-*b*-$PGlu_{2k}$ nanoparticles could counterbalance unfavourably protein binding by masking a significant amount of cisplatin molecules during the distribution process, as far as it is not released in biological media. From this point of view, it should be remarked that the low release kinetics was favourable to the transport of large platin

amounts to the targeted organs with minimal exposure of cisplatin to proteins binding. However, because some of the cisplatin molecules are likely to be exposed on the outer shell of the nanoparticles and therefore their interactions with proteins should be further evaluated.

6- *In vivo* fate of bone targeted nanoparticles

The *in vivo* fate of nanoparticles following intravenous administration is a complex issue that involves different kinetic processes and that will determine their biodistribution. Clearly, the biodistribution of drugs and nanomedicines can be considerably modified in diseased organisms, with considerable modifications of the efficacy of different barriers in the body. For example, it is well known that the permeability of the vasculature of solid tumors may be considerably increased, leading to the so-called enhanced permeation and retention (EPR) effect. Local metabolism or pH modifications are other examples. However, in the present work, it has been decided to investigate the fate of the bone targeted nanoparticles in a physiological model rather than a pathological model, as it was primarily necessary to understand the ability of the nanoparticles to reach bone tissues and the relationship with their composition and structure, not only for antitumoral delivery but also in a general purpose.

The biodistribution properties of nanoparticles are determined by anatomo-physiological characteristics and physico-chemical properties of nanoparticles. As a rule of thumb, the main parameter that determines nanoparticle biodistribution is their recognition by the reticuloendothelial system (RES), which often lead to their capture and their consequent elimination. In general, for active targeted nanoparticles, stealthiness is required in order to have long plasma half-lives so that targeted nanoparticles can progressively attain their target.

Another essential parameter that should be taken into account is the whole body microvasculature. Liver capillary microvasculature consists of reticuloendothelial sinusoids with open fenestrae vessels that allow transvascular flow of nanoparticles up to 180 nm in humans and rabbits and up to 280 nm in

mice and rats. Spleen consists of sinusoidal non reticuloendothelial microvasculature in the terminal splenic red pulp arterial blood capillary that allows a transvascular flow of particles up to 5 µm [60]. Information regarding the microstructure of myeloid bone marrow microvasculature remains controversial. Literature mentioning that bone marrow sinusoids are fenestrated capillaries with pores up to 80 nm [8, 61-64] is extensive. However, others have revisited these data in more recent reviews and state that bone marrow sinusoids are formed by a continuous endothelium [60, 65]. A recent review by Sarin et al. [60] stated that myeloid bone marrow sinusoids are reticuloendothelial blood capillaries with macula occludens interendothelial junctions that determines a transvascular flow for lipid insoluble particles limited to 5 nm. Considering this approach, non endogenous macromolecules smaller than 60 nm that could evade phagocytosis by hepatic Kuppfer cells and splenic red pulp macrophages, could remain in the bloodstream a sufficient time so as to be phagocytosed by the capillary wall of the reticuloendothelial cells.

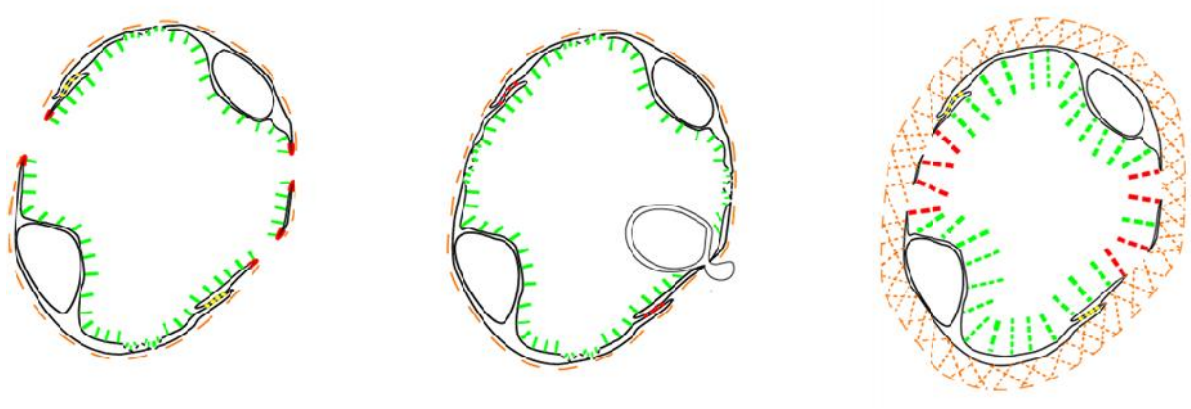

Figure 8: Schematic depictions of the capillary wall ultrastructure in different blood capillary microvasculature. Left: liver; center: bone marrow; right: kidney glomerulus**.** Green pillars represent the individual mucopolysaccharide fibers of glycocalyx; orange hatched region represents the collagenous basement layer. Schema adapted from [60]

Nanoparticles once endo-phagocytosed by the bone marrow reticuloendothelial cells, and upon transvascular release or spill over (saturation of the reticulo-endothelial cells of the bone marrow) could accumulate in the bone marrow interstitial spaces [60].

In the case of bone targeted nanoparticles, it has to be considered that in absence of an enhanced permeability effect, no pathological modification would increase favourably biodistribution to bone. For both theories of bone microvasculature the rational approach would be the development of small nanoparticles (around 60-80 nm, depending on the theory, this is not clear) with highly stealth properties. However, we should take into account that due to the whole body microvasculature (blood flow and much larger fenestrations of liver and spleen) and the eventual RES capture, nanoparticles might still be importantly distributed to liver and spleen. It has also been shown that specific coatings could favour the biodistribution of nanoparticles to the bone marrow [66, 67]. It was suggested for example, that poloxamer- 407 coated nanospheres could accumulate in bone marrow mediated by plasma components or cellular adhesion molecules [66]. In our study, PBLG-derivate nanoparticles have been shown to also distribute to bone, and this might be due both to their small size (under 60 nm) and to the stealthiness provided by the poloxamer coating (and by the PEG chains in the case of pegylated nanoparticles).

Once nanoparticles have attained bone microenvironment, mineralized bone surfaces are not readily next to the vessels. There is still an important barrier to overcome which is the high number of cells present in the bone marrow and specifically macrophages. Bone marrow homes the production of a large variety of cells derived from the hematopoietic stem cells (HSC) or mesenchymal stem cells (MSC) and giving rise to erythrocytes, platelets and leucocytes in the first case and to chondrocytes, adipocytes, osteoblast, fibroblast or myocytes in the second case. In the case of HSC cells it has been shown the existence of different niches, the vascular one, next to the sinusoids, involved in the differentiation and further mobilization through the endothelium via specific interactions [68, 69].

Nanoparticles could interact with these cells and thus less number of nanoparticles would be available to attain the bone mineralized tissue. At this level, stealthiness of nanoparticles would be again very favourable so as to avoid interaction of nanoparticles with cells. If we take into consideration all the intra-bone barriers to attain bone mineralized surfaces, it should be considered that the amount of nanoparticles that has overcome all these barriers and could attain bone mineralized surfaces is probably low. Indeed, the amount of nanoparticles able to bind to the mineralised tissue would be the result of the different kinetic processes: the main ones being: penetration of nanoparticles within the bone marrow, interaction with macrophages and other cells and binding to the extracellular matrix.

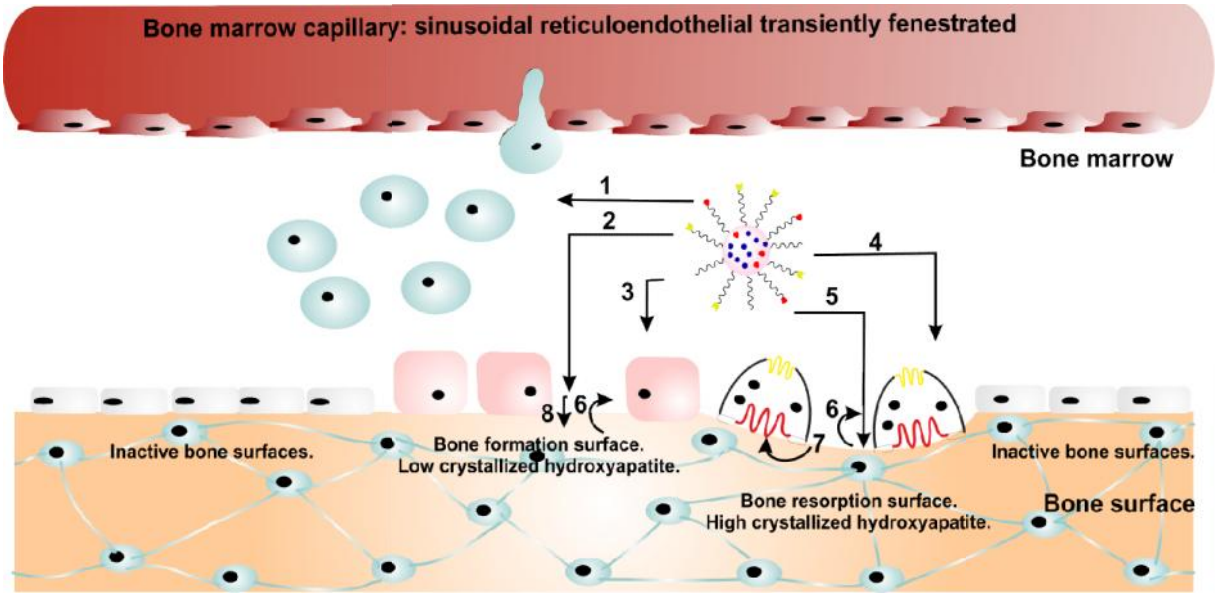

Figure 9: Nanoparticle interaction in the bone microenvironment once extravasated into the bone tissue. Nanoparticles can interact with different cell types and extracelullar matrix domains present in the bone microenviroment: 1- bone marrow cells, including phagocyting cells 2- low crystallized HAP corresponding to bone formation sites 3- osteoblasts 4-osteoclast 5- highly crystallized HAP corresponding to bone resorption sites. Once attached to the bone surface nanoparticles could: 6-detach from it, being

available to interact with bone cells or to reattach to the bone surface; 7-being resorbed by osteoclast 8-being embedded within the osteoid

Once nanoparticles have attained the bone mineralized surfaces, a retention mechanism that would prevent them from returning to the bone marrow (and interacting with macrophages and other bone cells) and from being cleared from the organism would be very useful. This is the reason why HAP binding properties have been conferred to nanoparticles either by coupling alendronate or/and poly(glutamic acid) moieties onto nanoparticle surface. The advantage of bone binding nanoparticles would be the reduced clearance of nanoparticles and thus a prolonged time of residence within the bone.

Whatever the type of HAP targeting nanoparticles, their binding to HAP in the PBS medium was a very rapid process, total binding was achieved in less than 20 minutes except for poly(glutamic acid) and poly(glutamic acid/PEG PBLG nanoparticles, for which it took approximately 45 minutes. This fast kinetics is in favour of a rapid immobilization of nanoparticles into the bone mineralised matrix when they attain this microenvironment. However, the *in vivo* bone binding kinetics is unknown and is likely to be dependent on the nanoparticle surface characteristics after circulation in the bloodstream and on their possible protein corona formed by plasma protein adsorption [70]. Moreover, kinetics of other processes involved at this stage: mainly penetration and interaction with bone marrow cells are unknown. Therefore, the *in vivo* fate of nanoparticles is impossible to predict or to attribute to any property. So as to be able to predict in a more accurate way *in vivo* fate of nanoparticles in bone, bone matrix could be used as a model instead. It would be very interesting to study these two main kinetic processes: uptake by macrophages and binding to the bone matrix to predict *in vivo* fate of nanoparticles in bone microenvironment. In order to evaluate this, an *in vitro* co-culture of macrophages and bone matrix forming osteoblasts would be highly valuable, although the feasibility of this model should be evaluated. Moreover, direct capture of decorated nanoparticles by the different cell types were out of the scope of this work. But unexpected effects are not excluded since

biphosphonates are currently used in the treatment of bone pathologies and malignancies. Finally, biodistribution modelling for the prediction of the *in vivo* fate of nanoparticles in the bone microenvironment is an appealing but very difficult task since the rates as well as extensive knowledge of these processes are ignored.

Once nanoparticles are bound to bone, they are subjected to chemical or biological detachment. Detachment is inversely related to affinity. Higher affinity binders would result in less detachment and more reattachment to the bone surface [20]. If we compare the different PBLG derivate nanoparticles and based on literature findings, poly(glutamic acid) and poly(glutamic acid/PEG PBLG nanoparticles would be more prone to chemical desorption than alendronate decorated PBLG nanoparticles. Moreover, the influence of the multivalency displayed by nanoparticles (nanoparticles can be decorated by a variable number of bone binding moieties on their surface) on the binding affinity should be evaluated for all types of nanoparticles.

As shown by the histological experiments of femurs after IV administration of nanoparticles, all types of nanoparticles can attain bone mineralized surfaces to a certain degree although alendronate nanoparticles showed an enhanced biodistribution to these surfaces. Alendronate nanoparticles were the most efficiently bound, even if they showed the lowest biodistribution to overall bone. This could be in part due to the rapid bone binding kinetics, as evidenced by the HAP binding assay. Bnz and PEG nanoparticles, although they lack an active bone targeting moiety, could effectively bind to bone mineralized surfaces, in coherence with the bone binding assay. Interestingly, alendronate/poly (glutamic acid) nanoparticles did not display *in vivo* bone binding in spite of the effective *in vitro* binding properties to HAP and *ex vivo* to bone, probably as a result of the complex processes involved as indicated above.

Discrepancy between bone uptake visualized by *in vivo* imaging and histological examination

Results concerning *in vivo* bone uptake obtained by *in vivo* imaging and by histological examination of bone slices differs substantially. This is completely coherent. *In vivo* imaging results give us a relative biodistribution of nanoparticles in bone, including the bone marrow, whereas for the histological examination we have focused on the relative microdistribution of nanoparticles in the bone mineralized tissue. The first is determined by the biodistribution of nanoparticles, including the bone marrow and its role as a RES system. The second consist of the ability of nanoparticles that have been distributed into the bone organ to attain bone mineralized surfaces and relies on all factors discussed above. It would be very interesting to study the biodistribution of the different types of nanoparticles within the bone and bone marrow microenvironment, to determine if some types have more interaction with the bone marrow cell types or others are rather located in the bone mineralized tissue and to determine the parameters involving this.

Diseased state: bone cancer pathology

In the case of a bone cancer pathology, the biodistribution of nanoparticles within in the bone will be favoured by the EPR effect [71]. Again, nanoparticles with stealth properties are desired to avoid the main RES organs, liver and spleen, and to be distributed into the tumour site. Cancers are known to have leaky vasculature. This is derived from the abnormality of endothelial cells which do not form a monolayer barrier but are rather disorganised and irregularly shaped. Endothelial cells have trans-endothelial cell fenestrations, caveolae and vesiculo-vacuolar vesicles and loose interendothelial junctions, which are likely to be responsible for much of the vessel leakiness [72, 73]. Besides, they produce high amounts of vascular permeability factors [71]. However, EPR effect has been often overestimated, should be evaluated for each type of cancer and is subjected to inter-individual variation. Interestingly, in a specific animal model of bone metastasis, the enhanced permeability effect could be evidenced [74].

As stated in the previous section, HAP targeted nanoparticles could result in an enhanced accumulation in the bone if they can attain and remain bound to the bone mineralised surfaces. Indeed, it would not increase nanoparticle arrival into the bone, which is determined by the ability of nanoparticles to be endocytosed and release by the bone marrow endothelial cells. In case of a bone cancer pathological microenvironment, tumours are generally located before bone mineralized surfaces and nanoparticles might not be able to overcome the tumour to attain the mineralised matrix due to difficulty in tumour penetration. However, some studies have shown that biphosphonate decorated PLGA and PIBCA nanoparticles present an enhanced biodistribution to bone [74-76]. Indeed, this is a global effect that could be due to other properties, including the enhanced internalisation of the zoledronate nanoparticles by breast cancer cells as authors evidenced [74]. Biphosphonates are approved for the treatment of bone metastases and therefore the issue of a non identified active targeting of bone cancer cells by these nanoparticles could be raised. Recent studies suggest that these effects are likely to be due to the effect in host cells and bone microenvironment and not to a direct effect on bone cancer cells [77]. In any case, as it has been evidenced by Chaudhari et al. that zoledronate nanoparticles are indeed more rapidly internalised that those without zoledronate [74].

Once in the bone, nanoparticles are subjected to interaction with macrophages and other bone cells as well as with metabolically active cancerous cells. If nanoparticles attained mineralized tissue, they could constitute a drug reservoir for intra-bone delivery and drug could be either released in the extracellular media or after desorption, being able to interact with bone cancer and other cells. Therefore, intra-bone toxicity derived both from the lack of targeting of bone cancer cells (a priori) themselves could not be excluded.

7- Conclusion

Bone targeted nanoparticles were foreseen for the treatment of various bone pathologies, including bone metastasis. This approach involves the retention of nanoparticles within the bone tissue to constitute drug reservoirs for intra-skeletal delivery. The main objective of this work was to investigate (i) the feasibility of bone targeted nanoparticles, (ii) their biodistribution and their possible bone affinity and finally (iii) their possible application for cisplatin delivery in view of treatment for bone metastasis.

In this work, various types of bone targeted PBLG nanoparticles were conceived, one type of them could exhibit both potential bone targeting and sustained anticancer properties. *In vivo* studies in a healthy animal model carried out with the blank $PBLG_{25k}$-*b*-$PGlu_{2k}$ nanoparticles were encouraging. They showed *in vivo* bone targeting properties and retention for at least five days. These nanoparticles were able to interact with HAP *in vitro* and *in vivo* and thus could potentially act as local reservoirs within bone tissue, releasing loaded drugs locally.

However, quantitative biodistribution of both nanoparticles and loaded drug should be further evaluated since the drug delivery potential of these nanomedicines depends on the amount of nanoparticles distributed at the right localization as well as on the amount of drug delivered at the right localization.

The bone targeted nanoparticle approach might be useful to some extent in some bone disease states such as bone cancer where the EPR effect would favour an improved biodistribution in the tumour and locally in the bone environment. Therefore, treatment of bone metastasis was identified as a possible application for these osteotropic nanoparticles. Their ability to encapsulate appreciable amounts of cisplatin (up to 6% w/w) and to sustain its delivery on a time-scale compatible with long-term skeletal durations have been shown.

For the bone metastasis application, if we consider the *in vivo* situation of a bone cancer not only localisation on the bone mineralized surfaces but rather a direct internalisation of the nanoparticles by the metastatic cancer cells should be foreseen. Biphosphonate-decorated nanoparticles could be favourably internalized in tumoural cells due to the biphosphonate moiety present on nanoparticle surface, as it has been shown for zoledronate-decorated nanoparticles. Consequently, $PBLG_{40k}$-*b*-PEG_{6k}-alendronate/ $PBLG_{25k}$-*b*-$PGlu_{2k}$ nanoparticles could eventually constitute a better approach in this case. Besides, acidic environment might trigger cisplatin release, which would be very favourable to enhance both tumour extracellular and intracellular cisplatin delivery.

Biodistribution and efficacy studies in an animal model of bone metastatic tumour should be performed as well as *in vitro* internalisation studies, which would confirm which type of nanoparticle, $PBLG_{25k}$-*b*-$PGlu_{2k}$ or $PBLG_{25k}$-*b*-$PGlu_{2k}$ / $PBLG_{50k}$-*b*-PEG_{6k}-alendronate could be a more suitable approach. Therefore, cisplatin loaded-PBLG-derivate nanoparticles remain as a promising approach for the treatment of bone metastasis.

References

[1] Shi J, Votruba AR, Farokhzad OC, Langer R. Nanotechnology in Drug Delivery and Tissue Engineering: From Discovery to Applications. Nano Letters. 2010;10:3223-30.
[2] Mundy GR. Metastasis to bone: causes, consequences and therapeutic opportunities. Nat Rev Cancer. 2002;2:584-93.
[3] Schulman KL, Kohles J. Economic burden of metastatic bone disease in the U.S. Cancer. 2007;109:2334-42.
[4] Deming TJ. Living polymerization of α-amino acid-N-carboxyanhydrides. Journal of Polymer Science Part A: Polymer Chemistry. 2000;38:3011-8.
[5] Curtin SA, Deming TJ. Initiators for end-group functionalized polypeptides via tandem addition reactions. J Am Chem Soc. 1999;121:7427-8.
[6] Gref R, Lück M, Quellec P, Marchand M, Dellacherie E, Harnisch S, et al. "Stealth" corona-core nanoparticles surface modified by polyethylene glycol (PEG): influences of the corona (PEG chain length and surface density) and of the core composition on phagocytic uptake and plasma protein adsorption. Colloids Surf, B. 2000;18:301-13.
[7] Russell RG. Bisphosphonates: the first 40 years. Bone. 2011;49:2-19.
[8] Ozcan I, Bouchemal K, Segura-Sanchez F, Ozer O, Guneri T, Ponchel G. Synthesis and characterization of surface-modified PBLG nanoparticles for bone targeting: In vitro and in vivo evaluations. J Pharm Sci. 2011;100:4877-87.

[9] Takahashi-Nishioka T, Yokogawa K, Tomatsu S, Nomura M, Kobayashi S, Miyamoto K. Targeted drug delivery to bone: pharmacokinetic and pharmacological properties of acidic oligopeptide-tagged drugs. Curr Drug Discov Technol. 2008;5:39-48.
[10] Higashi N, Koga T, Niwa M. Helical superstructures from a poly(γ-benzyl-l-glutamate)−poly(l-glutamic acid) amphiphilic diblock copolymer: monolayer formation on water and its specific binding of amino acids. Langmuir. 2000;16:3482-6.
[11] Vayaboury W, Giani O, Cottet H, Deratani A, Schué F. Living Polymerization of α-Amino Acid N-Carboxyanhydrides (NCA) upon Decreasing the Reaction Temperature. Macromol Rapid Commun. 2004;25:1221-4.
[12] Habraken GJM, Wilsens KHRM, Koning CE, Heise A. Optimization of N-carboxyanhydride (NCA) polymerization by variation of reaction temperature and pressure. Polymer Chemistry. 2011;2:1322-30.
[13] Cauchois O. Conception, Préparation & Caractérisation de Nanoparticules de Formes Complexes. Etude de leur Devenir In Vivo: Physico-chimie, Pharmacotechnie, Biopharmacie, UMR 8612, Université Paris-Sud, Paris 2011.
[14] Brzezinska KR, Curtin SA, Deming TJ. Polypeptide end-capping using functionalized isocyanates: preparation of pentablock copolymers. Macromolecules. 2002;35:2970-6.
[15] Favier A, Ladavière C, Charreyre M-T, Pichot C. MALDI-TOF MS investigation of the RAFT polymerization of a water-soluble acrylamide derivative. Macromolecules. 2004;37:2026-34.
[16] Gautrot JE, Zhu XX. Molar mass of main-chain bile acid-based oligo-esters measured by SEC, MALDI-TOF spectrometry and NMR spectroscopy: A comparative study. Anal Chim Acta. 2007;581:281-6.
[17] Sánchez-Ferrer A, Mezzenga R. Secondary structure-induced micro- and macrophase separation in rod-coil polypeptide diblock, triblock, and star-block copolymers. Macromolecules. 2009;43:1093-100.
[18] Hirabayashi H, Fujisaki J. Bone-specific drug delivery systems: approaches via chemical modification of bone-seeking agents. Clin Pharmacokinet. 2003;42:1319-30.
[19] Ishizaki J, Waki Y, Takahashi-Nishioka T, Yokogawa K, Miyamoto K-i. Selective drug delivery to bone using acidic oligopeptides. J Bone Miner Metab. 2009;27:1-8.
[20] Nancollas GH, Tang R, Phipps RJ, Henneman Z, Gulde S, Wu W, et al. Novel insights into actions of bisphosphonates on bone: Differences in interactions with hydroxyapatite. Bone. 2006;38:617-27.
[21] Sekido T, Sakura N, Higashi Y, Miya K, Nitta Y, Nomura M, et al. Novel drug delivery system to bone using acidic oligopeptide: pharmacokinetic characteristics and pharmacological potential. J Drug Targeting. 2001;9:111-21.
[22] Barroug A, Kuhn LT, Gerstenfeld LC, Glimcher MJ. Interactions of cisplatin with calcium phosphate nanoparticles: In vitro controlled adsorption and release. J Orthop Res. 2004;22:703-8.
[23] Barroug A, Glimcher MJ. Hydroxyapatite crystals as a local delivery system for cisplatin: adsorption and release of cisplatin in vitro. J Orthop Res. 2002;20:274-80.
[24] Marks Jr SC, Odgren PR, John PB, Lawrence G. Raisz and Gideon A. Rodan A2 - John P. Bilezikian LGR, Gideon AR. Chapter 1 - Structure and development of the skeleton. Principles of bone biology (second edition). San Diego: Academic press; 2002. p. 3-15.
[25] Cho G, Wu Y, Ackerman JL. Detection of hydroxyl ions in bone mineral by solid-state NMR spectroscopy. Science. 2003;300:1123-7.

[26] Lee W-H, Zavgorodniy AV, Loo C-Y, Rohanizadeh R. Synthesis and characterization of hydroxyapatite with different crystallinity: Effects on protein adsorption and release. Journal of Biomedical Materials Research Part A. 2012;100A:1539-49.
[27] El Rhilassi A, Mourabet M, Bennani-Ziatni M, El Hamri R, Taitai A. Interaction of some essential amino acids with synthesized poorly crystalline hydroxyapatite. Journal of Saudi Chemical Society. 2013.
[28] Yamamoto T, Tamaki H, Katsuda C, Nakatani K, Terauchi S, Terada H, et al. Molecular basis of interactions between mitochondrial proteins and hydroxyapatite in the presence of Triton X-100, as revealed by proteomic and recombinant techniques. J Chromatogr A. 2013;1301:169-78.
[29] Yarbrough DK, Eckert R, He J, Hagerman E, Qi F, Lux R, et al. Rapid probing of biological surfaces with a sparse-matrix peptide library. PLoS ONE. 2011;6:e23551.
[30] Vaupel P. Tumor microenvironmental physiology and its implications for radiation oncology. Seminars in Radiation Oncology. 2004;14:198-206.
[31] Xu S, Olenyuk BZ, Okamoto CT, Hamm-Alvarez SF. Targeting receptor-mediated endocytotic pathways with nanoparticles: Rationale and advances. Adv Drug Delivery Rev. 2013;65:121-38.
[32] Georges S, Ruiz Velasco C, Trichet V, Fortun Y, Heymann D, Padrines M. Proteases and bone remodelling. Cytokine & Growth Factor Reviews. 2009;20:29-41.
[33] Väänänen K. Mechanism of osteoclast mediated bone resorption--rationale for the design of new therapeutics. Adv Drug Delivery Rev. 2005;57:959-71.
[34] Dinand E, Zloh M, Brocchini S. Competitive reactions during amine addition to cis-aconityl anhydride. Australian Journal of Chemistry. 2002;55:467-74.
[35] Coleman RE. Clinical features of metastatic bone disease and risk of skeletal morbidity. Clin Cancer Res. 2006;12:6243s-9s.
[36] Desoize B, Madoulet C. Particular aspects of platinum compounds used at present in cancer treatment. Crit Rev Oncol Hematol. 2002;42:317-25.
[37] Nowotnik DP, Cvitkovic E. ProLindac (AP5346): a review of the development of an HPMA DACH platinum Polymer Therapeutic. Adv Drug Deliv Rev. 2009;61:1214-9.
[38] Stathopoulos GP, Boulikas T. Lipoplatin formulation review article. J Drug Deliv. 2012:581363.
[39] Plummer R, Wilson RH, Calvert H, Boddy AV, Griffin M, Sludden J, et al. A Phase I clinical study of cisplatin-incorporated polymeric micelles (NC-6004) in patients with solid tumours. Br J Cancer. 2011;104:593-8.
[40] Nishiyama N, Yokoyama M, Aoyagi T, Okano T, Sakurai Y, Kataoka K. Preparation and characterization of self-assembled polymer metal complex micelle from cis-dichlorodiammineplatinum(II) and poly(ethylene glycol)-poly(L-aspartic acid) block copolymer in an aqueous medium. Langmuir. 1998;15:377-83.
[41] Xia Y, Wang Y, Wang Y, Tu C, Qiu F, Zhu L, et al. A tumor pH-responsive complex: Carboxyl-modified hyperbranched polyether and cis-dichlorodiammineplatinum(II). Colloids and Surfaces B: Biointerfaces. 2011;88:674-81.
[42] Zhu W, Li Y, Liu L, Zhang W, Chen Y, Xi F. Biamphiphilic triblock copolymer micelles as a multifunctional platform for anticancer drug delivery. Journal of Biomedical Materials Research Part A. 2010;96A:330-40.

[43] Ye H, Jin L, Hu R, Yi Z, Li J, Wu Y, et al. Poly(gamma-L-glutamic acid) cisplatin conjugate effectively inhibits human breast tumor xenografted in nude mice. Biomaterials. 2006;27:5958-65.
[44] Feng Z, Lai Y, Ye H, Huang J, Xi XG, Wu Z. Poly (gamma- L-glutamic acid)-cisplatin bioconjugate exhibits potent antitumor activity with low toxicity: a comparative study with clinically used platinum derivatives. Cancer Sci. 2010;101:2476-82.
[45] Nishiyama N, Kataoka K. Preparation and characterization of size-controlled polymeric micelle containing cis-dichlorodiammineplatinum(II) in the core. J Control Release. 2001;74:83-94.
[46] Verschraagen M, van der Born K, Zwiers THU, van der Vijgh WJF. Simultaneous determination of intact cisplatin and its metabolite monohydrated cisplatin in human plasma. Journal of Chromatography B. 2002;772:273-81.
[47] Rabik CA, Dolan ME. Molecular mechanisms of resistance and toxicity associated with platinating agents. Cancer Treat Rev. 2007;33:9-23.
[48] Jamieson ER, Lippard SJ. Structure, Recognition, and Processing of Cisplatin DNA Adducts. Chem Rev. 1999;99:2467-98.
[49] Fuertes MA, Alonso C, Perez JM. Biochemical modulation of cisplatin mechanisms of action: enhancement of antitumor activity and circumvention of drug resistance. Chem Rev. 2003;103:645-62.
[50] Gonzalez VM, Fuertes MA, Alonso C, Perez JM. Is cisplatin-induced cell death always produced by apoptosis? Mol Pharmacol. 2001;59:657-63.
[51] Yonou H, Yokose T, Kamijo T, Kanomata N, Hasebe T, Nagai K, et al. Establishment of a novel species- and tissue-specific metastasis model of human prostate cancer in humanized non-obese diabetic/severe combined immunodeficient mice engrafted with human adult lung and bone. Cancer Res. 2001;61:2177-82.
[52] Wang P, Henning SM, Heber D. Limitations of MTT and MTS-based assays for measurement of antiproliferative activity of green tea polyphenols. PLoS ONE. 2010;5:e10202.
[53] McGowan EM, Alling N, Jackson EA, Yagoub D, Haass NK, Allen JD, et al. Evaluation of cell cycle arrest in estrogen responsive MCF-7 breast cancer cells: pitfalls of the MTS assay. PLoS ONE. 2011;6:e20623.
[54] Miller SE, House DA. The hydrolysis products of cis-dichlorodiammineplatinum(II) 3. Hydrolysis kinetics at physiological pH. Inorg Chim Acta. 1990;173:53-60.
[55] Wang K, Lu J, Li R. The events that occur when cisplatin encounters cells. Coord Chem Rev. 1996;151:53-88.
[56] Ivanov AI, Christodoulou J, Parkinson JA, Barnham KJ, Tucker A, Woodrow J, et al. Cisplatin Binding Sites on Human Albumin. J Biol Chem. 1998;273:14721-30.
[57] Aryal S, Hu C-MJ, Zhang L. Polymer−Cisplatin Conjugate Nanoparticles for Acid-Responsive Drug Delivery. ACS Nano. 2009;4:251-8.
[58] Graf N, Bielenberg DR, Kolishetti N, Muus C, Banyard J, Farokhzad OC, et al. αVβ3 Integrin-Targeted PLGA-PEG Nanoparticles for Enhanced Anti-tumor Efficacy of a Pt(IV) Prodrug. ACS Nano. 2012;6:4530-9.
[59] Graf N, Lippard SJ. Redox activation of metal-based prodrugs as a strategy for drug delivery. Adv Drug Delivery Rev. 2012;64:993-1004.

[60] Sarin H. Physiologic upper limits of pore size of different blood capillary types and another perspective on the dual pore theory of microvascular permeability. J Angiogenes Res. 2010;2:2-14.
[61] Wang D, Miller S, Sima M, Kopeckova P, Kopecek J. Synthesis and evaluation of water-soluble polymeric bone-targeted drug delivery systems. Bioconjug Chem. 2003;14:853-9.
[62] Choi S-W, Kim J-H. Design of surface-modified poly(d,l-lactide-co-glycolide) nanoparticles for targeted drug delivery to bone. J Control Release. 2007;122:24-30.
[63] Pan H, Kopečková P, Wang D, Yang J, Miller S, Kopeček J. Water-soluble HPMA copolymer—prostaglandin E1 conjugates containing a cathepsin K sensitive spacer. J Drug Targeting. 2006;14:425-35.
[64] Recent developments in nanoparticle-based drug delivery and targeting systems with emphasis on protein-based nanoparticles. Expert Opin Drug Deliv. 2008;5:499-515.
[65] Moghimi SM. Exploiting bone marrow microvascular structure for drug delivery and future therapies. Adv Drug Delivery Rev. 1995;17:61-73.
[66] Sou K. Advanced drug carriers targeting bone marrow, recent advances in novel drug carrier systems In: (Ed.) PADS, editor.2012.
[67] Harris TJ, Green JJ, Fung PW, Langer R, Anderson DG, Bhatia SN. Tissue-specific gene delivery via nanoparticle coating. Biomaterials. 2010;31:998-1006.
[68] Yin T, Li L. The stem cell niches in bone. The Journal of Clinical Investigation. 2006;116:1195-201.
[69] Kopp H-G, Avecilla ST, Hooper AT, Rafii S. The bone marrow vascular niche: home of HSC differentiation and mobilization. Physiology. 2005;20:349-56.
[70] Salvati A, Pitek AS, Monopoli MP, Prapainop K, Bombelli FB, Hristov DR, et al. Transferrin-functionalized nanoparticles lose their targeting capabilities when a biomolecule corona adsorbs on the surface. Nat Nano. 2013;8:137-43.
[71] Fang J, Nakamura H, Maeda H. The EPR effect: unique features of tumor blood vessels for drug delivery, factors involved, and limitations and augmentation of the effect. Adv Drug Delivery Rev. 2011;63:136-51.
[72] Sarin H, Kanevsky A, Wu H, Sousa A, Wilson C, Aronova M, et al. Physiologic upper limit of pore size in the blood-tumor barrier of malignant solid tumors. Journal of Translational Medicine. 2009;7:51-64.
[73] McDonald DM, Baluk P. Significance of blood vessel leakiness in cancer. Cancer Res. 2002;62:5381-5.
[74] Ramanlal Chaudhari K, Kumar A, Megraj Khandelwal VK, Ukawala M, Manjappa AS, Mishra AK, et al. Bone metastasis targeting: a novel approach to reach bone using zoledronate anchored PLGA nanoparticle as carrier system loaded with docetaxel. J Control Release. 2012;158:470-8.
[75] Chaudhari KR, Kumar A, Khandelwal VKM, Mishra AK, Monkkonen J, Murthy RSR. Targeting efficiency and biodistribution of zoledronate conjugated docetaxel loaded pegylated PBCA nanoparticles for bone metastasis. Adv Funct Mater. 2012;22:4101-14.
[76] Thamake SI, Raut SL, Gryczynski Z, Ranjan AP, Vishwanatha JK. Alendronate coated poly-lactic-co-glycolic acid (PLGA) nanoparticles for active targeting of metastatic breast cancer. Biomaterials. 2012;33:7164-73.
[77] Chinault SL, Prior JL, Kaltenbronn KM, Penly A, Weilbaecher KN, Piwnica-Worms D, et al. Breast cancer cell targeting by prenylation inhibitors elucidated in living animals with a bioluminescence reporter. Clin Cancer Res. 2012;18:4136-44.

CONCLUSION GENERALE
ET PERSPECTIVES

CONCLUSION GENERALE ET PERSPECTIVES

L'objectif de ce travail a consisté à concevoir des nanoparticules possédant un tropisme pour l'os, en vue du traitement ciblé de diverses pathologies osseuses. Pour cela, nous avons réalisé: (i) la conception, (ii) la préparation et la caractérisation de nanoparticules possédant un tropisme pour l'os, (iii) l'étude de leur biodistribution dans les tissus osseux et finalement (iv) la mise en œuvre de ces nanoparticules en vue de transporter et délivrer de manière contrôlée du cisplatine aux métastases osseuses. Ce travail a été mené à deux niveaux, avec en premier lieu la problématique d'essayer de comprendre les mécanismes de la distribution de nanoparticules vers et dans les tissu osseux puis, en second lieu, avec l'objectif de mettre en œuvre ces particules dans le cadre du traitement des métastases osseuses.

Ainsi, des nanoparticules multifonctionnelles ont été préparées par autoassemblage de divers dérivés fonctionnalisés du poly(gamma-benzyl–L-glutamate), préalablement synthétisés et caractérisés. Ces nanoparticules sont qualifiées de multifonctionnelles puisqu'elles ont été dotées simultanément : (i) de molécules d'alendronate ou de poly(acide glutamique), toutes les deux utilisées comme ligands de reconnaissance de l'os (notamment via leurs interactions avec l'hydroxyapatite) et (ii) de poly(acide glutamique) à nouveau, permettant l'association de quantités importantes de cisplatine (jusqu'à 6%) et un contrôle prolongé dans le temps et très efficace de sa libération, déclenchée par un pH acide et/ou la présence d'ions chlorure, (ii) de groupements PEG dans certains cas, destinés à diminuer les phénomènes de reconnaissances non spécifiques dans l'organisme et d'élimination précoce par le système réticuloendothélial, sans oublier (iv), les entités fluorescentes nécessaires à l'imagerie des nanoparticules.

Des études de distribution des différents types de nanoparticules préparées ont été menées chez l'animal sain et ont montré des résultats encourageants puisque les nanoparticules décorées par les ligands ostéotropes (alendronate ou poly(acide glutamique) ont été retrouvées dans les tissus osseux et que leur rémanence a été mise en évidence jusqu'à 5 jours après leur administration intraveineuse grâce à leur capacité d'interagir avec l'hydroxyapatite. Plus précisément, des études histologiques ont permis d'établir que les nanoparticules portant de l'alendronate en surface avaient un tropisme net pour les surfaces en cours de minéralisation dans l'os, très certainement en raison de l'affinité vérifiée de ce biphosphonate pour l'hydroxyapatite. Au total, ces nanoparticules possèdent donc un tropisme osseux intéressant qui pourrait donc leur permettre de constituer localement un réservoir de principe actif et qu'elles pourraient libérer progressivement dans cet environnement, en concentrations plus élevées et soutenues dans le temps.

Clairement, la biodistribution de ces nanoparticules mériterait d'être mieux comprise, notamment en utilisant des modèles animaux pathologiques, afin de pouvoir sélectionner les nanoparticules possédant la microdistribution dans les tissus osseux la mieux adaptée à l'application thérapeutique. De ce point de vue, le traitement des foyers métastatiques osseux, fréquemment disséminés, constitue un objectif extrêmement intéressant au plan thérapeutique mais qui nécessite aussi de poursuivre ces travaux afin de mieux comprendre les mécanismes de la distribution dans les tissus osseux métastatiques. Il s'agira tout particulièrement de mieux comprendre le trafic des particules dans ces tissus extrêmement complexes, leur microdistribution, les modalités de leur éventuelle capture par les cellules tumorales, afin d'être finalement capables de multifonctionnaliser efficacement ces nanoparticules et qu'elles atteignent au mieux leur objectif.

CURRICULUM VITAE

De Miguel, Laura
31 Boulevard Jourdan ,75014 Paris
28 years, Spanish
Tél : 0698608411
Email: laura.de-miguel@u-psud.fr

SCIENTIFIC EDUCATION AND EXPERIENCE

2009-2013	**PhD in Pharmaceutical Nanotechnology:** Galien Institute Paris-Sud, UMR-CNRS 8612, School of Pharmacy, University Paris-Sud XI, Châtenay-Malabry, France. **(PhD Thesis defense: 1st October 2013)**. Research Supervisor: Pr. G. Ponchel "***Multifunctional poly (benzylglutamate) nanoparticles for bone targeting and anticancer drug delivery into bone tissues"*** 4 awarded scholarships from three different foundations: "La Caixa" (two years: 09/2009-09/2011), "Ibercaja" (one year, 09/2011-09/2012) and "Caja Madrid" (one year: 09/2012-09/2013)
2011-2012	**Part-time temporary lecturer and research assistant (ATER)**, Galien Institute Paris-Sud, UMR-CNRS 8612, School of Pharmacy, University Paris-Sud XI.
2008-2009	**Master of Research II in Pharmaceutical Technology:** School of Pharmacy, University Complutense of Madrid, Spain. Score: 97/100. Research Supervisor: Pr. J. Torrado. "***Insulin containing microspheres with modified release: design, physico-chemical characterisation and in vivo efficacy*** "
2003-2008	**Master of Pharmacy:** School of Pharmacy, University of Navarre, Spain. Score > 90/100. Finalist of the best degree award. Internships in the Laboratory of Pharmaceutical Technology (research supervisor: Pr. J.M. Irache) and Physico-chemistry (research supervisors: Pr. C. Martinez, Pr. A. Zornoza).6 month internship in Clinical Pharmacy at St Thomas'Hospital (London).
2007	2 month awarded research fellowship at the Center of Molecular Biology Severo Ochoa(CBMSO), CSIC. Supervisor: Dr F. Wandosell. "***Treatment of ovarian tumour cells TOV-112D with estradiol"***

SKILLS

Scientific: Design of optimal approaches for active targeted polymeric nanoparticulate systems for intravenous administration, including functionalised polymer synthesis, nanoparticle preparation, optimal drug association for controlled release and study of nanoparticle surface properties and interactions.

Technical: Polymer synthesis (ring opening polymerizations, under inert conditions), coupling reactions (carbodiimide, click chemistry and living polymerizations) and characterization techniques (NMR, IR, MALDI-TOF, viscosimetry, TLC). Physico-chemistry of nanoparticulate systems (design of new nanoprecipitation methods), their surface properties (DLS, TEM, ITC, Fluorescence) and drug analytical tools (AAS, HPLC). *In vitro* cell culture, *in vivo* animal experience and histological studies.

Organisational: Project management, identification of project needs and contact of scientific and technical collaborations, supervision of research trainees, oral and written communication.

Computer software: Microsoft Office Suite, Chem Draw, Corel Draw, Adobe Illustrator, Image J, Origin, End Note, MesRenova.

LANGUAGES

Spanish: mother tongue

English: very fluent (iTOEFL:114/120, December 2008)

French : very fluent (DALF C1, February 2009 and afterwards 4 years living in Paris)
German : basic

PUBLICATIONS

Effect of PLGA hydrophilia on the drug release and the hypoglucemic activity of different insulin-loaded PLGA microspheres. C. Presmanes, L. de Miguel, R. Espada, C. Alvarez, E. Morales, J. J. Torrado. *Journal of Microencapsulation, 2011*

Poly(γ-benzyl-L-glutamate)-PEG-alendronate multivalent nanoparticles for bone targeting. L. de Miguel, M. Noiray, G. Surpateanu, B. Iorga, G. Ponchel (submitted to *International Journal of Pharmaceutics*)

Osteotropic poly(γ- benzyl-L-glutamate) co poly(glutamic acid) nanoparticles for cisplatin delivery. L. de Miguel, I. Popa, M. Noiray, E. Caudron, L. Arpinati, D. Desmaële, G. Cebrián-Torrejón, A. Doménech-Carbó, G. Ponchel (submitted to *Journal of Controlled Release*)

Bone targeted cisplatin-complexed poly(γ-benzyl-L-glutamate) co poly(glutamic acid) nanoparticles: an electrochemical approach. L. de Miguel, G. Cebrián-Torrejón, E. Caudron, L. Arpinati, A. Domenech-Carbó, G. Ponchel (to be submitted)

Osteotropicity and microbiodistribution in bones of self-assembled multifunctional poly(benzylglutamate) nanoparticles. L. de Miguel, C. Charrueau, G. Moriceau, M.-F. Bureau, P. J Marie, G. Ponchel (to be submitted)

Bone targeted nanoparticle therapeutics (review). L. de Miguel, G. Ponchel (to be submitted)

POSTER COMMUNICATIONS

Bone targeted multivalent PBLG-PGlu nanoparticles for bone cancer applications.
L. de Miguel, I. Popa, C. Charrueau, E. Caudron, and G. Ponchel. *6th European CLINAM & ETPN Summit, Basel, June, 2013*. ***First prize for poster communication***.

Multivalent poly(γ-benzylglutamate) nanoparticles with enhanced affinity to bone tissue.
L. de Miguel, M. Noiray, I. Popa, G. Surpateanu, B. Iorga and G. Ponchel. *27th GTRV (Groupe Thématique de Recherche sur la Vectorisation) Scientific Meeting, Paris, December 2012.*

Multifunctional nanoparticles of poly (γ-benzyl-L-glutamate) for bone-targeting.
L. de Miguel, C. Gueutin, M. Noiray and G. Ponchel. *26th GTRV (Groupe Thématique de Recherche sur la Vectorisation) Scientific Meeting, Brussels, December 2011*.

Bone-targeting multifunctional nanoparticles of poly (γ-benzyl-l-glutamate).
L. de Miguel, M. Noiray and G. Ponchel. *ULLA Summer School. Parme, July 2011*.

Drug Release and Hypoglycemic Effect of Different Insulin-Loaded PLGA Microspheres.
J. Torrado, C. Presmanes, L. de Miguel, R. Espada, C. Alvarez. *36th Annual Meeting and Exposition of Controlled Release Society, Copenhagen, July 2009.*

INTERESTS

Cooperation with charitable organisations, sports (swimming, hiking, skiing), culture (theatre, art expositions, travelling, discovering other cultures), classical ballet, scouts.

PROFESSIONAL REFERENCES

Professor Gilles Ponchel; PhD supervisor; Institut Galien Paris-Sud; gilles.ponchel@u-psud.fr

Doctor Christine Charrueau; Collaborator; Laboratoire de Pharmacie Galénique, EA4466, Univ Paris Descartes; christine.charrueau@parisdescartes.fr

RESUME

Des nanoparticules multifonctionnelles polymères, préparées par auto-assemblage de plusieurs dérivés du poly (L-glutamate de gamma-benzyle) (PBLG), ont été conçues afin d'assurer le ciblage des tissus osseux et la libération contrôlée de molécules actives. Des propriétés d'attachement aux tissus osseux leur ont été conférées par la présentation en surface de différents ligands ostéotropes, l'alendronate et l' acide poly(glutamique), seuls ou en combinaison. Leur affinité pour les tissus osseux a été évaluée *in vivo* ainsi que leur distribution fine dans ces tissus. Par ailleurs, des propriétés anticancéreux ont été conférées aux nanoparticules grâce à un mécanisme originale d'association du cisplatin par complexation. Le procédé mis en œuvre permet d'obtenir des cinétiques de libération très progressives de dérivés actifs du platine et déclenchée par la présence des ions chlorure. Enfin, leur cytotoxicité a été mesurée. Cette stratégie constitue donc une approche prometteuse en vue d'améliorer le traitement des métastases osseuses.

MOTS-CLES:: nanoparticules, ciblage de l'os, délivrance du principe actif, poly(glutamate de benzyle), alendronate, poly(acide glutamique), cisplatine.

ABSTRACT

Multifunctional bone targeted polymeric nanoparticles prepared by self-assembly of several poly(gamma-benzyl-L-glutamate) (PBLG) derivates have been developed. Their bone binding properties were provided by two different osteotropic moieties, alendronate or/and poly(glutamic acid) exposed on the nanoparticle surface. Their affinity for bone tissues has been evaluated *in vitro*, *ex vivo* and *in vivo*, including their detailed distribution in bone tissues structures. Further, in view of bone cancer therapeutics, nanoparticles were provided with anticancer properties thanks to the complexation of cisplatin, which leaded to very well controlled release properties. Finally, cytotoxicity were studied. Therefore, this strategy constitute a promising approach for the improvement of bone cancer therapeutics.

KEYWORDS: nanoparticles, bone targeting, drug delivery, poly(benzylglutamate), alendronate, poly(glutamic acid), cisplatin, hydroxyapatite.

POLE: PHARMACOTECHNIE ET PHYSICO-CHIMIE

LABORATOIRE DE RATTACHEMENT Equipe "Amélioration du Passage des Barrières par les Molécules actives". INSTITUT GALIEN PARIS SUD UMR CNRS 8612-UNIVERSITE PARIS-SUD XI

UFR DE PHARMACIE DE CHATENAY-MALABRY

5, rue Jean Baptiste Clément

92296, Châtenay-Malabry Cedex